The Manufacture of Polymer Nanocomposite Materials Using Supercritical Carbon Dioxide

Chen Chen

Dissertation submitted to the Faculty of

Virginia Polytechnic Institute and State University

in partial fulfillment of the requirements for the degree of

DOCTOR OF PHILOSOPHY

in

Chemical Engineering

Donald G. Baird, Chairman

Eva Marand

Robert B. Moore

John Y. Walz

November 30, 2011

Blacksburg, VA

Keywords: nanocomposite, supercritical CO_2, carbon nanotube, nano-clay

The Manufacture of Polymer Nanocomposite Materials Using Supercritical Carbon Dioxide

Chen Chen

Abstract

The use of supercritical carbon dioxide ($scCO_2$) as a processing aid to help exfoliate nano-clays and improve their dispersion during melt blending in polymer matrices has been reported in the literature. One of the best processes in terms of improving the degree of nano-clay dispersion and composite mechanical properties was developed in our laboratory. This process allows the clay to be in direct contact with $scCO_2$ and expanding the clay-CO_2 mixture via rapid depressurization into a two-stage screw extruder to mix with the polymer pellets. However, composites with clay loading higher than 6.6 wt % were not reported. In addition, the $scCO_2$ aided processing method has not been applied to carbon nanotube (CNT) based composites.

This dissertation initially focused on applying the $scCO_2$ aided processing technique to the field of CNT expansion and CNT/polymer composite preparation. The relationship with the expanded CNT morphology and the experimental conditions of the expansion procedure (including pressures, temperatures, exposure time, and depressurization rates) was studied. Microscopy results showed improved CNT dispersion in the polymer matrix and more uniform networks formed with the use of $scCO_2$, which indicated that CO_2 expanded CNTs are easier to disperse into the polymer matrix during the blending procedure. The CNT/ poly(phenylsulfone) (PPSF) composites prepared with $scCO_2$ aided method provided continuous improvements in Young's modulus up to the addition of 7 wt % CNTs. However, the Young's modulus of the

composite prepared by means of conventional direct melt blending failed to increase beyond the addition of 1 wt % CNT.

The second part of this work is concerned with the development of a semi-continuous process using $scCO_2$ to process polymer-clay composites with clay loading higher than 6.6 wt % (i.e. 10 wt %). Two major modifications are involved in the new procedure: exfoliating the nano-clay directly into the hopper filled with pellets followed by processing the composite immediately and sequentially mixing the clay into the melt. Transmission electron microscopy (TEM) and wide angle X-ray diffraction (WAXD) results show that this modified procedure help to reduce the clay collapse when processing the composites with high clay loadings. Surface modified montmorillonite (MMT) nano-clay/polypropylene (PP) composite at 10 wt % nano-clay with improved clay dispersion was obtained with increased modulus and tensile strength of 63 % and 16%, respectively, compared to the pure PP matrix.

Additional mechanical property improvements for nano-clay based composites are then obtained with the use of high crystallinity polypropylene (HCPP) and polypropylene grafted with maleic anhydride (PP-g-MA). HCPP has higher crystallinity and stiffness than conventional PP and, therefore, composites made from HCPP have better mechanical properties to start with. PP-g-MA has polar groups grafted on the PP chains that promote the intercalation of PP with clay. By using the newly developed procedure, the HCPP nanocomposite at 10 wt % of nano-clay has a Young's modulus as high as 3.236 GPa, and the modulus of the 10% MMT/PP-g-MA sample is found to be 2.595 GPa, both higher than that of the composite prepared by the direct blending method and that of a composite based on a conventional PP matrix.

Acknowledgements

The author would like to first thank Dr. Donald G. Baird for his constant support and guidance throughout the project, which has made the completion of this dissertation possible. The author would also like to thank Dr. Michael Bortner from NanoSonic Inc. for his advice for the first part of this work. In addition, the author wishes to thank her committee members for their guidance and appreciated input: Dr. John Walz, Dr. Robert Moore, and Dr. Eva Marand.

The thanks must then go to her parents for their unconditional love and endless support whenever and wherever she needs them.

The author would like to especially thank the people who gave her priceless support during the unexpected challenge and helped her to regain the courage to finish up this dissertation:

- Dr. Chitwood and Dr. Goldthmich;
- Dr. Y.A. Liu and his wife Hinghar for their thoughtful help;
- Kim and Karen in Cranwell International Center for their thorough assistance;
- Dr. Baird and his wife Treesha, Bob & Jen Lowell, Dr. Walz, Haiyan, Rixin, Zhenxing, Yanfang, Dan Li, and many more friends for their concern and help.

In addition, the author would like to thank the following people who had an impact on this work and her life:

- Former and current members of the polymer processing lab group: Jianhua, Joe, David, John Quigley, Aaron, Christ, Myoungbae, Desmond, Kevin O, Mike, Kevin M, Syed, John H, Gregorio, and Neeraj;

- Staff of the Chemical Engineering Department for their kindly assistance: Mike, Riley, Diane, Tina, Nora, and Jane;
- Her friends: Phuong Bui, Xiaoyue Zhang, Qing He, Yazhe Feng, Yin Fan, Yunping Shao, Xuerong Yao, Xin Qu, and Keyu Chen for their valuable friendship.

At last, the author would like to thank her boyfriend, Jing Yu, for his love, patience, and the faith that he always has for her.

Original Contributions

The following are considered to be significant original contributions of this research:

- Application of the $scCO_2$ technique in CNT expansion and the investigation of the relationship between the CNT morphology and the expansion procedure conditions (including pressures, temperatures, exposure time, and depressurization rates). This work was the first to report the use of $scCO_2$ to expand the entangled CNT bundles. In addition, these experiments were the first experiments to study the influence on the CNT morphology with different experimental conditions. The expanded CNTs using the best conditions have a significant bulk volume increase and disentangled structure.

- The preparation of CNT/polymer composites using the $scCO_2$ expansion techniques coupled with the melt blending method: Continuous improvement of the composite mechanical properties was obtained up to 7 wt % addition of CNTs due to the disentangle structure of the expanded CNTs. This work was the first one to use the $scCO_2$ expansion technique and melt blending method together to prepared CNT based polymer composites. To the author's knowledge, this work was also the first work to show a continuous improvement of the composite mechanical properties up to such a high CNT loading using a single screw extruder.

- A semi-continuous process that effectively reduced the clay collapse was developed. This process utilized the benefits of the $scCO_2$ technique and introduced two important original modifications: exfoliating nano-clay into the polymer pellets and sequentially mixing and adding the clay into the polymer composite. A PP composite

consisting 10 wt % nano-clay with intercalated structure was obtained using this process. The Young's modulus and tensile strength of this composite increased by 63% and 16%, respectively, compared to that of the pure PP matrix. This improvement was the best improvement that has been achieved in PP based polymer-clay composites prepared by modified melt blending methods without using compatilizers.

Format of Dissertation

This dissertation is written in journal format. Chapters 3 and 4 are self-contained papers that have been submitted for journal publications. Chapter 5 is a separate chapter satisfying the last research objective of this study written in a journal format but is not submitted. Pertinent details regarding the experiments, results, and conclusions are separately described in each chapter. With the exception of the literature review and the appendices, the figures and tables referenced in a chapter are provided following the reference section of the respective chapter.

Attribution

The co-authors in chapter 3, 4, and 5 and their contribution for the work are introduced as following.

Dr. Donald G. Baird is the Alexander F. Giacco Professor of Chemical Engineering at Virginia Tech. He gave tremendous direction and guidance to this work. He also provided assistance in the editing of the dissertation, especially in chapter 3, 4, and 5.

Dr. Michael Bortner is the Director of Manufacturing Process Development at NanoSonic, Inc. (Pembroke, VA). He provided valuable suggestions in the experiment design of the work done in chapter 3.

John P. Quigley is a PhD student in Chemical Engineering Department at Virginia Tech. He assisted some of the experiment of composites preparation for the work in chapter 3, 4 and 5. He also proofread these chapters.

Joseph Samaniuk completed his Master Degree in Chemical Engineering Department at Virginia Tech in 2008 and is now a PhD student in University of Wisconsin-Madison. He obtained the XRD data regarding the clay collapsing over the storage time in chapter 4.

Gilles Devoux is completing his PhD degree in Chemistry Department at Virginia Tech currently. He performed the XRD characterization for the nano-clay/PP composites in chapter 4.

Robert B. Moore is the Associate Director of Institute for Critical Technology and Applied Science (ICTAS) and professor of Chemistry. He provided suggestions about the morphology interpretation and provided the device for the XRD characterization of the nano-clay composites in chapter 4.

Table of Contents

List of Figures

Chapter 2

Chapter 3

List of Tables

Chapter 1

Introduction

1.1 Nanoparticles and Polymer Nanocomposites

Carbon nanotubes (CNTs) and montmorillonite (MMT) nano-clay are two of the widely used materials for generating nanocomposites. The potential chemical, physical and mechanical property enhancements that can be achieved in nanoparticle/polymer have attracted tremendous interest for the past two decades [1-8].

CNTs are hollow cylinders of graphite sheets. They can be classified into two main types: single wall nanotubes (SWNT) and multi-wall nanotubes (MWNT). SWNT can be modeled as a rolled graphite sheet and MWNT can be modeled as concentric arranged graphite sheets cylinders. Since Iijima's publication on multi-wall carbon nanotubes in Nature in 1991 [9] and following the discovery of single walled carbon nanotubes two years later [10], there has been an extraordinary explosion of related research. The combination of low density, high respect ratio, and mostly important, extremely high Young's modulus (~1TPa) and tensile strength (~30 GPa)[11], makes CNTs an ideal candidate for composite reinforcement materials. The outstanding potential of CNTs as reinforcements in polymer composites is evident from the super-tough composite fibers contain around 60 wt % SWNTs fabricated by Dalton et al. [12], which had a tensile strength of 1.8 GPa and a Young's Modulus of 80 GPa. One of the promising examples is from Liu et al. [13] involving a Nylon-6 nanocomposite. The elastic modulus and the yield strength of the CNT composite produced are improved by about 214% and 162%, respectively, with incorporating 2 wt % MWNTs. However, in general the generation of composites based on the use of nanotubes for the reinforcement of composites has not been successful, especially for the non-polar polymer systems [14-16].

The structure of MMT is promising for mechanical reinforcement firstly due to its high aspect ratio. The individual MMT layer has the thickness on the order of 1 nm and its lateral dimension is approximately 200 nm [17]. Moreover, ion-exchange reactions with cationic surfactants made the silicate layers compatible with hydrophobic engineering polymers, which means increased surface interactions between the polymer and clays [18, 19]. The Toyota research group produced and characterized the first nanoclay/polymer composites material using Nylon-6 proved the nanoclay composite has potential to not only improve the barrier properties but the mechanical properties of a polymer [2]. The tensile modulus of Nylon-6 based nanoclay composite was reported to be doubled by modest additions of clay <5 wt% [20]. However, limited success has been achieved for other polymers by conventional processing procedures, especially for polyolefins. In addition, intensively reports are focused on composites with clay loading lower than 5 wt% because exfoliation is difficult to achieve at clay concentration higher than that.

The properties of nanocomposite are affected by nanoparticle type, aspect ratio, and polymer matrix properties, etc. [21]. In addition to that, the properties of nanoparticle reinforced composite also depend on the orientation [22], dispersion, and morphology (i.e. degree of exfoliation) of nanoparticles in matrices [23], which will be greatly affected by the compounding process.

1.2 Nanocomposites Compounding Methods

One of the main challenges in manufacturing high performance nanoparticle/polymer composite is achieving homogeneous dispersion of the nanoparticles in a polymer matrix. This criterion is vital because good dispersion of the individual nanoparticles in the polymer matrix is the basis for obtaining promising material properties [23].

Currently, the three most widely applied techniques for compounding nanoparticles into polymer matrices are solution blending, in-situ polymerization and melt compounding method. For the solution blending method, nanoparticles are usually dispersed in a solvent, mixed with polymer and then the composites can be recovered by precipitating or casting a film [24-28]. It only requires small amounts of material to conduct the process and is effective for CNTs or clay/polymer matrix mixing [19, 25]. As a true solvent for pristine nanotubes has yet to be found, the choice of solvent used is generally made based on the solubility of the polymer, and ultra-sonication was usually involved [14, 29-32]. However, it was proven that sonication with a long sonication time at low power can be sufficient to shorten the nanotube length with limited unbundling, which is detrimental to the composite properties [33]. Although functionalization of CNTs surfaces and commercially available organically modified nanoclay (organoclay) are solutions for this issue, the solution blending method still has this major limitation due to the requirement to find a suitable polymer/solvent pair for each filler-polymer system. Another limitation of this method is due to the large volume of organic solvent that is usually involved, which is costly and maybe environmentally hazardous. In addition current research is mostly on a small scale and may not be industrially desirable.

The first nanoclay/polymer (Nylon-6/MMT) composite reported by the Toyota research group was prepared by in-situ polymerization [34-36]. It is a developing technique for CNTs composite preparation. The method starts by dispersing nanotubes in monomer followed by polymerizing the monomers [37-40]. The in-situ polymerization process is useful for polyamide and epoxy-based composites [34-36, 41-43], and it enables covalent bonding between the polymer macromolecules and the nanoparticle surfaces [44-46]. However, the application of this method is not general to other kinds of polymers. This technique also requires extended

processing time as well as a solvent while polymerizing certain types of polymer. These concerns limit the application for in-situ polymerization to industrial practice.

Melt blending for attempting to disperse nanoparticles into polymer matrices is now the best scalable method for industrial applications and it is also economical and environmentally friendly. The melt blending process generally involves the melting of polymer pellets to form a viscous liquid. The nanoparticles are dispersed into the polymer matrix by high shear rate combined with diffusion at high temperature [13, 47, 48]. The problem with this method is that good dispersion is usually hard to obtain, especially in non-polar polymers. Although using polypropylene oligomers (PP-MA) as a compatibalizer, the exfoliation of nanoclay within the PP matrix was improved, the elongation at break greatly decreased and the composite changed from flexible material to brittle material [49]. In addition, the properties of the composites failed to increase at a high nanoparticle loading (>10 wt%) due to the aggregation of nanoparticles [50]. Hence, although melt compounding has shown some promise for producing composites with improved properties, it does not provide a general means applicable to all polymers. Furthermore, we can expect an improvement of properties of about 100% at 5 to 6 wt% but little improvement with further loading levels [51]. The improvement in composite properties such as modulus is significantly below what is expected theoretically [52].

1.3 Super Critical Carbon Dioxide($scCO_2$) and its Application for Nanocomposite Processing

Carbon dioxide is non-toxic, non-flammable, environmentally benign, abundant, recoverable, and it has a relatively low critical point (Tc=31.1°C, Pc=1073 psi) [53]. $ScCO_2$ possesses a unique combination of properties from both the liquid and gas states, having similar solubility to that of organic solvents, and exhibiting a liquid like density combined with low

viscosity and high permeability of a gas phase. For these and many other factors, $scCO_2$ has proven to be a very useful alternative to the use of organic solvents in polymer composite processing, such as foaming agents [54], plasticizers during melt compounding [55-58], and a processing solvent in the in-situ polymerization procedure [59, 60].

To overcome the issues of poor nanoclay dispersion using melt blending method, and modified PP and other solvent-based techniques, several techniques using $scCO_2$ with the combination of melt bending method to prepare nanoclay/polymer nanocomposites have been developed. In a more common procedure, the nanoclay and polymer pellets are allowed to be saturated in the pressurized container first and then the melt blending was conducted. Evident of improved exfoliation was reported but properties of the nanocomposites were not reported [61]. Manke et al. [62] reported a process that allows clay particles to be pre-treated with $scCO_2$ in a pressurized vessel and then rapidly depressurized into another vessel at atmospheric pressure to force the clay platelets apart. The result showed exfoliated nanoclay particles by X-Ray diffraction. However, they did not provide any mechanism for assuring that the exfoliated particles remain exfoliated when they are combined with the polymer via conventional melt blending. Two years later, the same group [63] proposed a method to directly inject $scCO_2$ with polymer and $scCO_2$ treated nanoclay into an extruder. They claimed that the silicate layers will further exfoliate when the melt mixture exited the extruder. However, no WAXD or TEM evidence of exfoliated morphology was presented. Nguyen et al. [51] reported improved nanoclay/PP mechanical properties and clay exfoliation using a new technique. In this technique, the nanoclay was pre-treated and rapidly released into a port of a modified two-stage single screw extruder causing the nanoparticles to flow back through the barrel to the hopper, where solid pellets were coated with the exfoliated nanoclay. The technique was effective for the

nanoclay concentration up to 6.6 wt%. However, the further improvement in modulus for the PP nanocomposites with nanoclay concentration higher than 6.6 wt% was not achieved.

The $scCO_2$ aided melt blending method has not been widely extended to the area of CNTs/polymer nanocomposite preparation. Our early work [64] for preparing MWNTs/polyphenylsulfone using $scCO_2$ aided melt blending method showed great improvement of the dispersion of CNTs in polymer matrix and composite mechanical properties compared to direct blending method. By combining the conventional melt blending method with $scCO_2$ technique, one could expect the benefits from both sides, which are excellent dispersion from $scCO_2$ and simplicity, fast speed, and industrial compatibility from melt blending method.

1.4 Research Objectives

The first objective is to extend the $scCO_2$ aided processing technique to improve CNT dispersion in a polymer matrix and hence improve the composite mechanical properties.

The second objective is to extend the previous research of nanoclay/polymer composite using $scCO_2$ to a higher clay concentration level (>6.6 wt %) and obtain better properties with modified processing route aimed at improving the dispersion of nanoclay in polymer matrices (e.g. PP).

The third objective of this work is to determine whether additional improvement by using high crystalline PP and maleic anhydride grafted polypropylene.

1.5 Reference:

[1] G. Galgali, S. Agarwal, A. Lele, Polym. J., 45 (2004) 6059-6069.

[2] Y. Kojima, A. Usuki, M. Kawasumi, A. Okada, Y. Fukushima, T. Kurauchi, O. Kamigaito, J. Mater. Res., 8 (1993) 1185-1189.

[3] K.P. Pramoda, T. Liu, Z. Liu, C. He, H.-J. Sue, Polym. Degrad. Stab., 81 (2003) 47-56.

[4] M. Zanetti, S. Lomakin, G. Camino, Macromol. Mater. Eng., 279 (2000) 1-9.

[5] R.A. Vaia, G. Price, P.N. Ruth, H.T. Nguyen, J. Lichtenhan, Appl. Clay Sci., 15 (1999) 67-92.

[6] J.W. Gilman, Appl. Clay Sci., 15 (1999) 31-49.

[7] S.S. Ray, K. Okamoto, M. Okamoto, Macromolecules, 36 (2003) 2355-2367.

[8] P.B. Messersmith, E.P. Giannelis, J. Polym. Sci., Part A: Polym. Chem., 33 (1995) 1047.

[9] S. Iijima, Nature, 354 (1991) 56-58.

[10] S. Iijima, T. Ichihashi, Nature, 363 (1993) 603-605.

[11] P.M. Ajayan, L.S. Schadler, C. Giannaris, A. Rubio, Advanced Materials, 12 (2000) 750-753.

[12] A.B. Dalton, S. Collins, E. Munoz, J.M. Razal, V.H. Ebron, J.P. Ferraris, J.N. Coleman, B.G. Kim, R.H. Baughman, Nature, 423 (2003) 703-703.

[13] T.X. Liu, I.Y. Phang, L. Shen, S.Y. Chow, W.D. Zhang, Macromolecules, 37 (2004) 7214-7222.

[14] D. Qian, E.C. Dickey, R. Andrews, T. Rantell, Appl. Phys. Lett., 76 (2000) 2868-2870.

[15] B. Safadi, R. Andrews, E.A. Grulke, Journal of Applied Polymer Science, 84 (2002) 2660-2669.

[16] A. Dufresne, M. Paillet, J.L. Putaux, R. Canet, F. Carmona, P. Delhaes, S. Cui, J Mater Sci, 37 (2002) 3915-3923.

[17] B. Yalcin, M. Cakmak, Polymer, 45 (2004) 2691-2710.

[18] A. Blumstein, Journal of Polymer Science Part A: General Papers, 3 (1965) 2665-2672.

[19] R. Krishnamoorti, R.A. Vaia, E.P. Giannelis, Chemistry of Materials, 8 (1996) 1728-1734.

[20] B. Chen, J.R.G. Evans, H.C. Greenwell, P. Boulet, P.V. Coveney, A.A. Bowden, A. Whiting, Chem Soc Rev, 37 (2008) 568-594.

[21] M. Moniruzzaman, K.I. Winey, Macromolecules, 39 (2006) 5194-5205.

[22] J.I. Weon, H.J. Sue, Polymer, 46 (2005) 6325-6334.

[23] E.P. Giannelis, Advanced Materials, 8 (1996) 29-&.

[24] M. Lebron-Colon, M.A. Meador, J.R. Gaier, F. Sola, D.A. Scheiman, L.S. McCorkle, ACS Appl. Mater. Interfaces, 2 (2010) 669-676.

[25] M.S.P. Shaffer, A.H. Windle, Advanced Materials, 11 (1999) 937-941.

[26] X. Zhang, T. Liu, T.V. Sreekumar, S. Kumar, V.C. Moore, R.H. Hauge, R.E. Smalley, Nano Lett., 3 (2003) 1285-1288.

[27] H.G. Jeon, H.T. Jung, S.W. Lee, S.D. Hudson, Polym. Bull., 41 (1998) 107-113.

[28] C.R. Tseng, J.Y. Wu, H.Y. Lee, F.C. Chang, Polymer, 42 (2001) 10063-10070.

[29] J.W. Yang, J.H. Hu, C.C. Wang, Y.J. Qin, Z.X. Guo, Macromol. Mater. Eng., 289 (2004) 828-832.

[30] X.D. Cao, H. Dong, C.M. Li, L.A. Lucia, Journal of Applied Polymer Science, 113 (2009) 466-472.

[31] D.Y. Zhao, S.H. Wang, J. Wu, X.D. Bai, Q.Q. Lei, Pigm. Resin. Technol., 38 (2009) 305-309.

[32] L. Jin, C. Bower, O. Zhou, Appl. Phys. Lett., 73 (1998) 1197-1199.

[33] S. Badaire, P. Poulin, M. Maugey, C. Zakri, Langmuir, 20 (2004) 10367-10370.

[34] Y. Kojima, A. Usuki, M. Kawasumi, A. Okada, T. Kurauchi, O. Kamigaito, J. Polym. Sci. Pol. Chem., 31 (1993) 983-986.

[35] A. Usuki, M. Kawasumi, Y. Kojima, A. Okada, T. Kurauchi, Kobunshi Ronbunshu, 52 (1995) 440-444.

[36] A. Usuki, Y. Kojima, M. Kawasumi, A. Okada, Y. Fukushima, T. Kurauchi, O. Kamigaito, J Mater Res, 8 (1993) 1179-1184.

[37] A.A. Koval'chuk, A.N. Shchegolikhin, V.G. Shevchenko, P.M. Nedorezova, A.N. Klyamkina, A.M. Aladyshev, Macromolecules, 41 (2008) 3149-3156.

[38] S. Kumar, T. Rath, B.B. Khatua, A.K. Dhibar, C.K. Das, J. Nanosci. Nanotechnol., 9 (2009) 4644-4655.

[39] K. Saeed, S.Y. Park, Journal of Applied Polymer Science, 106 (2007) 3729-3735.

[40] Z.J. Jia, Z.Y. Wang, C.L. Xu, J. Liang, B.Q. Wei, D.H. Wu, S.W. Zhu, Mater. Sci. Eng. A-Struct. Mater. Prop. Microstruct. Process., 271 (1999) 395-400.

[41] Z. Spitalsky, G. Tsoukleri, D. Tasis, C. Krontiras, S.N. Georga, C. Galiotis, Nanotechnology, 20 (2009).

[42] T. Lan, T.J. Pinnavaia, Chem. Mater., 6 (1994) 2216-2219.

[43] J.B. Gao, M.E. Itkis, A.P. Yu, E. Bekyarova, B. Zhao, R.C. Haddon, J. Am. Chem. Soc., 127 (2005) 3847-3854.

[44] K.F. Fu, W.J. Huang, Y. Lin, L.A. Riddle, D.L. Carroll, Y.P. Sun, Nano Lett., 1 (2001) 439-441.

[45] G. Viswanathan, N. Chakrapani, H.C. Yang, B.Q. Wei, H.S. Chung, K.W. Cho, C.Y. Ryu, P.M. Ajayan, J. Am. Chem. Soc., 125 (2003) 9258-9259.

[46] M.H. Liu, T. Zhu, Z.C. Li, Z.F. Liu, J. Phys. Chem. C, 113 (2009) 9670-9675.

[47] R.E. Gorga, R.E. Cohen, J. Polym. Sci. Pt. B-Polym. Phys., 42 (2004) 2690-2702.

[48] J.M. Yuan, Z.F. Fan, X.H. Chen, Z.J. Wu, L.P. He, Polymer, 50 (2009) 3285-3291.

[49] J. Pascual, E. Fages, O. Fenollar, D. Garcia, R. Balart, Polym. Bull., 62 (2009) 367-380.

[50] S.S. Ray, M. Okamoto, Prog. Polym. Sci., 28 (2003) 1539-1641.

[51] Q.T. Nguyen, D.G. Baird, Polymer, 48 (2007) 6923-6933.

[52] Q.T. Nguyen, D.G. Baird, Advances in Polymer Technology, 25 (2006) 270-285.

[53] Y.T. Shieh, J.H. Su, G. Manivannan, P.H.C. Lee, S.P. Sawan, W.D. Spall, Journal of Applied Polymer Science, 59 (1996) 707-717.

[54] C.C. Zeng, N. Hossieny, C. Zhang, B. Wang, Polymer, 51 (2010) 655-664.

[55] J.S. Chiou, J.W. Barlow, D.R. Paul, Journal of Applied Polymer Science, 30 (1985) 2633-2642.

[56] A. Garg, E. Gulari, C.W. Manke, Macromolecules, 27 (1994) 5643-5653.

[57] M. Lee, C. Tzoganakis, C.B. Park, Advances in Polymer Technology, 19 (2000) 300-311.

[58] M.D. Wilding, D.G. Baird, Polym. Eng. Sci., 49 (2009) 1990-2004.

[59] Z.M. Liu, X.H. Dai, J. Xu, B.X. Han, J.L. Zhang, Y. Wang, Y. Huang, G.Y. Yang, Carbon, 42 (2004) 458-460.

[60] A.S. Zerda, T.C. Caskey, A.J. Lesser, Macromolecules, 36 (2003) 1603-1608.

[61] G.M. A.J. Lesser, in: ANTEC 2004, 2004, pp. 1528-1532.

[62] E.G. C.W Manke, D.F Mielewski, E.C Lee, in, 2002.

[63] L.E. Mielewski DF, Manke CW, Gulari E., in, 2004.

[64] C. Chen, D.G. Baird, M. Bortner, in: ANTEC, Orlando, FL, 2010.

Chapter 2

Literature Review

A review of carbon nanotube (CNT) and nanoclay nanoparticles based polymer nanocomposites is presented here with particular emphasis on the advantages and limitations of various compounding techniques including the procedures using supercritical carbon dioxide ($scCO_2$) to produce nanocomposite material with desirable properties. The background of the two types of nanoparticles is provided and the enhancements of various composite properties including mechanical, thermal, electrical, rheological properties are reviewed.

2.1 Background

2.1.1 Carbon Nanotubes

Since Iijima's publication on multi-wall carbon nanotubes in Nature in 1991[1] and following the discovery of single walled carbon nanotubes two years later [2], there has been an extraordinary explosion of related research. Because of their unique mechanical, electrical and thermal properties combined with low density, CNTs have a wide range of applications in various areas. CNT structures, synthesis methods, properties and applications are introduced in this section.

2.1.1.1 CNT Structures

Carbon nanotubes are hollow cylinders of graphite sheets. They can be classified into two main types: single wall nanotubes (SWNT) and multi-wall nanotubes (MWNT). SWNT can be modeled as a rolled graphite sheet and MWNT can be modeled as concentric arranged graphite sheets cylinders. However, the nanotubes are not simply rolled up like a scroll, as originally proposed by Bacon [3], but have a large number of potential helicities and chiralities [1]. The chiralities of SWNTs are specified as zig-zag, armchair and chiral, as shown as Fig. 2.1. The properties of CNTs highly depend on the

chirality of the nanotubes. MWNT contains a variety of tube chiralities, and so their properties are even harder to predict.

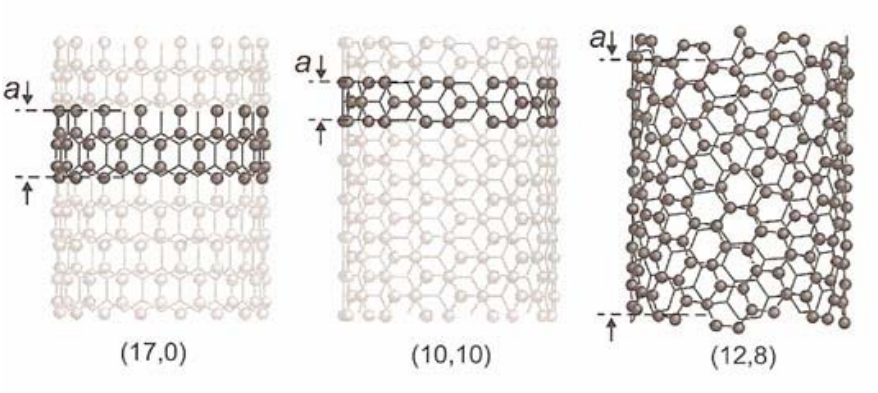

Figure 2.1 Zig-zag, armchair and chiral single wall carbon nanotubes (SWNTs) [1]

MWNTs were first found by Iijima in high resolution transmission electron microscopy in 1991 [1]. After that, various characterization techniques have been used for CNT structure determination. The structure of CNTs can be investigated by high resolution imaging techniques or electron diffraction techniques, such as STM, TEM, neutron diffraction, X-ray diffraction, X-ray photoelectron spectroscopy, infrared and Raman spectroscopy [4, 5]. Each of the methods has its own advantages, and all these techniques must be used in complementary ways.

2.1.1.2 CNT Synthesis Methods

The synthesis methods have been widely studied and developed since the discovery of CNTs. Numerous reports and reviews on the synthesis of CNTs in detail have been published. The following section will briefly summarize the three most popular synthesis techniques: arc discharge, laser ablation and chemical vapor deposition (CVD).

The first MWNT was produced by arc discharge method [1]. It is similar to the Kratschmer-Huffman method which was used to generate fullerences [6]. In this method, a low-voltage (~12 to 25 V), high-current (50 to 120 amps) power supply was used. An inert gas such as He or Ar is used as the atmosphere for the reaction, at a pressure of 100-1000 torr. An arc is produced across a 1mm gap between two graphite electrodes 5 to 20 mm in diameter [4]. Both SWNT and MWNT can be synthesized by arc discharge, but SWNTs could only be formed by adding certain kinds of metal catalyst to the anode, such as using a Fe:C anode in a methane: argon environment or Co:C anode with a He environment [2, 7]. The current standard widely used method for SWNTs production is a Y:Ni mixture, which yielded up to 90% SWNT [8]. This method is one of the most developed and inexpensive ways to produce CNTs, but the CNTs produced required purification before application.

The second synthesis method for CNTs is laser ablation method. In 1995, Smalley's research group first reported the laser vaporization synthesis of SWNTs [9]. In the following year, the first large scale production of SWNTs was reported by refinement of this method [10]. The furnace used to grow CNTs is heated to approximately 1200 °C and an inert gas of ~500 Torr of Ar or He flows through the 5 cm diameter tube. A cylindrical graphite composite target doped with small amounts of catalyst metal (typically 0.5-1.0% each of Co and Ni) is mounted at the center of the furnace. Vaporization of the target and the formation of CNTs is performed by a pulsed- or continuous-wave Nd:YAG laser [4, 11]. The diameter distribution of SWNTs made by this method is roughly between 1.0 and 1.6 nm [4]. The CNTs produced by this method also require purification before application. The mechanism of CNT synthesis in the laser

ablation process is very similar to arc discharge and both appear to be fairly simple, which is majorly governed by the dynamics of hot vapor cooling and carbon diffusion [12]. Both of the methods produce SWNTs by using a metal-impregnated graphite target (or anode), and produce MWNTs when pure graphite is used instead.

CVD and related methods are the route that can provide large amount of products. CVD was first reported to produce defective MWNTs in 1993 by Endo et al [13]. In 1996, Dai et al. successfully adapted Co-based CVD to produce SWNTs [14]. CVD and related methods are categorized according to the energy source. When a conventional heat source such as a resistive or inductive heater, furnace, or IR lamp is used, the technique is called thermal CVD, or just CVD in some literature. Plasma-enhanced CVD (PECVD), refers to the case where a plasma source is used to create glow discharge. Both CVD and PECVD have been extensively used to grow a variety of CNT structure [12].

In a typical basic CVD apparatus, gaseous carbon feedstock is flowed over metal catalyst nanoparticles at medium to high temperature (550°C to 1200 °C) and reacts with the nanoparticles to produce CNTs. For CNT synthesis in the direct PECVD system, the researchers heated the substrate up to 550 °C to 850 °C, utilized a CH_4/H_2 gas mixture at 500 mT, and applied 900 W of plasma power as well as an externally applied magnetic field [4].

Compared with the previous two methods, CVD and related methods have the advantages of amenability to scale up and more controllable over the growth process [13]. With the help of catalytic techniques, it is possible to grow arrays of aligned nanotubes on substrates [15]. However, CNTs produced in this way are structurally inferior to those made by the high-temperature arc and laser techniques, especially for MWNTs.

2.1.1.3 CNT Properties

It is widely accepted that CNT is one of the stiffest and strongest materials that has been discovered. The Young's Modulus of the CNTs can be as high as 1 TPa, which is approximately 5 times higher than the steel. Their tensile strength can be up to 63 GPa, around 50 times higher than steel. These properties are even more attractive when combined with its low density.

Theoretical calculations of CNT mechanical properties have been carried out in many different ways. The empirical force constant model calculation on single-walled tubes is one of the earliest theoretical calculations. It found a Young's modulus of 970 GPa for SWNTs with diameters from 0.34 to 13.5 nm, and to be independent of tube structure or diameter [16]. However, later studies including calculations using continuum mechanics [17], electronic energy-band theory [18], and molecular-mechanics simulations [19] all support the opposite – modulus depends on tube diameter and structure. The stiffness of small tubes will always tend to be less than for larger tubes. Fracture mechanism studies showed that the early stages of the fracture may involve the formation of Stone-Wall defect, which is a rearrangement of carbon atoms instead of hexagonal carbon networks on CNT walls [20]. In a simulation of nanotubes brittle fracture, the researchers found that a defect is formed at a strain of 0.24. As the strain increases, more defects are generated, and when the strain reaches 0.256, two bonds are broken leading to two holes [20]. With increasing strain, more bonds are broken and the holes become larger until the tube fractures.

Experimental measurement of CNT mechanical properties is a great challenge because of the dimension of CNTs. The first quantitative measurement was carried out

using TEM in 1996 [21]. In this technique, TEM images of a number of individual, freely vibrating nanotubes were recorded at temperatures up to 800 °C. The Young's modulus was then obtained by analyzing the mean-square amplitude as a function of temperature, which ranged from 410 GPa to 4.15 TPa, with an average of 1.8 TPa. In 1997, the scanning probe microscopy method was developed for CNT mechanical property measurements and the results implied a value of 1.28 TPa for the elastic modulus [22]. Subsequent studies on CNT mechanical property measurements including 3 point bending method [23] and Raman spectroscopy [24] all suggest exceptional stiffness and strength of the nanotubes.

The first theoretical calculations for CNT electrical properties was carried out in 1992 [25], and details can also be found in the work later on of Dresselhaus et al. [26, 27]. The bonding and anti-bonding π bonds point perpendicular to the nanotubes' surface play the most important roles for the electronic properties. The conductivity of nanotubes depends on nanotube structure. All armchair single-walled tubes are expected to be metallic, while approximately one-third of zigzag and chiral tubes should be metallic, with the remainder being semiconducting.

The experimental measurement of electrical properties of CNTs is a great challenge as well. The first attempts on individual nanotubes electrical measurements were carried out on MWNTs in 1996 [28]. Resistance was found to rise with the decrease of temperature, indicating that the CNT was semiconducting. Thomas Ebbesen and colleagues [26] carried out a series of four-probe resistance measurements for eight individual nanotubes. The resistance of eight different nanotubes differed widely, ranging from 2×10^2 Ω to 10^8 Ω. Although these values are only approximate, they show that the

room temperature resistivity of nanotubes can in some cases be comparable, or lower, than the in-plane resistivity of graphite [11]. Bundles of nanotubes behave very differently from the individual nanotubes. The bundling of the nanotubes changes the nanotube properties by tube-tube interaction and opens a gap in armchair tubes but also closes the band gap in semiconducting tubes. Rao et al. [29] claimed that they mostly observed the peaks of electronic density of states in a nanotube bundle shift away from the Fermi level, which means the bundle is less conductive. However, a general trend is hard to find.

CNT have also been theoretically predicted as materials that display the highest thermal conductivity, according to the calculations carried out by David Tomanek and colleagues [30]. However, existing theoretical predictions range from several dozen to 9500 W/(m·K) and existing molecular dynamics simulation results for isolated nanotubes range from several hundred to 6600 W/(m·K) [31]. Experimental measurement of CNTs also varies a lot. Hone et al. [32] presented the early experimental work for CNT bundles thermal properties. They obtained CNT ropes conductivity in the range of 2-35 W/(m·K). These values are low because the tangled nature of the ropes plays an important part. If translated into thermal conductivities for individual ropes, the values should fall in the range of 1750-5800 W/(m·K). Kim et al. [33] found the thermal conductivity of individual MWNTs can be greater than 3000 W/(m·K) at room temperature by using a microfabricated suspended device. Li et al. [34] used a non-contact Raman spectra shift method and found the thermal conductivities for SWNTs and MWNTs are 2400 W/(m·K) and 1400 W/(m·K), respectively.

2.1.1.4 CNT Applications

Due to the combination of small diameters, high aspect ratios and reversibly, CNTs have a great potential as probes in the fields of imaging, measurement and sensing. In 1996, Smalley et al. [35] used nanotubes as nanoprobes in scanning probe microscopy. They attached an individual MWNT to the tip of conventional atomic force microscopes and obtained images of sharp recesses in surface topography. However, this method of mechanically attaching nanotube bundles for tip fabrication is time consuming and limited in nanotube selections. In 1999, Lieber's group [36] developed a technique for growing individual carbon nanotube probe tips directly with control over the orientation by CVD from the ends of silicon tips. Ultra-high resolution images for bio-molecules have also been obtained using nanotube AFM tips [37]. A review of the carbon nanotubes application in AFM tips is available in the literature [38].

CNTs also have extraordinary potential applications for sensors, including chemical sensors, physical sensors, and biosensors. In a paper published in Science in 2005 [39], the researchers found that electronic transport in metallic SWNTs was sensitive to collisions with inert gas atoms or small molecules, including He, Ar, Ne, Kr, Xe and N_2, which are difficult to detect with current measurement technologies. Bourlon et al. [40] demonstrated that the CNT conductance changes in response to the flow rate, functioning as a nanoscale physical flow sensor. An enormous amount of work on CNT biosensors has also been done, including analyzing DNA [41], enzymes [42], proteins [43] and glucose [44].

Composites are another huge application area for carbon nanotubes. A very large amount of work has been carried out on CNT composites [45-56]. The extraordinary

mechanical properties combined with low density, high respect ratio and unique electrical, thermal properties made CNTs one of the best candidates for composite materials [57, 58]. There is some interest in ceramics and metals for matrix materials [59-61], but in more cases, polymer materials were used as the matrices [45-53, 55, 58, 62-141]. The preparation techniques, composite properties and current challenges will be discussed in section 2.2 and 2.3.

2.1.2 Montmorillonite (MMT) nanoclay

2.1.2.1 Structure and properties of MMT

Nanosilicates have various kinds of structures, cations and surface charges [142]. MMT is one of the widely used nanoclay filler materials for nanocomposites, which is also one subtype of 2:1 layered structure, or phillosilicates [143]. The nominal composition of MMT is $Na_{1/3}(Al_{5/3}Mg_{1/3})Si_4O_{10}(OH)_2$ [144]. The crystal structure of MMT can be illustrated as Fig. 2.2. A single aluminum hydroxide octahedral sheet is sandwiched between two layers of silicon oxide tetrahedral sheets [145]. The layer thickness of each platelet is on the order of 1 nm and its lateral dimension is approximately 200 nm [145]. The individual layers of these clay platelets are attracted to each other through van der Waal forces. The space between the layers, which is referred to as the interlayer or gallery spacing, is approximately 1nm [143]. The galleries of MMT are occupied by hydrated Na^+ or K^+ cations [146].

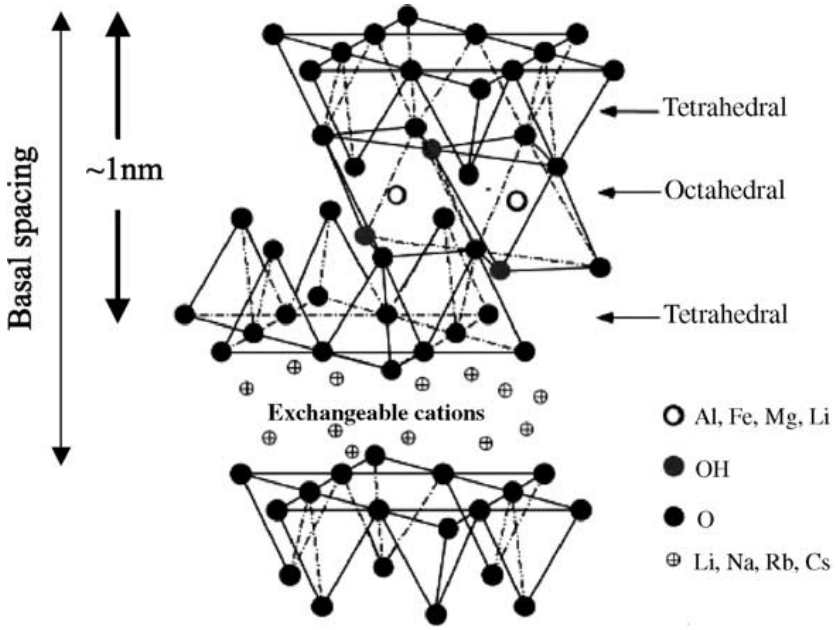

Figure 2.2: Basic structure of a 2:1 phyllosilicate [146]

Due to the physical dimensions of MMT, it has unique properties as a filler material. Firstly, it has high aspect ratio sheets and consequently large surface areas. The tremendous surface area available for polymer-clay interaction allows polymer chains to effectively transfer stress into filler particles [147]. In addition, high aspect ratio particles can be used to improve the barrier properties of polymer membranes by increasing the tortuosity of the material [148].

2.1.2.2 Organically Modified MMT

Organically modified nanoclay is also called organoclay. In this pristine state, layered silicates are only miscible with hydrophilic polymers, such as poly(ethylene oxide) (PEO) [149], because nature layered silicates usually contain hydrated Na^+ or K^+ cations [146]. It is proven that high dispersion degree of the stacks of MMT, or nanoplatelest, into individual layers is vital for preparing nanocomposites [150]. This

requires the ability to fine-tune the surface chemistry to be compatible with a chosen polymer matrix [147].

Ion-exchange reactions with cationic surfactants such as quarternary alkylammonium or alkylphosphonium cations render the normally hydrophilic silicate surface organophilic, thus making it compatible with non-polar polymers [151, 152]. A list of commercial available organic modified MMT and its counter ions is shown in Table 2.1 [153].

Table 2.1 Common counter ions for organic modified clay [153]

Product Name	Counter Ion	Modifier Concentration (meq/100g clay)
Cloisite 10A	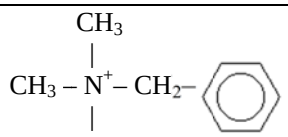	125
Cloisite 15A	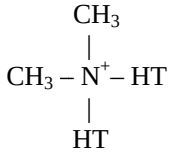	125
Cloisite 20A	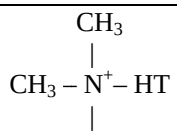	95
Cloisite 25A	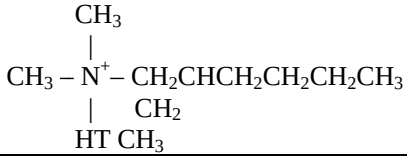	95
Cloisite 30B	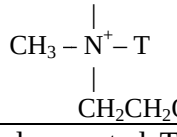	90

Where HT is Hydrogenated Tallow (~65% C18; ~30% C16; ~5% C14), and T is Tallow (~65% C18; ~30% C16; ~5% C14)

These cationic surfactants modify interlayer interactions by lowering the surface energy of the inorganic component and improve the wetting characteristics with the polymer [151, 154]. They can also provide functional groups that can react with the polymer or initiate polymerizations of monomers and thereby improve the strength of the interface between the polymer and inorganic [144, 154]. In addition, cation exchange carried out with long chain surfactant molecules increase the gallery spacing between silicate layers [153]. This increasing of gallery spacing helps the diffusion of polymer chains into individual layers, thus is important for the degree of dispersion for final composite morphology after processing.

2.1.3 MMT Clay/Polymer Nanocomposite Morphologies

The properties of nanoclay/polymer composites are significantly related to the silicate layers morphology in polymer matrix. Thus, it is important to understand each type of the nanocomposites. Four types of morphologies introduced in the following are -- exfoliated morphology, intercalated morphology, flocculated morphology and a mixture of both exfoliation and intercalation in the same nanocomposite.

2.1.3.1 Intercalated

Intercalated clay morphology occurs when polymer chains diffuse into the gallery spacings of layered structure [146]. One or a few of the polymer chains are inserted between unaltered silicate layers with their regular alternation of galleries and lamina. Gallery distance is typically on the order of a few nanometers. As its name suggests, in the second class the silicate is totally delaminated and dispersed in the polymer matrix [143]. The principle scheme and a SEM picture of exfoliated silicate morphology are

shown in Fig. 2.3 (a) and (b) [155], respectively. Properties of the composites typically resemble those of ceramic materials [146].

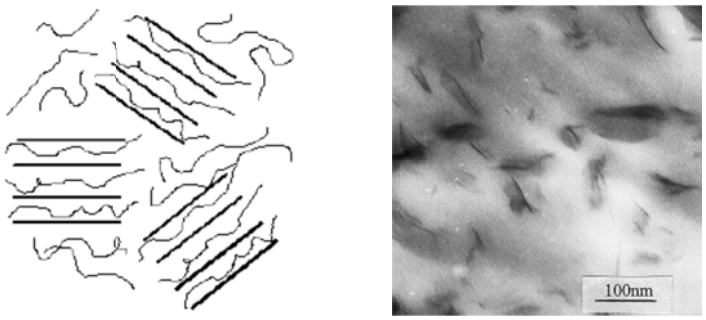

(a) (b)

Fig. 2.3: Intercalated silicate morphology (a) principle scheme (b) SEM picture

2.1.3.2 Exfoliated

An exfoliated structure occurs when silicate layers are separated by regions of polymer matrix at distances on the order of the radius of gyration of the polymer chains [143]. The individual clay layers are separated in a continuous polymer matrix by an average distances that depends on clay loading [146]. The separation may be uniform or variable. The principle and a SEM picture of exfoliated silicate morphology are shown in Fig. 2.4 (a) [155] and (b) [156], respectively.

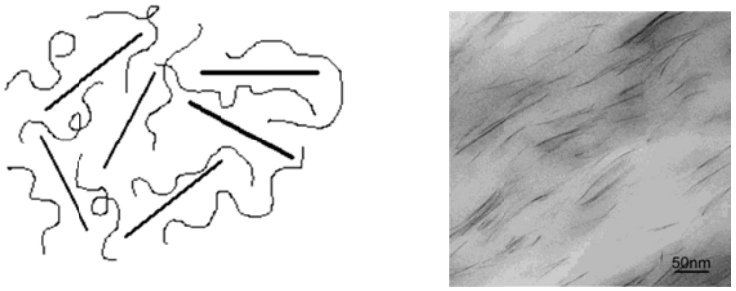

(a) (b)

Fig. 2.4: Exfoliated silicate morphology (a) principle scheme (b) SEM picture

Exfoliated morphology is preferred because it usually provides better property improvements than intercalated morphology [157]. The benefit of an exfoliated structure is the ability to take advantage of the high aspect ratio of individual silicate layers [158]. Bae et al. [159] prepared exfoliated polyaniline (PANI)/clay nanocomposites by in-situ polymerization. They also rationalized that the higher the degree of exfoliation in polymer/clay nanocomposites, the greater the enhancement of these properties. Sheng et al. [160] used a multi-scale micromechanical model and predicted a steady, gradual increase in stiffness up to a fully exfoliated state. Usually, the nanoclay content of an exfoliated nanocomposite is much lower than that of an intercalated nanocomposite [146].

2.1.3.3 Flocculated

In addition to the two clay morphologies above, a less commonly found clay morphology is flocculation. Flocculation occurs when the edges of silicate layers are attracted to one another end to end due to edge–edge interaction of the silicate layers. Conceptually this is same as intercalated nanocomposites [146]. The principle scheme of flocculated silicate layers is shown in Fig. 2.5 (a) [155] and (b) [24], respectively.

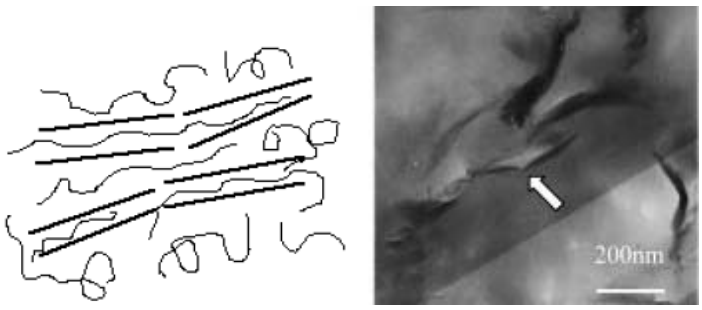

(a) (b)

Fig. 2.5: Flocculated silicate morphology (a) principle scheme (b) SEM picture

A flocculated structure has a strong effect on mechanical properties of the nanocomposite [161]. In the flocculation morphology, the silicate layers combined with each other through end to end hydrogen bonding and results in a large increase in the aspect ratio. Wu et al. [162] used epoxy resin as a reactive compatilizer to prepare poly(butylene terephthalate) (PBT) /clay composite and a flocculated morphology formed. The hydrogen bonding and PBT chains extension might be the reason of this morphology formation. Therefore a percolated strong-associated-tactoids network formed and resulted in the stress overshoot for the ternary nanocomposites. This behavior is consistent with what one would expect from an increase in effective particle aspect ratio resulting from the combination of layers in an end to end fashion.

2.1.3.4 Mixture of Exfoliation and Intercalation

Although we discussed each of the above morphologies separately, more than one morphologies exist within the same nanocomposites in most cases. The most common nanoclay morphology is a mixture of intercalation and exfoliation. Usually, nanoclay morphology is characterized as a point in-between the extremes of intercalation and exfoliation. The clay loading, strength of polymer-clay interaction and the compounding technique used all have an effect on the resulting percentage of each morphology.

2.2 Compounding Methods for Producing Nanoparticle/Polymer Composites

The properties of reinforced composite greatly depend on the compounding methods for producing the composites, which will affect the orientation, dispersion and morphology of the nanoparticles in matrices. The processing method employed limits both the type of polymer that can be used and the volume of composite materials that can be produced. Solution blending, melt blending and in-situ polymerization are the three

most widely used compounding methods for nanoparticle reinforced composite. Each of them has its own advantages and disadvantages. A list of other compounding methods and a review of compounding methods involving supercritical CO_2 is also provided.

2.2.1 Solution Blending

Solution blending is probably the most common method for preparing CNT/polymer and nanoclay/polymer nanocomposite. It only requires a small amount of materials to conduct the process, and is effective on CNTs or clay/polymer matrix mixing. In this method, three major steps are usually involved: 1) disperse nanoparticles in a suitable solvent or polymer solution, 2) mix the nanoparticles and polymer in the solution, and 3) recover the composite by precipitating or casting a film. Shaffer and Windle [55] produced CNT/poly(vinyl alcohol) composite by blend the components to form a stable mixture, where each nanotube become covered with an adsorbed layer of polymer before it is able to interact with a significant number of other nanotubes. The composite film prepared contains up to 60 wt % CNTs. Krishnamoorti et al. [163] used solution mixing nanoclay with a polystyrene-polyisoprene block copolymer in toluene as the solvent. The toluene used as a solvent had to be removed with extensive drying. The resulting nanocomposite morphology showed a mixture of intercalation and exfoliation in X-ray diffraction.

For both nanoclay and CNT polymer nanocomposites, the major limitation of this process is the requirement to find a suitable polymer/solvent pair and well disperse the nanoparticles into the solution. The solvent used must be able to swell the nanoparticle spacing as well as dissolve the polymer chains. The extent to which the solvent swells controls the final morphology of the nanocomposite.

As a true solvent for pristine nanotubes is yet to be found, the choice of solvent used is generally made based on the solubility of the polymer. In order to well-disperse the pristine nanotubes in most of these solvents, ultrasonication techniques, either high-power or mild sonication in a bath, are always involved [49, 52, 127, 164, 165]. This technique is involved in CNT/polymer composite in very early examples for solution blending. For example, Jin et al. [165] performed ultrasonication twice during the preparing of polyhydroxyaminoether (PHAE)/MTNT nanocomposite. The first time was just to mix the ground MWNTs powders and the second mixing was performed after adding in PHAE. The final product, a black thin film was formed by precipitating and the CNT weight concentration up to 50 wt % was achieved with relatively good dispersion. However, it was proven that sonication with a long sonication time at low power was sufficient to deduce the nanotubes with limited unbundling [81], and thus reduce the aspect ratio of CNTs. Most of the time, the ultrasonication solely is not sufficient to disperse CNTs in the solution, and thus other techniques are always combined with sonication.

The use of surfactants is another attempt to achieve more efficient dispersion of CNTs in solvent. O'Connell et al. [166] obtained individual nanotubes by ultrasonically agitating an aqueous dispersion of raw SNWTs in sodium dodecyl sulfate (SDS) and then centrifuging to remove tube bundles, ropes, and residual catalyst. The use of derivatives of SDS becomes the most common choice of surfactant, and this technique results in good dispersion with no derogatory effects on CNTs/polymer composite film properties [129]. However, using surfactants to improve nanotube dispersion can be problematic. Sundararajan et al. [56] showed that the surfactant molecules Triton X-100

(polyoxyethylene isooctylcyclohexyl ether) can alter the crystallization in the polycarbonate (PC) matrix, which might in turn affect the transparency and mechanical properties of the composites.

Du et al. [167] carried out a similar method in which a solution was used to blend CNTs and the polymer matrix, which they called the coagulation method. In this method, the SWNTs were added to dimethylformamide (DMF) and a sonication bath was performed for 24 h. The chosen matrix poly(methylmethacrylate) (PMMA) was then dissolved in the SWNT and DMF mixture. The composite formed by dripping the suspension into a large amount of distilled water. PMMA and SWNTs participated together because PMMA is insoluble in the DMF/water mixture and the SWNTs were trapped by the participated PMMA chains. This procedure is effective in CNT dispersing and the extensional flow during melt fiber spinning aligned the SWNTs according to SAXS, which may benefit the thermal, electrical and mechanical properties. The use of a large amount of water and solvent could be a problem when scaling up the process.

The nanoclay surface modification, or the use of organoclay, is widely applied to improve the dispersion of nanoclay into the solvents. In 1998, Jeon et al. [168] investigated high density polyethylene (HDPE) and a nitrile-based copolymer with organically modified MMT. The modified MMT could be finely dispersed in the solvent benzonitrile. The results showed a partially exfoliated structure with clay layers to be aggregated in thin stacks consisting of a few (two to five) individual layers. Tseng et al. [169] successfully prepared syndiotactic polystyrene (s-PS) organically modified clay nancomposites by mixing pure s-PS and organophilic clay with adsorbed cetyl pyridinium chloride. The clay is well dispersed into the s-PS matrix with scale in 1-2 nm.

Various types of organically modified MMT are now commercially available, which makes this problem less challenging for nanoclay/polymer composite than for the CNTs.

However, much of the current literature using solution blending is concerned with the preparation of nanoclay–polymer systems where the volume or weight of nanoclay present in the polymer is fairly low, in the range of less than 5 wt %, because higher clay concentration usually leads to aggregation of the clay layers and thus there is no improvement in mechanical properties. Avella et al. [170] investigated the crystallization behavior and properties of exfoliated isotactic polypropylene (iPP)/organoclay nanocomposites prepared by a solution technique. From the XRD results, it was shown that the nanocomposite filled with 1 wt% of nanoclay possesses exfoliated structure, while the sample with 3 wt% contained both exfoliated and intercalated structures. Above 3 wt%, clay aggregation was observed. Young's moduli increased with increasing clay content and reached a maximum at 3 wt% filler content. Above 3 wt%, tensile moduli actually decreased due to the agglomeration and collapse of the clay layers.

Functionalization of CNTs is also of interest in current research as one alternative to surfactant-aided dispersion to improve dispersion and interfacial adhesion to the polymer matrix. Covalent [171-174] functionalization of CNTs has been demonstrated to improve their dispersibility in various polymer matrices and enhance interfacial bonding between the polymer and the carbon nanotubes. Liu et al [78] prepared CNTs/PMMA nanocomposite by using the MWNTs surface functionalized by covalent linking of long alkyl chains. The results showed that functionalized multi-wall carbon nanotubes were well dispersed in the PMMA matrix. However, these methods often involve the conversion of side-wall carbons from sp^2 to sp^3 hybrization. This bonding change disrupts

conjugation within the nanotubes and can lead to reduced electrical conductivity and mechanical properties [175].

Accordingly, noncovalent methods such as wrapping or complexation have been explored as an alternative to the covalent functionalization methods described above. Noncovalent functionalization of carbon nanotubes using highly aromatics molecules have been proved to be also effective [176-179]. It has been demonstrated that pyrene interact strongly on the surface wall of either single [176] or multiwall carbon nanotubes [179]. Such methods lead to enhanced solubility and good carbon nanotubes polymer interactions. Yang et al [180] used polyethylene glycol-200 as a noncovalent functionalization agent and successfully prepared polyimide nanocomposite films containing dispersed individual nanotubes, with CNT percentage up to 43 wt %. However, functionalization procedure for CNTs is not commercially available.

With all the efforts that have been put in, the solution blending method is still expensive and not expandable due to the requirement to find a suitable polymer/solvent pair for each filler-polymer system, and the challenge to efficiently functionalize CNT surfaces. Although some water-soluble polymers such as PEO does not require organic solvents for nanoclay/polymer composite preparation, a large volume of organic solvent is usually involved, which is costly and maybe environmentally hazardous.

2.2.2 In-situ Polymerization

The first nanoclay/polymer (Nylon-6/MMT) nanocomposites that attracted tremendous attention for this field by the Toyota research group reported was prepared by the in-situ polymerization [181-183]. This method applied to the perpetration of CNT nanocomposite has also been studied intensively for the recent few years [82, 83, 85, 91-

93, 97]. This preparation strategy mainly involved two steps: 1) disperse nanoparticles in the monomers and 2) polymerization reaction of the monomers. Jia et al [85] is one of the early examples for CNTs/polymer composite preparation using in-situ polymerization strategy. In their approaching, CNTs were dispersed into MMA at first and followed by the addition polymerization process to form the CNTs/PMMA composite. From the results, it is shown that CNTs were initiated by AIBN to open their π-bonds, which imply that CNTs may participate in PMMA polymerization and form a strong combining interface between the CNTs and the PMMA matrix.

In-situ polymerization process is useful for polyamide based composites [5, 84, 93, 94]. Usuki et al. [184] produced the first Nylon-6 based nanoclay nanocomposite using a ring opening polymerization with caprolactam. X-ray diffraction analysis and TEM imaging showed that below 15 wt% silicate the morphology was primarily exfoliated. Above 15 wt% a mixture of intercalated and exfoliated silicate layers were apparent. Gao et al. [84] reported a chemical processing technology that allows the continuous spinning of SWNT–nylon 6 fibres by the in situ ring opening polymerization of caprolactam in the presence of SWNT. This process increases the tensile modulus and tensile strength about 2.7 and 1.9 times compared to neat matrix material, respectively, with the incorporation of 1.5 wt % SWNTs into nylon-6. The results showed excellent compatibility between the SWNTs and nylon 6.

Epoxy as the polymer matrix of nanocomposites comprise the majority of reports using in-situ polymerization methods [48, 76, 78-80, 185], where usually the nanoparticles are dispersed in the resin followed by curing the resin with the hardener. The first reported epoxy–nanotube composites comes from a paper by Ajayan in 1994

[75]. In this work, the resin is prepared by mixing the epoxy resin, curing agents, methyl nadic anhydride (MNA), and an accelerating agent by magnetic stirring. The nanotube-resin mixture is then hardened by keeping it over 24 hours at above 60 °C. In-situ polymerization in the application of epoxy is also capable for high CNT loading nanocomposite. Spitalsky et al [80] presented a versatile processing technique for fabricating epoxy nanocomposites with a high weight fraction of CNTs. In their approach, the functional CNT buckypapers was firstly prepared by a dispersion–filtration protocol [77]. These buckypapers, composed of randomly oriented tubes with tailored chemical environment, were used as a preform for fabricating CNT/epoxy composites by just immersing in a pre-polymerized epoxy/curing agent solution in acetone. Subsequently, the soaked buckypaper was removed from the acetone bath, left to dry for 1 h and then cured. MWNT based nanocomposites with CNT weight fraction up to 70 wt % were prepared with improved mechanical and electrical properties. Lan et al. [186] used epoxy to determine the effect that extent of polymerization has on nanoclay morphology. The authors showed that the extent of intercalation and exfoliation in nanoclay composite can be controlled while using in-situ polymerization by controlling the extent of polymerization. X-ray diffraction results taken at different times in the polymerization step show a steady decrease in the amount of intercalated material present and a steady increase in exfoliation.

One advantage of in-situ polymerization method for preparing CNT composite is that it enables the grafting of polymer macromolecules onto the walls of CNTs thus covalently attached to CNTs. Two categories of grafting methods have been reported as “grafting to” or “grafting from” approaches [129]. In the “grafting to” approach, polymer

is prepared firstly and followed by the reaction with the functional groups of CNTs. The advantage of this method is that preformed commercial polymers of controlled mass and distribution can be used. The limitation is that attachment of a small number of chains hinders diffusion of additional macromolecules to the surface, thereby leading to low grafting density. One of the first examples of the ‘‘grafting to’’ approach was published by Fu et al. in 2001 [83]. In this work, carboxylic acid groups on the nanotube surface were converted to acyl chlorides by refluxing the samples in thionyl chloride. Then the acyl chloride functionalised carbon nanotubes were reacted with hydroxyl groups of dendritic PEG (polyethylene glycol) polymers via the esterification reactions. The “grafting from” approach, on the other hand, allows high grafting density, in which nanotube surface is first covalently attached with initiators and the resulting nanotube-based macroinitiators are then exposed to monomers. This method requires a strict control of amounts of initiator and substrate as well as a control of conditions for polymerization reaction. The attachment of atom transfer radical polymerization initiators to CNTs has been used to graft different polymers to CNTs successfully, either by multiple steps, [82, 86, 92, 97, 99] or in simple one step [91, 97].

Along with intensively report of in-situ polymerization processing of CNT polymer nanocomposite, only few of them considered the feasibility for industrial applications. Koval'chuk et al. [87] proposed a technique using MAO-activated C2- and C1-symmetry ansazirconocenes to prepare isotactic polypropylene and elastomeric stereoblock polypropylene nanocomposites containing MWNTs. In their work, bulk of liquid propylene is used as a medium for CNT dispersion and subsequent polymerization reaction. The author claimed that the utilization of liquid monomer as a reaction medium

made the synthesis easily scalable and feasible to the industrial realization. However, with consideration of as the increasing viscosity during the polymerization progresses, the extent of in situ polymerization reactions might be limited.

A great disadvantage to this technique is the extended processing time as well as the necessity for a solvent while polymerizing certain types of polymer. These concerns limited the application for in-situ polymerization to industrial practice.

2.2.3 Melt Blending

The melt blending process generally involves the melting of polymer pellets to form a viscous liquid. The nanoparticles are dispersed into the polymer matrix by high shear rate combined with diffusion at high temperature. Samples can then be fabricated by followed compression molding, injection molding, or fiber production techniques.

Melt blending methods are proved to have decent improvement for the nanoclay dispersion and widely used in nanoclay/polymer composite preparing. Vaia et al. [187] showed that direct intercalation of polymer chains into clay gallery spacings is a viable compounding procedure. In a follow up paper, the same group used in-situ x-ray diffraction to determine that the rate of diffusion of polymer chains between silicate layers was on the same order of magnitude as polymer self-diffusion [188]. This work showed that melt compounding was not only possible but it could be carried out under the same conditions as one would melt process a pure polymer material.

Cho et al. [189] carried out one of the first extensive studies on the effects of melt compounding conditions on nanoclay morphology and nanocomposite properties. Both a single screw and a twin screw extruder were employed to produce polyamide based nanoclay composite. Results from samples produced using the single screw extruder at

40rpms showed a poor exfoliation. A second pass through the single screw extruder was also attempted but the poor exfoliation was still existed. Composite produced using the twin screw extruder showed considerable property improvements compared to composite processed with the single screw extruder. Exfoliation in the twin screw processed material was found to be extensive after only a single pass. Fornes et al. [190] showed that the molecular weight of the polymer matrix affects nanoclay morphology due to the ability of high molecular weight polymers to transfer shear stresses more effectively than low molecular weight polymers. This difference in exfoliation levels are attributed the trend of increasing melt viscosity and stress transfer ability of the polymer melt with increasing molecular weight.

Nevalainen et al. [191] prepared MMT/PC composite using melt-compounding method in a twinscrew extruder. Pellet samples with 0, 1, 3, and 5 wt% filler content were prepared. XRD and TEM results showed that a mixture of exfoliated, intercalated, and confined (i.e., the collapse of the interlayer distance) nanocomposites are obtained. The Young's modulus and yield strength increased based on nanoclay possess. However, their ductility upon tensile loading is significantly affected. A transition from ductile to brittle deformation occurs at studied clay loadings.

This technique is successful in effectively dispersing the nanoclays in the polymer matrix for the polar polymer system, however, limited success has been achieved from extending this technology to non-polar polymers, such as polyolefins [192]. This is because the non-polar polymer is not completely compatible with the nano-clays. Although the clay surface can be modified with non-polar groups, such as hydrogenated tallows, there are still some charges exist on the clay surface, which is repulsive to the

non-polar polymer matrix. Many attempts at generating polyolefin based nanocomposites have been partially successful only by use of large amounts of compatiblizer, which may lower the molecular weight and mechanical properties. Zhang et al. [193] prepared organoclay/maleic anhydride-modified polypropylene nanocomposites using a conventional twin-screw extruder. The particles of silicate layers were exfoliated and dispersed into the nanometer level. The impact strength is greatly improved at lower MMT content. However, the tensile strength of nanocomposites is not increased much compared with that of polypropylene and conventional filled composite, especially at higher clay concentration (i.e. 5 wt%).

Jin et al. [112] presented one of the early examples for CNTs nanocomposite produced by melt-blending method. They mixed polymethylmethacrylate (PMMA) with 26 wt % MWNT in a laboratory mixing molder at 200 ^{o} C. The melt was then compression molded (under 8–9 MPa at 210 ºC) in a hydraulic press to give composite slabs. A following report from the same group improved the approach by using poly(vinylidene fluoride) (PVDF) covered MWNTs [113]. The result shows that PVDF assists in MWNTs dispersion and increases the interfacial adhesion between MWNT and PMMA, thus leads to a significant improvement in the storage moduli of the MWNT/PMMA composites at low temperatures.

The melt blending method is also very attractive for thermoplastic polymers based CNTs nanocompostes, particularly for those are not able to process by solution blending [105]. Liu et al. [115] successively prepared MWNTs/PA6 nanocomposite film samples by using a twin-screw mixer and get great improved mechanical properties. However, the processing conditions should be optimized for the whole range of polymer–nanotube

combinations, because nanotubes can affect melt properties such as viscosity, resulting in unexpected polymer degradation under conditions of high shear rates [118]. Some other successful example can be found for of melt blending including SWNT/polypropylene [106, 117], SWNT/polyimide[120], MWNT/PMMA [110], and MWNT/PET [116].

The main disadvantage for melt-blending is the high viscosities of the composite melt at high CNTs loadings. This fact results is not only difficulty of processing and less efficiency of CNT dispersing, but also the damage to CNTs during processing. It was found that the average nanotube length fell with mixing energy. For the samples with the best dispersion, the nanotube length had fallen to a quarter of its initial value [105]. To overcome this disadvantage, a combination of solution and melt techniques was reported by Thostenson and Chou [121]. They initially dispersed CVD-MWNT in a solution of PS in tetrahydrofurane (THF) and prepared a film, then extruded the cut film though a rectangular die. However, this approach may lose the initial advantage of melt-blending method and draw it back to the solution blending.

Of the three compounding techniques discussed above, melt compounding has the advantage of being simple, fast and compatible with current industrial techniques. The primary challenge to melt compounding that must be overcome is the inability to disperse the nanoparticles in non-polar polymer matrices such as polypropylene and get continuous improvement of the mechanical properties at high nanoparticle concentration.

2.2.4 Other Method

In addition to the three most widely used methods, some other methods have been developed include co-vulcanization [194], electrospinning [195], solid-state intercalation [119, 196-202], sol–gel [203], latex fabrication [50, 204-206] and etc. These methods are

able to prove unique properties of the nanocomposites and are useful in their specific research area, but strict limitations of these methods restrict the widely application.

2.2.5 Compounding Methods Involving Supercritical CO_2 ($scCO_2$)

Supercritical fluids have solubility comparable to a gas, but a tunable density near that of a liquid. They have been receiving attention in various applications from including food and pharmaceutical industries as well as in the plastics industry. Particularly, carbon dioxide is non-toxic, non-flammable, abundant, recoverable, and it has a relatively low critical point (Tc=31.1 °C, Pc=1073 psi) [207]. Using $scCO_2$ as a processing aid does not producing CO_2 because it only borrow the CO_2 from the atmosphere, therefore is an environmental friendly benign process.

$ScCO_2$ can be used in a wide range of applications in polymer processing including plasticizers, foaming agents, processing solvents and processing aids used for the impregnation of polymer matrices with additives [208].

One of the earliest application for $scCO_2$ as an aid for polymer processing is plasticizing agents. $ScCO_2$ behaves like a polar, highly volatile organic solvent, which swells and plasticizes polymers when it interacts with them [209]. $ScCO_2$ is proven to be efficient for lowering the viscosity of high molecular weight polymers of various polymer melts [210-212]. Wilding et al. [213] used $scCO_2$ to plasticize and reduce the viscosity of 65% and 85% acrylonitrile (AN) copolymers in an extrusion process and render it melt processable. The viscosity was reduced by up to 56% at adding 7 wt% CO_2 in melt for the 65% AN copolymer. A chemorheological analysis determined that the 85% AN copolymer would be suitably stable for over 30 min of extrusion at temperatures up to 200 °C. The foaming of the extrudate in this application is always a problem when

homogenous extrudates are desired, and the suppressing of the foaming becomes an issue. Wilding et al.[213] extruded the polymer melts into a pressurized chamber attached to the end of the die. The author claimed that the chamber was operated in batch mode, but could be adapted to run continuously, similar to the steam pressurized chambers used to pressurize PAN plasticized with water and organic solvents [214, 215]. Re-pelletizing, compression molding, or injection molding of the foamed pellets is always an option, but they costs extra effort and are not perfectly effective.

Currently, there is no literature reported about CNT reinforced materials using $scCO_2$ as a plasticizer. Zeng et al. [216] reported using CO_2 as a foaming agent to produce PMMA/MWCNTs nanocomposites foams. However, CO_2 in this study is not used in super critical status.

$ScCO_2$ has been widely used as a polar and low viscosity solvent with the combination of the in-situ polymerization method to prepare nanocomposites. Zerda et al. [217] used $scCO_2$ for the synthesis of PMMA/organo-MMT nanocomposites by mixing organo-MMT, MMA, initiator in the $scCO_2$ in a high pressure apparatus. The primary purpose of the $scCO_2$ was to allow MMA monomers to readily diffuse and homogeneously disperse within the gallery spacings of the silicate layers. After the saturation period for mixing, the temperature was raised to complete the polymerization step. Once polymerization was complete, the pressure was reduced to atmospheric conditions over a period of 15hrs. Removal of trapped CO_2 was accomplished by exposing the samples to temperatures above the glass transition to allow foaming to occur. The foamed material was then pulverized and melt processed. This technique produced well dispersed, intercalated nanoclay/polymer composites with clay concentration of 40

wt %. Isotropic forms of the 40 wt % composite showed a 50% increase in tensile modulus while melt processed samples containing orientation showed an increase in the tensile modulus of 220%.

Similar methods applied to CNT/polymer composites have also been developed. Liu et al. [218] successfully prepared CNT/PS composite by impregnating styrene and an initiator into the CNTs with the aid of $ScCO_2$ followed by the polymerization. A composite material, in which CNTs were consistently filled with polystyrene, was obtained. Dai et al. [219] prepared CNTs coated poly(2,4-hexadiyne-1,6-diol) (polyHDiD) with the aid of $scCO_2$. CNTs were first dispersed in an ethanol solution of HDiD, and CO_2 was then introduced into the mixture. After heating the mixture at 200 °C, poly(HDiD)/CNT composites were produced. It was shown that poly(HDiD) existed in two forms in the composites: either as a coating on the outer surface of the CNTs with a thickness of less than 10 nm or being impregnated in the inner cavities of the CNTs. Other polymer based CNT nanocomposites as polypyrrole [220], polyacetylene [221], PMMA [222], etc, have also been reported using this technique. However, few of the reports showed the mechanical properties and none of these reports showed the potential for application in industry due to the limited product amount.

The techniques using $scCO_2$ with the combination of melt bending method to prepare nanoclay/polymer nanocomposites have been developed. In 2002, Manke et al. [223] developed a process that allows clay particles to be pre-treated with $scCO_2$ in a pressurized vessel and then rapidly depressurized into another vessel at atmospheric pressure to force the clay platelets apart. The result showed exfoliated nanoclay particles by X-Ray diffraction. However, they did not provide any mechanism for assuring that the

exfoliated particles remain exfoliated when they are combined with the polymer via conventional melt blending. Two years later, the same group [224] proposed a method to directly inject $scCO_2$ with polymer and $scCO_2$ treated nanoclay into an extruder. The polymer and nanoclay were disposed through two separated hopper into the extruder substantially. The extruder was heated so that the silicate-polymer mixture was a flowable melt. The pressurized melt was then got contact with $scCO_2$ to above 1100 psi gauge and the temperature was controlled as the melting temperature of the polymer. They claimed that the silicate layers will further exfoliate when melt mixture exiting the extruder. No WAXD or TEM evidence of exfoliated morphology was presented. In a different procedure, Lesser et al. [225] firstly let $scCO_2$ absorb into the nanoclay particles and pellets in a pressurized hopper and then the melt blending was conducted. WAXS and TEM results showed the increase in the clays d-spacing was as much as 100%. However, properties of the nanocomposites were not reported.

Nguyen et al. [226] developed another technique by first saturate the nanoclay in $scCO_2$ and then releasing the nanoclay rapidly back through a stopped extruder filled with polymer pellets. The saturation was conducted in a custom pressure chamber designed with an inlet for the addition of CO_2 and an exit with a ball valve for the subsequent release of the mixture, which has the ability to release its contents through an inlet in the second stage of a single screw extruder. The polymer pellets were loaded into a hopper attached to the extruder with the ability to trap released clay. The extruder was brought to melt temperature with the screw turned off. The ball valve on the pressure chamber was opened and the mixture of silicate and $scCO_2$ rapidly expanded throughout the extruder screw and up into the modified hopper where it immediately mixed with the

polymer pellets. Results from WAXD showed an increase in the exfoliation levels of the $scCO_2$ produced material as compared to samples produced with dry mixing of polymer and clay. Mechanical tests showed a 17% improvement in the Young's modulus of $scCO_2$ produced composite containing 6.5wt% silicate over composite with the same wt% silicate produced from dry mixing of the silicate and clay. The combination of $scCO_2$ facilitated silicate exfoliation with melt compounding makes this particular technique ideal for use with polymer matrices that stand to benefit from the addition of layered silicate but are unable to achieve a suitable level of silicate exfoliation with simple melt compounding. However, the property of the nanocomposites with nanoclay over concentration of 6.6 wt% failed to increase further as the theory predicted. This may due to the limitation of the facility size or the procedure itself.

The $scCO_2$ aided melt blending method has not been extended to the area of CNTs/polymer nanocomposite preparing. By combining the conventional melt blending method with $scCO_2$ technique, one should expect the benefits from both sides, which are excellent dispersion from $scCO_2$ and simplicity, fast speed, and industrial compatibility from melt blending method.

2.3 CNT/Polymer Composite Properties

2.3.1 Mechanical Properties

The outstanding potential of carbon nanotubes as reinforcements in polymer composites is evident from the super-tough composite fibers contain around 60% SWNTs by weight fabricated by Dalton et al. [130]. However, among the early studies using nanotubes for reinforcement of composites and the following intensive reports, successful system for CNT/polymer nanocomposite was not quite common [50, 52, 139].

The main challenges for the successfully reinforcement are: first, good dispersion of nanotube within the polymer matrix and, second, a good interface interaction for the load transfer. Till the year of 2004, functionalized CNT within the matrix of Nylon-6 was found to be a good system that showed great improvement on the mechanical properties. Chen et al. [227] used melt blending followed by compression molding to prepare Nylon-6 nanocomposites reinforced with surface-functionalized CNTs. The modulus of the composite was increased from 1899 MPa to 3556 MPa or by 87% with the addition of 1 wt % CNT. Their transmission electron microscopy (TEM) and SEM results showed evidence of both uniform dispersion of the CNTs and a strong interfacial adhesion with the matrix. Liu et al. [115] successively prepared MWNTs/nylon-6 nanocomposite film samples by melt blending followed by the compression molding. Compared with neat polymer, the elastic modulus and the yield strength of the composite produced are greatly improved by about 214% and 162%, respectively, with incorporating only 2 wt % MWNTs. Uniform dispersion of MWNTs throughout the polymer matrix and a strong interfacial adhesion achieved by the functionalization of CNT surfaces are responsible for the remarkable enhancements in mechanical properties of the nanocomposites.

Achievements for thermal setting polymer matrix based CNT nanocomposites are presented during similar time period. Breton et al. [125] carried out the research about CVD-MWNT–epoxy composites. Significant increases in modulus from 2.75 GPa to 4.13 GPa were observed on addition of 6 wt% nanotubes corresponding. They attributed the large reinforcement values to residual oxygen containing groups that had covalently bonded to the nanotubes during purification. Bai et al. [124] observed a doubling of Young’s modulus from 1.2 to 2.4 GPa on addition of 1 wt% MWNT to an epoxy resin. In

addition, significant increases in strength from 30 to 41MPa were obtained. McClory et al. [104] prepared thermosetting polyurethane (PU) containing MWNTs. The Young's modulus of MWNT/PU resin increased by 561% from 6.4 to 42.34 MPa on the addition of 1 wt % MWNTs. The ultimate tensile strength and the percentage elongation at break also increased by about 397% and 272%, respectively, compared to the pure thermoset material. Beside the outstanding properties of MWNTs, these enhancements in mechanical properties can be attributed to the high dispersion of MWNTs throughout the polymer matrix and good interfacial interaction between materials, which could be both physical and chemical.

In an attempt to understand the reinforcement mechanism, Qian et al. [52] initiated crack formation inside a TEM, shown in Fig. 2.6(a). They observed the appearance of crazes where cracks were bridged by nanotubes. When the crazes reached widths of 800 nm, the nanotubes were seen to either fracture or pull out of the matrix. From the SEM images (Fig. 2.6(b)), Lau et al. [102] showed that the local deformations of the matrix adjacent to stiff nanotubes and deformed the surrounding matrix, thus enlarging the holes from where they came. These researches show that the CNTs aligned perpendicularly to a crack are able to slow down its propagation by bridging the crack faces. Thus, these materials may be used to improve the out-of-plane and interlaminar properties of advanced composite structures by increasing the matrix strength and linking up the individual laminar layers with these tiny, pin-like structures [228].

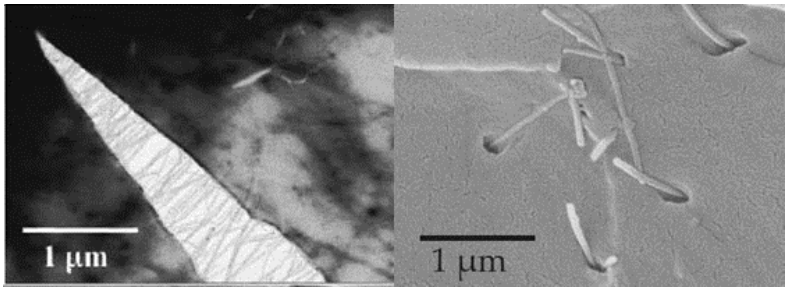

Figure 2.6: TEM (a) [52] and SEM (b) [102] proof of CNT/polymer nanocomposite reinforcement mechanism

2.3.2 Electrical Conductivity

The CNT can be metallic or semiconductive depending on the CNT structure [4, 11]. Conductive nanotube–polymer composites are regarded as promising materials for use in the areas such as lithium batteries, supercapacitors, polyactuators, [67] biosensors[69], flexible transparent electrodes[73], etc. [66, 68]. The electrical properties of CNT/polymer composite can be affected by filler concentration, filler morphology, different states of dispersion [71], nanotube orientation [45], and are much more sensitive to the nanotube–nanotube contacts made through their entanglements. [65] Ramasubramaniam et al. [47] reported that SWNT/polycarbonate (PC) composites with SWNT loading compositions >0.3 wt % and >3 wt % are sufficient for applications in electrostatic painting and electromagnetic interference (EMI) shielding, respectively, in these solution-blended composites. New transparent and electrically conductive coatings and films have a variety of fast-growing applications ranging from window glass to flat-panel displays [229].

The electrical percolation threshold is an important index for the CNT composite electrical property, which is the critical filler concentration when the electrical conductivity of the composite is reached to form conductive pathways. This property is

typically determined by plotting the electrical conductivity as a function of the reduced mass fraction of nanotubes and fitting with a power law function [47]. More than 200 publications have reported on the electrical percolation threshold of CNT in different polymer systems [71]. Higher aspect ratio [62, 64], better dispersion [230] but slight local aggregation [70] usually lead to a lower percolation threshold, while alignment of a nanotubes worsens the electrical conductivity and shifts the percolation threshold higher [167]. A comprehensive review for CNT composite electrical percolation threshold is available from Bauhofer and KovacsBohofer [63].

2.3.3 Thermal Properties

Excellent thermal conductivity of individual nanotubes led to early expectations that it will enhance the thermal conductivity of CNT polymer composite. Unlike electronic conductivity, even relatively more promising results that cited below are well below the prediction of the engineering rule of mixing

The thermal conductivity, κ, of carbon materials is dominated by atomic vibrations or phonons. The thermal conductivities of composites are controlled by filler concentration [231], filler conductivity, filler geometry [231], interface conductance between filler and polymer, and homogeneity of the filler dispersion [232].

Pradhan and Iannacchione [232] showed that higher thermal conductivity of CNT/polymer composites can be achieved by using suitable dispersion methods and higher quality nanofiller materials. Choi et al. [231] reported a 300% increase in thermal conductivity at room temperature with 3 wt % SWNT in epoxy, with an additional increase (10%) when aligned magnetically. Guthy et al. [233] found an enhancement of thermal conductivity of about 250% for SWNT/PMMA with 11% SWNTs. Cheng et al.

[234] showed that the ternary composites of Nylon-6 with conductive carbon black (CBB) and CNTs has higher electrical conductivity over the binary composites filled only with CCB or MWNT only, because it has better conductive network structure formed in the presence of two kinds of fillers with different geometry. This proposal provided an innovative idea to the potential researchers in the fabrication of other composite systems with improved properties.

The existence of CNTs is also able to delay the onset of thermal degradation of the polymer and increase the thermal stability. Diez-Pascual et al. [108] showed that the incorporation of SWNTs induced a remarkable increase of thermal stability in SWNTs/PEEK composites relative to the pure matrix polymers by using thermo gravimetric analysis (TGA). This thermal stabilization effect is mostly connected with the formation and stablilization of CNT-conded macroradicals [235] and nanotube's interfere with the mobility and crystallization of the polymer chains [236, 237], which enable the composite to be used for high temperature applications [238].

Using a cone calorimeter in air and a gasification device in a nitrogen atmosphere to measure the composite flammability, it is proved that CNTs are capable to reduce the mass loss rate of the composite of PMMA [239], ethylene-vinyl acetate [240] and PP [241]. The in-situ formation of a continuous, network structured protective layer from the tubes is critical for significant reduction in heat release rate, because the layer thus acts as a thermal shield from energy feedback from the flame. Kashiwagi et. al. [242] also compared the flame-retardant abilities of 0.5 wt % SWNT, MWNT, CNF, and carbon black particles in PMMA matrix. SWNT is the most effective flame retardant additive and the MWNT is the second most effective one.

2.3.4 Rheological Properties

The rheological properties of CNTs/polymer composites have both practical importance since they are related to composite processing and basic importance as a probe of the composite dynamics and microstructure. The general behavior reported in the literature for oscillatory shear rheological measurement at low progresses from a liquid-like response ($G' \propto \omega^{-2}$) to a solid-like response (G' independent of ω) as the nanotube concentration increases [243]. Applying a power law function to the G' vs CNT loading data provides a tool to estimate the percolation threshold, corresponding to the onset of solid-like behavior [116]. Du et al. [243] and Pötschke et al. [244] reported that the 'rheological' percolation is different to the 'electrical' percolation for PMMA/SWNT and PC/MWNT nanocomposites, respectively. Fundamentally, polymer chain immobility determines the rheological threshold, and the distance between neighboring nanotubes determines the electrical percolation threshold. The rheological percolation is a function of CNT dispersion, aspect ratio, and alignment. Different values of the percolation threshold can be found in the literature for several types of nanocomposites. Lower values as 0.12 wt% have been found in the case of CNT/PMMA systems [243]. Higher values as 7.5% have been reported in the case of CNT/PE systems [116]. In most cases, the percolation compositions are well below 3% [243-248].

Reported by several articles [111, 245, 249-251], CNT nanocomposites are highly shear thinning without the usual Newtonian plateau at low shear rates that is usually observed for the neat polymer. Huang et al. [111] studied the rheological properties of Nylon-11 nanocomposites with different loadings of MWNTs. Their results show that neat Nylon-11 and its composites containing less than 1 wt% MWNTs show similar

frequency dependence and reach a Newtonian plateau at low frequencies, while for the composite containing 2 wt% nanotubes exhibit an evident shear thinning effect. Kim et al. [251] found that the shear-thinning exponent of the PET/MWNT nanocomposites decreased with increasing MWNT content, indicating the significant dependence of the shear-thinning behavior of the polymer nanocomposites on the MWNT content. Bangarusampath et al. [252] estimated the elongational viscosity of PEEK/MWNTs composites by using a Göttfert Rheotens apparatus and Elongational Viscosity Fixture. The result provides information over a range of elongation rates, and showed that the enlongational viscosity of the composite also increases in viscosity at low rates and thinning at high rates.

Recently, the effects of the CNT aspect ratio [253] and the CNT dispersion [245, 254, 255] to the rheology properties have been evaluated. Cipriano et al. [253] found larger storage modulus and complex viscosities for the nanocomposites prepared with larger aspect ratio by comparing the rheological properties of MWNT/PS nanocomposites with different MWNT aspect ratio (L/D=49 and 150 MWNT were employed). Seyhan et al. [256] investigated the effect of functionalizing MWNT with amine groups in order to improve their dispersion within the matrix poly(vinyl ester)s. The nanocomposites prepared with 0.3% neat MWNT exhibited a viscous behavior ($G'' > G'$), however, the nanocomposite with functionalized MWNT of identical composition had amore viscoelastic behavior ($G'' \sim G'$).

2.4 Nanoclay/Polymer Composite Properties Enhancements

2.4.1 Mechanical properties

The Toyota group was the first to report significant improvements in the tensile

modulus of nanoclay reinforced composite. A 69% increase in tensile modulus from 1.11 GPa for pure Nylon-6 to 1.87 GPa for the composite was realized in a polyamide based composite containing 4.7wt% nanoclay using in-situ polymerization [257]. In the following reports, the tensile modulus of Nylon-6 based nanoclay composite was reported to be doubled by modest additions of clay <5 wt% [258]. This significant improvement in mechanical properties of polyamide-based nanocomposite was considered to have its origin in the existence of an exceptionally high interfacial surface area and the formation of ionic and/or hydrogen bonds between the organic polymer and inorganic silicate. [182, 259]

Reinforcement of nanoclay for non-polar polymer based composites has achieved only limited success. Kawasumi et al. [134] developed the method using the maleic anhydride modified PP-MA as a compatibelizaer to improve the exfoliation of nanoclay within the PP matrix. The excellent exfoliation of clay layers in the hybrids was confirmed by TEM and XRD results. Pascual et al. [260] showed that using the same technique, the overall effect of the addition of clay is a remarkable increase in elastic modulus up to 890 MPa with 2 wt% of nanclay relative to that of the unfilled material with an elastic modulus of about 220 MPa. The elongation at break changes from 440% for polypropylene without clay addition down to values around 12% for filled polypropylene. Nguyen et al. [261] used a novel technique without using PP-MA and increase the tensile modulus to 2.118 GPa relative to the pure PP modulus of 1.374 GPa at a nanoclay concentration of 6.6 wt%. In his work, comparisons of mechanical properties of composite prepared with different methods were provided, as shown in Fig. 2.7, his method provided the best improvement for the Young’s modulus of the nano-clay

composites out of all the processing methods. However, the modulus data for nanocomposite with nanoclay concentration higher than 6.6 wt% was not presented.

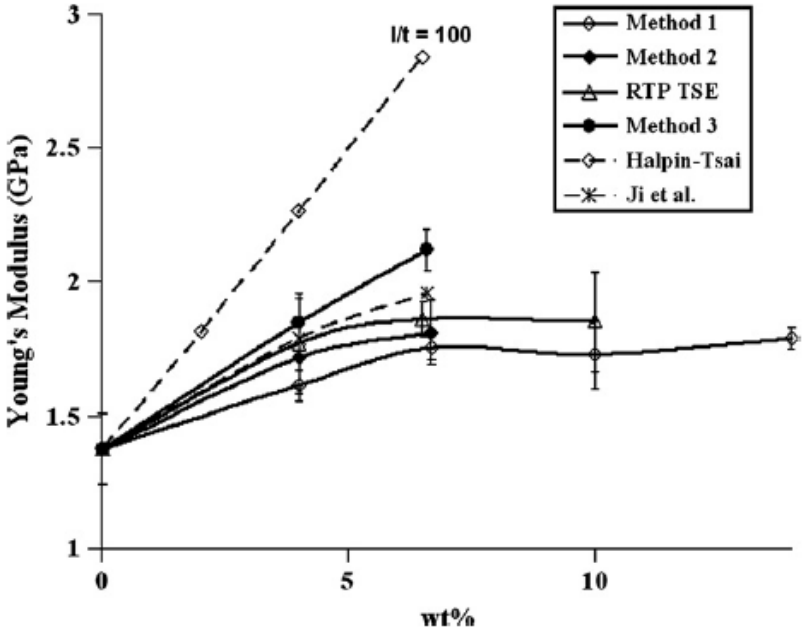

Figure 2.7: Young's modulus of different nanocomposites versus clay weight percent as a function of different processing techniques. (Method 1-- conventional melt blending method using a single screw; Method 2 -- conventional melt blending method with in-line CO_2 addition; Method 3 – $scCO_2$ aided melt blending method developed by Nguyen et al.. RTP TES -- commercial nano-clay composite prepared using a twin-screw extruder. Halpin-Tsai -- theoretical values predicted by Halpin-Tsai Model; Ji et al. model -- theoretical values predicted by Ji et al.Model.) [261]

The mobility and orientation of clay platelets should also be taken into account when interpreting mechanical property results. Weon and Sue [141] studied the mechanical properties of nylon-6/clay nanocomposites with various orientation and aspect ratio introduced by a large-scale simple shear process. The modulus and the tensile strength were found to decrease as the clay aspect ratio and degree of orientation were reduced. Galgali et al. [262] studied the effect of silicate orientation as well as polymer/clay compatibility on the tensile modulus of a polypropylene based nanoclay

composite. The orientation of clay was determined using TEM pictures. The results showed that samples containing compatiblizer had average silicate orientations that were dependent on the amount of shear they were exposed to during melt compounding. The tensile modulus of the compatiblized samples correlated very well with the average silicate orientation resulting in large modulus improvements. The uncompatiblized samples had average silicate orientations that were independent of the amount of shear they were exposed to during melt compounding. As a result, no improvement in the tensile modulus of the uncompatiblized samples with increasing shear exposure was found.

2.4.2 Heat Distortion Temperature

The heat distortion temperature (HDT) of the Nylon-6/clay composite was 87 °C higher than that of neat nylon 6 [182]. Ke et al. [37] found that the addition of 5 wt% layered silicate to PET matrix caused a 40 °C increase in the HDT. This dramatic increase in the HDT is attributed to the confinement of polymer chains between silicate layers. The extreme confinement of the polymer chains decreases their ability to move freely.

2.4.3 Flame Retardancy

Enhanced flame retardancy is found for naonoclay/polymer composites. Pramoda et al. [263] used nylone-6 to examine the thermal degradation behavior of nanoclay based composite. The results showed thermal degradation temperature was 12^{o}C higher for the composite containing 2.5wt% silicate than the neat nylon-6. Bourbigot et al. [264] showed that the heat release rate of nylon 6-made fabric was reduced by 40% with addition of 5 wt% organoclay. This is associated with char formation resulting from ceramic clay platelets and the barrier effect of clay platelets to the diffusion of the volatile

products formed by thermal degradation [258]. However it should be noted that presence of organic clay modifier could catalyze thermal degradation which somewhat compensates for these two effects [265].

2.4.4 Barrier Properties

Barrier properties are found to be significantly improved for nanoclay composite [148, 266]. Adding high aspect ratio particles to a polymer matrix will increases the tortuosity of a membrane formed from that polymer material. Yano et al. [267] showed that the permeation coefficient of water vapor of polyimides used for microelectronics was reduced by 54% with only 2 wt% montmorillonite, retaining the optical clarity of the unfilled polymer.

The barrier properties are closely related to the morphology of the nanoclay within the polymer matrix. Nazarenko et al. [268] found the oxygen permeability of intercalated PS/clay nanocomposites is lower than intercalated-exfoliated nanocomposites, which was attributed to layer aggregation effects. Ray et al. [10] found that at a silicate loading of 3.6wt% there is a steep drop in the oxygen permeability, which they claimed to be attributing to the formation of a flocculated structure.

2.5 Theoretical Modeling of Nanopartical nanocomposite Tensile Modulus

A large amount of theoretical works has been carried out with the aim of modeling the mechanical properties of nanopartical reinforced composites [258, 269, 270]. The theoretical modeling is one good way to test our understanding of the reinforcement mechanism of the nanocomposite system. The simple rule of mixing is not successful in predicting modulus values of CNT and nanoclay reinforced systems because a number of important factors are ignored. The Halpin-Tsai model [271]

developed from composite theory [272] are the result of the addition of mathematics to simple volume additivity and the effects of particle aspect ratio on composite modulus. For aligned fiber composites, the Halpin–Tsai model gives the composite modulus to be

$$E_c = E_m \left[\frac{1+\xi\eta\phi_f}{1-\eta\phi_f}\right] \qquad (1)$$

where $\xi = 2l/D$ and

$$\eta = \frac{[E_f/E_m - 1]}{[E_f/E_m + \xi]} \qquad (2)$$

E_f, E_m and E_c are the filler modulus, matrix modulus and composite modulus, respectively. ϕ_f is the filler volume fraction and l/D is the aspect ratio of the filler particles.

For randomly orientated composites the changed to:

$$\frac{E_c}{E_m} = \frac{3}{8}\left[\frac{1+\xi\eta_L\phi_f}{1-\eta_L\phi_f}\right] + \left[\frac{1+2\eta_T\phi_f}{1-\eta_T\phi_f}\right] \qquad (3)$$

where

$$\eta_L = \frac{[E_f/E_m - 1]}{[E_f/E_m + \xi]} \qquad (4)$$

and

$$\eta_T = \frac{[E_f/E_m - 1]}{[E_f/E_m + 2]} \qquad (5)$$

2.5.1 Halpin-Tsai Model in Nanoclay Composites

The Halpin-Tsai Model has been widely used for nanoclay composites [226, 273-275]. The assumptions of complete exfoliation and full alignment of silicate layers results in relatively accurate predictions of the modulus.

Under these assumptions, the modulus of the nanoclay composite can be estimated using equation (1) and (2). The aspect ratio of the filler particles is taken to be approximately 100 for nanoclay. The filler modulus is taken to be 172 GPa [276].

The simplicity of the model has led to its widespread use in the literature [258] as a way to draw conclusions about the state of silicate morphology and orientation in the nanoclay/polymer composites [277]. The assumptions made in the Halpin-Tsai model mean that the modulus values calculated from these equations are expected to be greater than the values obtained from any sample with partial exfoliation or incomplete alignment of silicate particles.

2.5.2 Halpin-Tsai Model in CNT Composites

In Halpin-Tsai Model, if the fiber length is much smaller than the thickness of the specimen, the fibers can be assumed randomly oriented in three dimensions [278]. Equation (3), (4) and (5) are appropriate for the calculation of CNT composite in randomly orientated cases. The density of MWNTs is taken as rods with an average density of 1.65 g/ml from the density of graphite by assuming that the outer diameter of the nanotubes was twice the inner [279]. The Young's modulus of MWNT is taken as 953 GPa, which is on the upper bound of the experimental results obtained by Yu et al. [2].

The Halpin–Tsai equation is known to fit some data very well at low volume fractions [129] and has been widely used in different polymer systems [52, 103, 280, 281]. Using this model, it is also possible to estimate the effective Young's modulus of MWNT from the reverse of Eq. (3) [282].

2.6 References

[1] S. Iijima, Nature, 354 (1991) 56-58.
[2] S. Iijima, T. Ichihashi, Nature, 363 (1993) 603-605.
[3] R. Bacon, J Appl Phys, 31 (1960) 8.
[4] M.J. O'Connell, Carbon nanotubes : properties and applications CRC Taylor & Francis, Boca Raton, 2006.
[5] P. Chen, H.S. Kim, H.J. Jin, Macromol. Res., 17 (2009) 207-217.
[6] H.W. Kroto, A.W. Allaf, S.P. Balm, Chem. Rev., 91 (1991) 1213-1235.
[7] D.S. Bethune, C.H. Kiang, M.S. Devries, G. Gorman, R. Savoy, J. Vazquez, R. Beyers, Nature, 363 (1993) 605-607.
[8] C. Journet, W.K. Maser, P. Bernier, A. Loiseau, M.L. delaChapelle, S. Lefrant, P. Deniard, R. Lee, J.E. Fischer, Nature, 388 (1997) 756-758.
[9] T. Guo, P. Nikolaev, A. Thess, D.T. Colbert, R.E. Smalley, Chem. Phys. Lett., 243 (1995) 49-54.
[10] A. Thess, R. Lee, P. Nikolaev, H.J. Dai, P. Petit, J. Robert, C.H. Xu, Y.H. Lee, S.G. Kim, A.G. Rinzler, D.T. Colbert, G.E. Scuseria, D. Tomanek, J.E. Fischer, R.E. Smalley, Science, 273 (1996) 483-487.
[11] P.J.F. Harris, Carbon nanotube science : synthesis, properties and applications Cambridge University Press, Cambridge, UK ; New York 2009.
[12] M. Meyyappan, Carbon nanotubes : science and applications CRC Press, Boca Raton, FL 2005.
[13] M. Endo, K. Takeuchi, S. Igarashi, K. Kobori, M. Shiraishi, H.W. Kroto, J Phys Chem Solids, 54 (1993) 1841-1848.
[14] H.J. Dal, A.G. Rinzler, P. Nikolaev, A. Thess, D.T. Colbert, R.E. Smalley, Chem Phys Lett, 260 (1996) 471-475.
[15] Z.F. Ren, Z.P. Huang, J.W. Xu, J.H. Wang, P. Bush, M.P. Siegal, P.N. Provencio, Science, 282 (1998) 1105-1107.
[16] J.P. Lu, Phys Rev Lett, 79 (1997) 1297-1300.
[17] S. Govindjee, J.L. Sackman, Solid State Commun, 110 (1999) 227-230.
[18] X. Zhou, J.J. Zhou, Z.C. Ou-Yang, Phys Rev B, 62 (2000) 13692-13696.
[19] A. Sears, R.C. Batra, Phys Rev B, 69 (2004) -.
[20] K.M. Liew, X.Q. He, C.H. Wong, Acta Mater, 52 (2004) 2521-2527.
[21] M.M.J. Treacy, T.W. Ebbesen, J.M. Gibson, Nature, 381 (1996) 678-680.
[22] E.W. Wong, P.E. Sheehan, C.M. Lieber, Science, 277 (1997) 1971-1975.
[23] J.P. Salvetat, J.M. Bonard, N.H. Thomson, A.J. Kulik, L. Forro, W. Benoit, L. Zuppiroli, Appl Phys a-Mater, 69 (1999) 255-260.
[24] O. Lourie, H.D. Wagner, J Mater Res, 13 (1998) 2418-2422.
[25] J.W. Mintmire, B.I. Dunlap, C.T. White, Phys Rev Lett, 68 (1992) 631-634.
[26] M.S. Dresselhaus, G. Dresselhaus, R. Saito, Carbon, 33 (1995) 883-891.
[27] M.S. Dresselhaus, G. Dresselhaus, P.C. Eklund, Science of Fullernes and Carbon Nanotubes, Academic Press, San Diego, 1996.
[28] L. Langer, V. Bayot, E. Grivei, J.P. Issi, J.P. Heremans, C.H. Olk, L. Stockman, C. VanHaesendonck, Y. Bruynseraede, Phys Rev Lett, 76 (1996) 479-482.
[29] A.M. Rao, J. Chen, E. Richter, U. Schlecht, P.C. Eklund, R.C. Haddon, U.D. Venkateswaran, Y.K. Kwon, D. Tomanek, Phys Rev Lett, 86 (2001) 3895-3898.
[30] S. Berber, Y.K. Kwon, D. Tomanek, Phys Rev Lett, 84 (2000) 4613-4616.
[31] J.R. Lukes, H.L. Zhong, J Heat Trans-T Asme, 129 (2007) 705-716.
[32] J. Hone, M. Whitney, A. Zettl, Synthetic Met, 103 (1999) 2498-2499.

[33] P. Kim, L. Shi, A. Majumdar, P.L. McEuen, Phys Rev Lett, 8721 (2001) -.
[34] Q.W. Li, C.H. Liu, X.S. Wang, S.S. Fan, Nanotechnology, 20 (2009) -.
[35] H.J. Dai, J.H. Hafner, A.G. Rinzler, D.T. Colbert, R.E. Smalley, Nature, 384 (1996) 147-150.
[36] J.H. Hafner, C.L. Cheung, C.M. Lieber, Nature, 398 (1999) 761-762.
[37] S. Carnally, K. Barrow, M.R. Alexander, C.J. Hayes, S. Stolnik, S.J.B. Tendler, P.M. Williams, C.J. Roberts, Langmuir, 23 (2007) 3906-3911.
[38] C.V. Nguyen, Q. Ye, M. Meyyappan, Meas Sci Technol, 16 (2005) 2138-2146.
[39] H.E. Romero, K. Bolton, A. Rosen, P.C. Eklund, Science, 307 (2005) 89-93.
[40] B. Bourlon, J. Wong, C. Miko, L. Forro, M. Bockrath, Nat Nanotechnol, 2 (2007) 104-107.
[41] H. Cai, X.N. Cao, Y. Jiang, P.G. He, Y.Z. Fang, Anal Bioanal Chem, 375 (2003) 287-293.
[42] A. Arvinte, F. Valentini, A. Radoi, F. Arduini, E. Tamburri, L. Rotariu, G. Palleschi, C. Bala, Electroanal, 19 (2007) 1455-1459.
[43] J.J. Gooding, R. Wibowo, J.Q. Liu, W.R. Yang, D. Losic, S. Orbons, F.J. Mearns, J.G. Shapter, D.B. Hibbert, J Am Chem Soc, 125 (2003) 9006-9007.
[44] G.L. Luque, N.F. Ferreyra, G.A. Rivas, Microchim Acta, 152 (2006) 277-283.
[45] L. Bokobza, Polymer, 48 (2007) 4907-4920.
[46] M.T. Byrne, Y.K. Gun'ko, Advanced Materials, 22 (2010) 1672-1688.
[47] R. Ramasubramaniam, J. Chen, H.Y. Liu, Appl. Phys. Lett., 83 (2003) 2928-2930.
[48] P.R. Thakre, Y. Bisrat, D.C. Lagoudas, Journal of Applied Polymer Science, 116 (2010) 191-202.
[49] D.Y. Zhao, S.H. Wang, J. Wu, X.D. Bai, Q.Q. Lei, Pigm. Resin. Technol., 38 (2009) 305-309.
[50] A. Dufresne, M. Paillet, J.L. Putaux, R. Canet, F. Carmona, P. Delhaes, S. Cui, J Mater Sci, 37 (2002) 3915-3923.
[51] J. Liu, A. Rasheed, M.L. Minus, S. Kumar, Journal of Applied Polymer Science, 112 (2009) 142-156.
[52] D. Qian, E.C. Dickey, R. Andrews, T. Rantell, Appl. Phys. Lett., 76 (2000) 2868-2870.
[53] J.F. Vega, J. Martinez-Salazar, M. Trujillo, M.L. Arnal, A.J. Muller, S. Bredeau, P. Dubois, Macromolecules, 42 (2009) 4719-4727.
[54] C.G. Hu, Z.L. Chen, A.G. Shen, X.C. Shen, H. Li, S.S. Hu, Carbon, 44 (2006) 428-434.
[55] M.S.P. Shaffer, A.H. Windle, Advanced Materials, 11 (1999) 937-941.
[56] P.R. Sundararajan, S. Singh, M. Moniruzzaman, Macromolecules, 37 (2004) 10208-10211.
[57] M. Moniruzzaman, K.I. Winey, Macromolecules, 39 (2006) 5194-5205.
[58] J.N. Coleman, U. Khan, Y.K. Gun'ko, Advanced Materials, 18 (2006) 689-706.
[59] Z. Burghard, D. Schon, J. Bill, F. Aldinger, Int J Mater Res, 97 (2006) 1667-1672.
[60] C.F. Deng, D.Z. Wang, X.X. Zhang, A.B. Li, Mat Sci Eng a-Struct, 444 (2007) 138-145.
[61] T. Kuzumaki, K. Miyazawa, H. Ichinose, K. Ito, J Mater Res, 13 (1998) 2445-2449.
[62] J.B. Bai, A. Allaoui, Compos. Pt. A-Appl. Sci. Manuf., 34 (2003) 689-694.
[63] W. Bauhofer, J.Z. Kovacs, Compos. Sci. Technol., 69 (2009) 1486-1498.
[64] M.B. Bryning, M.F. Islam, J.M. Kikkawa, A.G. Yodh, Advanced Materials, 17 (2005) 1186-+.
[65] L.M. Dai, Aust J Chem, 54 (2001) 11-13.
[66] G. Hansen, J. Adv. Mater., 38 (2006) 68-74.
[67] C. Kim, X.Y. Liu, Int. J. Mod. Phys. B, 20 (2006) 3727-3732.
[68] K.T. Lau, H.Y. Cheung, J. Lu, Y.S. Yin, D. Hui, H.L. Li, J Comput Theor Nanos, 5 (2008) 23-35.
[69] Y.F. Ma, S.R. Ali, A.S. Dodoo, H.X. He, J Phys Chem B, 110 (2006) 16359-16365.
[70] C.A. Martin, J.K.W. Sandler, M.S.P. Shaffer, M.K. Schwarz, W. Bauhofer, K. Schulte, A.H. Windle, Compos. Sci. Technol., 64 (2004) 2309-2316.

[71] K. Masenelli-Varlot, L. Chazeau, C. Gauthier, A. Bogner, J.Y. Cavaille, Compos. Sci. Technol., 69 (2009) 1533-1539.
[72] O. Meincke, D. Kaempfer, H. Weickmann, C. Friedrich, M. Vathauer, H. Warth, Polymer, 45 (2004) 739-748.
[73] J.H. Zou, H. Chen, A. Chunder, Y.X. Yu, Q. Huo, L. Zhai, Advanced Materials, 20 (2008) 3337-+.
[74] P.M. Ajayan, L.S. Schadler, C. Giannaris, A. Rubio, Advanced Materials, 12 (2000) 750-753.
[75] P.M. Ajayan, O. Stephan, C. Colliex, D. Trauth, Science, 265 (1994) 1212-1214.
[76] S. Bal, Bull. Mat. Sci., 33 (2010) 27-31.
[77] D. Kastanis, D. Tasis, K. Papagelis, J. Parthertios, C. Tsakiroglou, C. Galiotis, Adv. Compos. Lett., 16 (2007) 243-248.
[78] L.Q. Liu, H.D. Wagner, Compos. Interfaces, 14 (2007) 285-297.
[79] L.S. Schadler, S.C. Giannaris, P.M. Ajayan, Appl. Phys. Lett., 73 (1998) 3842-3844.
[80] Z. Spitalsky, G. Tsoukleri, D. Tasis, C. Krontiras, S.N. Georga, C. Galiotis, Nanotechnology, 20 (2009).
[81] S. Badaire, P. Poulin, M. Maugey, C. Zakri, Langmuir, 20 (2004) 10367-10370.
[82] D. Baskaran, J.W. Mays, M.S. Bratcher, Angew. Chem.-Int. Edit., 43 (2004) 2138-2142.
[83] K.F. Fu, W.J. Huang, Y. Lin, L.A. Riddle, D.L. Carroll, Y.P. Sun, Nano Lett., 1 (2001) 439-441.
[84] J.B. Gao, M.E. Itkis, A.P. Yu, E. Bekyarova, B. Zhao, R.C. Haddon, J. Am. Chem. Soc., 127 (2005) 3847-3854.
[85] Z.J. Jia, Z.Y. Wang, C.L. Xu, J. Liang, B.Q. Wei, D.H. Wu, S.W. Zhu, Mater. Sci. Eng. A-Struct. Mater. Prop. Microstruct. Process., 271 (1999) 395-400.
[86] H. Kong, C. Gao, D.Y. Yan, J. Am. Chem. Soc., 126 (2004) 412-413.
[87] A.A. Koval'chuk, A.N. Shchegolikhin, V.G. Shevchenko, P.M. Nedorezova, A.N. Klyamkina, A.M. Aladyshev, Macromolecules, 41 (2008) 3149-3156.
[88] S. Kumar, T. Rath, B.B. Khatua, A.K. Dhibar, C.K. Das, J. Nanosci. Nanotechnol., 9 (2009) 4644-4655.
[89] E. Lafuente, M. Pinol, M.T. Martinez, E. Munoz, L. Oriol, J.L. Serrano, J. Polym. Sci. Pol. Chem., 47 (2009) 2361-2372.
[90] S.D. Lee, O.J. Kwon, B.C. Chun, J.W. Cho, J.S. Park, Fiber. Polym., 10 (2009) 71-76.
[91] M.H. Liu, T. Zhu, Z.C. Li, Z.F. Liu, J. Phys. Chem. C, 113 (2009) 9670-9675.
[92] S.H. Qin, D.Q. Oin, W.T. Ford, D.E. Resasco, J.E. Herrera, J. Am. Chem. Soc., 126 (2004) 170-176.
[93] K. Saeed, S.Y. Park, Journal of Applied Polymer Science, 106 (2007) 3729-3735.
[94] Y. Takahashi, H. Awano, O. Haba, T. Takahashi, K. Yonetake, Kobunshi Ronbunshu, 65 (2008) 679-687.
[95] D. Tasis, N. Tagmatarchis, A. Bianco, M. Prato, Chem. Rev., 106 (2006) 1105-1136.
[96] B. Vigolo, B. Vincent, J. Eschbach, P. Bourson, J.F. Mareche, E. McRae, A. Muller, A. Soldatov, J.M. Hiver, A. Dahoun, D. Rouxel, J. Phys. Chem. C, 113 (2009) 17648-17654.
[97] G. Viswanathan, N. Chakrapani, H.C. Yang, B.Q. Wei, H.S. Chung, K.W. Cho, C.Y. Ryu, P.M. Ajayan, J. Am. Chem. Soc., 125 (2003) 9258-9259.
[98] K.-L. Wu, S.-C. Chou, Y.-Y. Cheng, Journal of Applied Polymer Science, 116 (2010) 3111-3117.
[99] Z.L. Yao, N. Braidy, G.A. Botton, A. Adronov, J. Am. Chem. Soc., 125 (2003) 16015-16024.
[100] M. Abdalla, D. Dean, P. Robinson, E. Nyairo, Polymer, 49 (2008) 3310-3317.
[101] A. Eitan, F.T. Fisher, R. Andrews, L.C. Brinson, L.S. Schadler, Compos. Sci. Technol., 66 (2006) 1162-1173.
[102] K.-T. Lau, D. Hui, Carbon, 40 (2002) 1605-1606.

[103] X.D. Li, H.S. Gao, W.A. Scrivens, D.L. Fei, X.Y. Xu, M.A. Sutton, A.P. Reynolds, M.L. Myrick, J. Nanosci. Nanotechnol., 7 (2007) 2309-2317.
[104] C. McClory, T. McNally, G.P. Brennan, J. Erskine, J Appl Polym Sci, 105 (2007) 1003-1011.
[105] R. Andrews, D. Jacques, M. Minot, T. Rantell, Macromol. Mater. Eng., 287 (2002) 395-403.
[106] A.R. Bhattacharyya, T.V. Sreekumar, T. Liu, S. Kumar, L.M. Ericson, R.H. Hauge, R.E. Smalley, Polymer, 44 (2003) 2373-2377.
[107] W. De Zhang, L. Shen, I.Y. Phang, T.X. Liu, Macromolecules, 37 (2004) 256-259.
[108] A.M. Diez-Pascual, M. Naffakh, M.A. Gomez, C. Marco, G. Ellis, M.T. Martinez, A. Anson, J.M. Gonzalez-Dominguez, Y. Martinez-Rubi, B. Simard, Carbon, 47 (2009) 3079-3090.
[109] L.F. Giraldo, B.L. Lopez, W. Brostow, Polym. Eng. Sci., 49 (2009) 896-902.
[110] R.E. Gorga, R.E. Cohen, J Polym Sci Pol Phys, 42 (2004) 2690-2702.
[111] S. Huang, M. Wang, T.X. Liu, W.D. Zhang, W.C. Tjiu, C.B. He, X.H. Lu, Polym Eng Sci, 49 (2009) 1063-1068.
[112] Z. Jin, K.P. Pramoda, G. Xu, S.H. Goh, Chem. Phys. Lett., 337 (2001) 43-47.
[113] Z.X. Jin, K.P. Pramoda, S.H. Goh, G.Q. Xu, Mater Res Bull, 37 (2002) 271-278.
[114] J.Y. Kim, Journal of Applied Polymer Science, 112 (2009) 2589-2600.
[115] T.X. Liu, I.Y. Phang, L. Shen, S.Y. Chow, W.D. Zhang, Macromolecules, 37 (2004) 7214-7222.
[116] T. McNally, P. Potschke, P. Halley, M. Murphy, D. Martin, S.E.J. Bell, G.P. Brennan, D. Bein, P. Lemoine, J.P. Quinn, Polymer, 46 (2005) 8222-8232.
[117] Y.Z. Pan, L. Li, S.H. Chan, J.H. Zhao, Compos. Pt. A-Appl. Sci. Manuf., 41 (2010) 419-426.
[118] P. Potschke, A.R. Bhattacharyya, A. Janke, H. Goering, Compos. Interfaces, 10 (2003) 389-404.
[119] S. Pujari, T. Ramanathan, K. Kasimatis, J. Masuda, R. Andrews, J.M. Torkelson, L.C. Brinson, W.R. Burghardt, J. Polym. Sci. Pt. B-Polym. Phys., 47 (2009) 1426-1436.
[120] E.J. Siochi, D.C. Working, C. Park, P.T. Lillehei, J.H. Rouse, C.C. Topping, A.R. Bhattacharyya, S. Kumar, Compos. Pt. B-Eng., 35 (2004) 439-446.
[121] E.T. Thostenson, T.W. Chou, J Phys D Appl Phys, 35 (2002) L77-L80.
[122] X.L. Xie, Y.W. Mai, X.P. Zhou, Mater. Sci. Eng. R-Rep., 49 (2005) 89-112.
[123] J.M. Yuan, Z.F. Fan, X.H. Chen, Z.J. Wu, L.P. He, Polymer, 50 (2009) 3285-3291.
[124] J. Bai, Carbon, 41 (2003) 1325-1328.
[125] Y. Breton, G. Desarmot, J.P. Salvetat, S. Delpeux, C. Sinturel, F. Beguin, S. Bonnamy, Carbon, 42 (2004) 1027-1030.
[126] P.H.C. Camargo, K.G. Satyanarayana, F. Wypych, Mater. Res.-Ibero-am. J. Mater., 12 (2009) 1-39.
[127] X.D. Cao, H. Dong, C.M. Li, L.A. Lucia, Journal of Applied Polymer Science, 113 (2009) 466-472.
[128] H. Cebeci, R.G. de Villoria, A.J. Hart, B.L. Wardle, Compos. Sci. Technol., 69 (2009) 2649-2656.
[129] J.N. Coleman, U. Khan, W.J. Blau, Y.K. Gun'ko, Carbon, 44 (2006) 1624-1652.
[130] A.B. Dalton, S. Collins, E. Munoz, J.M. Razal, V.H. Ebron, J.P. Ferraris, J.N. Coleman, B.G. Kim, R.H. Baughman, Nature, 423 (2003) 703-703.
[131] A. Dasari, Z.Z. Yu, Y.W. Mai, Polymer, 50 (2009) 4112-4121.
[132] A.M.K. Esawi, H.G. Salem, H.M. Hussein, A.R. Ramadan, Polymer Composites, 31 (2010) 772-780.
[133] Q.M. Gong, Z. Li, X.D. Bai, D. Li, Y. Zhao, J. Liang, Mater. Sci. Eng. A-Struct. Mater. Prop. Microstruct. Process., 384 (2004) 209-214.

[134] M. Kawasumi, N. Hasegawa, M. Kato, A. Usuki, A. Okada, Macromolecules, 30 (1997) 6333-6338.
[135] X.D. Li, H.S. Gao, W.A. Scrivens, D.L. Fei, X.Y. Xu, M.A. Sutton, A.P. Reynolds, M.L. Myrick, Nanotechnology, 15 (2004) 1416-1423.
[136] D. Mari, R. Schaller, Mater. Sci. Eng. A-Struct. Mater. Prop. Microstruct. Process., 521-22 (2009) 255-258.
[137] A.L. Martinez-Hernandez, C. Velasco-Santos, V.M. Castano, Curr. Nanosci., 6 (2010) 12-39.
[138] H.S. Peng, X.M. Sun, Chem. Phys. Lett., 471 (2009) 103-105.
[139] B. Safadi, R. Andrews, E.A. Grulke, Journal of Applied Polymer Science, 84 (2002) 2660-2669.
[140] Z. Spitalsky, D. Tasis, K. Papagelis, C. Galiotis, Prog. Polym. Sci., 35 (2010) 357-401.
[141] J.I. Weon, H.J. Sue, Polymer, 46 (2005) 6325-6334.
[142] J. Lusis, R.T. Woodhams, M. Xanthos, Polymer Engineering & Science, 13 (1973) 139-145.
[143] M. Zanetti, S. Lomakin, G. Camino, Macromol Mater Eng, 279 (2000) 1-9.
[144] T. Pinnavaia, G. Beall, Polymer-Clay Nanocomposites, John Wiley & Sons, Ltd., New York, 2000.
[145] B. Yalcin, M. Cakmak, Polymer, 45 (2004) 2691-2710.
[146] S.S. Ray, M. Okamoto, Prog. Polym. Sci., 28 (2003) 1539-1641.
[147] H.Z. Shi, T. Lan, T.J. Pinnavaia, Chemistry of Materials, 8 (1996) 1584-&.
[148] P.B. Messersmith, E.P. Giannelis, J. Polym. Sci. Pol. Chem., 33 (1995) 1047-1057.
[149] P. Aranda, E. Ruizhitzky, Chemistry of Materials, 4 (1992) 1395-1403.
[150] E.P. Giannelis, Advanced Materials, 8 (1996) 29-&.
[151] A. Blumstein, Journal of Polymer Science Part A: General Papers, 3 (1965) 2665-2672.
[152] R. Krishnamoorti, R.A. Vaia, E.P. Giannelis, Chemistry of Materials, 8 (1996) 1728-1734.
[153] S.C. Products, in, 2006.
[154] B.K.G. Theng, Formation and properties of clay–polymer complexes, Elsevier, Amsterdam, 1979.
[155] J.R. Samaniuk, in: Chemical Engineering, Virginia Tech, Blacksburg, 2008.
[156] G.D. Barber, B.H. Calhoun, R.B. Moore, Polymer, 46 (2005) 6706-6714.
[157] K. Masenelli-Varlot, E. Reynaud, G. Vigier, J. Varlet, J. Polym. Sci. Pt. B-Polym. Phys., 40 (2002) 272-283.
[158] W.J. Boo, L.Y. Sun, J. Liu, E. Moghbelli, A. Clearfield, H.J. Sue, H. Pham, N. Verghese, J. Polym. Sci. Pt. B-Polym. Phys., 45 (2007) 1459-1469.
[159] W.J. Bae, K.H. Kim, W.H. Jo, Y.H. Park, Macromolecules, 37 (2004) 9850-9854.
[160] N. Sheng, M.C. Boyce, D.M. Parks, G.C. Rutledge, J.I. Abes, R.E. Cohen, Polymer, 45 (2004) 487-506.
[161] S.S. Ray, K. Okamoto, M. Okamoto, Macromolecules, 36 (2003) 2355-2367.
[162] D.F. Wu, C.X. Zhou, W. Yu, X. Fan, J. Polym. Sci. Pt. B-Polym. Phys., 43 (2005) 2807-2818.
[163] R. Krishnamoorti, J. Ren, A.S. Silva, J. Chem. Phys., 114 (2001) 4968-4973.
[164] J.W. Yang, J.H. Hu, C.C. Wang, Y.J. Qin, Z.X. Guo, Macromol. Mater. Eng., 289 (2004) 828-832.
[165] L. Jin, C. Bower, O. Zhou, Appl Phys Lett, 73 (1998) 1197-1199.
[166] M.J. O'Connell, S.M. Bachilo, C.B. Huffman, V.C. Moore, M.S. Strano, E.H. Haroz, K.L. Rialon, P.J. Boul, W.H. Noon, C. Kittrell, J. Ma, R.H. Hauge, R.B. Weisman, R.E. Smalley, Science, 297 (2002) 593-596.
[167] F.M. Du, J.E. Fischer, K.I. Winey, J. Polym. Sci. Pt. B-Polym. Phys., 41 (2003) 3333-3338.
[168] H.G. Jeon, H.T. Jung, S.W. Lee, S.D. Hudson, Polym Bull, 41 (1998) 107-113.

[169] C.R. Tseng, J.Y. Wu, H.Y. Lee, F.C. Chang, Polymer, 42 (2001) 10063-10070.
[170] M. Avella, S. Cosco, G.D. Volpe, M.E. Errico, Advances in Polymer Technology, 24 (2005) 132-144.
[171] J. Chen, M.A. Hamon, H. Hu, Y.S. Chen, A.M. Rao, P.C. Eklund, R.C. Haddon, Science, 282 (1998) 95-98.
[172] H.L. Zeng, C. Gao, D.Y. Yan, Adv. Funct. Mater., 16 (2006) 812-818.
[173] C.A. Dyke, J.M. Tour, J. Phys. Chem. A, 108 (2004) 11151-11159.
[174] Y.P. Sun, W.J. Huang, Y. Lin, K.F. Fu, A. Kitaygorodskiy, L.A. Riddle, Y.J. Yu, D.L. Carroll, Chemistry of Materials, 13 (2001) 2864-2869.
[175] M. Lebron-Colon, M.A. Meador, J.R. Gaier, F. Sola, D.A. Scheiman, L.S. McCorkle, Acs Appl Mater Inter, 2 (2010) 669-676.
[176] R.J. Chen, Y.G. Zhang, D.W. Wang, H.J. Dai, J. Am. Chem. Soc., 123 (2001) 3838-3839.
[177] P. Lauffer, A. Jung, R. Graupner, A. Hirsch, L. Ley, Phys Status Solidi B, 243 (2006) 3213-3216.
[178] N. Nakayama-Ratchford, S. Bangsaruntip, X.M. Sun, K. Welsher, H.J. Dai, J. Am. Chem. Soc., 129 (2007) 2448-+.
[179] T. Lemek, J. Mazurkiewicz, L. Stobinski, H.M. Lin, P. Tomasik, J. Nanosci. Nanotechnol., 7 (2007) 3081-3088.
[180] Z. Yang, X.H. Chen, Y.X. Pu, L.P. Zhou, C.S. Chen, W.H. Li, L.S. Xu, B. Yi, Y.G. Wang, Polym. Adv. Technol., 18 (2007) 458-462.
[181] Y. Kojima, A. Usuki, M. Kawasumi, A. Okada, T. Kurauchi, O. Kamigaito, J. Polym. Sci. Pol. Chem., 31 (1993) 983-986.
[182] A. Usuki, M. Kawasumi, Y. Kojima, A. Okada, T. Kurauchi, Kobunshi Ronbunshu, 52 (1995) 440-444.
[183] A. Usuki, Y. Kojima, M. Kawasumi, A. Okada, Y. Fukushima, T. Kurauchi, O. Kamigaito, J Mater Res, 8 (1993) 1179-1184.
[184] A. Usuki, Y. Kojima, M. Kawasumi, A. Okada, Y. Fukushima, T. Kurauchi, O. Kamigaito, J. Mater. Res., 8 (1993) 1179-1184.
[185] S. Abbasi, P.J. Carreau, A. Derdouri, Polymer, 51 (2010) 922-935.
[186] T. Lan, T.J. Pinnavaia, Chem. Mater., 6 (1994) 2216-2219.
[187] R.A. Vaia, H. Ishii, E.P. Giannelis, Chem. Mater., 5 (1993) 1694-1696.
[188] R.A. Vaia, K.D. Jandt, E.J. Kramer, E.P. Giannelis, Macromolecules, 28 (1995) 8080-8085.
[189] J.W. Cho, D.R. Paul, Polym. J., 42 (2001) 1083-1094.
[190] T.D. Fornes, P.J. Yoon, H. Keskkula, D.R. Paul, Polym. J., 42 (2001) 9929-9940.
[191] K. Nevalainen, J. Vuorinen, V. Villman, R. Suihkonen, P. Jarvela, J. Sundelin, T. Lepisto, Polym. Eng. Sci., 49 (2009) 631-640.
[192] E.C. Lee, D.F. Mielewski, R.J. Baird, Polym. Eng. Sci., 44 (2004) 1773-1782.
[193] Q. Zhang, Q. Fu, L.X. Jiang, Y. Lei, Polym Int, 49 (2000) 1561-1564.
[194] A. Usuki, A. Tukigase, M. Kato, Polymer, 43 (2002) 2185-2189.
[195] F. Ko, Y. Gogotsi, A. Ali, N. Naguib, H.H. Ye, G.L. Yang, C. Li, P. Willis, Advanced Materials, 15 (2003) 1161-+.
[196] F. Gao, S. Chen, J.B. Hull, J. Mater. Sci. Lett., 20 (2001) 1807-1810.
[197] N. Furgiuele, A.H. Lebovitz, K. Khait, J.M. Torkelson, Macromolecules, 33 (2000) 225-228.
[198] H.S. Xia, Q. Wang, K.S. Li, G.H. Hu, J Appl Polym Sci, 93 (2004) 378-386.
[199] A.H. Lebovitz, K. Khait, J.M. Torkelson, Polymer, 44 (2003) 199-206.
[200] M.F. Mu, A.M. Walker, J.M. Torkelson, K.I. Winey, Polymer, 49 (2008) 1332-1337.
[201] J. Masuda, J.M. Torkelson, Macromolecules, 41 (2008) 5974-5977.
[202] N. Khaorapapong, K. Kuroda, H. Hashizume, M. Ogawa, Appl. Clay Sci., 19 (2001) 69-76.

[203] J.M. Sequaris, F. Bassmann, A. Hild, H.D. Narres, M.J. Schwuger, Colloid Surf. A-Physicochem. Eng. Asp., 159 (1999) 503-512.
[204] O. Regev, P.N.B. ElKati, J. Loos, C.E. Koning, Advanced Materials, 16 (2004) 248-+.
[205] E.J. Park, S. Hong, D.W. Park, S.E. Shim, Colloid Polym Sci, 288 (2010) 47-53.
[206] M. Xu, Y.S. Choi, Y.K. Kim, K.H. Wang, I.J. Chung, Polymer, 44 (2003) 6387-6395.
[207] Y.T. Shieh, J.H. Su, G. Manivannan, P.H.C. Lee, S.P. Sawan, W.D. Spall, Journal of Applied Polymer Science, 59 (1996) 695-705.
[208] D.L. Tomasko, H. Li, D. Liu, X. Han, M.J. Wingert, L.J. Lee, K.W. Koelling, Ind. Eng. Chem. Res., 42 (2003) 6431-6456.
[209] A.R. Berens, G.S. Huvard, Acs Symposium Series, 406 (1989) 207-223.
[210] J.S. Chiou, J.W. Barlow, D.R. Paul, Journal of Applied Polymer Science, 30 (1985) 2633-2642.
[211] A. Garg, E. Gulari, C.W. Manke, Macromolecules, 27 (1994) 5643-5653.
[212] M. Lee, C. Tzoganakis, C.B. Park, Advances in Polymer Technology, 19 (2000) 300-311.
[213] M.D. Wilding, D.G. Baird, Polym. Eng. Sci., 49 (2009) 1990-2004.
[214] Y.S.K. G.P. Daumit, C.R. Slater, J.G. Venner, and C.C.Young, in, 1990.
[215] H. Porosoff, in, 1979.
[216] C.C. Zeng, N. Hossieny, C. Zhang, B. Wang, Polymer, 51 (2010) 655-664.
[217] A.S. Zerda, T.C. Caskey, A.J. Lesser, Macromolecules, 36 (2003) 1603-1608.
[218] Z.M. Liu, X.H. Dai, J. Xu, B.X. Han, J.L. Zhang, Y. Wang, Y. Huang, G.Y. Yang, Carbon, 42 (2004) 458-460.
[219] X.H. Dai, Z.M. Liu, B.X. Han, Z.Y. Sun, Y. Wang, J. Xu, X.L. Guo, N. Zhao, J. Chen, Chem. Commun., (2004) 2190-2191.
[220] J. Steinmetz, S. Kwon, H.J. Lee, E. Abou-Hamad, R. Almairac, C. Goze-Bac, H. Kim, Y.W. Park, Chem. Phys. Lett., 431 (2006) 139-144.
[221] J. SteinmetZ, H.J. Lee, S. Kwon, D.S. Lee, C. Goze-Bac, E. Abou-Hamad, H. Kim, Y.W. Park, Curr. Appl. Phys., 7 (2007) 39-41.
[222] B.H. Yue, Y.B. Wang, C.Y. Huang, R. Pfeffer, Z. Iqbal, J Nanosci Nanotechno, 7 (2007) 994-1000.
[223] C.W Manke, E. Gulari, D.F Mielewski, E.C Lee, U.S. Patent 6,753,360 (2002)
[224] D.F. Mielewski, E.C. Lee, C.W. Manke, E. Gulari, U.S. Patent 6,469,073 (2004)
[225] G.M. A.J. Lesser, in: ANTEC 2004, 2004, pp. 1528-1532.
[226] Q.T. Nguyen, in: Chemical Engineering, Virginia Tech, Blacksburg, 2007, pp. 195.
[227] G.X. Chen, H.S. Kim, B.H. Park, J.S. Yoon, Polymer, 47 (2006) 4760-4767.
[228] O. Breuer, U. Sundararaj, Polymer Composites, 25 (2004) 630-645.
[229] R.H. Baughman, A.A. Zakhidov, W.A. de Heer, Science, 297 (2002) 787-792.
[230] S. Barrau, P. Demont, E. Perez, A. Peigney, C. Laurent, C. Lacabanne, Macromolecules, 36 (2003) 9678-9680.
[231] E.S. Choi, J.S. Brooks, D.L. Eaton, M.S. Al-Haik, M.Y. Hussaini, H. Garmestani, D. Li, K. Dahmen, J Appl Phys, 94 (2003) 6034-6039.
[232] N.R. Pradhan, G.S. Iannacchione, J Phys D Appl Phys, 43 (2010).
[233] C. Guthy, F. Du, S. Brand, K.I. Winey, J.E. Fischer, J Heat Trans-T Asme, 129 (2007) 1096-1099.
[234] H.K.F. Cheng, N.G. Sahoo, Y.Z. Pan, L. Li, S.H. Chan, J.H. Zhao, G. Chen, J. Polym. Sci. Pt. B-Polym. Phys., 48 (2010) 1203-1212.
[235] N.R. Raravikar, L.S. Schadler, A. Vijayaraghavan, Y.P. Zhao, B.Q. Wei, P.M. Ajayan, Chemistry of Materials, 17 (2005) 974-983.
[236] K. Lozano, E.V. Barrera, Journal of Applied Polymer Science, 79 (2001) 125-133.

[237] M. Cadek, J.N. Coleman, V. Barron, K. Hedicke, W.J. Blau, Appl. Phys. Lett., 81 (2002) 5123-5125.
[238] J.R. Wood, Q. Zhao, M.D. Frogley, E.R. Meurs, A.D. Prins, T. Peijs, D.J. Dunstan, H.D. Wagner, Phys Rev B, 62 (2000) 7571-7575.
[239] T. Kashiwagi, F.M. Du, K.I. Winey, K.A. Groth, J.R. Shields, S.P. Bellayer, H. Kim, J.F. Douglas, Polymer, 46 (2005) 471-481.
[240] G. Beyer, Fire Mater., 26 (2002) 291-293.
[241] T. Kashiwagi, E. Grulke, J. Hilding, K. Groth, R. Harris, K. Butler, J. Shields, S. Kharchenko, J. Douglas, Polymer, 45 (2004) 4227-4239.
[242] T. Kashiwagi, F.M. Du, J.F. Douglas, K.I. Winey, R.H. Harris, J.R. Shields, Nat Mater, 4 (2005) 928-933.
[243] F.M. Du, R.C. Scogna, W. Zhou, S. Brand, J.E. Fischer, K.I. Winey, Macromolecules, 37 (2004) 9048-9055.
[244] P. Potschke, M. Abdel-Goad, I. Alig, S. Dudkin, D. Lellinger, Polymer, 45 (2004) 8863-8870.
[245] M. Abdalla, D. Dean, D. Adibempe, E. Nyairo, P. Robinson, G. Thompson, Polymer, 48 (2007) 5662-5670.
[246] Q.H. Zhang, D.R. Lippits, S. Rastogi, Macromolecules, 39 (2006) 658-666.
[247] C.A. Mitchell, J.L. Bahr, S. Arepalli, J.M. Tour, R. Krishnamoorti, Macromolecules, 35 (2002) 8825-8830.
[248] A.K. Kota, B.H. Cipriano, M.K. Duesterberg, A.L. Gershon, D. Powell, S.R. Raghavan, H.A. Bruck, Macromolecules, 40 (2007) 7400-7406.
[249] D.F. Wu, L. Wu, M. Zhang, J. Polym. Sci. Pt. B-Polym. Phys., 45 (2007) 2239-2251.
[250] D.F. Wu, L. Wu, M. Zhang, Y.L. Zhao, Polym Degrad Stabil, 93 (2008) 1577-1584.
[251] J.Y. Kim, H.S. Park, S.H. Kim, Journal of Applied Polymer Science, 103 (2007) 1450-1457.
[252] D.S. Bangarusampath, H. Ruckdaschel, V. Altstadt, J.K.W. Sandler, D. Garray, M.S.P. Shaffer, Polymer, 50 (2009) 5803-5811.
[253] B.H. Cipiriano, T. Kashiwagi, S.R. Raghavan, Y. Yang, E.A. Grulke, K. Yamamoto, J.R. Shields, J.F. Douglas, Polymer, 48 (2007) 6086-6096.
[254] Y.S. Song, Polym. Eng. Sci., 46 (2006) 1350-1357.
[255] D. Wu, L. Wu, Y. Sun, M. Zhang, J. Polym. Sci. Pt. B-Polym. Phys., 45 (2007) 3137-3147.
[256] A.T. Seyhan, F.H. Gojny, M. Tanoglu, K. Schulte, Eur Polym J, 43 (2007) 2836-2847.
[257] Y. Kojima, A. Usuki, M. Kawasumi, A. Okada, Y. Fukushima, T. Kurauchi, O. Kamigaito, J. Mater. Res., 8 (1993) 1185-1189.
[258] B. Chen, J.R.G. Evans, H.C. Greenwell, P. Boulet, P.V. Coveney, A.A. Bowden, A. Whiting, Chem Soc Rev, 37 (2008) 568-594.
[259] A. Usuki, A. Koiwai, Y. Kojima, M. Kawasumi, A. Okada, T. Kurauchi, O. Kamigaito, Journal of Applied Polymer Science, 55 (1995) 119-123.
[260] J. Pascual, E. Fages, O. Fenollar, D. Garcia, R. Balart, Polym. Bull., 62 (2009) 367-380.
[261] Q.T. Nguyen, D.G. Baird, Polymer, 48 (2007) 6923-6933.
[262] G. Galgali, S. Agarwal, A. Lele, Polym. J., 45 (2004) 6059-6069.
[263] K.P. Pramoda, T. Liu, Z. Liu, C. He, H.-J. Sue, Polym. Degrad. Stab., 81 (2003) 47-56.
[264] S. Bourbigot, D.L. Vanderhart, J.W. Gilman, W.H. Awad, R.D. Davis, A.B. Morgan, C.A. Wilkie, J. Polym. Sci. Pt. B-Polym. Phys., 41 (2003) 3188-3213.
[265] F. Bellucci, G. Camino, A. Frache, A. Saffa, Polym Degrad Stabil, 92 (2007) 425-436.
[266] S.D. Burnside, E.P. Giannelis, Chemistry of Materials, 7 (1995) 1597-1600.
[267] K. Yano, A. Usuki, A. Okada, T. Kurauchi, O. Kamigaito, J. Polym. Sci. Pol. Chem., 31 (1993) 2493-2498.

[268] S. Nazarenko, P. Meneghetti, P. Julmon, B.G. Olson, S. Qutubuddin, J. Polym. Sci. Pt. B-Polym. Phys., 45 (2007) 1733-1753.
[269] K. Li, X.L. Gao, A.K. Roy, Mech Adv Mater Struc, 13 (2006) 317-328.
[270] T. Mori, K. Tanaka, Acta Metallurgica, 21 (1973) 571-574.
[271] J.C. Halpin, J.L. Kardos, Polym. Eng. Sci., 16 (1976) 344-352.
[272] R. Hill, Journal of the Mechanics and Physics of Solids, 12 (1964) 199-212.
[273] D. Chu, Q. Nguyen, D.G. Baird, Polymer Composites, 28 (2007) 499-511.
[274] H. Miyagawa, M.J. Rich, L.T. Drzal, J. Polym. Sci. Pt. B-Polym. Phys., 42 (2004) 4391-4400.
[275] Q.H. Zeng, A.B. Yu, G.Q. Lu, Prog. Polym. Sci., 33 (2008) 191-269.
[276] J. Lusis, R.T. Woodhams, M. Xanthos, Polym. Eng. Sci., 13 (1973) 139-145.
[277] Y. Ke, C. Long, Z. Qi, J. Appl. Polym. Sci., 71 (1999) 1139-1146.
[278] H.L. Cox, British Journal of Applied Physics, 3 (1952) 72.
[279] M.S.P. Shaffer, X. Fan, A.H. Windle, Carbon, 36 (1998) 1603-1612.
[280] M. Kim, Y.B. Park, O.I. Okoli, C. Zhang, Compos. Sci. Technol., 69 (2009) 335-342.
[281] S. Peeterbroeck, L. Breugelmans, M. Alexandre, J. Bnagy, P. Viville, R. Lazzaroni, P. Dubois, Compos. Sci. Technol., 67 (2007) 1659-1665.
[282] M.-K. Yeh, N.-H. Tai, J.-H. Liu, Carbon, 44 (2006) 1-9.

Chapter 3

Using Supercritical Carbon Dioxide in Preparing Carbon Nanotube Nanocomposite: Improved Dispersion and Mechanical Properties

Using Supercritical Carbon Dioxide in Preparing Carbon Nanotube Nanocomposite: Improved Dispersion and Mechanical Properties

Chen Chen[a], Michael Bortner[b], John P. Quigley[a], Donald G. Baird[a,*]

[a] Department of Chemical Engineering, Virginia Polytechnic Institute and State University, Blacksburg, Virginia 24061

[b] Nanosonic, Inc., Pembroke, Virginia 24136

3.1 Abstract:

Improvements in carbon nanotube (CNT) dispersion and subsequent mechanical properties of CNT/poly(phenylsulfone) (PPSF) composites were obtained by applying the supercritical CO_2 ($scCO_2$) aided melt blending technique that has been used in our laboratory for nanoclay/polymer composite preparation. The preparation process relied on rapid expansion of the CNTs followed by melt blending using a single-screw extruder. Scanning electronic microscopy (SEM) results revealed that the CNTs exposed to $scCO_2$ at certain pressures, temperatures, exposure time, and depressurization rates, have a more dispersed structure. Microscopy results showed improved CNT dispersion in the polymer matrix and more uniform networks formed with the use of $scCO_2$, which indicated that CO_2 expanded CNTs are easier to disperse into the polymer matrix during the blending procedure. The CNT/PPSF composites prepared with $scCO_2$ aided melt blending and conventional melt blending showed similar tensile strength and elongation at break. The Young's modulus of the composite prepared by means of conventional direct melt blending failed to increase beyond the addition of 1 wt% CNT, but the $scCO_2$ aided melt blending method provided continuous improvements in Young's modulus up to the addition of 7 wt% CNT.

3.2 Introduction

Since Iijima's discovery of multi-wall carbon nanotubes (MWNTs) in 1991[1], tremendous interest has focused on carbon nanotubes (CNTs) and their applications, especially in the area of CNT reinforced composite materials [2-26]. Their nano-scale diameter, high aspect ratio, unique physical properties, and low density make CNTs an ideal candidate for use as a reinforcing filler for high-performance polymers.

Currently, the three most widely used techniques for preparing CNT composites are: solution blending, *in situ* polymerization, and melt blending. In the solution blending method, CNTs are typically dispersed in a solvent and then mixed with polymer. Afterwards, the composites are recovered by precipitating the polymer/CNT mixtures or film casting and subsequent solvent removal [2-5]. This method is effective for CNT/polymer matrix mixing at relatively high CNT levels [6, 7]. Shaffer et al. [6] managed to fabricate CNT/Poly(vinyl alcohol) composites films with up to 60 wt% CNTs, and good dispersion was observed using scanning electron microscopy (SEM). However, current research using the solution blending method is mostly on a small scale and, therefore, is not practically desirable. The choice of the solvent is made by the solubility of the polymer. This leads to another disadvantage of this method: the use and subsequent removal of large volumes of organic solvents, which are costly and environmentally hazardous. Ultra-sonication is usually involved to help improve the dispersion of CNTs in the polymer solution [8-10]. It was shown that sonication can damage the nanotubes with limited unbundling, which is detrimental to the composite properties [11]. *In situ* polymerization method is a developing technique for CNT composite preparation. The method starts by dispersing nanotubes in monomer followed by polymerization [12-15]. The *in situ* polymerization process has proven to be useful for polyamide and epoxy-based composites [16-

21], but it is not general to other kinds of polymers. This technique also requires extended processing time and sometime organic solvent to help mixing the monomers and nanotubes. These facts limit the application of *in situ* polymerization as an industrially viable process. The melt blending method is now the best scalable method for industrial applications and is also economical and environmentally friendly. This process generally involves the melting of polymer pellets to form a viscous liquid. The nanotubes are forced to disperse into the polymer matrix by high shear at high temperature [22-24]. The problem with this method is that good dispersion is usually hard to obtain, especially for non-polar polymers. Improvements of the material mechanical properties are mostly achieved using polar polymer matrices, such as Nylon-6. Chen et al. [25] used melt blending followed by compression molding to prepare Nylon-6 nanocomposites reinforced with surface-functionalized CNTs. The modulus of the composite was increased from 1899 MPa to 3556 MPa or by 87% with the addition of 1 wt % CNT. Their transmission electron microscopy (TEM) and SEM results showed evidence of both uniform dispersion of the CNTs and a strong interfacial adhesion with the matrix. However, improvements of the mechanical properties of CNT composites based on non-polar polymer matrices are not as significant. For example, Kim [26] reported the preparation of CNT reinforced poly(butylene terephthalate) nanocomposite using the melt-blending process. The tensile modulus increased by 21.7% from 1.2 GPa to 1.46 GPa with 2 wt % of CNT. Using a very similar procedure, Deng et al. [27] prepared CNT/polypropylene (PP) composites and the tensile modulus only increased from 1.4 GPa to 1.75 GPa or by 25% with 1 wt % of CNT. In addition, the mechanical properties of the nanocomposites usually level off beyond 1 wt % to 2 wt % of CNT as the challenge of CNT dispersion increases [28]. This is probably the reason why only properties up to these or lower concentrations are reported in the literature [23, 24, 26, 29].

Hence, although melt compounding has shown some promise for producing composites with improved properties for some polymer matrices, it does not provide a promising reinforcement for non-polar polymers and at high CNT loadings greater than 2 wt %. Achieving a well dispersed nanoparticle morphology within any polymer matrix is one of the main challenges in polymer nanocomposites manufacturing using the melt blending procedure.

The techniques using supercritical carbon dioxide ($scCO_2$) coupled with the melt blending method have been studied in the field of nanoclay/polymer composite [30-33]. Lesser et al. [30] used a modified hopper in the feed section of the extruder to allow polymer and clay to interact with $scCO_2$ before processing. It was found that the presence of $scCO_2$ increased the clays d-spacing by as much as 100%, and the nanocomposite with an intercalated structure was produced. However, mechanical properties of the nanocomposites were not reported. Alternately, Manke et al. [32] developed a process that allows clay particles to be pre-treated with $scCO_2$ in a pressurized vessel and then catastrophically depressurized to atmospheric pressure so that the stacked nanoclay platelets were forced apart. The presence of exfoliated nanoclay particles was identified by wide angle X-ray diffraction (WAXD). However, they did not provide any procedure for combining the clay particles with polymers and any mechanism for assuring that the exfoliated particles remained exfoliated once combined with the polymer at high temperature. Two years later, the same group developed a procedure to combine polymer and nano-clay in presence of $scCO_2$ [31]. In this approach, the clay and polymer pellets were loaded through two separate hoppers into the extruder and $scCO_2$ was injected into the hopper containing the clays. The patent claimed that two factors result in the exfoliation of nano-clays: 1) decreased viscosity of composite melt caused by $scCO_2$ as a plasticizer, and 2) CO_2 nucleation and expansion within the extrudates when exiting the extruder die. However, no WAXD or TEM evidence of an

exfoliated morphology was presented and no mechanical properties were provided. In a different procedure, Nguyen et al. [33] developed a method to combine the benefits of melt compounding with the exfoliating capability of $scCO_2$. The process relied on rapid expansion of the clay followed by direct injection into the extruder. It was observed in the WAXD data that the composite contained a high degree of exfoliated nanoclay for concentrations as high as 6.6 wt%. The Young's modulus of the composites increased by 54% at this nanoclay loading. This technique ensured that the clay stayed exfoliated as the nanoparticles were processed immediately following exfoliation.

The $scCO_2$ aided melt blending method for CNT/polymer composites has not been well studied. Most applications of $scCO_2$ in the field of CNT nanocomposite preparation are as a polar and low viscosity solvent in the *in situ* polymerization process. For example, Liu et al. [34] prepared a CNT/polystyrene composite by impregnating styrene and an initiator into the CNTs with the aid of $scCO_2$ followed by polymerization. TEM images showed a composite material of CNTs filled with polystyrene was formed. Other polymer based CNT nanocomposites such as polypyrrole [35], polyacetylene [36], and poly(methyl methacrylate) [37], have also been reported using this technique. However, none of these studies reported the mechanical properties and, hence, we can't judge the degree of effectiveness of the process. Ma et al. [38] reported a method that used $scCO_2$ to assist the preparation of CNT/PP composites combined with batch melt mixing. In this method, a composite with 3 wt % CNT was prepared by mechanically mixing the polymer melt and CNTs at high temperature in an autoclave with the CO_2 present under supercritical conditions (15 MPa and 200 ^{o}C). Composites with lower concentrations were obtained by diluting this batch with pure polymer. By using $scCO_2$ assisted mixing, the yield stress and Young's modulus of the nanocomposites increased by 33% and 6%, respectively. This

improvement was mostly due to the reduced melt viscosity during mixing as $scCO_2$ acted as a plasticizer. This method didn't involve the crucial rapid expansion step as described in the $scCO_2$ aided melt blending method above that was applied to nanoclays, and is, therefore, different in terms of the dispersion mechanism. In addition, this method involves batch processing, a less preferable process compared to the $scCO_2$ aided continuous extrusion process.

In this study, the $scCO_2$ technique is extended to CNT expansion and the preparation of CNT/polymer composites. We want to determine whether the $scCO_2$ technique can expand and separate the CNT bundles as effectively as it exfoliated nanoclays. The structure and chemical properties of nanoclays and CNTs are very different. Nanoclays consist of a 2-D layered platelet structure and have negative charges on the clay surfaces with cations between the clay layers. The CNTs are 1-D tubes existing in entangled bundles and have neutral charges on the surfaces. Therefore, it is important to study the influence of this technique on the CNT morphology, which is still unknown. The variables used in the $scCO_2$ expansion process, such as chamber pressure, temperature, depressurization rate, and contacting time, are studied to reveal their effects on the CNT morphologies. We also want to ascertain whether the improvement in the CNT dispersion in polymer matrix can be achieved and lead to the enhancement of the composite mechanical properties. A series of CNT concentrations with both $scCO_2$ aided melt blending method and traditional melt blending are produced and examined to deduce the effect of this novel technique on the composite properties. To avoid the complex facilities required in the procedure developed by Nguyen et al. [33] in this work, the CNTs are simply expanded and collected first and then combined with the polymer by the means of mixing in an extruder.

3.3 Experimental

3.3.1 Materials

The polymeric matrix used in this work is poly(phenylsulfone) (PPSF, RADEL® R-5000) which was donated by Solvay Advanced Polymers (Alpharetta, GA). The melt index of the polymer is 17 g/10 min at 365°C and 5.0 kg of force. The pristine CNTs used were Nanocyl®-7000, which were obtained from Nanocyl Inc. (Sambreville, Belgium). The CNTs are thin multi-wall carbon nanotubes produced via acatalytic carbon vapor deposition (CCVD) process and are used as-received.

3.3.2 CNT Expansion

The CNTs were subjected to $scCO_2$ in a pressurized chamber at varying pressures, temperatures, and exposure times, which ranged from 2000 psi to 3000 psi, 40 °C to 100 °C, and 20 min to 12 hr, respectively. 3000 psi, 80 °C and 12 hr were chosen as the best set of experimental conditions based on results of the CNT morphology. These conditions were used to expand all CNTs before the melt compounding step in CNT composite preparation. The chamber used to contain CNTs and $scCO_2$ was a pressure chamber with 660 ml capacity obtained from Parr Instrument Company (Moline, IL). The inlet/outlet of the chamber was sealed by a ball valve from High Pressure Equipment Company (Erie, PA). Following pressurization, the CNTs and CO_2 mixture was released into a 5 gal pressure vessel using rapid depressurizing to achieve expansion. The expanded CNTs were then collected from the 5 gal pressure vessel.

3.3.3 Melt Compounding

PPSF pellets and the expanded CNTs were mechanically dry blended in a Kitchen Aid type mixer and dried at 115 °C for at least 12 hr in preparation for melt compounding. The mixture of CNTs and PPSF pellets was then fed to a single screw extruder (Killion 4335 series)

and re-pelletized. The nanocomposite was extruded using a screw speed of 25 rpm and an ascending temperature profile beginning at 230 °C in the solids conveying zone and progressing to 335 °C at the circular die. The single screw had a constant channel width and pitch angle (square pitch) design, a diameter of 2.54 cm, and a L/D of 20:1. The nanocomposite extrudate was quenched using a cold water bath at room temperature and pelletized into approximately 1.0 cm long by 0.2 cm diameter pellets.

In addition to the method just described, conventional direct blending method was used to prepare the nanocomposite for the purpose of comparison. In this method, the CNTs were used as received. The pristine CNTs and PPSF were mechanically dry blended and melt compounded using the same device and procedure as described above.

3.3.4 Tensile Properties

Composite pellets were compression molded into approximately 1.5 mm thick plaques and stamped to dogbone-shape samples of 65 mm long and 10 mm wide with a neck length of 20 mm and neck width of 3.15mm. Tensile tests on these dogbone samples were performed at room temperature using an Instron Model 4204 testing machine (Instron, Grove City, PA). An extensometer was used to accurately measure the Young's modulus. The load was measured with a 5 kN load cell. The crosshead speed was kept at 1.27 mm/min during all tensile tests. The average and standard deviation were calculated from at least five samples for all tests.

3.3.5 Rheological Properties

Rheological measurements on the nanocomposites were performed using an ARES rheometer from TA Instruments. Extruded pellets were dried for at least 12 hr at 115 °C and compression molded into 25 mm diameter disks. Dynamic frequency sweep experiments were performed under a continuous nitrogen atmosphere using a 25-mm parallel-plate fixture at

350 °C in the linear viscoelastic region of the materials. The linear viscoelastic limit was determined using strain sweeps at a frequency of 10 rad/s and at the same temperature (350 °C). It was found that dynamic frequency sweep experiments could be conducted at a strain of 1%. The elastic moduli (*G'*), loss moduli (*G"*), and complex viscosities (η^*) of the materials as functions of angular frequency (ω) (ranging from 0.1 rad/s to 100 rad/s) were obtained at a temperature of 350 °C.

3.3.6 Morphological Characterization

The morphology of the CNTs and the nanocomposites was analyzed by the use of scanning electron microscopy (SEM). SEM micrographs were generated by means of an LEO 1550 SEM device with an accelerating voltage of 5 kV.

3.4 Results and Discussion

3.4.1 Application of the $ScCO_2$ Technique to CNT Expansion

3.4.1.1 Morphological Characterization of CNTs before and after Expansion

Properties of the CNTs differ greatly before and after using the $scCO_2$ expansion technique. Both bulk density and texture of the CNTs change significantly, even by visual observation. Fig. 3.1 shows the CNTs before (left) and after (right) CO_2 expansion with the same sample weight (0.10g). The bulk volume of expanded CNTs is approximately 5 times larger than the pristine volume. After expansion, the CNTs are distended with a softer texture and tend to float upon shaking.

As shown in the SEM images in Fig. 3.2 (a and b), the aggregated CNT clumps which existed in the pristine CNTs have been expanded into separated CNT bundles, which explains the distended and soft texture observed visually. The CNT bundles in Fig. 3.3 (e) have an average diameter of 719 nm as measured by SEM. Although it would be ideal to obtain

individual nanotubes for the best reinforcement, the bundled structure of CNTs is also a great improvement compared to the entangled CNT clumps. The polymer chains can potentially penetrate into the gaps between the CNT bundles and even among individual tubes much easier than previously. In addition, the CNT bundles have a high respect ratio at the micro scale, which is beneficial for the composite mechanical properties. No noticeable damage occurred to the expanded CNTs as seen in Figs. 3.2 (c) and (f). The average diameter of the tubes is 14.5 nm for the unexpanded nanotubes and 18.5 nm for the expanded nanotubes, respectively. $ScCO_2$ may have penetrated into the CNT walls and loosened them slightly, but severe damage did not appear to take place. These factors suggest that the $scCO_2$ is effective for expanding CNTs and could be beneficial in the generation of the final composite physical properties when combined with a polymer during melt blending.

3.4.1.2 Morphological Characterization of CNTs Expanded at Different Conditions

The morphology of the CNTs is significantly affected by the conditions utilized for the $scCO_2$ expansion process. The depressurization rates, exposure time, pressures and temperatures are all important variables that can affect CNT morphology. The first variable controlled was the depressurization rate. In the case of a rapid depressurization rate, CNTs were released from high pressure (3000 psi) to atmospheric pressure within 2 seconds. For a slow depressurization rate, the ball valve was released in such a way that the high pressure vessel took about 5 minutes to reach atmospheric pressure. The other conditions for the $scCO_2$ expansion process were kept the same (CNTs exposed to $scCO_2$ for 1hr at 80°C and at 3000 psi) in order to investigate the effect of the depressurization rate. As can be seen in Fig. 3.3, the rapid release rate (Fig. 3.3 (b)) helped to disentangle the CNT bundles, while the slow release rate resulted in an aggregated CNT structure (Fig 3.3 (a)). This is probably because the fast release rate allows a rapid expansion of

the CO_2 and, thus, blows apart the entangled CNT bundles more effectively. The effect of pressure can be seen from Figs. 3.4(a) and 3.4(b). With other conditions fixed, CNTs exhibit a form of separated CNT bundles under higher pressure (Fig. 3.4 (b)). Conversely, at low pressures an entangled structure forms (Fig. 3.4(a)). This is because higher pressure ensures a better penetration of CO_2 into the gaps between the nanotubes. In addition, higher pressure provides more mass of CO_2 absorbed into the CNT bundles that can blow the nanotubes apart during the release of pressure. However, the pressure applied has a limitation due to the experimental equipment. The highest pressure listed for the chamber is 3500 psi. For safety considerations, no higher than 3000 psi was applied. Fig. 3.5 (a-d) shows the morphology of CNTs that were exposed to scCO_2 for different periods of time from 20 min to 12 hr. CNTs that were held in the chamber for 12 hr formed the most dispersed structure with long and thin CNT bundles. Longer exposure time allows more penetration of CO_2 into the gaps between the carbon nanotubes and, thus, better separation upon depressurization. For the optimal results, the nanocomposites prepared in this work were all subjected to a 12 hr exposure time. However, the differences between the CNTs that were exposed to the scCO_2 for 3 hr, 6 hr, and 12 hr are smaller than the difference between the CNTs that were treated to scCO_2 for 20 min and 3 hr. Fig. 3.6 (a-d) shows the CNT morphologies as a result of treatment with asCO_2 at 40 °C, 60 °C, 80 °C and 100 °C with fixed pressure (3000 psi), exposure time (12 hr), and release rate (fast). From the SEM images, it can be observed that at 40 °C and 60 °C, the CNTs are not quite as well separated and expanded, and part of the tube bundles are still entangled with each other. At 80 °C, CNTs are observed to exhibit a more expanded structure. The CNTs treated at 80 °C are slightly more expanded than those treated at 100 °C, and they formed thinner bundles. This phenomenon is possibly due to the balance of two opposing effects upon the temperature change.

First, higher temperature means easier and better penetration of the CO_2 into CNTs bundles and, thus, a more separated structure. Alternately, higher temperature means a reduced amount of $scCO_2$ in the container with the same pressure and, hence, less CO_2 will be involved in the pressure release process. Raising the temperature too much will lead to reduced CO_2 expansion during the release of pressure and result in a less separated CNT structure. Therefore, the best dispersion is obtained at the intermediate temperature, instead of the highest one.

3.4.2 CNT/PPSF Nanocomposite Properties

3.4.2.1 Linear Viscoelastic Properties

In this section, we look at the effect of the $scCO_2$ aided melt blending method on the rheological behavior of the nanocomposite melts at various CNT loadings. The storage modulus, *G'*, and complex viscosity, $|\eta^*|$, were obtained from dynamic frequency scan measurements. Values of *G'* and $|\eta^*|$ of the nanocomposite melt, that prepared by different methods at various CNT concentrations, are compared in Figs. 3.7 and 3.8, respectively. There are several factors that have a large impact on the *G'* values. First, as the nanotube loading increases, the magnitudes of *G'* increases and the slope of the *G'* curve decrease significantly. The *G'* of pure PPSF and 1 wt % CNT/PPSF samples processed using both methods (conventional direct blending and $scCO_2$ aided melt blending method) are essentially the same. The *G'* values of 3 wt % CNT/PPSF samples increases slightly, but the curves keep a similar shape with the pure PPSF *G'* curve. This is because the CNTs don't have strong interactions with one another at these low concentrations. The slight yield-like behavior at low frequencies is caused by existing sulfonic bonds within the polymer, which can be also observed in the pure matrix melt behavior. For higher CNT concentrations, the nanotube-nanotube interactions become much stronger as the interparticle distances decrease and the hydrodynamic volumes of the particles start to overlap.

As a result, *G'* of the nanocomposites containing 5 wt % and 7 wt % are much higher, and dramatic plateaus appear at low frequencies. Second, all samples prepared by the $scCO_2$ aided method have higher *G'* values and higher plateaus than the samples prepared by the direct melt blending method at the same CNT concentrations beyond 1 wt %. This suggests that the nanotube network formed using the CO_2 expanded CNTs is more uniform and contains stronger particle-particle interactions. It was reported that when the CNTs are well dispersed in the polymer matrix, a plateau in *G'* versus angular frequency can be observed at low frequencies [39-41]. Pujari et al. [41] reported the storage modulus of nanocomposites containing the same levels of CNT (3.5 wt %) but with different melt mixing times. Their results showed that *G'* evolved in shape towards a plateau as the mixing time increased from 15 min to 90 min. This plateau is the result of improvements in the CNT dispersion. Similar viscoelastic behavior was seen in clay and graphite nanocomposites [42, 43]. The increased plateau in the nanocomposites prepared by the $scCO_2$ aided method can also indicate a better dispersion of the CNTs within the matrix. However, the concentrated filled melt system can be very complicated and a variety of structured networks may display similar rheological responses [44]. It is not possible to draw any definite conclusions concerning the degree of CNT dispersion from the rheological measurement. Other comprehensive characterizations such as SEM are needed to determine the state of CNT dispersion.

The processing method has a pronounced impact on the complex viscosity, $|\eta^*|$, of the composite as well (shown in Fig. 3.8). Values of the complex viscosity of pure PPSF and the nanocomposite containing 1 wt % CNTs processed by means of both direct melt blending and $scCO_2$ aided methods are the same within experimental error. The existing sulfonic bonds contribute to the rise in $|\eta^*|$ at low frequencies which is attributed to the slight yield behavior at

low frequencies for the pure PPSF and the 1 wt % samples, similar to the behavior in *G'*. No significant difference can be observed from the composites prepared by different methods at 1 wt % due to the low CNT loadings. As the CNT concentration increases, the difference in $|\eta^*|$ caused by different processing techniques increases as well. Obvious yield-like behavior also starts to appear for the 5 wt % samples, which indicates network formations as did plateaus in the storage modulus at low frequencies [33, 39]. $ScCO_2$ processed nanocomposites with CNT concentration above 3 wt % have higher $|\eta^*|$ with the same CNT loadings, especially at low frequencies. This could be the result of the distended structure of expanded CNTs and the structural differences we saw in the CNT micrographs. It suggests that the $scCO_2$ aided procedure is more effective than the direct blending method at relatively high CNT concentrations (i.e. 5 - 7 wt %) because it improves the CNT dispersion in the polymer matrix.

3.4.2.2 Morphological Characterization

Rheological measurements suggested that a more uniform network of the CNTs in the PPSL matrix, as a result of improved CNT dispersion, is formed by using the $scCO_2$ aided processing method. As using rheology to determine the dispersion of the CNTs in the nanocomposites is ambiguous and the information obtained from it can only be used to probe the structure indirectly, scanning electron micrographs are provided as a complementary method to the rheological results in this section.

The SEM images for 1 wt% CNT/PPSF nanocomposites are not provided here because no significant difference in terms of CNT dispersion is observed in the samples prepared by different methods. The CNTs in both samples lack ideal dispersion. There are varying regions of the aggregated CNTs and sparse CNTs in both samples. However, one point can be made in the nanocomposite prepared by the $scCO_2$ aided method. It can be noticed on the fracture surface

that several CNTs were pulled out of the bulk and formed a strengthening structure in the gap, as shown in Fig. 3.9. A similar structure was observed for CNT reinforced Nylon-6 composite materials [23], where the interface interactions of the surface-functionalized nanotubes with the polar polymer matrix was strong. No such structure was found in the sample that was prepared by the direct blending method in our work. This suggests the possibility of better interactions of CNTs with the polymer matrix at the interface and could be one possible reason for the improved mechanical properties discussed below.

Unlike the 1 wt% CNT composites, the morphology of composites at higher CNT concentrations shows greater difference in the CNT dispersion for different processing methods. Samples with 7 wt% nanotubes showed the greatest improved dispersion of the CNTs by using $scCO_2$ among the samples with all the concentrations. Figs. 3.10 (a-c) and (d-f) show the SEM images of the fracture surfaces of 7 wt% CNT/PPSF nanocomposites prepared by the direct blending method and the $scCO_2$ aided method, respectively, at different magnifications. Aggregation of the CNTs can be observed for both composite samples as the bright regions in Figs. 3.10 (a) and (b). The directly blended sample contains less, but much larger areas of aggregation, than the sample prepared by the $scCO_2$ aided method. The sample prepared by sCO_2 still has some regions with CNT aggregation, but these regions are more in the number and smaller in the area. The enlarged aggregation areas (Figs. 3.10 (c) and (f)) for these two composites are not very different as they both contain large amounts of CNTs. The well dispersed regions (Figs. 3.10 (b) and (e)) are quite different, though. The nanocomposite prepared by $scCO_2$ aided method has significantly more CNTs embedded in the polymer matrix in these regions. The CNTs in these regions are most likely to involve in the composite reinforcement because they exist as individual tubes or fairly thin CNT bundles and, therefore,

have a large surface area to interact with the polymer matrix. The improvement of the CNTs dispersion in the nanocomposite is caused by the use of expanded CNTs. This agrees with the rheological data, which indicates an increased CNT network in the nanocomposites. Although structures of "pulled out CNTs" are still noticed, the improved dispersion should be crucial for improved mechanical property as discussed below.

3.4.2.3 Mechanical Properties

The mechanical properties of the CNT/PPSF nanocomposite compression molded plaques are shown in Table 3.1 and compared in Fig. 3.11. The improvements in Young's modulus depend on the processing method used as well as CNT concentration. PPSF used in this study has a Young's modulus of 2.124 ± 0.074 GPa. With the addition of 1 wt % CNT and direct blending the CNTs into the polymer matrix, a Young's modulus of 2.339 ± 0.054 GPa is obtained which is a 10% increase compared to the pure matrix material. Using the same technique, at concentration of 3 wt%, 5 wt%, and 7 wt% of CNTs, the nanocomposites are found to have Young's moduli of 2.334 ± 0.153 GPa, 2.470 ± 0.114 GPa, and 2.282 ± 0.136 GPa, respectively. In other words, the modulus shows little increase beyond the addition of 3 wt % of CNTs (when direct blended), which is a frequent observation [9, 26, 28]. This could be due to poor dispersion of CNTs in the nanocomposite. Aggregation of CNT particles has been shown to reduce the amount of reinforcement that the CNTs can provide, resulting in less enhancement of the Young's modulus [45, 46]. As shown in Fig. 3.11, by using the $scCO_2$ aided processing method, the average moduli of samples at all CNT concentrations have higher values than the ones prepared by the direct blending method. Although their error bars overlap at lower concentrations, the diverging trend becomes more and more obvious as the CNT concentration increases. The Young's moduli of the CNT/PPSF prepared by the means of $scCO_2$ continue to

increase after 1 wt %. At 7 wt %, the Young's modulus is as high as 2.937 ± 0.176 GPa, a 38% improvement compared to the base matrix. This indicates an essential contribution of the $scCO_2$ technique to the melt blending process in terms of aiding the dispersion of the CNTs in the polymer matrix and, therefore, improves the nanocomposite mechanical properties.

The tensile strength results (shown in Table 3.1) of the nanocomposites show another advantage of the $scCO_2$ aided method. Pure PPSF used in this work has a tensile strength of 64.75 ± 1.14 MPa. Using 1 wt % CNTs prepared by the direct blending method leads to a slight increase in strength of 66.69 ± 2.39 MPa, while using the $scCO_2$ aided method only provided a tensile strength of 54.41 ± 5.70 MPa. This result is reasonable because the $scCO_2$ sample has a higher modulus and is more brittle. A slight decrease in tensile strength is acceptable. However, at a CNT concentration of 3 wt %, the tensile strength of the nanocomposites prepared by the $scCO_2$ aided method is 70.18 ± 0.68 MPa, outperforming the one prepared by the direct melt blending method which exhibits a tensile strength of 67.88 ± 0.64 MPa. At 7 wt % CNT loading, the tensile strength increases to 77.32 ± 6.18 MPa, which is a 19% increase relative to that of the pure PPSF. This is a significant improvement in tensile strength considering the modulus also improved significantly. It is probably due to the improved CNT dispersion achieved with the use of $scCO_2$ expanded CNTs.

Another critical set of mechanical properties, the values of elongation at break of the nanocomposites, are reported in Table 3.1 as well. Apparently, the increase in elastic modulus leads to a decrease in mechanical ductile properties. The elongation at break changed from around 12% for pure PPSL polymer to values between 3.18% to 5.39% for CNT filled PPSF nanocomposites.

3.4.2.4 Comparison of Modulus Values with Composite Theory

In order to realize the full potential of the mechanical property increase, it is necessary to compare the observed property enhancements, such as modulus, to those predicted by theories such as Halpin-Tsai model [47]. For aligned fiber composites, Halpin and Tsai's model, shown below in Eq. (1), assumes perfectly uniform dispersion and unidirectional oriented nanotubes, as well as a high degree of adhesion of the filler particles to the surrounding polymer matrix.

$$E_c = E_m \left[\frac{1+\xi\eta\phi_f}{1-\eta\phi_f}\right] \qquad (1)$$

where $\xi = 2l/D$ and

$$\eta = \frac{[E_f/E_m - 1]}{[E_f/E_m + \xi]} \qquad (2)$$

E_f, E_m and E_c are the filler modulus, matrix modulus and composite modulus, respectively. ϕ_f is the filler volume fraction and l/D is the aspect ratio of the filler particles. The length, l, and diameter, D, of CNTs are taken as 1.5 micron and 9.5 nanometers, respectively, based on material datasheet provided by the CNT supplier. The Young's modulus of a CNT is taken as 953 GPa, which is on the upper margin of the experimental results obtained by Yu et al. [48]. With the density of the matrix, ρ_m, equal to 1.29 g/ml and the density of CNTs, ρ_f, equal to 1.65 g/ml (calculated from the density of graphite by assuming that the outer diameter of the nanotubes was twice the inner [49]), the volume fraction of the CNTs, ϕ_f, can be found from the weight percentage, w_f, as

$$\phi_f = \rho_m w_f / (\rho_f - \rho_f w_f + \rho_m w_f) . \qquad (3)$$

The theoretical composite moduli with 1 wt %, 3 wt %, 5 wt % and 7 wt % of CNT are 7.19 GPa, 17.45 GPa, 27.92 GPa, and 38.59 GPa, respectively. The experimental Young's

moduli are significantly below those predicted by the Halpin-Tsai model. This may be due to some important issues such as lack of complete dispersion of CNTs as individual tubes, lack of complete orientation of the filler particles in the flow direction, lack of a high degree of adhesion of the CNTs to the matrix, and the aspect ratio may be less than the calculated value based on the individual tube dimension data. It should be noted that the nanocomposites in this work were prepared by heating up the pellets to the melt temperature and solidifying them while pressing. There was little flow of the melt during this post-processing and, thus, no preferential orientation of the nantoubes was achieved. Better mechanical properties are expected from injection molding or other post-processing technique after CNT orientation is acheieved, which is critical to the modulus of the composite.

3.5 Conclusions

The $scCO_2$ technique was successfully applied to CNT expansion and CNT/PPSF composite preparation. The significant bulk volume increase and disentangled CNTs observed in the SEM images lead us to believe that using $scCO_2$ is efficient in expanding entangled CNT bundles. CO_2 in the supercritical state retains a low viscosity with high density, which allows a large amount of CO_2 to penetrate into the gaps between CNT bundles as completely as possible, forcing the entangled CNT bundles apart as the CO_2 expands upon rapid depressurization. The CNTs gained a distended structure with bundles disentangled after the expansion procedure. The degree of CNT expansion was found to be positively correlated to chamber pressure and contacting time with CO_2. Optimized values of these two conditions should be determined by taking into consideration the equipment limitation and processing cost. The best operating temperature for the expansion process was found at an intermediate temperature around 80 °C. At this condition, ample penetration of the CO_2 into the CNT bundles can be achieved and the

amount of CO_2 is sufficient to ascertain the best separation of CNTs. Expanded CNTs were found to be easier to disperse into the polymer matrix during the blending procedure while retaining the distended structure to form more uniform networks based on microscopy observations. This explained the significant yield-behavior for the composite melts in their linear viscoelastic properties. CNT/PPSF composites prepared by the conventional direct melt compounding methods did not show any considerable improvements in the mechanical properties above the addition of 1 wt % CNTs due to their inability to adequately disperse the entangled CNTs into the polymer matrix. However, continuous improvement of the mechanical properties was seen as a function of increasing CNT concentrations up to 7 wt % for samples prepared using the $scCO_2$ aided method. The increase of Young's modulus was 38% for the CNT/PPFL nanocomposite prepared by $scCO_2$ method while the sample made using the direct blending only had a 7% increase. Better mechanical properties are expected from samples with further improvement in CNT dispersion and post-processing methods that may introduce orientation of CNTs, such as injection molding. This work shows the advantage of using the $scCO_2$ aided melt blending method in preparation of CNTs/polymer nanocomposite.

3.6 Acknowledgements

The authors would like to acknowledge the financial support from the Office of Naval Research (ONR) Small Business Technology Transfer (STTR) programs (Phase I, Grant number A-2006) through Nansonic, Inc. and the Institute for Critical Technology and Applied Science (ICTAS) at Virginia Tech. The authors would also like to thank Solvay Advanced Polymers, L.L.C. for donating PPSF polymer material. In addition, we would like to thank Steve McCartney at the Nanoscale Characterization and Fabrication Laboratory in ICTAS for aid in conducting the SEM studies.

3.7 References

[1] S. Iijima, Nature, 354 (1991) 56-58.

[2] M. Lebron-Colon, M.A. Meador, J.R. Gaier, F. Sola, D.A. Scheiman, L.S. McCorkle, ACS Appl. Mater. Interfaces, 2 (2010) 669-676.

[3] X. Zhang, T. Liu, T.V. Sreekumar, S. Kumar, V.C. Moore, R.H. Hauge, R.E. Smalley, Nano Lett., 3 (2003) 1285-1288.

[4] H.G. Jeon, H.T. Jung, S.W. Lee, S.D. Hudson, Polym. Bull., 41 (1998) 107-113.

[5] C.R. Tseng, J.Y. Wu, H.Y. Lee, F.C. Chang, Polymer, 42 (2001) 10063-10070.

[6] M.S.P. Shaffer, A.H. Windle, Advanced Materials, 11 (1999) 937-941.

[7] R. Krishnamoorti, R.A. Vaia, E.P. Giannelis, Chemistry of Materials, 8 (1996) 1728-1734.

[8] X.D. Cao, H. Dong, C.M. Li, L.A. Lucia, Journal of Applied Polymer Science, 113 (2009) 466-472.

[9] D.Y. Zhao, S.H. Wang, J. Wu, X.D. Bai, Q.Q. Lei, Pigm. Resin. Technol., 38 (2009) 305-309.

[10] L. Jin, C. Bower, O. Zhou, Appl. Phys. Lett., 73 (1998) 1197-1199.

[11] S. Badaire, P. Poulin, M. Maugey, C. Zakri, Langmuir, 20 (2004) 10367-10370.

[12] A.A. Koval'chuk, A.N. Shchegolikhin, V.G. Shevchenko, P.M. Nedorezova, A.N. Klyamkina, A.M. Aladyshev, Macromolecules, 41 (2008) 3149-3156.

[13] S. Kumar, T. Rath, B.B. Khatua, A.K. Dhibar, C.K. Das, J. Nanosci. Nanotechnol., 9 (2009) 4644-4655.

[14] K. Saeed, S.Y. Park, Journal of Applied Polymer Science, 106 (2007) 3729-3735.

[15] Z.J. Jia, Z.Y. Wang, C.L. Xu, J. Liang, B.Q. Wei, D.H. Wu, S.W. Zhu, Mater. Sci. Eng. A-Struct. Mater. Prop. Microstruct. Process., 271 (1999) 395-400.

[16] Y. Kojima, A. Usuki, M. Kawasumi, A. Okada, T. Kurauchi, O. Kamigaito, J. Polym. Sci. Pol. Chem., 31 (1993) 983-986.

[17] A. Usuki, M. Kawasumi, Y. Kojima, A. Okada, T. Kurauchi, Kobunshi Ronbunshu, 52 (1995) 440-444.

[18] A. Usuki, Y. Kojima, M. Kawasumi, A. Okada, Y. Fukushima, T. Kurauchi, O. Kamigaito, J Mater Res, 8 (1993) 1179-1184.

[19] Z. Spitalsky, G. Tsoukleri, D. Tasis, C. Krontiras, S.N. Georga, C. Galiotis, Nanotechnology, 20 (2009).

[20] T. Lan, T.J. Pinnavaia, Chem. Mater., 6 (1994) 2216-2219.

[21] J.B. Gao, M.E. Itkis, A.P. Yu, E. Bekyarova, B. Zhao, R.C. Haddon, J. Am. Chem. Soc., 127 (2005) 3847-3854.

[22] R.E. Gorga, R.E. Cohen, J. Polym. Sci. Pt. B-Polym. Phys., 42 (2004) 2690-2702.

[23] T.X. Liu, I.Y. Phang, L. Shen, S.Y. Chow, W.D. Zhang, Macromolecules, 37 (2004) 7214-7222.

[24] J.M. Yuan, Z.F. Fan, X.H. Chen, Z.J. Wu, L.P. He, Polymer, 50 (2009) 3285-3291.

[25] G.X. Chen, H.S. Kim, B.H. Park, J.S. Yoon, Polymer, 47 (2006) 4760-4767.

[26] J.Y. Kim, Journal of Applied Polymer Science, 112 (2009) 2589-2600.

[27] H. Deng, E. Bilotti, R. Zhang, T. Peijs, Journal of Applied Polymer Science, 118 (2010) 30-41.

[28] T. McNally, P. Potschke, P. Halley, M. Murphy, D. Martin, S.E.J. Bell, G.P. Brennan, D. Bein, P. Lemoine, J.P. Quinn, Polymer, 46 (2005) 8222-8232.

[29] P. Maiti, M. Okamoto, Macromol. Mater. Eng., 288 (2003) 440-445.

[30] G.M. A.J. Lesser, in: ANTEC 2004, 2004, pp. 1528-1532.

[31] C.W Manke, E. Gulari, D.F Mielewski, E.C Lee, U.S. Patent 6,753,360 (2002)

[32] D.F. Mielewski, E.C. Lee, C.W. Manke, E. Gulari, U.S. Patent 6,469,073 (2004)

[33] Q.T. Nguyen, D.G. Baird, Polymer, 48 (2007) 6923-6933.

[34] Z.M. Liu, X.H. Dai, J. Xu, B.X. Han, J.L. Zhang, Y. Wang, Y. Huang, G.Y. Yang, Carbon, 42 (2004) 458-460.

[35] J. Steinmetz, S. Kwon, H.J. Lee, E. Abou-Hamad, R. Almairac, C. Goze-Bac, H. Kim, Y.W. Park, Chem. Phys. Lett., 431 (2006) 139-144.

[36] J. SteinmetZ, H.J. Lee, S. Kwon, D.S. Lee, C. Goze-Bac, E. Abou-Hamad, H. Kim, Y.W. Park, Curr. Appl. Phys., 7 (2007) 39-41.

[37] B.H. Yue, Y.B. Wang, C.Y. Huang, R. Pfeffer, Z. Iqbal, J. Nanosci. Nanotechnol., 7 (2007) 994-1000.

[38] W.J. Boo, L. Sun, G.L. Warren, E. Moghbelli, H. Pham, A. Clearfield, H.J. Sue, Polymer, 48 (2007) 1075-1082.

[39] D.S. Bangarusampath, H. Ruckdaschel, V. Altstadt, J.K.W. Sandler, D. Garray, M.S.P. Shaffer, Polymer, 50 (2009) 5803-5811.

[40] G.D. Barber, B.H. Calhoun, R.B. Moore, Polymer, 46 (2005) 6706-6714.

[41] S. Pujari, T. Ramanathan, K. Kasimatis, J. Masuda, R. Andrews, J.M. Torkelson, L.C. Brinson, W.R. Burghardt, J. Polym. Sci. Pt. B-Polym. Phys., 47 (2009) 1426-1436.

[42] K. Masenelli-Varlot, E. Reynaud, G. Vigier, J. Varlet, J. Polym. Sci. Pt. B-Polym. Phys., 40 (2002) 272-283.

[43] W.J. Boo, L.Y. Sun, J. Liu, E. Moghbelli, A. Clearfield, H.J. Sue, H. Pham, N. Verghese, J. Polym. Sci. Pt. B-Polym. Phys., 45 (2007) 1459-1469.

[44] Q.T. Nguyen, D.G. Baird, Advances in Polymer Technology, 25 (2006) 270-285.

[45] in.

[46] X.L. Xie, Y.W. Mai, X.P. Zhou, Mater. Sci. Eng. R-Rep., 49 (2005) 89-112.

[47] J.C. Halpin, J.L. Kardos, Polym. Eng. Sci., 16 (1976) 344-352.

[48] M.-F. Yu, O. Lourie, M.J. Dyer, K. Moloni, T.F. Kelly, R.S. Ruoff, Science, 287 (2000) 637-640.

[49] M.S.P. Shaffer, X. Fan, A.H. Windle, Carbon, 36 (1998) 1603-1612.

Figure 3.1: Photo picture of carbon nanotubes with same weight (0.10g) before (left) and after (right) expansion using supercritical CO_2

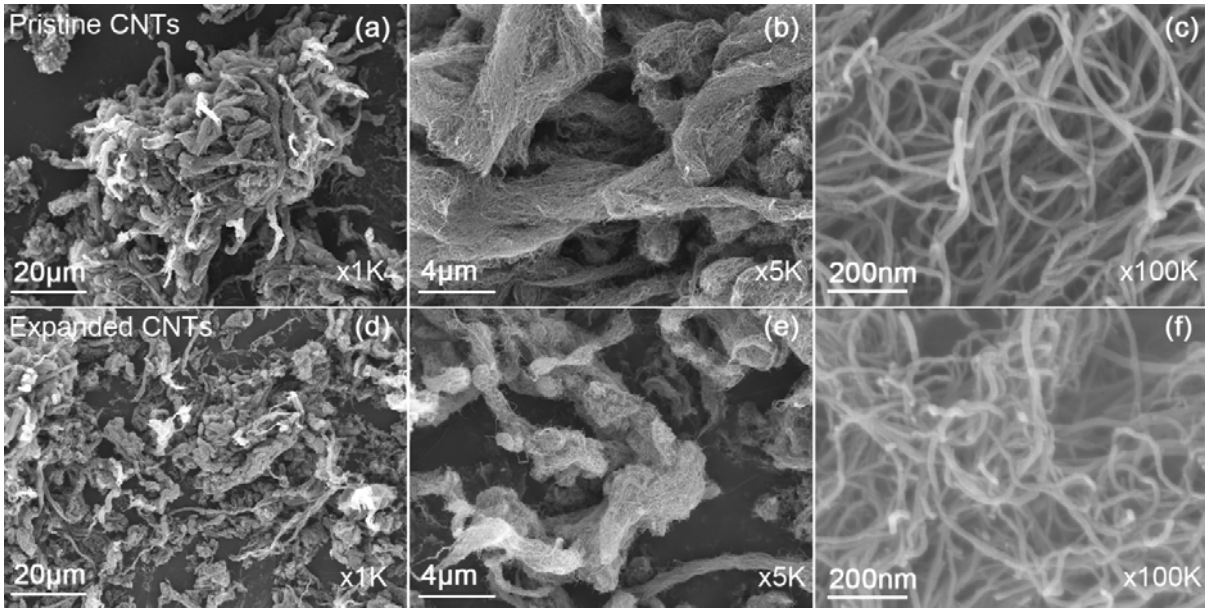

Figure 3.2: Scanning electron micrographs of pristine carbon nanotubes (a-c) and expanded carbon nanotubes (d-f) at (a, d) 1K magnification, (b, e) 5K magnification, or (c, f) 100K magnification

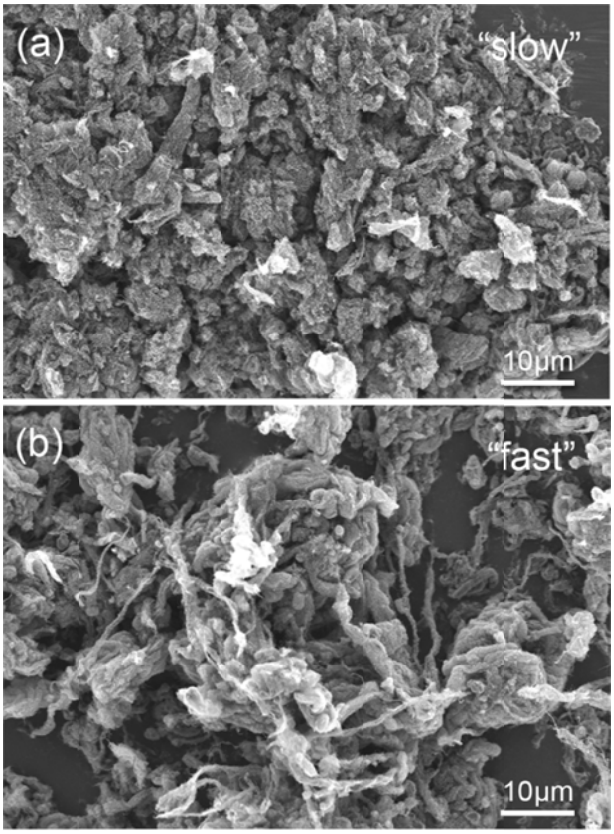

Figure 3.3: Scanning electron micrographs of carbon nanotubes expanded at (a) slow or (b) fast depressurization rates with other processing conditions fixed (temperature: 80 ^{o}C, pressure: 3000 psi, and exposure time: 1 hr)

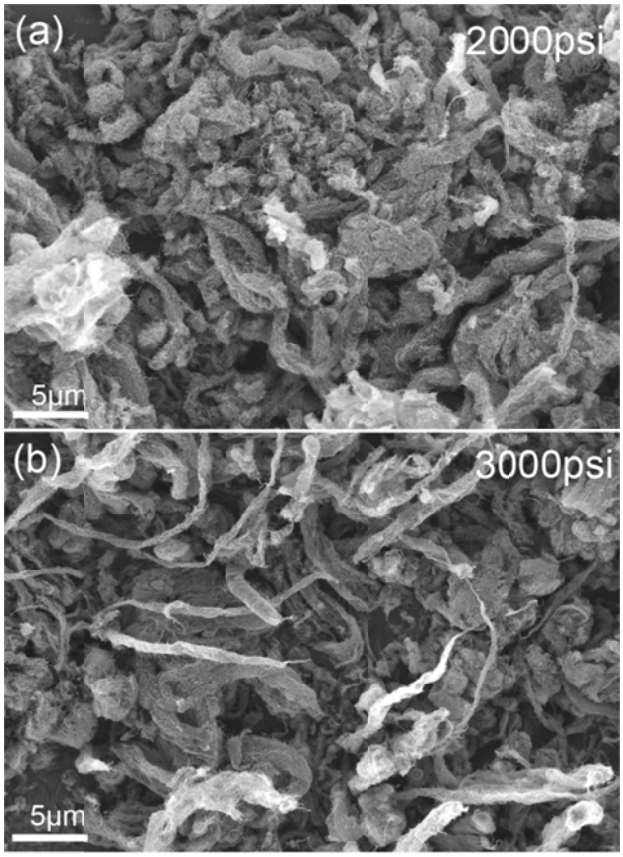

Figure 3.4: Scanning electron micrographs of carbon nanotubes exposed to $scCO_2$ at pressures of (a) 2000 psi or (b) 3000 psi with other processing conditions fixed (temperature: 80 ^{o}C, depressurization rate: fast, and exposure time: 12 hr)

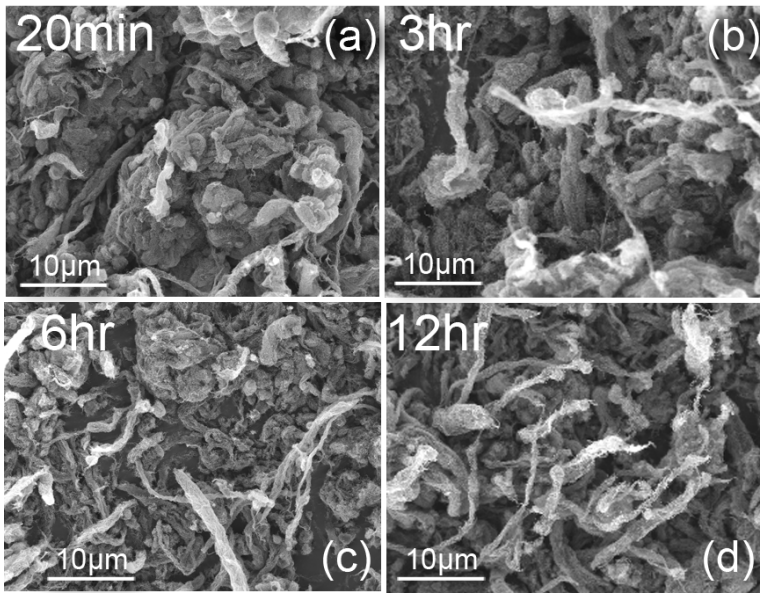

Figure 3.5: Scanning electron micrographs of carbon nanotubes exposed to $scCO_2$ for (a) 20 min, (b) 3 hr, (c) 6 hr, or (d) 12 hr with other processing conditions fixed (temperature: 80 ^{o}C, pressure: 3000 psi, and depressurization rate: fast)

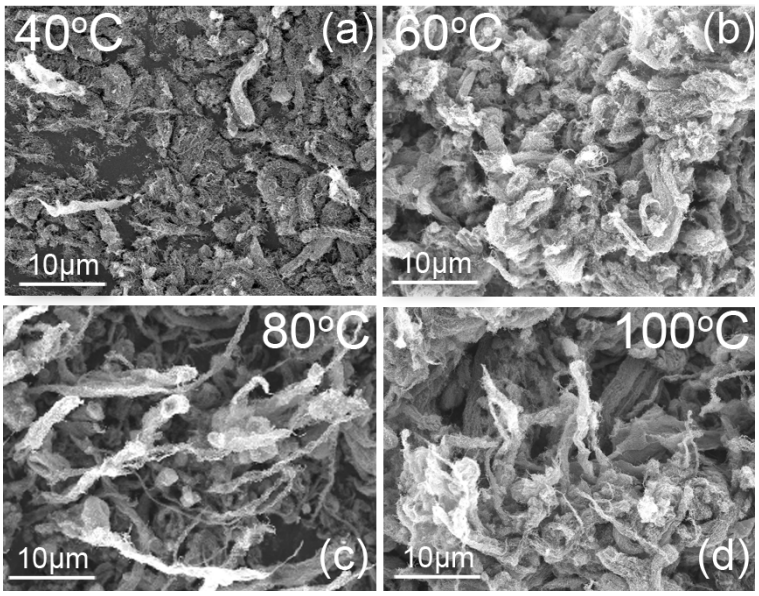

Figure 3.6: Scanning electron micrographs of carbon nanotubes exposed to $scCO_2$ at the temperature of (a) 40 ^{o}C (b) 60 ^{o}C, (c) 80 ^{o}C, or (d) 100 ^{o}C with other processing conditions fixed (pressure: 3000 psi, exposure time: 12 hr, and depressurization rate: fast)

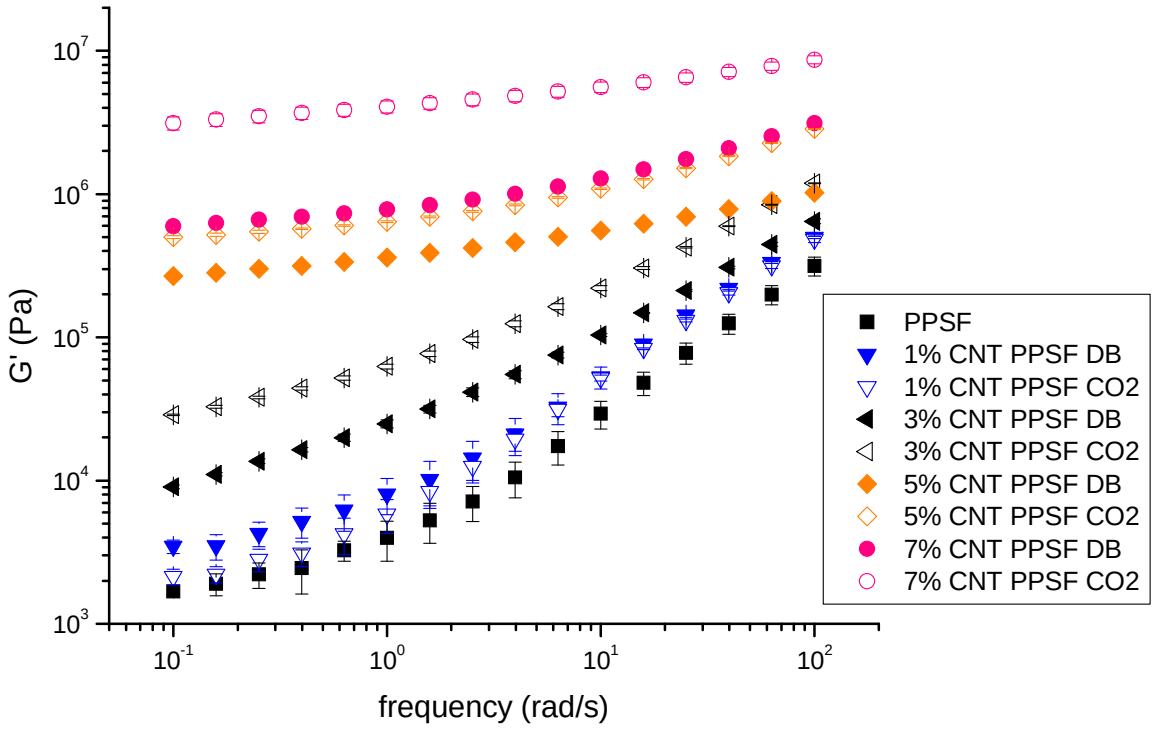

Figure 3.7: Storage modulus, *G'*, vs. frequency, ω, for the carbon nanotubes/PPSF nanocomposites prepared by $scCO_2$ aided method (labeled as CO2, hollow symbols) and direct blending method (labeled as DB, solid symbols) at 350 °C

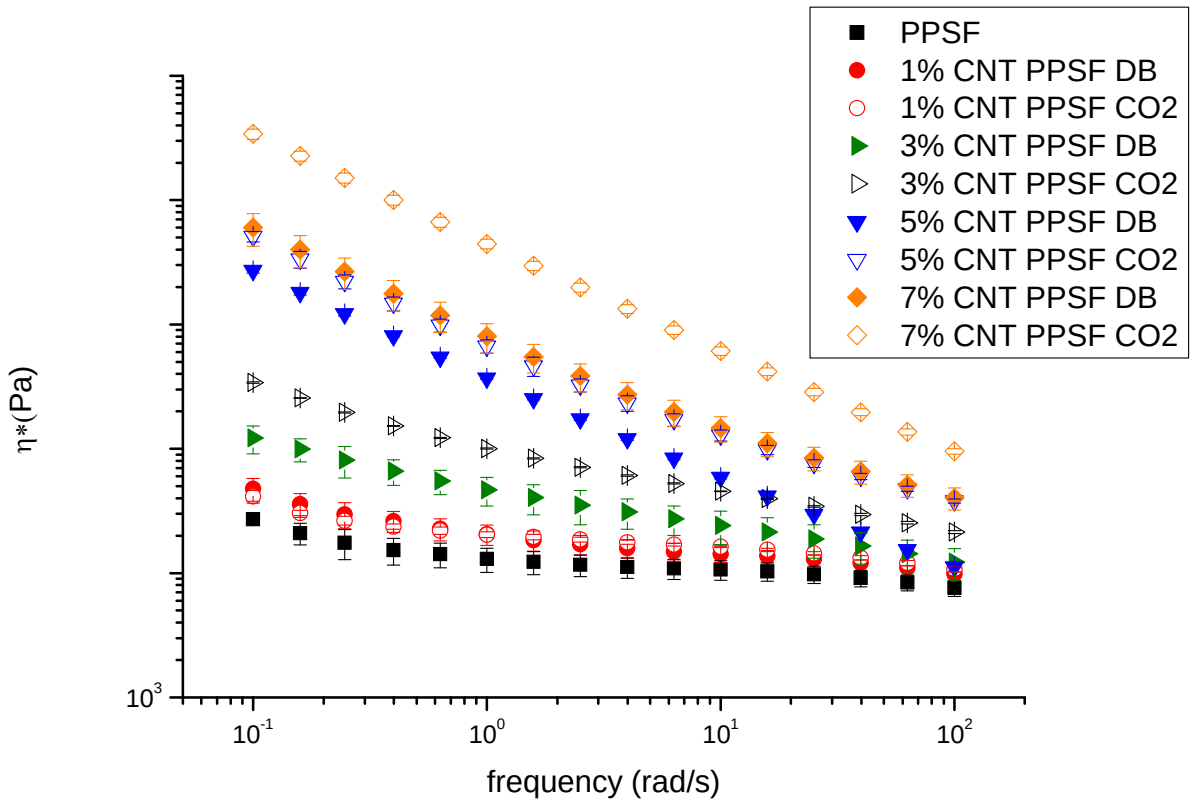

Figure 3.8: Complex viscosity, $|\eta^*|$, vs. frequency, ω, for the carbon nanotubes/ poly(phenylsulfone) nanocomposites prepared by $scCO_2$ aided method (labeled as CO2, hollow symbols) and direct blending method (labeled as DB, solid symbols) at 350 °C

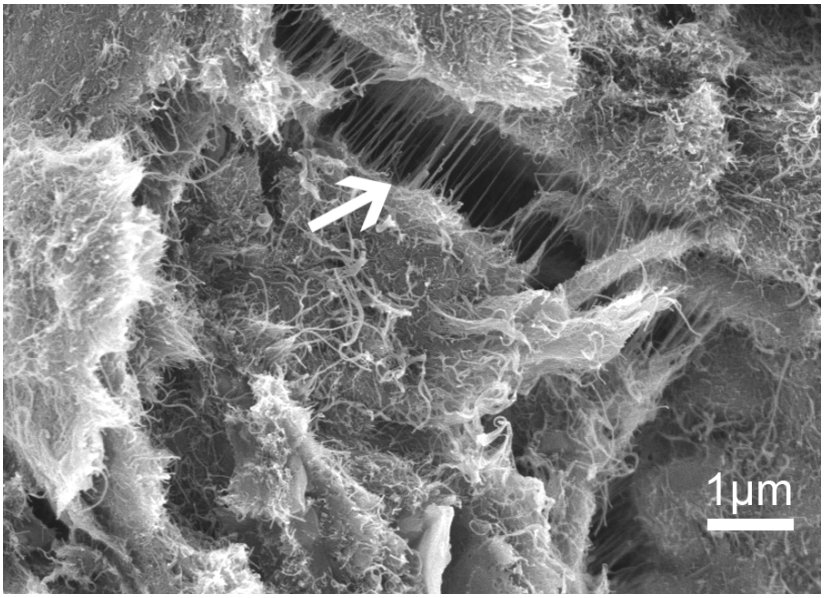

Figure 3.9: Scanning electron micrographs of the fracture surface of 1 % carbon nanotube/poly(phenylsulfone) nanocomposites processed by $scCO_2$ aided method showing the carbon nanotube strings pulled out from the bulk material

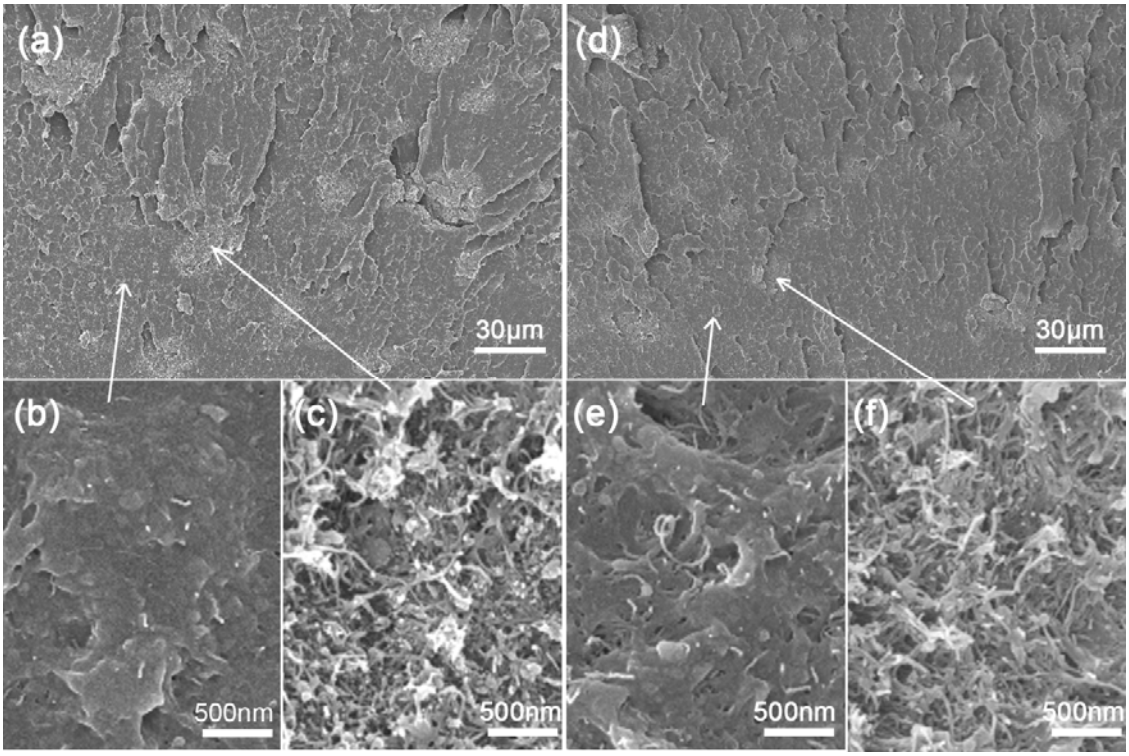

Figure 3.10: Scanning electron micrographs of 7 % carbon nanotube/poly(phenylsulfone) nanocomposites processed by direct blending method (a-c) and the $scCO_2$ aided method (d-f). (b, e) and (c, f) show the CNT well dispersed region and aggregated region, respectively, for the indicated samples.

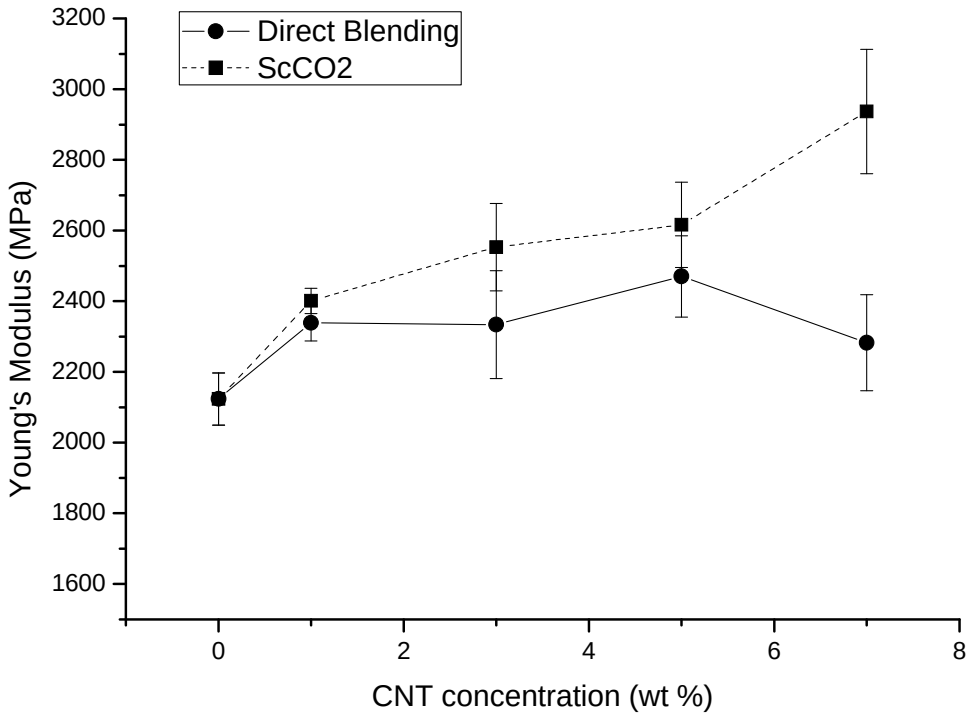

Figure 3.11: Young's modulus of carbon nanotube/poly(phenylsulfone) composite processed by direct blending (dash) and $scCO_2$ aided method (solid)

Table 3.1: Mechanical properties of carbon nanotube/poly(phenylsulfone) nanocomposite prepared using different processing methods

Materials	Young's Modulus (GPa)	S.D.	% Increase	Yield Strength (MPa)	S.D.	% Elongation	S.D.
Pure PPSF	2.124	0.074	-	64.75	1.14	12.23	2.14
1% CNT/PPSF DB	2.339	0.054	10	66.69	2.39	5.39	0.67
1% CNT/PPSF CO2	2.401	0.036	13	54.40	5.70	3.51	1.01
3% CNT/PPSF DB	2.334	0.153	9	67.88	0.64	3.47	0.55
3% CNT/PPSF CO2	2.553	0.124	20	70.18	0.68	3.53	0.30
5% CNT/PPSF DB	2.470	0.114	16	67.25	4.82	5.00	0.60
5% CNT/PPSF CO2	2.615	0.120	23	71.00	3.82	3.18	0.50
7% CNT/PPSF DB	2.282	0.136	7	73.69	2.53	5.18	0.07
7% CNT/PPSF CO2	2.937	0.176	38	77.32	6.18	4.18	1.07

Chapter 4

The Preparation of Nano-Clay/Polypropylene Composite Materials with Improved Properties Using Supercritical Carbon Dioxide and a Sequential Mixing Technique

The Preparation of Nano-Clay/Polypropylene Composite Materials with Improved Properties Using Supercritical Carbon Dioxide and a Sequential Mixing Technique

Chen Chen[a], Joseph Samaniuk[a], Donald G. Baird[a,*], Gilles Devoux[b], Robert B. Moore[b], John P. Quigley[a]

[a] Department of Chemical Engineering, Virginia Polytechnic Institute and State University, Blacksburg, Virginia 24061

[b] Department of Chemistry, Virginia Polytechnic Institute and State University, Blacksburg, Virginia 24061

4.1 Abstract:

The use of supercritical carbon dioxide ($scCO_2$) as a processing aid to help exfoliate nano-clays and improve their dispersion during melt blending in polymer matrices has been reported in the literature. The collapse of the nano-clay platelets after reaching a certain concentration level has become an issue that has prevented continuous enhancement in mechanical properties at high clay content. In this work, a semi-continuous process using $scCO_2$ is reported for processing polymer-clay composites with high clay loading (i.e. 10 wt%) by reducing the collapse of the exfoliated clays. Two major modifications are involved in the new procedure: exfoliating the nano-clay directly into the hopper filed with pellets followed by processing the composite immediately and sequentially mixing the clay into the melt. This latter approach helped to minimize the clay collapse when processing the composites with high clay loadings. Transmission electron microscopy (TEM) and wide angle X-ray diffraction (WAXD) results are provided to investigate the effect of sequential mixing on reducing the clay collapse in the nanocomposite. Surface modified montmorillonite (MMT) nano-clay/polypropylene (PP) composite at 10 wt % nano-clay with improved clay dispersion was obtained with increased modulus and tensile strength of 63 % and 16%, respectively, compared to the pure PP matrix.

4.2 Introduction

Polymer-clay nanocomposites have attracted tremendous interest over the past two decades because of their potential enhanced thermal, barrier, physical, and mechanical properties compared to other types of composite materials, such as glass-filled polymer composites. In 1993, the Toyota research group revealed a major breakthrough by successfully preparing nano-clay/nylon-6 composites using *in situ* polymerization [1]. The group found a 68% increase in tensile modulus, a 224% increase in flexural modulus, and an 87% increase in the heat distortion temperature relative to neat polymer material with the addition of 4.7 wt% clay. The study of polymer-clay composites has since been extended to others polymer systems, including polycarbonate [2], polyurethane [3], poly(vinyl chloride) [4], polypropylene [5], and epoxy [6]. However, the improvements of the composite mechanical properties are not as significant as for the case of nylon-6.

The properties of polymer-clay nanocomposites are significantly related to the clay morphology in polymer matrices. Particle aggregation decreases the particle surface area and effective aspect ratio, resulting in limited enhancement of composite properties. Among the three most common morphologies, phase separated, exfoliated and intercalated, the phase separated morphology is least desired, where the polymer does not enter the clay spacing galleries and the material only gains micro-scale reinforcement. The intercalated and exfoliated morphology both involve nano-scale reinforcement. Intercalated clay morphology occurs when polymer chains diffuse into the gallery spacings of layered structure, resulting in a gallery distance on the order of a few nanometers [7]. If the clay layers are completely pushed apart to create a disordered array, the composite is considered to be “exfoliated”. One of the main challenges in preparing nano-clay composites is to overcome the attractions of the stacked silicate layers and disperse

them into the polymer matrix in order to achieve the exfoliated state, or if not, the intercalated state.

The first step toward good dispersion of the nano-clay in a matrix is organic modification of the inorganic nano-clay particle surface. In the pristine state, montmorillonite (MMT) nano-clay contains hydrated Na^+ or K^+ cations in the gallery spacings and is not compatible with non-polar polymers such as polypropylene [7]. Ion-exchange reactions, utilizing cationic surfactants such as quarternary alkylammonium cations, render the normally hydrophilic surface hydrophobic compatibilizing the interface for interactions with non-polar polymers [8, 9]. In addition, cation exchange carried out with long chain surfactant molecules such as hydrogenated tallow increase the gallery spacing between the silicate layers. The increase of gallery spacing helps to separate the stacked nano-clay layers and is beneficial for the final composite properties.

The next step in effective nanoparticle dispersion is the combination of polymer and nano-filler by a compounding method. Various methods have been used to compound the clay with the polymer matrix, including *in situ* polymerization [10], solution blending [11, 12], and melt blending [13, 14]. A major disadvantage of *in situ* polymerization and solution blending method is the organic solvent usually involved, which can be costly and environmentally hazardous. Conversely, melt blending processing is more economical, flexible for formulation, and compatible with commercial practice [15]. However, the homogeneous dispersion of nano-clays and resulting significant properties improvements was achieved only in polymers containing polar functional groups. For example, Chavarria and Paul [16] prepared nylon-6 composites by melt blending using a twin screw extruder. They showed increases of modulus and yield strength of 67% and 31%, respectively, with the addition of 4.9 wt% MMT. Conventional melt blending is not as effective in the case of non-polar polymer matrices.

To improve the dispersion of nano-clay in the composite, compatibilizers or processing aids are usually used during melt intercalation. Maleic anhydride grafted PP (PP-g-MA) was proved to be effective in facilitating the intercalation of PP in nano-clay platelets [5, 17]. However, a large amount of PP-g-MA must be used in order to achieve a good level of intercalation at high clay concentration. This can be expensive and may reduce the nanocomposite's elongation at break significantly. Pascual et al. [18] showed that using PP-g-MA as a compatibilizer to prepare nano-clay composite increased the elastic modulus of the nanocomposite, but the elongation at break of the materials changeed from 440% for pure PP to around 12% for clay filled PP composites. Santos et al. [19] reported using two other types of processing aids, poly(propyleneglycol) (PPG) and EMCA (65% paraffinic carbon, 12% naphthenic carbon and 23% aromatic carbon), to prepare PP/nano-clay composites. PPG showed a better affinity than EMCA for aiding the dispersing clay into the polymer matrix and the impact strength of the composites increased by a factor of 3 (at clay concentration of 5 wt%) because of its polarity. However, both of the processing aids resulted in reduced flexural moduli.

The use of supercritical carbon dioxide ($scCO_2$) to exfoliate nano-clay coupled with the melt blending method has been considered as an alternative route for the preparation of polymer-clay nanocomposites in order to overcome some of the issues of using conventional melt intercalation with a compatibilizer or processing aids [20-23]. Lesser et al. [20] used a modified hopper in the feed section of the extruder to allow polymer and clay to interact with $scCO_2$ before processing. It was found that the presence of $scCO_2$ increased the clay d-spacing by as much as 100%, and a nanocomposite with an intercalated structure was produced. However, mechanical properties of the nanocomposites were not reported. Alternately, Manke et al. [22] developed a process that allows clay particles to be pre-treated with $scCO_2$ in a pressurized

vessel and then catastrophically depressurized to atmospheric pressure so that the stacked nano-clay platelets were forced apart. The presence of exfoliated nano-clay particles was identified by wide angle X-ray diffraction (WAXD). However, they did not provide any procedure for combining the clay particles with polymers and any mechanism for assuring that the exfoliated particles remained exfoliated once combined with the polymer at high temperature. Two years later, the same group developed a procedure to combine polymer and nano-clay in presence of $scCO_2$ [21]. In this approach, the clay and polymer pellets were loaded through two separate hoppers into the extruder and $scCO_2$ was injected into the hopper containing the clays. The patent claimed that two factors result in the exfoliation of nano-clays: 1) decreased viscosity of composite melt caused by $scCO_2$ as a plasticizer, and 2) CO_2 nucleation and expansion within the extrudates when exiting the extruder die. However, no WAXD or TEM evidence of an exfoliated morphology was presented and no mechanical properties were provided. In a different procedure, Nguyen et al. [23] developed a method to combine the benefits of melt compounding with the exfoliating capability of $scCO_2$. The process relied on rapid expansion of the clay followed by direct injection into the extruder. It was observed in the WAXD data that the composite contained a high degree of exfoliated nano-clay for concentrations as high as 6.6 wt%. The Young's modulus of the composites increased by 54% at this nano-clay loading. Nguyen's technique ensured that the clay stay exfoliated as the nanoparticles were processed immediately following exfoliation. However, the improvement on clay dispersion and composite mechanical properties was not observed beyond the addition of 6.6 wt % in this method, which may have been due to the size of the equipment. In addition, a special two-stage screw extruder is required for this procedure. The process in its present form is only a batch operation because the continuous feeding of the clay cannot be achieved.

In this study, we first develop a process that is as effective as Nguyen's method [23] in terms of improving the composite mechanical properties, but requires simpler operation and facilities. The comparison of these two systems is shown schematically in Fig. 4.1. It uses a pressurized CO_2 chamber to assist in the exfoliation of the clay into the extruder hopper, followed by melt compounding using a single-screw extruder. This process keeps the important feature of Nguyen's method by minimizing the time between clay exfoliation and the melt blending process. The limit of 6.6 wt% clay loading on property improvements is then investigated. A further modification is developed in order to accommodate the $scCO_2$ aided melt blending method to processing composites with higher clay loadings (i.e. 10 wt%). It involves a sequential addition and further mixing of the clay into the polymer matrix. A series of 10 wt% nano-clay/PP composites is then prepared by different processing methods and examined to deduce the effect of these techniques, including the use of $scCO_2$ and sequential mixing, on the composite properties. Composites with higher clay loadings are not included in this paper due to the reduced processability and only a gradual increase of the mechanical properties.

4.3 Experimental

4.3.1 Materials

The polymer matrix used in this work is polypropylene (Pro-Fax 6523) which was obtained from Lyondell Basell (Houston, TX) and was used as received. The melt index of the polymer is 4 g/10 min at 230 °C and at a load of 2.16 kg. The nano-clay used was surface modified montmorillonite (Cloisite 20A), which was obtained from Southern Clay Products, Inc. (Gonzalez, TX) and was used as-received. Cloisite 20A is a surface modified montmorillonite obtained through a cation exchange reaction, where the sodium cation is replaced by dimethyl, dihydrogenated tallow, quaternary ammonium cation.

4.3.2 Clay Concentration

Clay concentrations were determined by a burn-off technique in an ashing oven at 500 °C for 2 hr. The reported concentrations are an average of three burn-off samples. The clay concentrations reported here include the intercalants or the organic modifiers.

4.3.3 Preparation of Nano-clay/PP Composites

Four different processing methods were used in this work in order to reveal the relationships between the processing routes and composite morphologies. Table 4.1 shows the abbreviations used to refer to the individual processing method that will be introduced below in the rest of the article.

The first method is referred to as $scCO_2$ aided melt blending method. It is simplified from a procedure developed by Nguyen et al. [23] in our laboratory, and involves exfoliating the nano-clay directly into the hopper filled with polymer pellets and followed by processing the composite immediately. Before melt compounding, PP pellets and organic modified nano-clays were dried separately at 80 °C overnight. The nano-clays were then put in a pressurized chamber and allowed to be in direct contact with $scCO_2$ at 3000 psi and at 80 °C for 12 hr. The dried PP pellets were put into a 5 gal pressure vessel. The nano-clay and PP pellets were mixed as the clay was released rapidly with the CO_2 into the 5 gal pressure vessel. The nano-clay and polymer mixture was then collected and fed into the extruder hopper. A pressure chamber of 660 ml was used to contain nano-clays and was obtained from Parr Instrument Company (Moline, IL). The inlet/outlet of the chamber was sealed by a ball valve from High Pressure Equipment Company (Erie, PA). PP/clay mixture was then extruded at a melt temperature of approximately 190 °C and a screw speed of 20 rpm using a single screw extruder (Killion 4335 series) with a 25.4 mm (1 in) diameter and an L/D of 20:1. A capillary die of 1.59 mm diameter and 20:1 L/D was

attached to the end of the extruder. The nanocomposite were then chopped into pellets and dried at 80°C in an air circulation oven overnight. The dried composite pellets were injection molded with an Arburg Allrounder (model 221-55-250) injection molding machine. The Arburg Allrounder operated with a 22-mm diameter barrel, L/D of 24:1, and a screw with a variable root diameter from approximately 14.25 mm at the feed to 19.3 mm at the exit. A check ring non-return valve and an insulated nozzle that was 2 mm in diameter were included in the apparatus. The composites were injection molded with a melt temperature of 200 °C, a mold temperature of 80 °C, a holding pressure of 5 bar, a screw speed of 200 rpm, and a rectangular end-gated mold with dimensions 80 x 76 x 1.5 mm^3.

Another approach was the modification of the $scCO_2$ aided melt blending method which consisted of the sequential adding and mixing of nano-clays with the polymer pellets and extruded composite pellets. This method is referred to as $scCO_2$ aided method with sequential mixing. It is modified based on the $scCO_2$ aided melt blending method just described. It is used to prepare the high clay loading sample of 10 wt % in this study. First, the 5% clay/PP composite pellets were obtained using $scCO_2$ aided melt blending. Second, the dried 5% composite pellets were put back in the 5 gal pressure vessel to mix with more released clays yielding a total clay concentration of 10 wt %. The mixture of the 5 wt % composite pellets and the nano-clay was fed into the hopper of the injection molding machine and nanocomposite plaques containing 10 wt % of nano-clay were obtained.

In addition to the two methods just described, the conventional direct blending method was used to prepare nanocomposites for comparison purposes. This method is referred to as the direct blending method. In this approach, the organically modified nano-clay was used as

received. The clay and PP were mechanically mixed in a Kitchen Aid type mixer and dried together at 80 °C overnight. The mixture was then fed to an extruder and re-pelletized.

In the last procedure, direct blending method was used as the first step in the sequential mixing procedure to prepare a 10 wt % clay/PP sample for comparison purposes as well. In this method, the clay and PP were mechanically mixed and extruded to form 5% clay/PP composite pellets. The mixture of the 5 wt% composite pellets and the nano-clay was dry blended again and fed into hopper of the injection molding machine and nanocomposite plaques containing 10 wt % of nano-clay were obtained. This method is referred to as direct blending method with sequential mixing.

4.3.4 Tensile Properties

The injection-molded plaques were cut into rectangular bars lengthwise along the flow direction and were approximately 6 mm wide, 1.5 mm thick, and 80 mm long. Tensile tests on these bars were performed at room temperature with an Instron Model 4204 testing machine (Instron, Grove City, PA). An extensometer was used to accurately measure Young's modulus. The load was measured with a 5-kN load cell, and the crosshead speed was kept at 1.27 mm/min during all tensile tests. For all tests, the average and the standard deviation were calculated from at least six samples, and data points greater than 2 standard deviations from the mean were omitted.

4.3.5 Rheological Properties

Rheological measurements on the nanocomposites were performed using an ARES rheometer from TA Instruments. The 1.5 mm thick injection molded plaques were stamped into 25 mm diameter disks. Dynamic frequency sweep experiments were performed under a continuous nitrogen atmosphere using a 25 mm parallel plate fixture at 200 °C in the linear

viscoelastic region of the materials. The linear viscoelastic limit was determined using strain sweeps at a frequency of 10 rad/s and at the same temperature (200°C), and it was found that dynamic frequency sweep experiments could be conducted at a strain of 5%. The elastic moduli (G'), loss moduli (G''), and complex viscosities (η^*) of the materials as functions of angular frequency (ω) (ranging from 0.1 rad/s to 100 rad/s) were obtained at a temperature of 200°C.

4.3.6 Structure and Morphological Characterization

The state of exfoliation and morphology of pure clay was determined using WAXD obtained by means of a Scintag XDS 2000 diffractometer (wavelength of 1.542 nm). The data were obtained in the range of the scattering angle, 2θ, from 1.5° to 10° at a scanning rate of 0.1°/min and a step size of 0.05°. Due to the facility availability, the WAXD characterization for the polymer-clay nanocomposite structure was conducted using a different X-ray diffractometer (Rigaku Ultima III X-ray diffractometer) with Cu Ka radiation (wavelength of 1.542 nm) operating at 40 kV and 44 mA at a step size of 0.01° and a scan rate of 0.5°/min from 2° to 10°. Injection molded nanocomposite samples were ground into a powder using a rotating blade micro-grinder before WAXD analysis. Particle size was controlled by using an ultrafine metal mesh for separation purposes.

Transmission electron microscopy (TEM) was used as a supplemental technique to the WAXD measurements. TEM measurements were generated with a Philips EM420T with an accelerating voltage of 100 kV. The TEM samples, around 70 nm thick, were cut with a cryomicrotom equipped with a diamond knife at -60 °C. Injection molded samples were used for the TEM measurements.

4.4 Results and Discussion

4.4.1 X-ray diffraction analysis

X-ray diffraction was first used to determine the clay morphology changes with different storage time after exfoliation. The degree of exfoliation was justified based on the diffraction peak position and peak intensity. A lower 2θ value of a peak indicates a higher d-spacing due to Bragg equation:

$$2d\sin\theta = n\lambda \qquad (1)$$

where d represents the average basal spacing between silicate sheets, θ represents the diffraction angle, n is the wave number, and λ is the X-ray wavelength which is 1.542 nm. Consequently, the degree of clay dispersion and exfoliation is understood to be better if the peak is positioned at lower diffraction angles. As the peak intensity implies the concentration of the ordered structure, a lower peak means, therefore, less ordered structure and a higher degree of exfoliation with the same testing conditions and same clay level of the samples. Repeat WAXD measurements on the same sample prepared multiple times reveal that basal spacings from 2θ values are accurate to within 2%.

The WAXD patterns of the nanoclay (Cloisite 20A) showing the time sensitivity of the degree of exfoliation since release of the CO_2 are illustrated in Fig. 4.2. It's clear that the WAXD peak intensity at $2\theta \sim 3.5°$ increases with increasing storage time following exfoliation. The diffraction peak intensity is related to the concentration of ordered structure correspondening to that degree of spacing. With the testing conditions fixed, a diffraction peak with higher intensity implies less exfoliated structure and, therefore, the possible collapse of the previously separated silicate clay layers. The nano-clay tested 4 weeks after the exfoliation process showed a diffraction peak almost as high as the as-received clays without the $scCO_2$ treatment. This

implied that the clays require immediate processing once exfoliated. In addition, mechanical dry blending, such as that suggested in Manke's procedure [22], might cause a loss in the degree of exfoliation of the nano-clays. In Nguyen's method [23], the nano-clay was released into the extruder to coat the polymer pellets and processed immediately. This could be one of the reasons that Nguyen's method showed improved properties relative to the other methods involving the use of $scCO_2$. In the method proposed in this work, the nano-clay was released into the larger vessel and fed into the extruder immediately for processing. This ensures that the clay collapse is minimized. Conceptually, the clay can be released into a modified hopper to further shorten the storage time.

The WAXD patterns of the composite pellets and the injection molded plaques are compared in Fig. 4.3 in order to reveal the effect of the processing time on composite morphology. The injection molded composites were heated up to the melting temperature and mixed in the screw a second time during injection molding and, therefore, had one more processing cycle and a longer processing time than the pellets. It is clear that the diffraction peak of the 5% MMT/PP plaques shifted to a higher 2θ angle of 3.91° from the composite pellets with the same clay loading and processing method of 3.57°. The intensity of the peak also increased for the composite plaque. These two facts indicated that the d-spacings of the silicate layers decreased, and the degree of the clay dispersion decreased with longer processing times, which is evidence for the clay collapsing during processing at high temperatures and shear rate. Nguyen et al. [23] also reported similar observations. Their 6.6 wt% MMT/PP composite regained a WAXD peak after being injection molded. The difference between the two 10 wt% samples was less significant. A slight increase of peak intensity can be observed for higher clay loading samples with the addition of 10 wt% nano-clay as well. The peak shifting was not obvious. This

might be because most silicate layers of the nano-clay already collapsed during extrusion at this high clay loading. Therefore, to avoid processing the composite at high clay loading is necessary in order to prevent the silicate layers from collapsing.

The morphology of the 10 wt% MMT/PP nanocomposites prepared by the four different processing methods (DB, CO2, DB S, CO2 S) was also compared using WAXD to reveal the relationship between the composite morphology and the processing routes. The WAXD patterns of these composites are illustrated in Fig. 4.4. The diffraction peak and calculated average basal spacing between intercalated silicate sheets (d-spacing) are listed in Table 4.2. The d-spacings are evaluated using the Bragg equation (equation 1). The WAXD patterns are almost identical to each other for the composites prepared by direct melt blending, the $scCO_2$ aided method, and direct melt blending with sequential mixing. None of these methods was able to successfully increase the d-spacings of the nano-clay. Each of these samples had slightly decreased d-spacings compared to that of the pure clay shown in Table 4.2. This might be caused by the degradation of the modified surface (hydrogentated tallow in this case). Samaniuk [24] showed that surface modification groups of other types of hydroxyl-modified clay (cloisite 30B) can degrade, reducing the d-spacing that was originally increased by further separating the galleries. More specifically, Monticelli et al. [25] found that after treating hydroxyl-modified clay at 250 °C for 4 hr, the surface modification degraded until the basal spacing fell from 18.5 Å (2θ = 4.8°) to 12.9 Å (2θ = 6.85°). The alkyl modified clays are usually more stable due to less reactive groups, but the thermo degradation under high processing temperature could be a reason of the decrease of the clay d-spacings. The onset decomposition temperature of Cloisite 20A is 198 °C based on the measurement using thermogravimetric analysis by Cervantes-Uc et al. [26]. In this work, the processing temperature is about 200 °C, based on the melting temperature of PP. At

these temperatures, it is possible to cause the degradation of the alkyl chain on the modified surface, and therefore, reduce the nano-clay d-spacings in the composites. When the clay loading is high and a good clay dispersion is not achieved, the clays are more likely to interact with one another, increasing stresses and friction leading to collapsed galleries and displaced alkyl modifiers. The only composite that had an increased d-spacing was the one prepared by the $scCO_2$ aided method with sequential mixing. In this case, the d-spacing increased 15.5% compared to that of the pure clay. This is indicative of improved nano-clay dispersion.

Although WAXD can offer a convenient method to determine the nanocomposite structure, not much can be concluded about the spatial distribution of the silicate layers. The peak broadening and intensity changes are very difficult to study systematically, and thus, conclusions based solely on WAXD patterns are only tentative when concerning the mechanism of nanocomposite morphologies. TEM is a technique that allows a qualitative understanding of the internal structure and can be used to supplement the deficiencies of WAXD. It shows spatial distribution of the various phases, and views of the defect structure through direct visualization. TEM also has limitations. It is time consuming and only gives qualitative information at a very small scale, which may not entirely represent the microstructure of the nanocomposite as a whole. TEM and WAXD together, however, provide a more thorough analysis for evaluating the nanocomposite structure.

4.4.2 Transmission Electron Microscopy Analysis

TEM analysis was carried out as a supplemental characterization method to further evaluate the morphology of the nano-clay in the matrix. TEM images of the 10 wt% MMT/PP nanocomposites prepared using the four different processing methods (DB, CO2, DB S, CO2 S) are presented in Figs. 4.5 and 4.6. Images with magnification at 17,000x are shown in Fig. 4.5

and images with magnification at 34,000x are shown in Fig. 4.6. As can be seen from Figs. 4.5 (a) and 4.6 (a), the clay aggregation in the direct blended nanocomposite was significant with the addition of 10 wt % MMT. The system appears to be a phase separated morphology with tactoids on the order of hundreds of individual silicate layers. Many larger aggregated tactoids were found during the scan than the ones shown in the image. Apparently the conventional melt intercalation is not effective in exfoliating/intercalating the nano-clay at this high loading. Better clay dispersion can be observed in the composite prepared by the $scCO_2$ aided melt blending method in Figs. 4.5(b) and 4.6(b). However, the size of the tactoid is still large. This could be the reason for low modulus for the 10 wt% MMT/PP CO2 sample, which will be discussed in the following section. The morphology of the composite prepared by direct blending with the combination of sequential mixing (shown in Figs. 4.5(c) and 4.6(c)) did not show good dispersion of the nano-clays. The tactoids were smaller in size compared to those in Figs. 4.5(a) and 4.6(a), but similar in form when observing how the clay platelets stack together. Sequential mixing might help to avoid some further collapsing of the silicate layers but good dispersion could not be obtained simply because the clays were not delaminated in the first place. The best dispersion can be seen in the nanocomposite prepared using $scCO_2$ aided melt blending method with sequential mixing (Figs. 4.5(d) and 4.6(d)). Although there were still some aggregates, most showed fairly well dispersed clay platelets even at high magnification. These tactoids consisted of in the order of tens of individual clay layers. The delaminated clay layers were observed to be well dispersed in the polymer matrix. Moreover, the tactoids had a relatively high aspect ratio and are already aligned along the flow direction, which is a great benefit to the materials mechanical properties. This TEM observation confirms the WAXD patterns discussed in the previous section.

4.4.3 MMT/PP Nanocomposite Mechanical Properties

In this section, we look at the effects of the different processing methods on the mechanical properties of the composite materials. The mechanical properties of the injection molded MMT/PP nanocomposite are shown in Table 4.3. The Young's moduli of the composites are compared in Fig. 4.7. The pure PP used in this study has a Young's modulus of 1.549 ± 0.065 GPa. By adding approximately 5 wt % of MMT using the conventional melt blending method, the nanocomposite is found to have a Young's modulus of 1.968 ± 0.033 GPa, an increase of about 27% compared to the pure PP matrix. Raising the nano-clay loading to 10 wt% only yielded a Young's modulus of 2.011 ± 0.107 GPa, which is statistically the same with the addition of 5 wt % of clays. In other word, the Young's modulus leveled off after beyond a clay concentration close to 5 wt %. It is probably due to large agglomerates existing in the nanocomposite. This phenomenon is very common for polymer-clay composites prepared by simple melt compounding using single or twin screw extruder [27]. Aggregation of clay particles has been shown to reduce the amount of reinforcement that the clays can provide, resulting in less enhancement of the Young's modulus [28]. With the the $scCO_2$ aided processing method, the average modulus of the 5 wt% sample had a Young's modulus of 2.178 ± 0.043 GPa, a 41% increase compared to the matrix. The degree of improvement obtained from this method is very comparable to the improvement Nguyen reported [23]. In achieving this, the advantages of this potentially continuous new process are verified. However, the Young's modulus of a 10 wt % sample prepared by this $scCO_2$ aided method was only 2.104 ± 0.133 GPa, which showed no further improvement compared to the direct blended composite. This value is even lower than that of the 5 wt % sample prepared by the same procedure. This indicated an obstacle in applying this procedure to higher clay loading in nanocomposites. A possible reason for this failure is the

collapse of the clays due to over-processing at high clay loadings, which was shown to be detrimental to the exfoliation in the section on morphology. The biggest improvement is seen at the nanocomposites prepared using the $scCO_2$ technique with sequential mixing. The sample prepared in this manner also showed the best clay dispersion in the TEM and WAXD characterizations on earlier section. This confirms the common observation that better particle dispersion is related to enhancement in mechanical properties. At 10 wt % MMT, the nanocomposite was determined to have a Young's modulus of 2.524 ± 0.107 GPa, an increase of about 63% compared to pure PP. The composite prepared by the direct blending method with sequential mixing did not show any improvement compared to the direct blending method, which indicates that the sequential mixing technique should be used together with the $scCO_2$ technique. The nano-clay needs to be delaminated or swelled by the CO_2 first in order to better disperse it into the matrix. The sequential mixing is helpful to prevent collapse of the silicate layers due to over processing, but it is not effective in dispersing the nano-clay in the matrix by itself.

The tensile strength results of the nanocomposites show another advantage of the $scCO_2$ aided method with sequential mixing. The tensile strengths of the composites are compared in Fig. 4.8, and the values can be found in Table 4.3. The tensile strength of pure PP is 28.80 ± 0.69 MPa. Improvements in tensile strength were not obvious for the composites prepared by the conventional melt blending method and $scCO_2$ aided melt blending method. Regardless of the clay concentration, the tensile strength of the composites prepared by these two methods ranged from 29 MPa to 31 MPa, which were only improvements of the order of 8% and less compared to pure PP. This result is not disappointing considering higher modulus materials are usually more brittle and have lower tensile strength. Using the sequential mixing technique with the $scCO_2$ aided method, however, helped to raise the tensile strength of the 10 wt % MMT/PP to

33.42 ± 0.52 MPa, which is a 16% increase. This is a good improvement, especially when considering the significant modulus improvement of the material. The tensile strength of the 10% MMT/PP sample prepared by the melt blending method with sequential mixing is the lowest among all the samples. This is probably due to the insufficient mixing of the clay with polymer and consequently poor clay dispersion. Therefore, using $scCO_2$ and sequential mixing together is necessary to obtain good mechanical properties for the high loading of nano-clays in nanocomposites. The mixing must be enough to disperse the nano-clay layers but not too much to cause their collapse. The balance between these two situations should be optimized to gain optimal mechanical properties.

The values of elongation at break of the nanocomposites were not obtained due to the device limitations at the time of measurement. An oven was attached so that the maximum elongation at break that could be measured was about 20%. For all the samples measured the values of elongation exceeded this value. The increase in elastic modulus did not lead to a significant decrease in the ductility.

4.4.4 Comparison of Modulus Values with Composite Theory

In this section, the measured modulus values are compared with those predicted by composite theory models in order to determine if we were realizing the full potential increase of the mechanical properties. Two models that are commonly used to estimate the properties of polymer composites are the Halpin-Tsai [29] and the Ji et al. models [30]. Both models provide estimates of the composite Young's moduli based on filler and matrix properties but are based on different assumptions about the degree of dispersion of the filler particles and particle orientation.

The Halpin-Tsai model is often used because of its simplicity despite the existence of more accurate theoretical predictions. Halpin and Tsai's model shown below in Eq. (1) assumes

fully exfoliated and unidirectional clay platelets, as well as a high degree of adhesion of the filler particles to the surrounding polymer matrix,

$$E_c = E_m \left[\frac{1+\xi\eta\phi_f}{1-\eta\phi_f}\right] \qquad (2)$$

where $\xi = 2(1/t)$ and

$$\eta = \frac{[E_f/E_m - 1]}{[E_f/E_m + \xi]} \qquad (3)$$

E_f, E_m and E_c are the filler, matrix, and composite modulus, respectively. ϕ_f is the filler volume fraction and $1/t$ is the aspect ratio of the filler particles. The Young's modulus of nano-clay E_f was taken as 178 GPa [28] and the aspect ratio of the silicate platelets (l/t) was taken to be approximately 100 for fully exfoliated platelets [28]. With the density of the matrix, ρ_m, equals to 0.9 g/cm^3 and the density of nano-clays, ρ_f, equals to 1.77 g/cm^3, the volume fraction of the nano-clays ϕ_f can be found from the weight percentage w_f as

$$\phi_f = \rho_m w_f / (\rho_f - \rho_f w_f + \rho_m w_f) \quad (4).$$

The model developed by Ji et al. makes more realistic assumptions about the morphological state of a polymer composite than the Halpin-Tsai model. It makes no assumption as to the state of clay orientation and so is valid for randomly oriented systems. Also, the model does not assume fully exfoliated clay particles. Both of these assumptions result in predicted modulus values that are much closer to actual experimental values than those predicted by the Halpin-Tsai equations. Ji's model can be described as follows,

$$\frac{1}{E_c} = \frac{1-\alpha}{E_m} + \frac{\alpha-\beta}{(1-\alpha)E_m + \frac{\alpha(k-1)E_m}{\ln k}} + \frac{\beta}{(1-\alpha)E_m + \frac{(\alpha-\beta)(k+1)E_m}{2} + E_f\beta} \quad (5)$$

where

$$\alpha = \sqrt{[2\left(\frac{\tau}{t_c}\right) + 1]}, \quad (6)$$

$$\beta = \sqrt{\phi_f}, \quad (7)$$

$$k = E_f/E_m, \quad (8)$$

τ is the thickness of the interphase region taken to be the dspacing, and t_c is the thickness of individual MMT layer, taken to be approximately 1 nm. Ji et al.'s model takes into account the interphase separation between clay particles and makes no assumption about the state of intercalation or exfoliation of the clay platelets. If d-spacing data are available, then the dependence of Young's modulus on the degree of intercalation can be predicted.

The theoretical and experimentally measured moduli of the composites versus weight percent of MMT are compared in Fig. 4.7. As can be seen, the experimental Young's moduli are far below those predicted by the Halpin-Tsai model. For the nanocomposites prepared using $scCO_2$ method and sequential mixing at 10 wt % MMT, the Young's modulus is about 50% lower the theory prediction. For the other methods, the differences are even bigger. This may be due to some important issues such as the lack of fully exfoliation for the nano-clays, the lack of complete orientation of the filler particles in the flow direction, the lack of significant bonding between MMT and polypropylene, and a lower actual aspect ratio than the one assumed (100).

Ji et al.'s model provides a closer prediction of Young's modulus because it is more valid for randomly oriented particles and does not assume full exfoliation of the clay platelets. The 5 wt% sample prepared by $scCO_2$ aided method well matches the prediction. However, the measured Young's moduli for the 10 wt % samples are all lower than this prediction. For the nanocomposites prepared using $scCO_2$ method and sequential mixing at 10 wt % MMT, the Young's modulus is about 13% lower than the predicted value. The reason for this could be part of the silicate layers were not fully intercalated by the polymer chains. Those clays cannot be

included in the calculations because they don't share an interface with the polymer, negating any interactions with the polymer matrix. The model over-predicted part of the reinforcement from the clay platelets as they are not equally intercalated by the matrix phase.

4.4.5 MMT/PP Nanocomposite Rheological Properties

In this section, we look at rheological behavior of the different nanocomposite melts at various nano-clay loadings. The storage modulus, *G'*, loss modulus, *G"*, and complex viscosity, $|\eta*|$, were obtained from the dynamic frequency scan measurements. The *G'*, *G"*, and $|\eta*|$ of the nanocomposite melt prepared by different methods at various MMT concentrations are compared in Figs. 4.9, 4.10, and 4.11, respectively. Repeat rheological measurements on the same sample prepared multiple times reveal that *G'*, *G"*, and $|\eta*|$ are accurate to about 5%.

The processing method has no significant effect on the nanocomposite rheological behavior. As can be seen in Figs. 4.9 – 4.11, the *G'*, *G"*, and $|\eta*|$ of the 10 wt % MMT/PP samples prepared by different methods overlap with each other and are well within experimental error, as well as the two 5 wt% samples. It is generally reported in the literature that a ''tail'' in the storage modulus, *G'*, versus angular frequency at low frequencies can be observed when the nano-clays are exfoliated [9]. However, Nguyen et al. [23] found that the "tail" could be a result of a network formed due to either interactions of clay surfaces with matrices when using PP-g-MA or large agglomerates of clay formed due to very high clay loadings. Their samples with exfoliated structure did not create this "tail" in *G'* while the sample that had large agglomerates with the addition of 24 wt% of nano-clay presented a "tail". In our work, the dynamic frequency scan measurements failed to pick up the morphology differences, although they were observed in both WAXD and TEM results. Therefore, the rheological characterization is capable of monitoring the networks formed in the melt system, but does not provide sufficient information

for accurate particle morphologies. Using rheology to determine the micro structure and morphology of the nanocomposites is still ambiguous.

The nano-clay concentration has a slight impact on the nanocomposite rheological behavior. As can be seen in Fig. 4.11, as the nano-clay concentration increases, the complex viscosity increases slightly. The increases in *G'* and *G"* are too minimal to distinguish with the scale of the figures, but they have the same trend as the changes of $|\eta *|$ with various clay loadings. By increasing the nano-clay concentrations, the interactions between the clay to polymer chains are stronger. The interparticle distances also decrease and the chance of clay to clay interactions may increase as well. These can all contribute to the increase of the melt viscosity. Despite the slight increase of magnitude, all the samples have the same rheological behavior as the polymer matrix. This indicates that no obvious network has formed in the composite melt up to the addition of 10 wt% of nano-clay and the processability of the polymer-clay nanocomposites remains good up to this clay loading. The complex viscosities of the nanocomposites prepared using compatiblizers, such as maleic anhydride grafted polypropylene (PP-g-MA), would be higher, especially at low frequencies [23]. The MMT/PP composites prepared via $scCO_2$ aided method with sequential mixing can provide comparable reinforcement while keeping a good degree of processability compared to those synthesized with the aid of a compatibilizer [23].

4.5 Conclusions

A semi-continuous process that effectively reduced the clay collapse was developed based on a previous procedure used in our laboratory [26]. This process utilizes the benefits of the $scCO_2$ technique and introduces two important modifications based on the previous method: exfoliating nano-clay into polymer pellets and sequential mixing. The collapse of nano-clay was

found to occur both after the exfoliation procedure and during processing at high clay loadings based on WAXD results. Exfoliating the nano-clay directly into the hopper and processing the composite immediately can help minimize the clay collapse after exfoliation. Evidence from TEM images and WAXD results lead us to believe that the sequential mixing step can successfully reduce the clay collapse during processing at high clay content (i.e. 10 wt %) and is, therefore, beneficial for the nano-clay dispersion. Nanocomposites that have 10 wt % nano-clay with intercalated nano-clay were obtained with modulus increases from 1.548 GPa for pure PP matrix to 2.524 GPa, a 63% increase. The tensile strengths increased by 16% from 28.80 MPa (pure PP) to 33.42 MPa. Other processing methods including conventional melt blending and $scCO_2$ aided melt blending without the sequential mixing only helped to increase the Young's modulus and tensile strength by 30~36% and 1.3~6.8%, respectively, at the same clay level. The improved Young's modulus did not reach the theoretical predictions for samples produced by any of the processing methods. However, agreement of the results was better with Ji's and coworker's model than with the Halpin-Tsai model, because Ji's model does not assume fully exfoliated and unidirectional orientated nano-clays. The predicted modulus is still 13% higher than the experimental value for the 10 wt % sample prepared by the $scCO_2$ aided method and sequential mixing. The relationship between composite morphology and rheological behavior was not readily apparent, but the good processability of the composite even at 10 wt % nano-clay prepared using the proposed technique was suggested.

4.6 Acknowledgements

The authors would like to acknowledge the funding support from Institute for Critical Technology and Applied Science (ICTAS) at Virginia Tech and Southern Clay Products for

donating the MMT nano-clays. We would also like to thank Steve McCartney at the Nanoscale Characterization and Fabrication Laboratory in ICTAS for aid in conducting the TEM studies.

4.7 References

[1] Y. Kojima, A. Usuki, M. Kawasumi, A. Okada, Y. Fukushima, T. Kurauchi, O. Kamigaito, J Mater Res, 8 (1993) 1185-1189.

[2] K. Nevalainen, J. Vuorinen, V. Villman, R. Suihkonen, P. Jarvela, J. Sundelin, T. Lepisto, Polym. Eng. Sci., 49 (2009) 631-640.

[3] Q.P. Ran, H. Zou, S.S. Wu, J. Shen, Polymer Composites, 29 (2008) 119-124.

[4] W.H. Awad, G. Beyer, D. Benderly, W.L. Ijdo, P. Songtipya, M.D. Jimenez-Gasco, E. Manias, C.A. Wilkie, Polymer, 50 (2009) 1857-1867.

[5] M. Kawasumi, N. Hasegawa, M. Kato, A. Usuki, A. Okada, Macromolecules, 30 (1997) 6333-6338.

[6] A. Boukerrou, J. Duchet, S. Fellahi, M. Kaci, H. Sautereau, Journal of Applied Polymer Science, 103 (2007) 3547-3552.

[7] S.S. Ray, M. Okamoto, Prog. Polym. Sci., 28 (2003) 1539-1641.

[8] A. Blumstein, Journal of Polymer Science Part A: General Papers, 3 (1965) 2665-2672.

[9] R. Krishnamoorti, R.A. Vaia, E.P. Giannelis, Chemistry of Materials, 8 (1996) 1728-1734.

[10] A. Usuki, Y. Kojima, M. Kawasumi, A. Okada, Y. Fukushima, T. Kurauchi, O. Kamigaito, J Mater Res, 8 (1993) 1179-1184.

[11] H.G. Jeon, H.T. Jung, S.W. Lee, S.D. Hudson, Polym. Bull., 41 (1998) 107-113.

[12] C.R. Tseng, J.Y. Wu, H.Y. Lee, F.C. Chang, Polymer, 42 (2001) 10063-10070.

[13] N.H. Abu-Zahra, A.M. Alian, R. Perez, H. Chang, J. Reinf. Plast. Compos., 29 (2010) 1153-1165.

[14] M. Kannan, S.S. Bhagawan, T. Jose, S. Thomas, K. Joseph, Polym. Eng. Sci., 50 (2010) 1878-1886.

[15] D.R. Paul, L.M. Robeson, Polymer, 49 (2008) 3187-3204.

[16] F. Chavarria, D.R. Paul, Polymer, 45 (2004) 8501-8515.

[17] P.H. Nam, P. Maiti, M. Okamoto, T. Kotaka, N. Hasegawa, A. Usuki, Polymer, 42 (2001) 9633-9640.

[18] J. Pascual, E. Fages, O. Fenollar, D. Garcia, R. Balart, Polym. Bull., 62 (2009) 367-380.

[19] K.S. Santos, C. Dal Castel, S.A. Liberman, M.A.S. Oviedo, R.S. Mauler, Journal of Applied Polymer Science, 119 (2011) 1567-1575.

[20] G.M. A.J. Lesser, in: ANTEC 2004, 2004, pp. 1528-1532.

[21] C.W Manke, E. Gulari, D.F Mielewski, E.C Lee, U.S. Patent 6,753,360 (2002)

[22] D.F. Mielewski, E.C. Lee, C.W. Manke, E. Gulari, U.S. Patent 6,469,073 (2004)

[23] Q.T. Nguyen, D.G. Baird, Polymer, 48 (2007) 6923-6933.

[24] J. Samaniuk, D. Litchfield, D. Baird, Polym. Eng. Sci., 49 (2009) 2329-2341.

[25] O. Monticelli, Z. Musina, A. Frache, F. Bellucci, G. Camino, S. Russo, Polym Degrad Stabil, 92 (2007) 370-378.

[26] J.M. Cervantes-Uc, J.V. Cauich-Rodríguez, H. Vázquez-Torres, L.F. Garfias-Mesías, D.R. Paul, Thermochimica Acta, 457 (2007) 92-102.

[27] N. Hasegawa, H. Okamoto, M. Kawasumi, M. Kato, A. Tsukigase, A. Usuki, Macromol. Mater. Eng., 280 (2000) 76-79.

[28] T.D. Fornes, P.J. Yoon, D.L. Hunter, H. Keskkula, D.R. Paul, Polymer, 43 (2002) 5915-5933.

[29] J.C. Halpin, J.L. Kardos, Polym. Eng. Sci., 16 (1976) 344-352.

[30] X.L. Ji, J.K. Jing, W. Jiang, B.Z. Jiang, Polym. Eng. Sci., 42 (2002) 983-993.

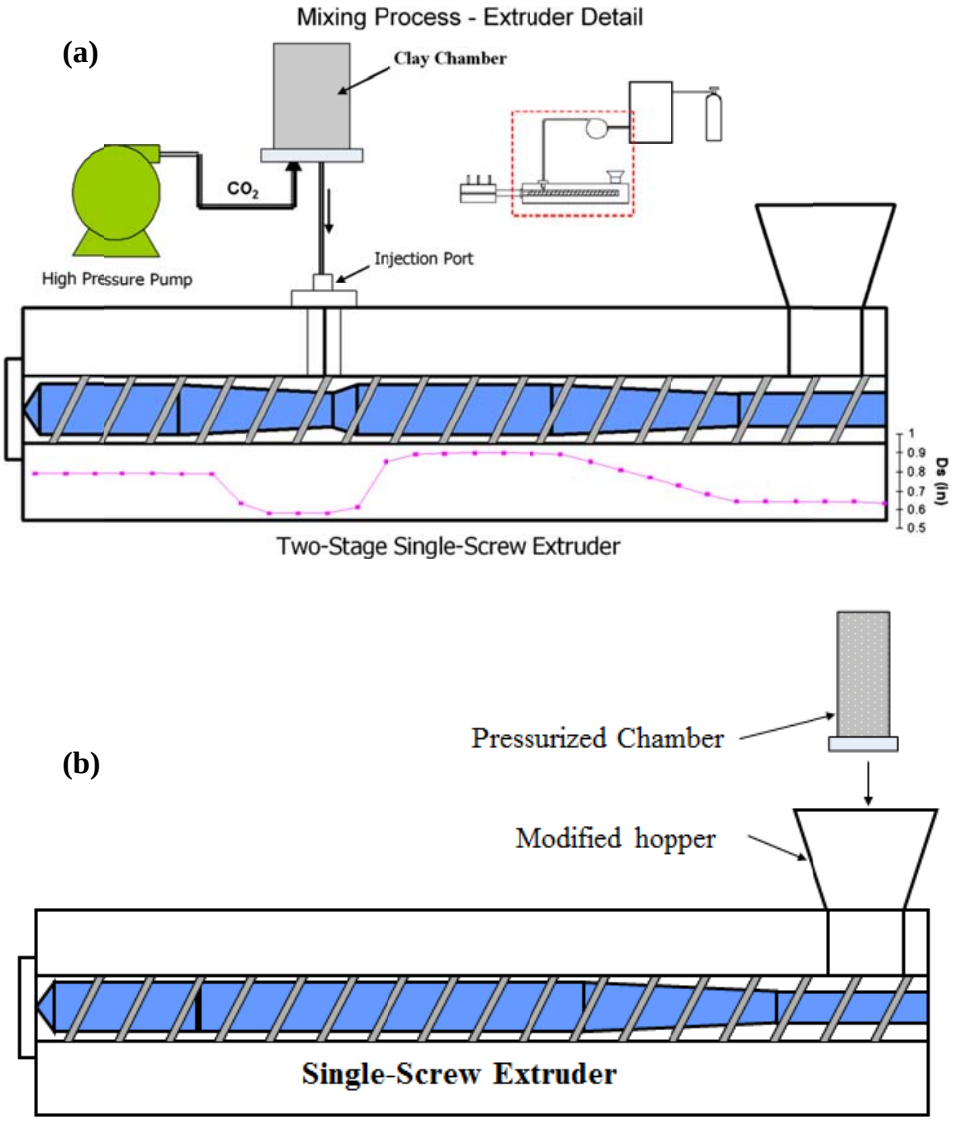

Figure 4.1: Comparison of (a) Nguyen et al.'s processing scheme [26] and (b) the simplified procedure used in this work

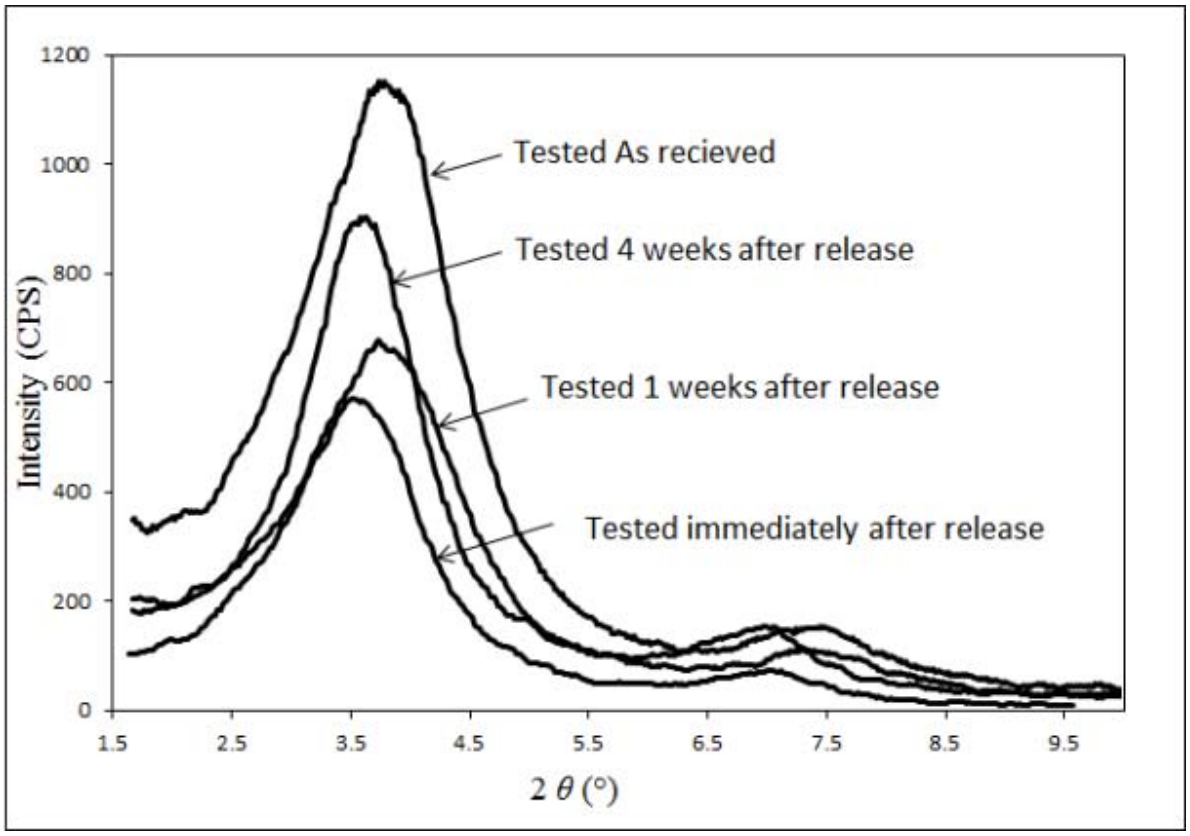

Figure 4.2: Wide angle X-ray diffraction (WAXD) patterns of as received and released nano-clay subsequently stored for different duration of times

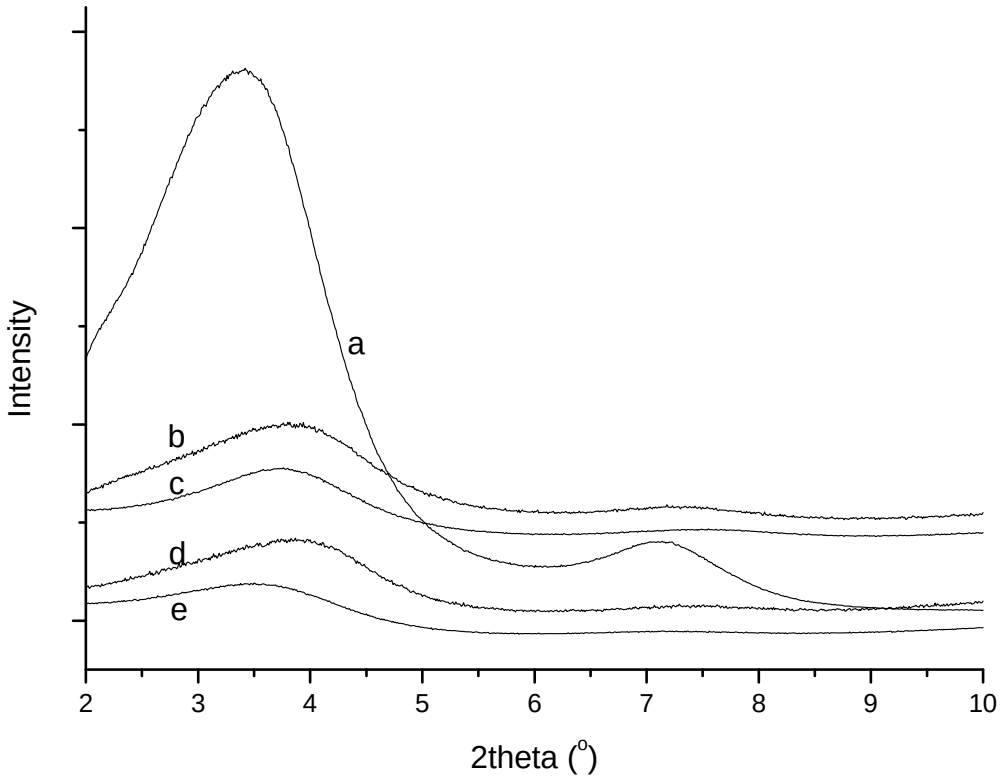

Figure 4.3: The wide angle X-ray diffraction patterns of (a) pure as-received nano-clay (Cloisite 20A), (b) injection molded plaque of 10 wt% MMT/PP, (c) extruded pellets of 10 wt% MMT/PP, (d) injection molded plaque of 5 wt% MMT/PP, and (e) extruded pellets of of 5 wt% MMT/PP composites. All composites were prepared by $scCO_2$ aided melt blending method.

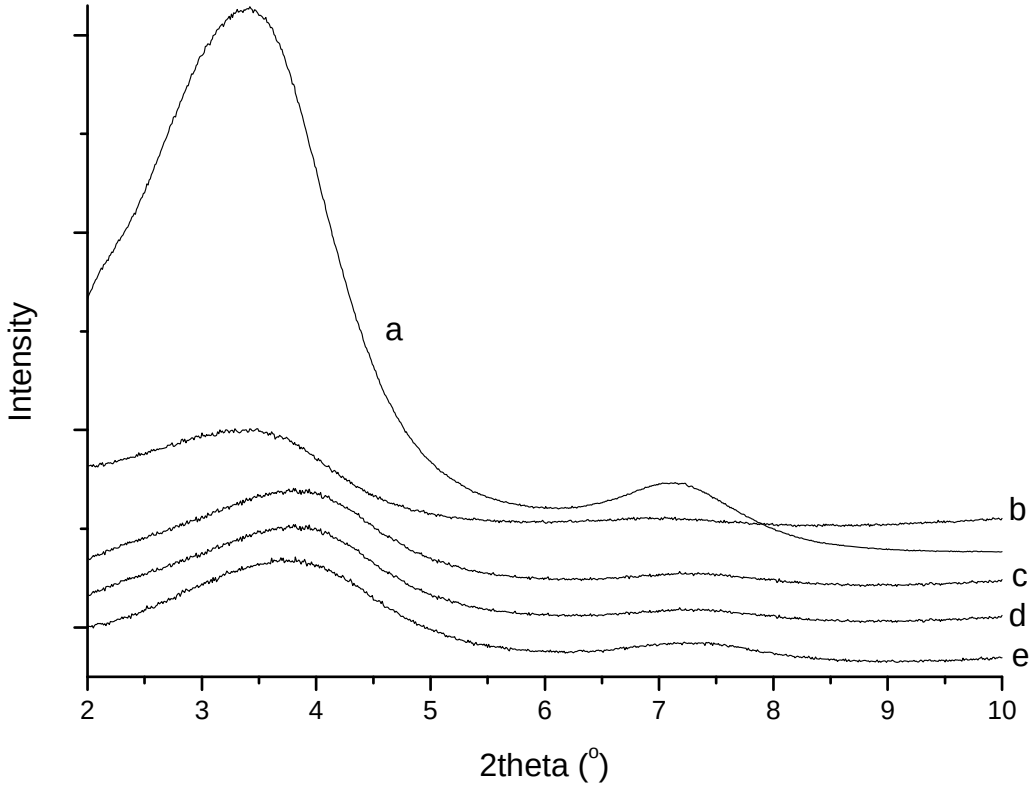

Figure 4.4: The wide angle X-ray diffraction patterns of (a) pure as-received nano-clay (Cloisite 20A), 10 wt% MMT/PP composite prepared by (b) $scCO_2$ aided melt blending with sequential mixing, (c) conventional direct blending method, (d) direct melt blending with sequential mixing, (e) $scCO_2$ aided melt blending method. All composites tested here are injection molded plaques.

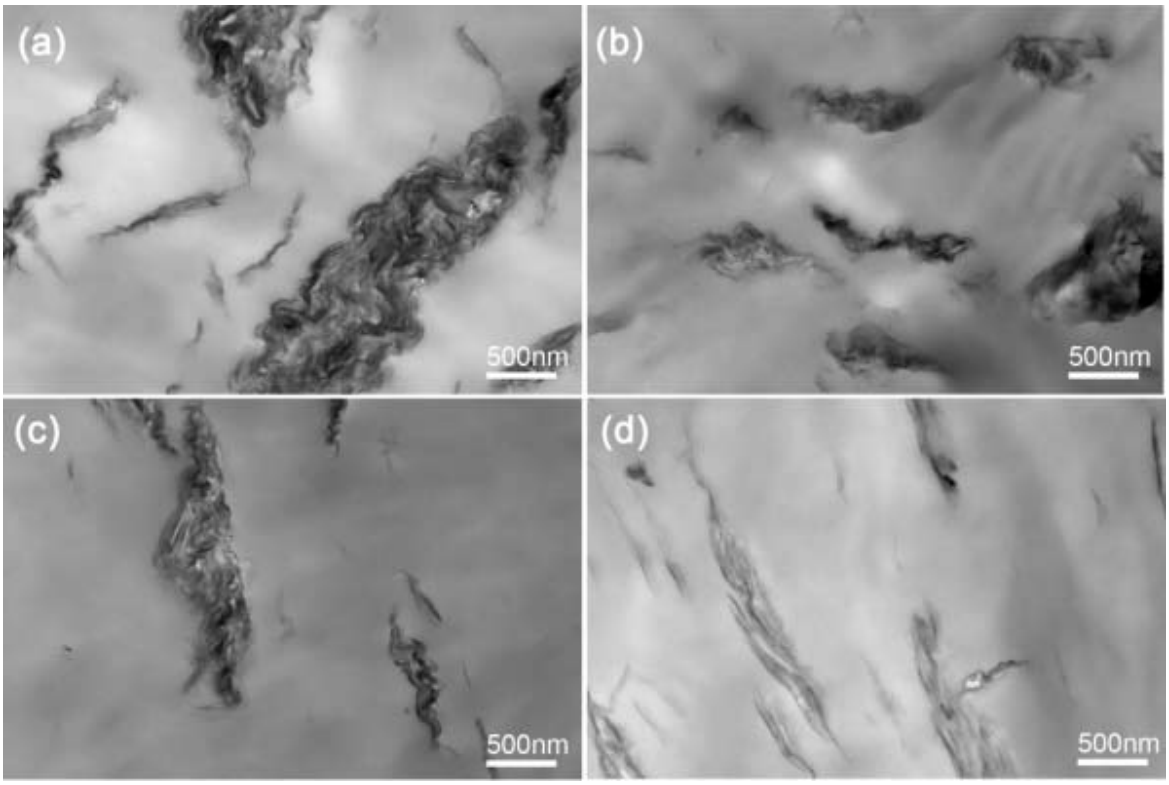

Figure 4.5: Transmission electron micrographs at 17,000x magnification of 10 wt% MMT/PP nanocomposites processed by (a) conventional melt blending, (b) $scCO_2$ aided melt blending, (c) direct blending with sequential mixing, and (d) $scCO_2$ aided melt blending with sequential mixing method

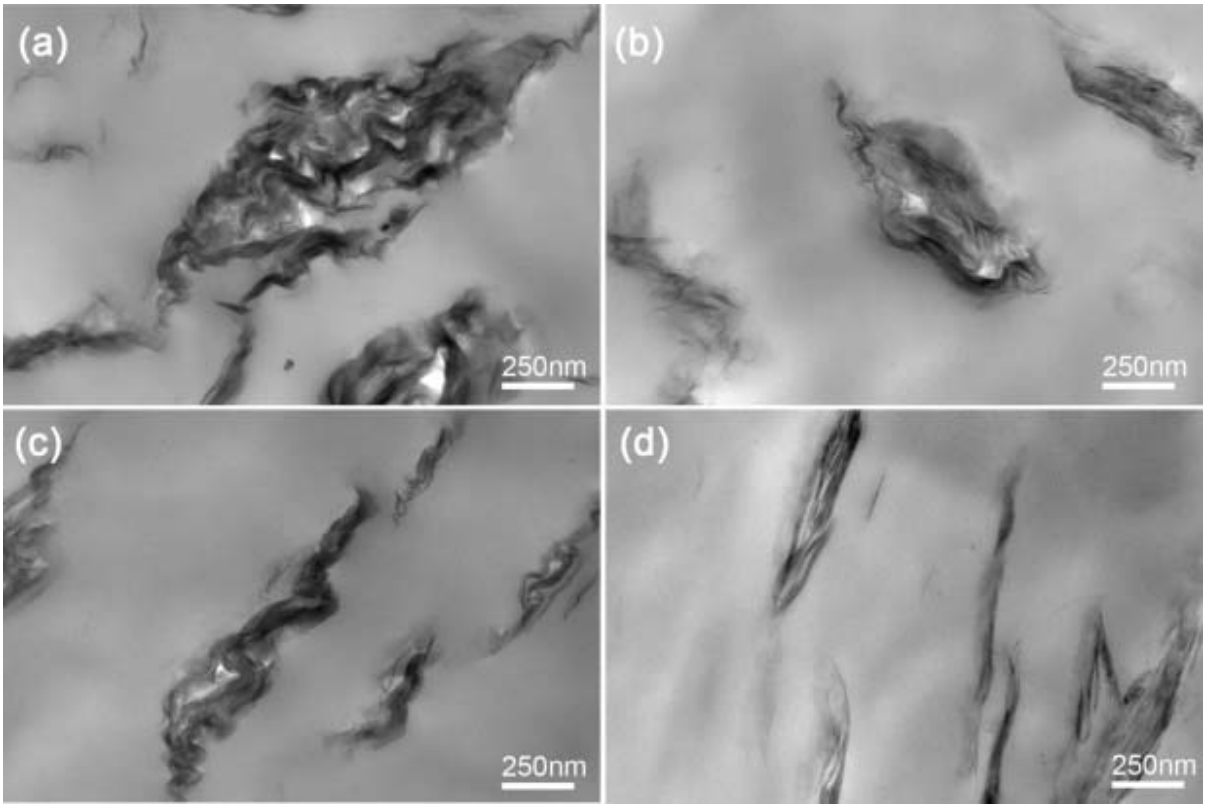

Figure 4.6: Transmission electron micrographs at 34,000x magnification of 10 wt% MMT/PP nanocomposites processed by (a) conventional melt blending, (b) $scCO_2$ aided melt blending, (c) direct blending with sequential mixing, and (d) $scCO_2$ aided melt blending with sequential mixing method

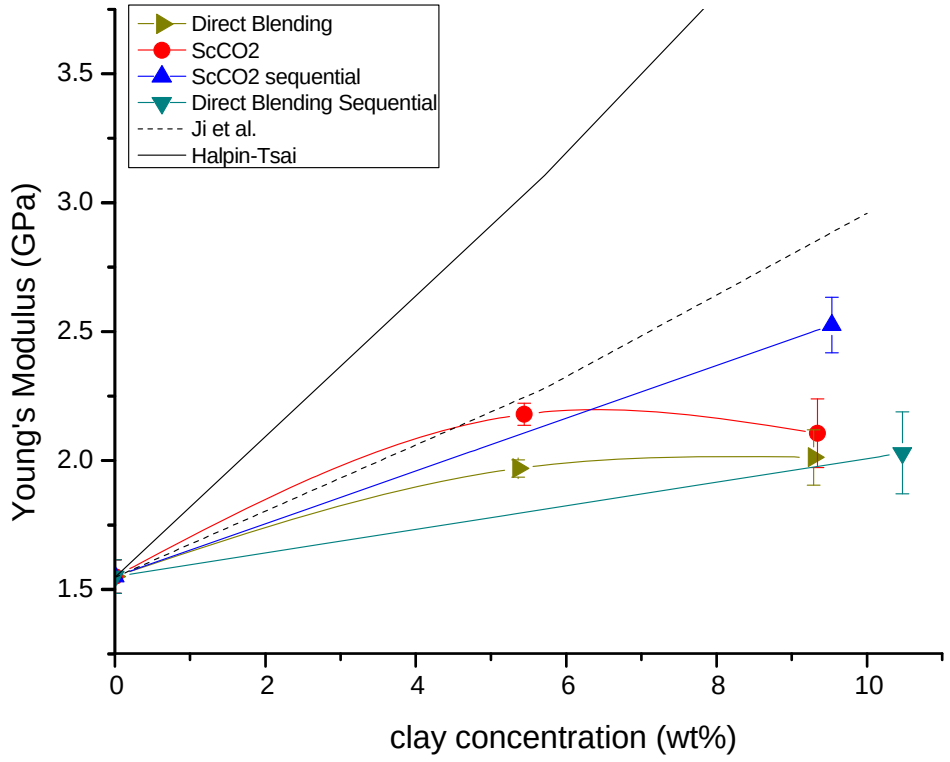

Figure 4.7: Young's moduli of MMT/PP nanocomposites processed by different methods and the comparison with theoretical predictions (Note: The lines for the experimental values are solely assisting to separate the data from processing methods. These lines are not intended to show any trend of the modulus change)

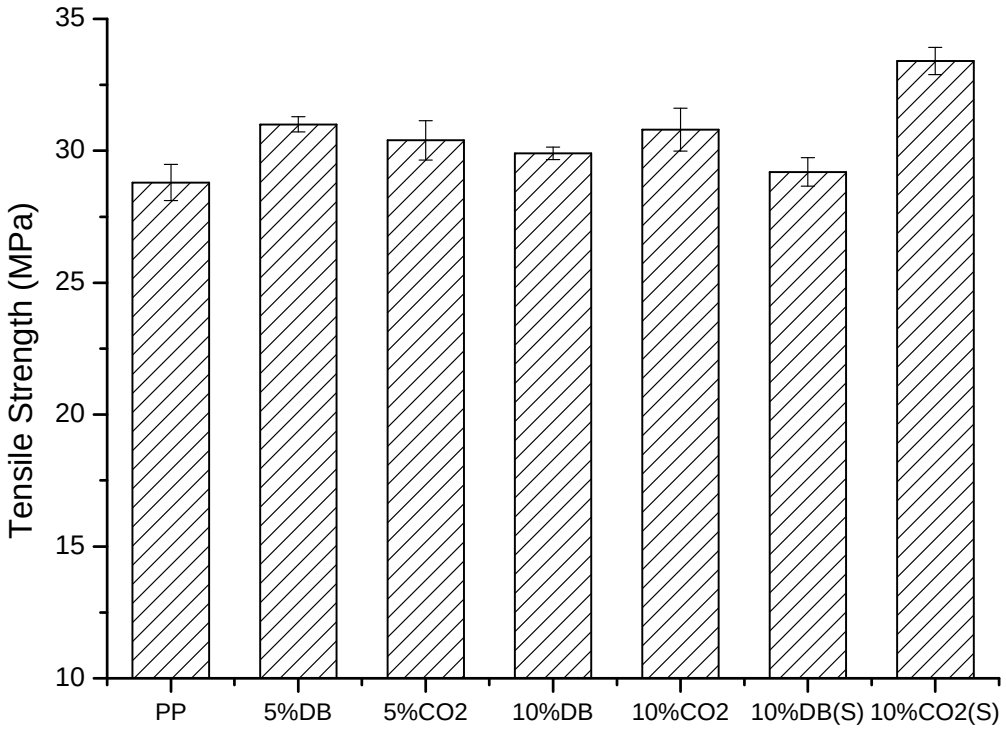

Figure 4.8: Tensile strengths of PP matrix different MMT/PP nanocomposite samples

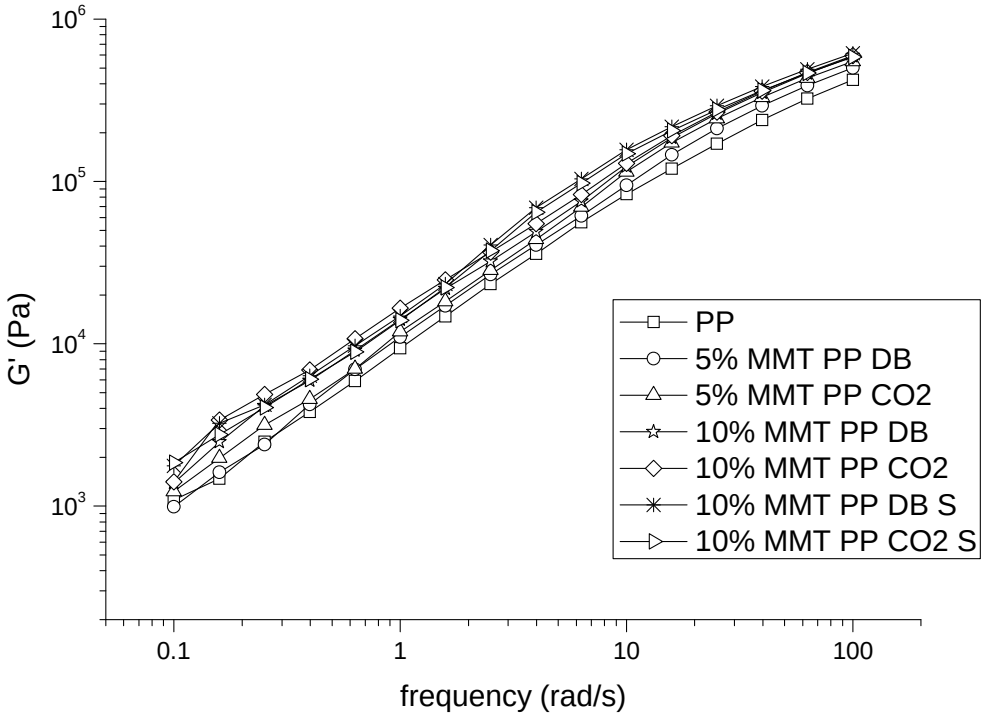

Figure 4.9: Storage modulus, *G'* vs. frequency, ω, of different nano-clay/PP nanocomposites at 200 °C

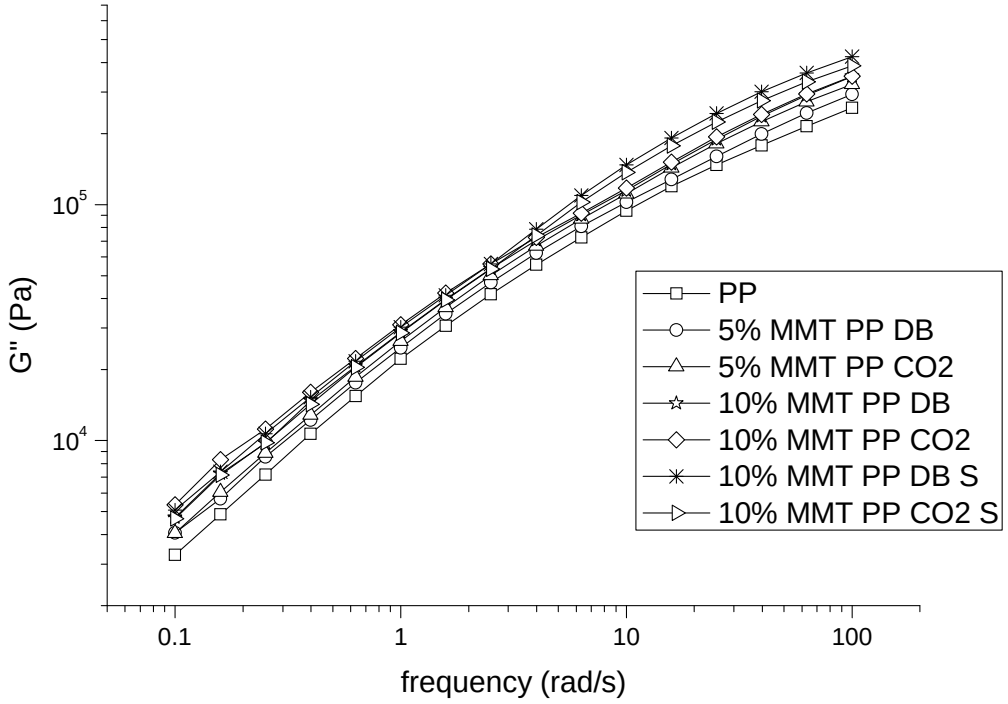

Figure 4.10: Loss modulus, *G"* vs. frequency, ω, of different nano-clay/PP nanocomposites at 200 °C

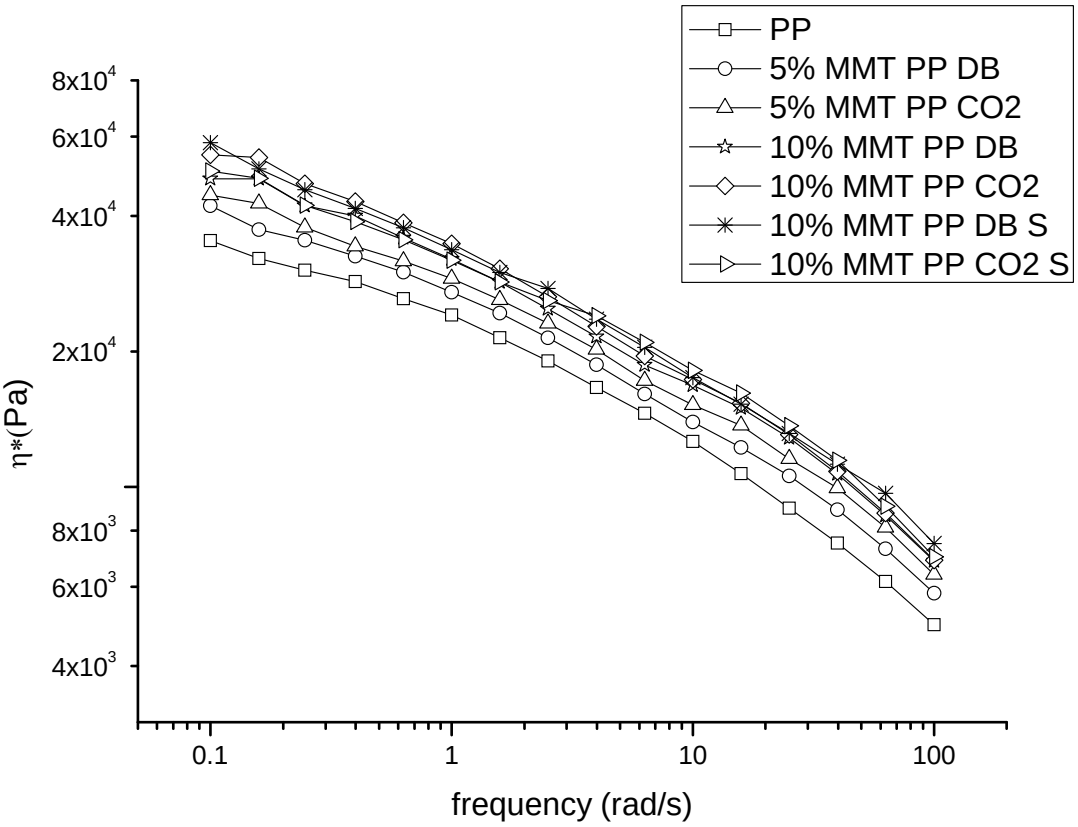

Figure 4.11: Complex viscosity, $|\eta^*|$, vs. frequency, ω, of different nano-clay/PP nanocomposites at 200 °C

Table 4.1: Abbreviation of processing methods used in tables and figures

Processing method	Abbreviation
Conventional direct melting blending	DB
$ScCO_2$ aided method (Simplified from Nguyen's method)	CO2
Conventional direct melting blending with sequential mixing	DB S
Simplified Nguyen's method with sequential mixing	CO2 S

Table 4.2: WAXD results and average basal spacing values calculated from Bragg's equation (1) with of 10 wt% MMT/PP injection molded plaque.

Sample	2θ (°)	d_{001}(nm)	% Increase
Clay 20A	3.65	2.42	- -
10% MMT/PP DB	3.82	2.31	-4.4
10% MMT/PP CO2	3.96	2.23	-7.8
10% MMT/PP DB S	3.72	2.37	-1.9
10% MMT/PP CO2 S	3.16	2.79	15.5

Table 4.3: Actual clay loading and mechanical properties of nano-clay/polypropylene nanocomposite prepared using different processing methods

Materials	Actual clay loading (wt%)	Young's Modulus (GPa)	S.D.	% Increase	Yield Strength (MPa)	S.D.	% Increase
PP	- -	1.548	0.065	- -	28.80	0.69	- -
5% MMT/PP DB	5.36	1.968	0.033	27	30.98	0.29	7. 6
5% MMT/PP CO2	5.44	2.178	0.043	41	30.40	0.75	5.6
10% MMT/PP DB	9.29	2.011	0.107	30	29.91	0.24	3.9
10% MMT/PP CO2	9.34	2.104	0.133	36	30.75	0.81	6.8
10% MMT/PP DB S	10.47	2.028	0.159	31	29.17	0.54	1.3
10% MMT/PP CO2 S	9.53	2.524	0.108	63	33.42	0.52	16.0

Chapter 5

The Manufacture of Nano-clay Polymer Composites Based on Polypropylene: Conventional Polypropylene, High Crystallinity Polypropylene, and Maleic Anhydride Grafted Polypropylene

The Manufacture of Nano-clay Polymer Composites Based on Polypropylene: Conventional Polypropylene, High Crystallinity Polypropylene, and Maleic Anhydride Grafted Polypropylene

Chen Chen, John P. Quigley, Donald G. Baird*

Department of Chemical Engineering, Virginia Polytechnic Institute and State University, Blacksburg, Virginia 24061

5.1 Abstract:

The use of supercritical carbon dioxide ($scCO_2$) and sequential mixing techniques was proven to be beneficial for surface modified montmorillonite (MMT) nano-clay dispersion in the polypropylene (PP) matrix and lead to improved material mechanical properties as reported in our earlier research. In order to obtain additional enhancements of the composite properties, the $scCO_2$ exfoliation and sequential mixing techniques are applied on MMT reinforced composites using high crystallinity polypropylene (HCPP) and polypropylene grafted with maleic anhydride (PP-g-MA) as polymer matrices. Morphological, rheological and mechanical properties of these composites are examined and compared for the composites using different matrices with different processing routes. Based on Transmission electron microscopy (TEM) observations, the degree of clay dispersion in the HCPP matrix is comparable with that of the clay dispersion in a conventional PP matrix showing intercalated structure. The PP-g-MA based nano-clay composites are found to have a high degree of exfoliated structure with the addition of approximately 10 wt % nano-clay when using $scCO_2$ aided method with sequential mixing technique. The HCPP nanocomposite at 10 wt % of nano-clay has a Young's modulus as high as 3.236 GPa, and the modulus of the 10% MMT/PP-g-MA sample is found to be 2.595 GPa, much higher than that of the composite prepared by the direct blending method and that of a composite based on PP matrix.

5.2 Introduction

Polymer-clay nanocomposites have attracted tremendous interest over the past two decades because of their potential to exhibit enhanced thermal, barrier, physical, and mechanical properties compared to other types of composite materials, such as glass-filled polymer composites. In 1993, the Toyota research group revealed a major breakthrough by successfully preparing nylon -6/nano-clay composites using *in situ* polymerization [1]. The group found a 68% increase in tensile modulus, a 224% increase in flexural modulus, and an 87% increase in the heat distortion temperature relative to neat polymer material with the addition of 4.7 wt% clay. The study of polymer-clay composites has since been extended to others polymer systems, including polycarbonate [2], polyurethane [3], poly(vinyl chloride) [4], polypropylene [5], and epoxy [6]. However, the improvements of the composite mechanical properties are not as significant as for the case of nylon-6.

The properties of polymer-clay nanocomposites are significantly related to the clay morphology in the polymer matrices. Particle aggregation decreases the particle surface area and effective aspect ratio, resulting in limited enhancement of the composite properties. Among the three most common morphologies, phase separated, intercalated and exfoliated, the phase separated morphology is least desired, where the polymer does not enter the clay gallery spacings between platelets and the material only gains micro-scale reinforcement. The intercalated and exfoliated morphology both involve nano-scale reinforcement. Intercalated clay morphology occurs when polymer chains diffuse into the gallery spacings of layered structure, resulting in a gallery distance on the order of a few nanometers [7]. If the clay layers are completely pushed apart to create a disordered array, the composite is considered to be “exfoliated”. One of the main challenges in preparing nano-clay composites is to overcome the

attractions of the stacked silicate layers and disperse them into the polymer matrix in order to achieve the exfoliated state, or if not, the intercalated state.

Various methods have been used to compound the clay with the polymer matrix. The most widely applied methods are *in situ* polymerization [8-11], solution blending [12, 13], and melt blending [14, 15], among which the melt blending processing is more economical, flexible for formulation, and compatible with commercial practice [16]. However, the homogeneous dispersion of nano-clays and resulting significant properties improvements was achieved only in polymers containing polar functional groups for the melt blending method. Many approaches using supercritical carbon dioxide ($scCO_2$) to exfoliate nano-clay compound by melt blending method have been developed in order to improve the clay dispersion in nanocomposites [17-20]. Nguyen et al. [20] developed a method to combine the benefits of melt compounding with the exfoliating capability of $scCO_2$. The process relied on rapid expansion of the clay followed by direct injection into the extruder. It was observed in the WAXD data that the PP composite contained a high degree of exfoliated nano-clay for concentrations as high as 6.6 wt%. The Young's modulus of the PP composites increased by 54% at this nano-clay loading while using the direct blending method can only provide a modulus increase of 28% compared to the pure PP matrix. In our recent study, we developed a method which utilizes the benefits of the $scCO_2$ technique and introduced two important modifications, exfoliating nano-clay into polymer pellets and sequential mixing the nano-clay with the polymer matrix. The collapse of nano-clay was found to occur both after the exfoliation procedure and during processing at high clay loadings based on WAXD results. Exfoliating the nano-clay directly into the hopper and processing the composite immediately can help minimize the clay collapse after exfoliation. Nanocomposites that have 10 wt % nano-clay with intercalated morphology were obtained with

a modulus increase from 1.548 GPa for the pure PP matrix to 2.524 GPa for the composite, a 63% increase.

In this work, the $scCO_2$ exfoliation and sequential mixing techniques for nano-clay composite preparation are applied to polypropylene with high crystallinity (HCPP) and maleic anhydride grafted polypropylene (PP-g-MA), in addition to the regular commercial polypropylene (PP), in order to determine the effectiveness of this new technique on different matrices. HCPP has higher crystallinity and stiffness than regular PP but with good processability. Composites made from HCPP are expected to have better mechanical properties to start with as the properties such as modulus are significantly higher than those of conventional PP. PP-g-MA has a polar group grafted on the PP chains that can help making the non-polar PP compatible with polar nano-clay layers by increasing interface interactions. We want to explore whether additional enhancements can be achieved using the two matrices as expected when applying the modified processing method we developed in the previous study. A series of nano-clay/polymer composites using these three matrices at various clay loadings is prepared by both conventional melt blending method and $scCO_2$ aided method, and the sequential mixing technique is applied to composites that consist of more than 5 wt % of nano-clays. Morphological, rheological and mechanical properties of these composites are examined and compared.

5.3 Experimental

5.3.1 Materials

Three polymer matrices were used in this work, and they were all used as received. The regular commercial polypropylene (PP, Pro-Fax 6523) was obtained from Lyondell Basell (Houston, TX). The melt index of the polymer is 4 g/10 min at 230°C and at a load of 2.16 kg.

The second matrix used was high crystallinity polypropylene (PP H 501 HC), which was obtained from Braskem (Brazil). The melt index of this polymer is 3.5 g/10 min at 230 °C and at a load of 2.16 kg. The final matrix investigated in this work was maleic anhydride grafted polypropylene (PP-g-MA, PB3150, MA content = 0.5 wt %), which was obtained from Chemtura Corp. (Middlebury, CT). The melt index of this polymer is 52.2 g/10 min at 230 °C and at a load of 2.16 kg. The nano-clay was surface modified montmorillonite (Cloisite 20A), which was obtained from Southern Clay Products, Inc. (Gonzalez, TX) and was used as-received. Cloisite 20A is a surface modified montmorillonite obtained through a cation exchange reaction, where the sodium cation is replaced by dimethyl, dihydrogenated tallow, quaternary ammonium cation.

5.3.2 Clay Concentration

Clay concentrations were determined by a burn-off technique in an ashing oven at 500 °C for 2 hr. The reported concentrations are an average of three burn-off samples. The clay concentrations reported here include the intercalants or the organic modifiers.

5.3.3 Preparation of Nano-clay/Polymer Composites

Before melt compounding, the polymer pellets and organic modified nano-clays were dried separately at 80°C under vacuum overnight. The nano-clays were then put in a pressurized chamber and allowed to be in direct contact with $scCO_2$ at 3000 psi and at 80 °C for 12 hr. The dried polymer pellets were put into a 5 gal pressure vessel. The nano-clay and polymer pellets were mixed as clay was released rapidly with the CO_2 into the 5 gal pressure vessel. The nano-clay and pellet mixture was then collected and fed into the extruder hopper. A pressure chamber of 660 ml was used to contain nano-clays and was obtained from Parr Instrument Company (Moline, IL). The inlet/outlet of the chamber was sealed by a ball valve from High Pressure

Equipment Company (Erie, PA). PP/clay mixture was then extruded at a melt temperature of approximately 200 °C, and the HCPP/clay and the PP-g-MA/clay mixture were extruded at a melt temperature of approximately 210 °C, and a screw speed of 20 rpm using a single screw Killion KL-100 extruder with a 25.4 mm (1 in) diameter, a L/D of 20:1, and variable channel depth from 12.80 mm at the feed to 7.90 mm at the exit. A capillary die of 1.59 mm diameter and 20:1 L/D was attached to the end of the extruder. The extruded nanocomposites were then chopped into pellets and dried at 80°C in an air circulation oven overnight. The dried composite pellets were injection molded with an Arburg Allrounder (model 221-55-250) injection molding machine. The Arburg Allrounder operated with a 22-mm diameter barrel, L/D of 24:1, and a screw with a variable root diameter from approximately 14.25 mm at the feed to 19.3 mm at the exit. A check ring non-return valve and an insulated nozzle that was 2 mm in diameter were included in the apparatus. The composites were injection molded with a melt temperature of 200 °C, a mold temperature of 80 °C, a holding pressure of 5 bar, a screw speed of 200 rpm, and a rectangular end-gated mold with dimensions 80 x 76 x 1.5 mm^3.

In our earlier research it was found that the exfoliated clay layers collapse during processing at high clay loadings, and sequential adding the nano-clays with the polymer pellets and extruded composite pellets can successfully reduce the clay collapse (Chapter 4). Therefore, the sequential mixing procedure was used to prepare the samples containing more than 5 wt % nano-clays. In this procedure, the 5% clay/polymer composite pellets were first obtained using $scCO_2$ aided melt blending. The dried 5% composite pellets were then put back in the 5 gal pressure vessel to mix with more exfoliated clays and injection molded into composite plaques yielding a total clay concentration of 10 wt %.

In addition to the two methods just described, the conventional direct blending method was used to prepare nanocomposites for comparison purposes. In this approach, the organically modified nano-clay was used as received. The clay and polymer pellets were mechanically mixed in a Kitchen Aid type mixer and dried together at 80 °C overnight. The mixture was then fed to an extruder and re-pelletized. The abbreviations used to refer to the individual samples in the rest of this article as well as the actual clay loading are listed in Table 5.1.

5.3.4 Tensile Properties

The injection-molded plaques were cut into rectangular bars lengthwise along the flow direction, and the bars were approximately 6 mm wide, 1.5 mm thick, and 80 mm long. Tensile tests on these bars were performed at room temperature with an Instron Model 4204 testing machine (Instron, Grove City, PA). An extensometer was used to accurately measure Young's modulus. The load was measured with a 5-kN load cell, and the crosshead speed was kept at 1.27 mm/min during all tensile tests. For all tests, the average and the standard deviation were calculated from at least six samples, and data points greater than 2 standard deviations from the mean were omitted.

5.3.5 Rheological Properties

Rheological measurements on the nanocomposites were performed using an ARES rheometer from TA instrument. The injected plaques were stamped into 25 mm diameter disks. Dynamic frequency sweep experiments were performed under a continuous nitrogen atmosphere using a 25 mm parallel plate fixture at 200 °C in the linear viscoelastic region of the materials. The linear viscoelastic limit was determined using strain sweeps at a frequency of 10 rad/s and at the same temperature (200°C). It was found that dynamic frequency sweep experiments could be conducted at a strain of 2%. The elastic moduli (G'), loss moduli (G''), and complex viscosities

(η^*) of the materials as functions of angular frequency (ω) (ranging from 0.1 rad/s to 100 rad/s) were obtained at a temperature of 200°C.

5.3.6 Structure and Morphological Characterization

Transmission electron microscopy (TEM) was used to characterize the morphology of the nanocomposites. TEM measurements were generated with a Philips EM420T with an accelerating voltage of 100 kV. The TEM samples, around 70 nm thick, were cut with a cryomicrotom equipped with a diamond knife at -55 °C. Injection molded samples were used for the TEM measurements.

5.4 Results and Discussion

5.4.1 Composite Mechanical Properties

In this section, we look at the effects of the different processing methods on the mechanical properties of the composite materials. HCPP-clay and regular PP composites exhibit similar improvement in Young's modulus as does the pure matrix material when employing the improved processing method, as shown in Table 5.2 and Fig. 5.1. The pure PP and HCPP used in this study have a Young's modulus of 1.548 ± 0.065 GPa and 2.051 ± 0.124 GPa, respectively. 5% and 10% MMT/PP composites prepared by the direct blending method are found to have Young's moduli of 1.968 ± 0.033 GPa and 2.011 ± 0.107 GPa, respectively. These two values are statistically the same. In the case of using HCPP as the matrix material, the Young's moduli of 5% direct blended MMT/HCPP sample is 2.714 ± 0.076 GPa. Raising the clay weight percent to around 10 wt %, the composite Young's modulus is found to be 2.935 ± 0.119 GPa, which is only slightly higher than that of the 5% sample. Considering the lower actual clay concentration of the HCPP 5% sample, it can be concluded that these two matrices behave very similarly when using the direct blending method. Their Young's moduli leveled off beyond a clay concentration

close to 5 wt %, which is probably due to large agglomerates existing in the nanocomposite as shown by TEM in the following section. This phenomenon is very common for polymer-clay composites prepared by simple melt compounding using single or twin screw extruder [21]. With the use of the $scCO_2$ aided processing method, the average modulus of the MMT/PP sample at 5 wt % concentration is 2.178 ± 0.043 GPa, a 41% increase compared to the matrix. The HCPP sample prepared by the same method has an increase of 37% and a Young's modulus of 2.804 ± 0.109 GPa. The biggest improvements for both samples are seen when the nanocomposites are prepared using the $scCO_2$ technique with sequential mixing at 10 wt % nano-clay. The Young's moduli of MMT/PP and MMT/HCPP sample are 2.524 ± 0.107 GPa and 3.236 ± 0.132 GPa respectively. The percentage increases in modulus of 10% MMT/PP CO2 sample and 10% MMT/HCPP CO2 sample are 63% and 58%, respectively, and their absolute increases are 1.0 GPa and 1.2 GPa, respectively, compared to the pure matrix materials. The improvements obtained from nano-clay inclusion are all very similar for these two matrices. This may be because these two matrices are similar in terms of the nature of their interactions with the filler nano-clay. There are no functional or polar groups in either of these matrices and, therefore, both matrices have no strong interactions with the naturally polar nano-clay surfaces, even after part of the surface are rendered hydrophobic by long alkyl chains. The order of improvement of the Young's modulus is based strongly on the processing method and resulting degree of the clay dispersion. However, with the same nano-clay content, the use of HCPP polymer provides an enhanced absolute Young's modulus. This increase in modulus is comparable to the lower margin of the Young's modulus for glass-filled polypropylene composites, which have a much higher glass fiber weight percentage. Therefore, the HCPP nanocomposite at 10% weight percent

clay provides an alternative material for applications using the polymer-glass composite with lighter weight and easier processing.

As shown in Table 5.2 and compared in Fig. 5.2, the clay composites using PP-g-MA have different response in the Young's modulus than the regular PP and HCPP based nanocomposites, especially for the composites prepared by the $scCO_2$ aided method. The pure PP-g-MA used in this study has a Young's modulus of 1.642 ± 0.193 GPa. By adding approximately 5 wt % of MMT using the conventional melt blending method, the nanocomposite is found to have a Young's modulus of 2.138 ± 0.147 GPa, an increase of about 30% compared to the pure PP-g-MA matrix. Further raising the nano-clay loading to 10 wt % only yields a Young's modulus of 2.133 ± 0.121 GPa. This shows that beyond the addition of 5 wt % clay, the modulus will level out for the PP-g-MA composite prepared by the melt blending method, a trend that was found for the HCPP and PP composites as well. The 5% MMT/PP-g-MA sample prepared by the $scCO_2$ aided method has a Young's modulus of 2.049 ± 0.118 GPa, which is statistically the same as the 5% sample prepared by direct blending. This is probably because the delamination of clay in the polymer matrix is already aided by inclusion of the MA compatibilizer which will be discussed in the morphology section. Using the $scCO_2$ aided method does not provide further improvement of the nano-clay platelets at this concentration, and thus, the Young's modulus does not increase regardless of processing approach. However, the 10 wt % sample prepared by the $scCO_2$ aided method with sequential mixing shows a significant improvement compared to the pure matrix. The nanocomposite was determined to have a Young's modulus of 2.595 ± 0.205 GPa, an increase of about 58% compared to pure PP-g-MA. This sample also showed higher degree of exfoliation of the nano-clay than the sample prepared by the direct blending method in the TEM image in the following section. This

confirms the common observation that better particle dispersion is related to enhancement in mechanical properties.

The tensile strength of composites does not show significant changes, compared to the pure matrix, with different clay concentrations and processing method for the three matrices tested (shown in Table 5.2). All the samples are found to have a tensile strength close to 30 MPa. It is encouraging that the improvements in modulus did not cause significant decrease in the tensile strength of the composites.

The value of elongation at break for different samples shows some variation due to the nature of the matrix that was used. These values can be found in Table 5.2. The regular PP based nanocomposites have the highest ductility among the three kinds of composites. The maximum value of elongation at break of the nanocomposites was about 20% due to the device limitations at the time of measurement. For the samples made of regular PP, each had values of elongation over 20%. The increase in elastic modulus did not lead to a significant decrease in the ductility for the PP samples. Composites of HCPP also showed good ductility. In addition, it can be noted that compounding nano-clay into HCPP may help to improve the ductility of the composites. The elongation at break for pure HCPP is only 6.8%. The 5% and 10% MMT/HCPP composites prepared by the direct blending method are found to have an elongation at break of 16.65% and 17.12%, respectively, and the elongation at break for the 5% MMT/HCPP prepared by the $scCO_2$ aided method is higher than 20%. Although the elongation at break of the 5% MMT/HCPP prepared by the $scCO_2$ aided method and sequential mixing decreases to 8.94%, it is still comparable with the pure HCPP. The HCPP has a higher degree of crystallinity and is, therefore, more rigid and brittle than regular PP. Adding in the clay platelets probably changes the crystallization behavior of the composite and, therefore, enhances the material ductility.

However, the values of elongation at break of clay filled PP-g-MA composites decrease as the clay concentration increases. The elongation of the PP-g-MA is already low at 5.28%. The 5% MMT/PP-g-MA samples have an elongation of less than 5%, and the 10% samples have even lower elongations.

5.4.2 Transmission Electron Microscopy Analysis

TEM analysis was carried out to evaluate the morphology of the nano-clay in the matrix. TEM images of the nano-clay composites prepared using different matrices, processing methods, and concentrations are compared in Figs. 5.3 and 5.4. Images with 5,800x magnification are shown in Fig. 5.3 to illustrate the general dispersion state of the nano-clay, and images with higher magnification at 34,000x are shown in Fig. 5.4 in order to show the detailed clay structure. As can be seen from Figs. 5.3 (a) and (b), the composite morphology for the 5% MMT/PP samples are visibly similar, regardless of the processing method. This system presented as a mixture of phase separated and intercalated morphology with tactoids in various sizes. At higher magnification, a slight difference can be noticed from these two samples. As shown in Figs. 5.4(a) and (b), most silicate layers of the clay in the 5% MMT/PP DB sample are stacked close together, while for the 5% MMT/PP CO2 sample, most of the clay layers have polymer chains intercepted in between them. This is probably the reason of slightly improved mechanical properties for the 5% MMT/PP composite prepared by the $scCO_2$ aided method. Similarly, the differences in morphologies for the 5% HCPP composite samples prepared by different processing methods are not significant. The only difference is that the sample prepared by the $scCO_2$ aided method seems to have a more intercalated structure, with a few individual clay layers noticeable in Fig. 5.4(f). The morphologies of the two 5% PP-g-MA samples are very different from the other composites. The nano-clays in both samples are very well dispersed.

Only a few silicate layers are stacked together, on the order of tens. A morphology with high degree of exfoliation is obtained. However, the morphologies of the two 5% PP-g-MA samples are very similar to each other on both scales. It looks like using compatibilizers is so effective in terms of improving the clay dispersion that the help from $scCO_2$ technique is not obvious at this loading. If the slight degradation of PP during the processing can be avoided, the mechanical properties of these two samples should be significantly higher than the MMT/PP composites with the same clay loading.

The 10 wt % samples using the three matrices all show a great dependence on the processing method in both scales (shown in Figs. 5.3 and 5.4). All of the 10 wt % samples prepared using the direct blending method have large, aggregated tactoids. The 10% MMT/PP DB sample has the poorest clay dispersion (Figs. 5.3(c) and 5.4(c)). Apparently the conventional melt intercalation is not effective in exfoliating/intercalating the nano-clay at this high loading in pure PP matrix. The clay dispersion is better in the composite prepared using HCPP as a matrix (Figs. 5.3(g) and 5.4(g)). There are clearly some polymer chains intercalated into the silicate layers and the aggregations in the system have smaller dimensions than in the PP matrix. The higher melt viscosity might help with the polymer chain intercalation. Therefore, the increase in dispersion for the 10% MMT/HCPP DB sample is larger than the 10% MMT/PP DB sample compared to the pure polymer matrices. However, the separated clay platelets appear as though they have rotated and collapsed to form a tactoid with reduced aspect ratio. Using the $scCO_2$ aided method and sequential mixing, the PP and HCPP based nano-clay composites (shown in Figs. 5.3(d, h) and 5.4(d, h)) have improved clay dispersion over those prepared by the direct blending method. Both samples show tactoids long and thin in shape, with polymer chains intercalated in between the clay layers. The 10% MMT/PP-g-MA DB sample has much higher

degree of clay dispersion and exfoliation than the samples processed with the same procedure but without compatibilizer. Although some large tactoids are still visible, a significant amount of clay layers are clearly dispersed into the matrix. The best dispersion can be seen in the MMT/PP-g-MA CO2 sample (Figs. 5.3(l) and 5.4(l)) at 10% nano-clay. Most of the clay layers are shown as exfoliated structures. Moreover, the exfoliated clay layers have a relatively high aspect ratio and are already aligned along the flow direction, which is a great benefit to the material's mechanical properties.

5.4.3 Composite Rheological Properties

In this section, we look at rheological behavior of the different nanocomposite melts. The storage modulus, *G'*, loss modulus, *G"*, and complex viscosity, $|\eta^*|$, were obtained from the dynamic frequency scan measurements. The rheological properties of the nanocomposite melt using the polymer matrices of PP, HCPP, and PP-g-MA are shown in Figs. 5.5, 5.6, and 5.7, respectively. Repeat rheological measurements on the same sample prepared multiple times reveal that *G'*, *G"*, and $|\eta^*|$ are accurate to about 2%.

The rheological behavior of MMT/PP and MMT/HCPP composite melts have no significant difference except the composites based on HCPP matrix have a slightly higher *G'*, *G"*, and $|\eta^*|$ values. The nano-clay concentration and the processing method used have an insignificant impact on the nanocomposite rheological behavior based on both PP and HCPP matrices. As can be seen in Figs. 5.5 and 5.6, the *G'*, *G"*, and $|\eta^*|$ of both the MMT/PP and MMT/HCPP samples prepared with different methods overlapped with each other and were well within experimental error at same clay loadings. The *G'*, *G"*, and $|\eta^*|$ of MMT/HCPP composite melts slightly increase as the nano-clay concentration increases, as well as the $|\eta^*|$ of MMT/PP composite. The increases in *G'* and *G"* for the MMT/PP samples were too minimal to distinguish

within the scale of the figures, but they presented the same trend as the changes of η^* values with various clay loadings. By increasing the nano-clay concentrations, the interactions between the clay to polymer chains are stronger. The interparticle distances also decrease, increasing the chance of clay to clay interactions. These could all contribute to the increase of the melt viscosity. Despite the slight increase of magnitude, all the samples show the same rheological behavior. This indicates that no obvious network has formed in the composite melt up to the addition of 10 wt % of nano-clay in both the matrices and the processability of the polymer-clay nanocomposites remains satisfactory up to this clay loading.

The rheological behavior of the nanocomposites using PP-g-MA as a matrix is very different, as shown in Fig. 5.7. The *G'*, *G"*, and $|\eta^*|$ of the MMT/PP-g-MA melt show a great dependence on both the clay loading and processing method. The increases of *G'*, *G"*, and $|\eta^*|$ with increasing clay loading are very obvious. The 5% MMT/PP-g-MA samples do not have significant differences in rheological properties, probably because they do not have appreciable differences in morphology, as discussed in the previous section. The difference between the *G'*, *G"*, and $|\eta^*|$ of 10% MMT/PP-g-MA composites prepared by the two difference methods greatly diverge from each other. The 10% MMT/PP-g-MA DB sample presents the same basic behavior as the composites with lower clay loading except a higher magnitude. The G' and $|\eta^*|$ of the 10% MMT/PP-g-MA CO2 sample, however, have obvious "tail" and yield-like behavior, respectively, at low frequencies. Its *G"* is much higher than the rest of the PP-g-MA samples as well. It is generally reported in the literature that a ''tail'' in the storage modulus, *G'*, or the yield-like behavior in the complex viscosity, $|\eta^*|$, versus angular frequency at low frequencies can be observed when the nano-clays are exfoliated [22]. Nguyen et al. [20] found that the "tail" could be a result of network formed due to either interactions of matrix groups or large agglomerates of

clay. Their samples with exfoliated structure did not create this “tail” in *G’* while the sample that had large agglomerates with the addition of 24 wt% of nano-clay exhibited a “tail”. In our work, the TEM image of the 10% MMT/PP-g-MA DB sample showed a mixture of phase separated, intercalated, and exfoliated structure. The degree of clay dispersion and exfoliation of this sample is obviously worse than the 10% MMT/PP-g-MA CO2 sample. In this case, the tail is not definitely indicative for an exfoliated morphology. A combination of poor clay dispersion and strong matrix interaction between the MA group causes the yield behavior of *G’* and $|\eta^*|$ at the low frequencies. The rheological characterization is capable of monitoring the networks formed in the melt system, but does not provide sufficient information for accurate particle morphology conclusions.

5.5 Conclusions

Additional enhancements in composite mechanical properties were achieved with the $scCO_2$ exfoliation and sequential mixing techniques on nano-clay composite preparation using HCPP and MA-g-PP as matrices relative to using regular PP as the polymer matrix. The enhanced mechanical properties of HCPP composite were mostly due to the high stiffness of pure HCPP matrix. Evidence from TEM results leads us to believe that the degree of clay dispersion in the HCPP matrix is comparable to that of the clay dispersion in the PP matrix. By using HCPP as the matrix, a similar amount of improvement in terms of mechanical properties was obtained upon using the same processing methods compared to the composites using PP as a matrix. The HCPP nanocomposite that has 10 wt % of nano-clay with the Young’s modulus as high as 3.236 GPa was obtained, which is a 58% increase compared to the matrix modulus. The mechanical property enhancements for MMT/PP-g-MA composites, however, benefit the most from the $scCO_2$ exfoliation and sequential mixing techniques at higher clay loading. Based on

TEM observations, the MA compatibilizer can greatly improve the clay dispersion within the polymer matrix at lower clay levels, but the $scCO_2$ and sequential mixing techniques are needed for good clay dispersion at higher clay loading. The Young's modulus of the 10% MMT/PP-g-MA sample is found to be 2.595 GPa, much higher than the composite prepared by the direct blending method and composite based on PP matrix.

5.6 Acknowledgements

The authors would like to acknowledge the funding support from Institute for Critical Technology and Applied Science (ICTAS) at Virginia Tech and Southern Clay Products for donating the MMT nano-clays. In addition, we would like to thank Steve McCartney at the Nanoscale Characterization and Fabrication Laboratory in ICTAS for aid in conducting the TEM studies.

5.7 References

[1] Y. Kojima, A. Usuki, M. Kawasumi, A. Okada, Y. Fukushima, T. Kurauchi, O. Kamigaito, J Mater Res, 8 (1993) 1185-1189.

[2] K. Nevalainen, J. Vuorinen, V. Villman, R. Suihkonen, P. Jarvela, J. Sundelin, T. Lepisto, Polym. Eng. Sci., 49 (2009) 631-640.

[3] Q.P. Ran, H. Zou, S.S. Wu, J. Shen, Polymer Composites, 29 (2008) 119-124.

[4] W.H. Awad, G. Beyer, D. Benderly, W.L. Ijdo, P. Songtipya, M.D. Jimenez-Gasco, E. Manias, C.A. Wilkie, Polymer, 50 (2009) 1857-1867.

[5] M. Kawasumi, N. Hasegawa, M. Kato, A. Usuki, A. Okada, Macromolecules, 30 (1997) 6333-6338.

[6] A. Boukerrou, J. Duchet, S. Fellahi, M. Kaci, H. Sautereau, Journal of Applied Polymer Science, 103 (2007) 3547-3552.

[7] S.S. Ray, M. Okamoto, Prog. Polym. Sci., 28 (2003) 1539-1641.

[8] J.B. Gao, M.E. Itkis, A.P. Yu, E. Bekyarova, B. Zhao, R.C. Haddon, J. Am. Chem. Soc., 127 (2005) 3847-3854.

[9] Y. Takahashi, H. Awano, O. Haba, T. Takahashi, K. Yonetake, Kobunshi Ronbunshu, 65 (2008) 679-687.

[10] P. Chen, H.S. Kim, H.J. Jin, Macromol. Res., 17 (2009) 207-217.

[11] K. Saeed, S.Y. Park, Journal of Applied Polymer Science, 106 (2007) 3729-3735.

[12] H.G. Jeon, H.T. Jung, S.W. Lee, S.D. Hudson, Polym. Bull., 41 (1998) 107-113.

[13] C.R. Tseng, J.Y. Wu, H.Y. Lee, F.C. Chang, Polymer, 42 (2001) 10063-10070.

[14] N.H. Abu-Zahra, A.M. Alian, R. Perez, H. Chang, J. Reinf. Plast. Compos., 29 (2010) 1153-1165.

[15] M. Kannan, S.S. Bhagawan, T. Jose, S. Thomas, K. Joseph, Polym. Eng. Sci., 50 (2010) 1878-1886.

[16] D.R. Paul, L.M. Robeson, Polymer, 49 (2008) 3187-3204.

[17] G.M. A.J. Lesser, in: ANTEC 2004, 2004, pp. 1528-1532.

[18] C.W Manke, E. Gulari, D.F Mielewski, E.C Lee, U.S. Patent 6,753,360 (2002)

[19] D.F. Mielewski, E.C. Lee, C.W. Manke, E. Gulari, U.S. Patent 6,469,073 (2004)

[20] Q.T. Nguyen, D.G. Baird, Polymer, 48 (2007) 6923-6933.

[21] N. Hasegawa, H. Okamoto, M. Kawasumi, M. Kato, A. Tsukigase, A. Usuki, Macromol. Mater. Eng., 280 (2000) 76-79.

[22] R. Krishnamoorti, R.A. Vaia, E.P. Giannelis, Chemistry of Materials, 8 (1996) 1728-1734.

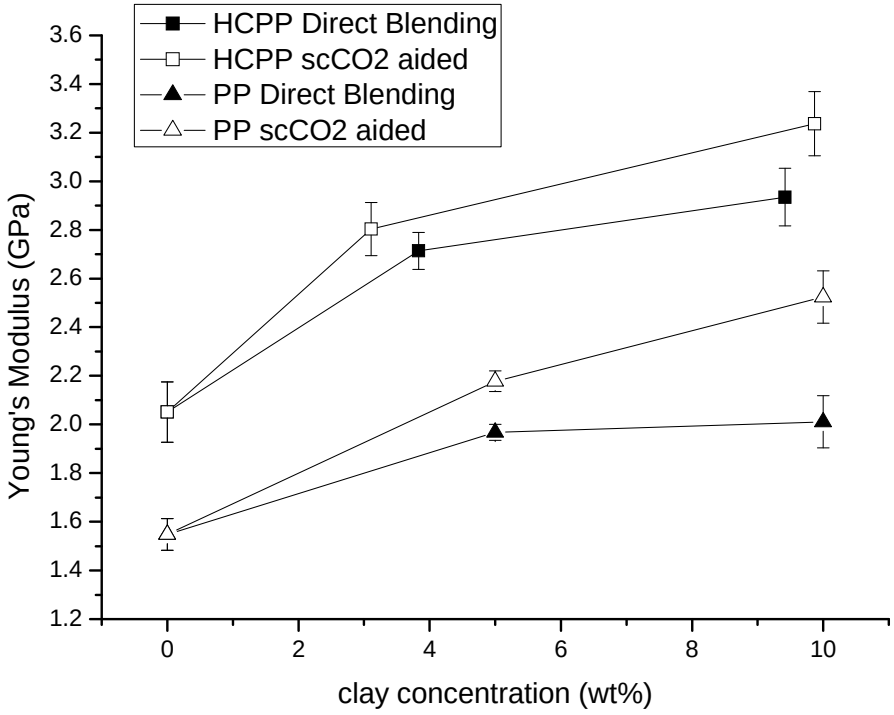

Figure 5.1: Comparison of Young's moduli of MMT/PP and MMT/HCPP nanocomposites processed by different methods

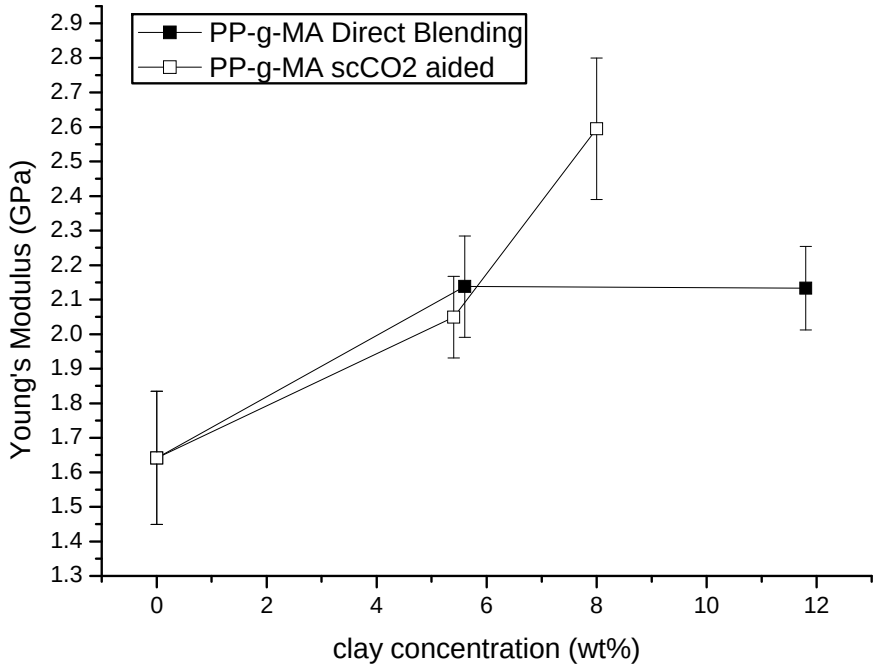

Figure 5.2: Comparison of Young's moduli of MMT/PP-g-MA nanocomposites processed by different methods

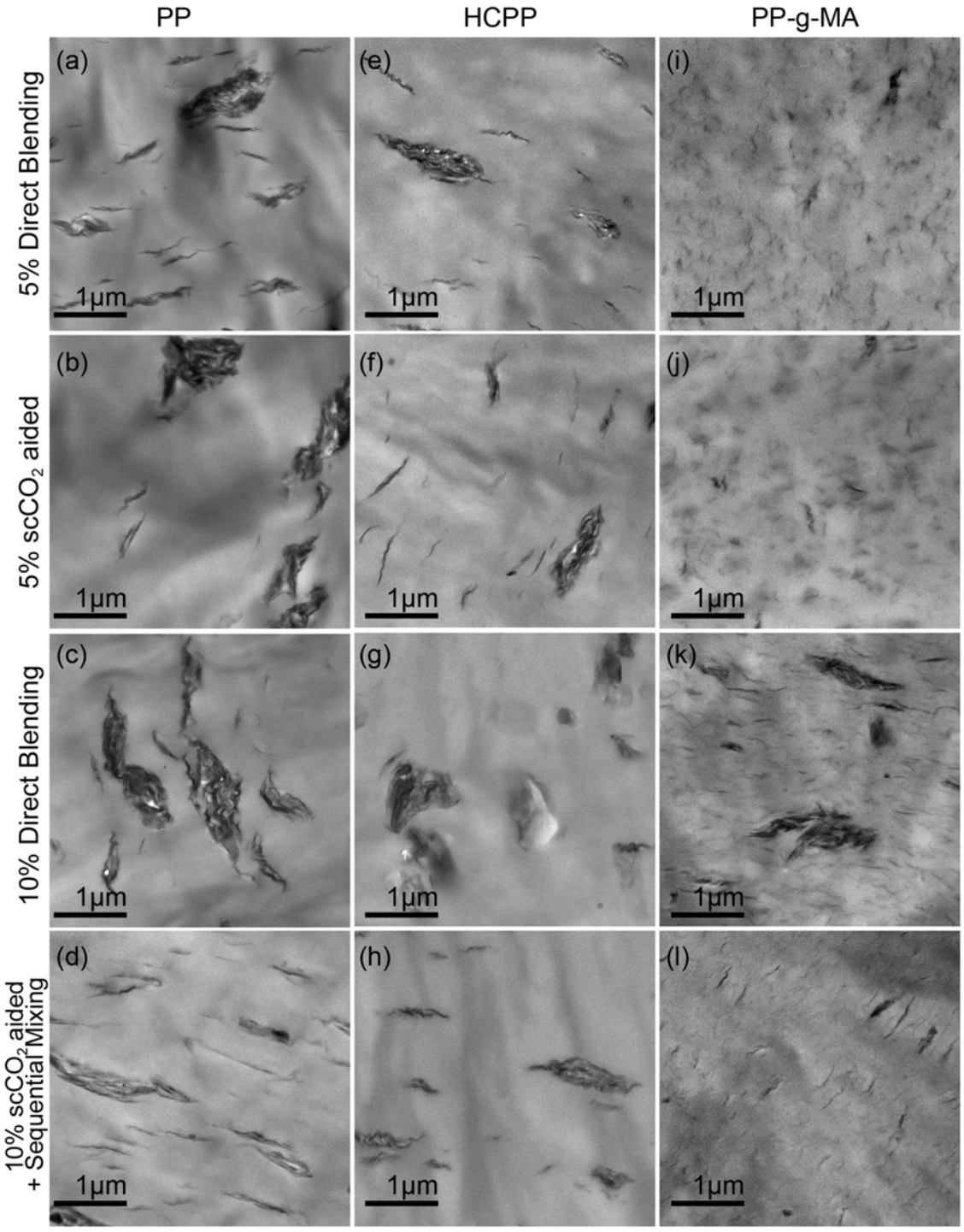

Figure 5.3: Transmission electron micrographs at 5,800x magnification of (a) 5 wt% MMT/PP nanocomposites processed by the direct blending method, (b) 5 wt% MMT/PP prepared by the $scCO_2$ aided melt blending, (c) 10 wt% MMT/PP prepared by the direct blending method, and (d) 10 wt% MMT/PP prepared by the $scCO_2$ aided melt blending method with sequential mixing

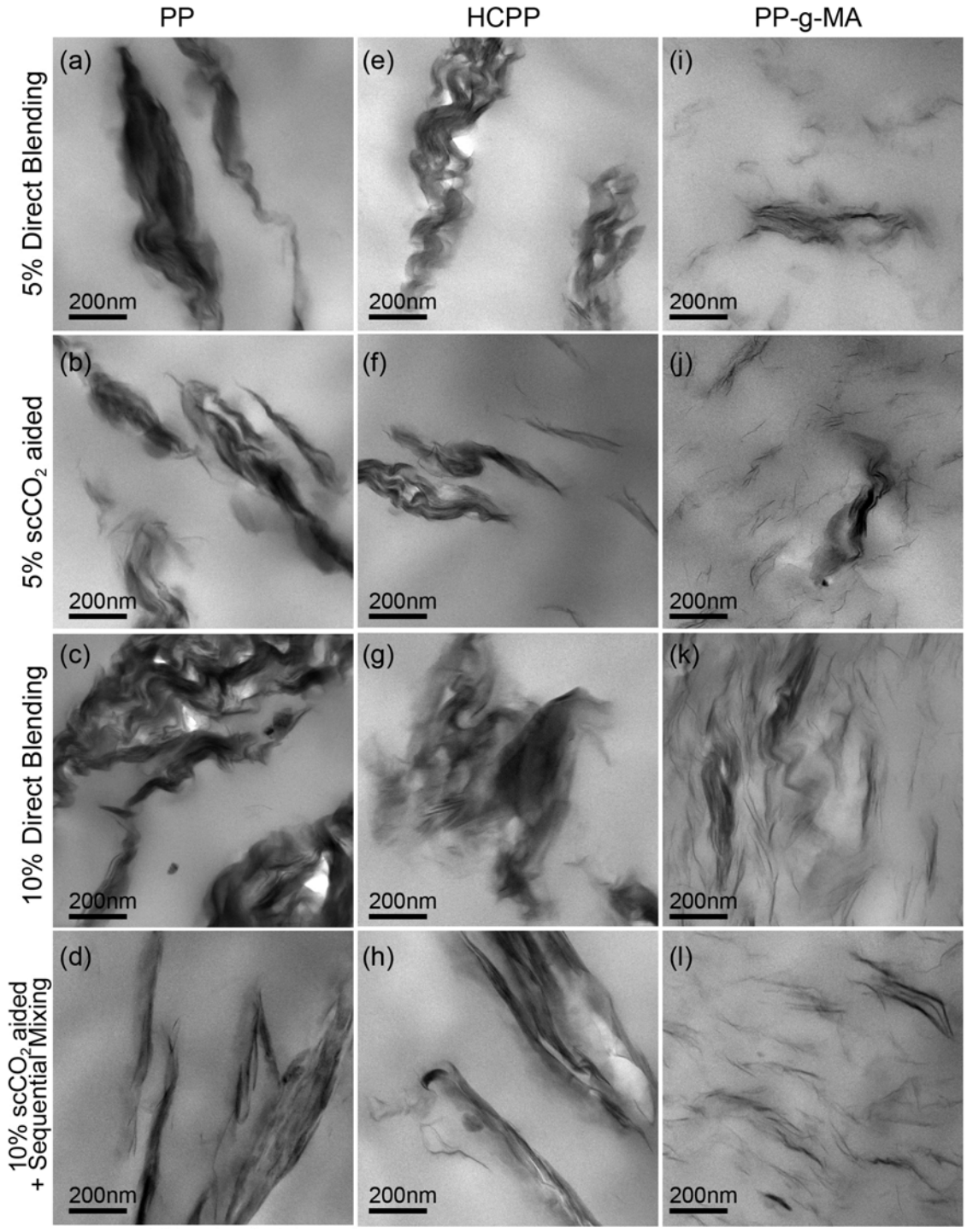

Figure 5.4. Transmission electron micrographs at 34,000x magnification of (a) 5 wt% MMT/PP nanocomposites processed by the direct blending method, (b) 5 wt% MMT/PP prepared by the $scCO_2$ aided melt blending, (c) 10 wt% MMT/PP prepared by the direct blending method, and (d) 10 wt% MMT/PP prepared by the $scCO_2$ aided melt blending method with sequential mixing.

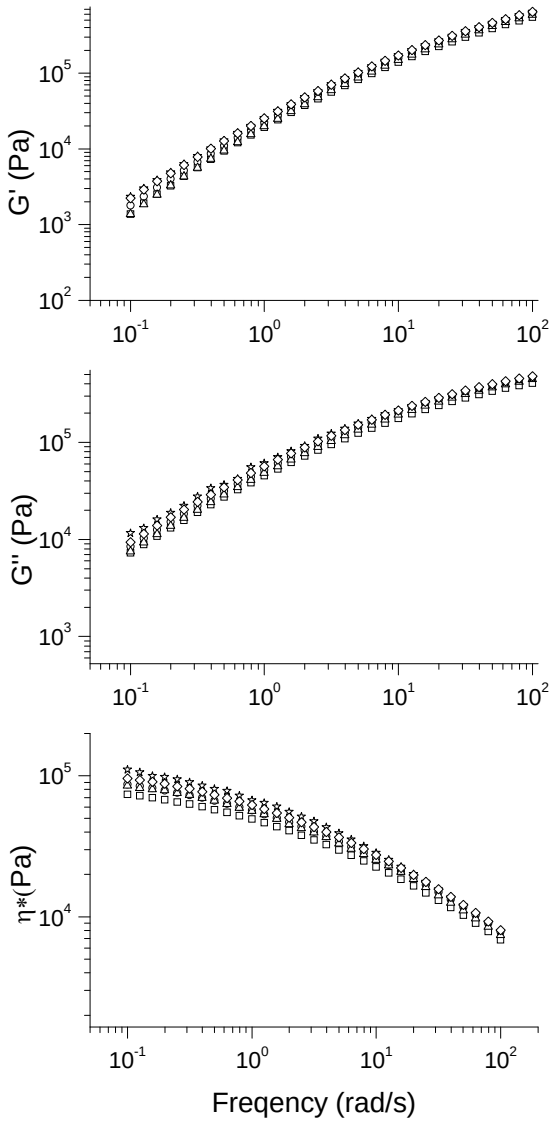

Figure 5.5: Storage modulus, *G'*, loss modulus, *G"*, and complex viscosity, $|\eta^*|$ vs. frequency, ω, of (□) PP, (○) 5 wt % MMT/PP composite prepared by the direct blending method, (△) 5 wt % MMT/PP composite prepared by the $scCO_2$ aided method, (☆)10 wt % MMT/PP composite prepared by the direct blending method, (◇)10 wt % MMT/PP composite prepared by the $scCO_2$ aided method and sequential mixing

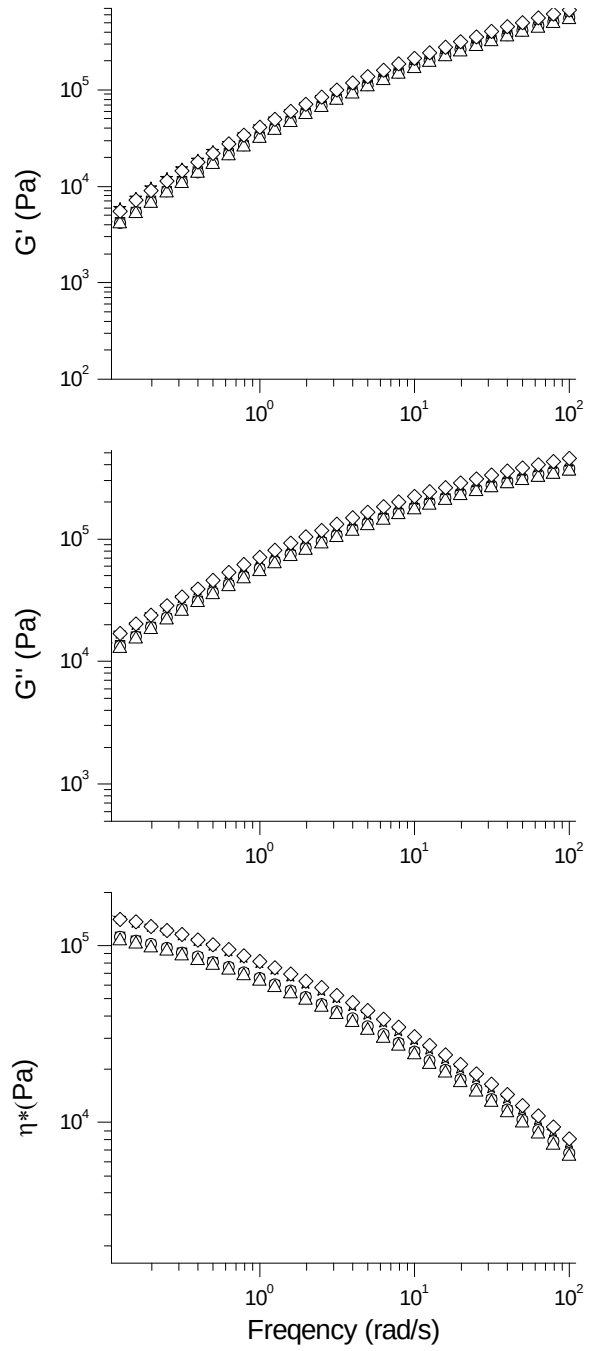

Figure 5.6: Storage modulus, *G'*, loss modulus, *G"*, and complex viscosity, $|\eta^*|$ vs. frequency, ω, of (□) HCPP, (○) 5 wt % MMT/HCPP composite prepared by the direct blending method, (Δ) 5 wt % MMT/HCPP composite prepared by the $scCO_2$ aided method, (☆)10 wt % MMT/HCPP composite prepared by the direct blending method, (◇)10 wt % MMT/HCPP composite prepared by the $scCO_2$ aided method and sequential mixing

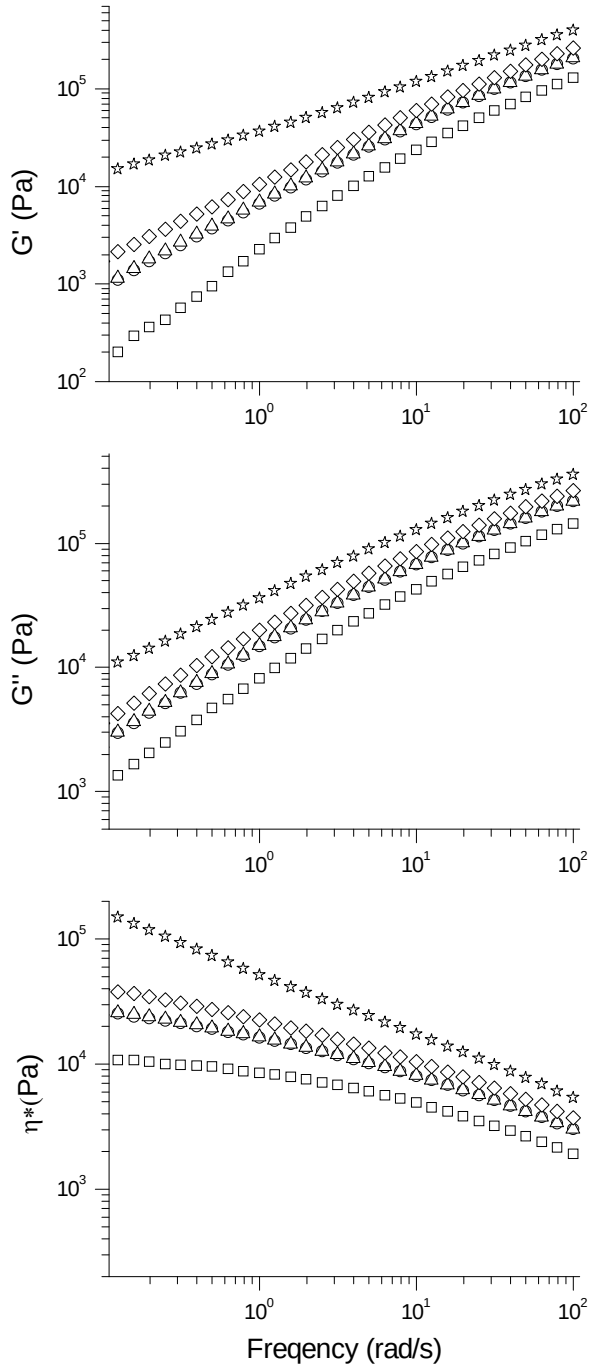

Figure 5.7: Storage modulus, *G'*, loss modulus, *G"*, and complex viscosity, $|\eta^*|$ vs. frequency, ω, of (□) PP-g-MA, (○) 5 wt % MMT/PP-g-MA composite prepared by the direct blending method, (△) 5 wt % MMT/PP-g-MA composite prepared by the $scCO_2$ aided method, (☆)10 wt % MMT/PP-g-MA composite prepared by the direct blending method, (◇)10 wt % MMT/PP-g-MA composite prepared by the $scCO_2$ aided method and sequential mixing

Table 5.1: Actual clay concentration and abbreviation of individual samples

Sample Abbreviation	Actual clay loading (wt %)	description
PP	- -	Pure PP
5% MMT/PP DB	5.36	MMT/PP prepared by direct melt blending method
5% MMT/PP CO2	5.44	MMT/PP prepared by $scCO_2$ aided method
10% MMT/PP DB	9.29	MMT/PP prepared by direct melt blending method
10% MMT/PP CO2	9.53	MMT/PP prepared by $scCO_2$ aided blending method and sequential mixing
HCPP	- -	Pure HCPP
5% MMT/HCPP DB	3.83	MMT/HCPP prepared by direct melt blending method
5% MMT/HCPP CO2	3.11	MMT/HCPP prepared by $scCO_2$ aided method
10% MMT/HCPP DB	9.42	MMT/HCPP prepared by direct melt blending method
10% MMT/HCPP CO2	9.87	MMT/HCPP prepared by $scCO_2$ aided blending method and sequential mixing
PP-g-MA	- -	Pure PP-g-MA (MA content = 0.5 wt %)
5% MMT/ PP-g-MA DB	5.60	MMT/PP-g-MA prepared by direct melt blending method
5% MMT/ PP-g-MA CO2	5.40	MMT/ PP-g-MA prepared by $scCO_2$ aided method
10% MMT/ PP-g-MA DB	11.8	MMT/ PP-g-MA prepared by direct melt blending method
10% MMT/ PP-g-MA CO2	8.02	MMT/ PP-g-MA prepared by $scCO_2$ aided blending method and sequential mixing

Table 5.2: Mechanical properties of nanoclay/polypropylene (MMT/PP) and nanoclay/high crystallinity polypropylene (MMT/HCPP), and nanoclay/PP-g-MA nanocomposite prepared using different processing methods

Materials	Young's Modulus (GPa)	S.D.	% Increase	Yield Strength (MPa)	S.D.	% Enlongation	S.D.
PP	1.548	0.065	- -	28.80	0.69	>20	- -
5% MMT/PP DB	1.968	0.033	27	30.98	0.29	>20	- -
5% MMT/PP CO2	2.178	0.043	41	30.40	0.75	>20	- -
10% MMT/PP DB	2.011	0.107	30	29.91	0.24	>20	- -
10% MMT/PP CO2	2.524	0.108	63	33.42	0.52	>20	- -
HCPP	2.051	0.124	- -	33.14	0.60	6.80	1.60
5% MMT/HCPP DB	2.714	0.076	32	34.71	0.65	16.65	2.96
5% MMT/HCPP CO2	2.804	0.109	37	34.95	0.84	>20	- -
10% MMT/HCPP DB	2.935	0.119	43	33.26	0.83	17.12	1.48
10% MMT/HCPP CO2	3.236	0.132	58	30.34	0.90	8.94	4.80
PP-g-MA	1.642	0.193	- -	29.58	0.20	5.28	0.43
5% MMT/ PP-g-MA DB	2.138	0.147	30	28.33	0.21	4.70	0.73
5% MMT/ PP-g-MA CO2	2.049	0.118	25	29.06	0.94	4.93	0.12
10% MMT/ PP-g-MA DB	2.133	0.121	30	27.74	0.67	3.93	0.27
10% MMT/ PP-g-MA CO2	2.595	0.205	58	29.75	1.34	3.05	0.41

Chapter 6

Overall Conclusions

Overall Conclusions

1. The $scCO_2$ technique was successfully extended to carbon nanotube (CNT) expansion and CNT/poly(phenylsulfone) (PPSF) composite preparation. Improved CNT dispersion in PPSF matrix and composite mechanical properties were obtained up to the addition of 7 wt % CNTs for samples prepared using the $scCO_2$ aided method, relative to those using the conventional melt blending method.

2. The previous research of nano-clay/polymer composite using $scCO_2$ was extended to a higher clay level (10 wt %). A modified processing route was successfully developed that effectively reduced the nano-clay collapse and improved the dispersion of nano-clay in the PP matrix at this high clay loading. The two important modifications of this process were: exfoliating nano-clay into polymer pellets and sequentially mixing the clay into the melt. Significant improvement of the composites mechanical properties were also obtained with Young's modulus and tensile strengths being increased by 68% and 16%, respectively, compared to that of the pure PP matrix.

3. Additional enhancements of composite mechanical properties were achieved by using HCPP and PP-g-MA as matrices instead of conventional PP. A high Young's modulus of 3.236 GPa was obtained by using this modified processing method and the HCPP as the matrix at 10 wt % nano-clay level. The modulus of

the 10 wt % nano-clay/PP-g-MA sample was found to be 2.595 GPa, which is also higher than that of the composites based on a conventional PP matrix.

Chapter 7

Recommendations for Future Work

Recommendations for Future Work

1. Limited to the vast bulk volume of the expanded CNTs and poor processability of CNT/PPSF composites at high CNT loading, it was not possible to prepare CNT composites with a CNT content over 7 wt %. Applying the sequential mixing procedure that was used for nano-clay/PP composite preparation in this work could be a potential solution to this limitation.

2. The orientation of the nano-clays and CNTs can significantly affect the composite mechanical properties because of their high aspect ratio. However, the control and influence of the particle orientation from additional post-processing, such as injection molding, mechanical squeezing and stretching, are complicated due the small scale of the nano-particles. This part of work was not fully investigated because of the limited time and facility access. A comprehensive and systematic study of the nano-particle orientation is recommended in the future to control the nano-particle orientation and reveal its influence on the composite mechanical properties.

3. The addition of micro-scale fillers, such as carbon fiber and glass fiber, with the nano-scale fillers can provide additional reinforcement to the composite. In addition, the aligned micro-scale filler can provide possibly easier orientation for the nano-scale fillers by forming channels in between the orientated micro-fibers. Therefore, future studies using the micro-scale fillers and nano-scale fillers together with the combination of orientation processes are recommended.

4. The modified melt processing procedure developed in this work is a semi-continuous process and can only reduce some of the collapse of the nano-clay during processing in the melt. It is recommended to develop a continuous process in which the exfoliated nano-clay is injected directly into the composite melt within the extruder to further reduce the collapse of the clay. In order to achieve this, this system should consist the following elements: 1) a extruder with a two stage screw that allows in-line addition of exfoliated clay in the melt; 2) two syringe pumps in series, which can provide continuous CO_2 with constant back pressure; 3) a feature that consists a mixing mechanism to prevent the settling of nanoparticles within the solid/gas mixture of nano-clay and CO_2, such as a fluidized bed; and 4) a slit die and attached gear pump that can manage and control and adjust the pressure within the extruding system. Employing a system like this should allow one to prepare nanocomposite continuously and further reduce clay collapse during processing.

Appendix A:

Preliminary Results of Poly(etheretherketon) Multi-scale Composites Reinforced by Carbon Fiber and Carbon Nanotube

A.0: Preliminary Results of Poly(etheretherketon) Multi-scale Composites Reinforced by Carbon Fiber and Carbon Nanotube

Composites, which use nano-reinforcements together with micro-scale reinforcements, are frequently referred to in the literature as multi-scale, (or three-phase, hybrid, hierarchical) composites [1]. Many interests have been attracted to the field of multi-scale composites using carbon nanotube (CNT) and carbon fiber (CF) as the filler materials. However, stiffness, strength and strain in the fiber direction are only slightly affected [2, 3]. The initial experiments of the preparation of CF and CNT reinforced poly(etheretherketon) (PEEK) composite using melt blending method with the aid of $scCO_2$ technique is studied in this work. We want to find out whether using the $scCO_2$ expanded CNTs together with micro-scale CFs is beneficial for the mechanical properties of the composites.

A.1 Experimental

A.1.1 Materials

The polymeric matrix used in this work was poly(etheretherketon) (PEEK) obtained from Victrex plc (Lancashire, United Kingdom). The carbon fiber (CF) reinforced PEEK was also obtained from Victrex plc, and contained 20 wt% of CF. Both pure PEEK and CF/PEEK were used as received. The pristine CNTs used were Nanocyl®-7000, which were obtained from Nanocyl Inc (Sambreville, Belgium). The CNTs were thin multi-wall carbon nanotubes produced via the catalytic carbon vapor deposition (CCVD) process and were used as-received.

A.1.2 CNT Expansion

The CNTs were allowed to be in direct contact with $scCO_2$ in a pressurized chamber at 3000 psi, at 80 ^{o}C for 12 hr. The CNTs and CO_2 mixture were then released into a 5 gal pressure vessel and depressurized rapidly to achieve expansion. The expanded CNTs were then collected.

The chamber used to contain CNTs and $scCO_2$ was a modified pressure chamber with 660 ml capacity obtained from Parr Instrument Company (Moline, IL). The inlet/outlet of the chamber was sealed by a ball valve from High Pressure Equipment Company (Erie, PA).

A.1.3 Melt Compounding

The compounding procedure for the CNT/CF/PEEK composite and 5%CNT/PEEK composite is described as follows. CF/PEEK pellets (or pure PEEK pellets in the case of 5%CNT/PEEK preparation) and the expanded CNTs were dry blended in a Kitchen Aid type mixer mechanically and dried together at 150 °C for at least 3 hrs in preparation of melt compounding. The mixture of CNTs and CF/PEEK (or PEEK) pellets was then fed to a single screw extruder (Killion 4335 series) and re-pelletized. The nanocomposite was extruded using a screw speed of 25 rpm and an ascending temperature profile beginning at 330 °C at the solids conveying zone and progressing to 380 °C at the circular die. The single screw a diameter of 2.54 cm, with a 25.4 mm (1 in) diameter, a L/D of 30:1, and variable channel depth from 12.80 mm at the feed to 7.90 mm at the exit. A capillary die of 1.59 mm diameter and 20:1 L/D was attached to the end of the extruder. The nanocomposite extrudate was quenched using a cold water bath at room temperature and collected in the form of strands with diameter around 3 mm.

A.1.4 Compression Molding

The CNT/CF/PEEK composite were then cut into strands of 10mm in length, and laid into a 10 mm x 10 mm mold, and compression molded into approximately 1.5 mm thick plaques at the temperature of 350 °C. In order to obtain plaques with similar CF orientation with the aligned CNT/CF/PEEK sample, the 30% CF/PEEK composite pellets were extruded and cut into strands of 10 mm long and compression molded into 1.5 mm thick plaques at 350 °C. This sample is labeled as “30% CF/PEEK aligned” in the rest of this chapter. The pure PEEK,

CF/PEEK pellets, and extruded 5%CNT/PEEK pellets were also compression molded into plaques using the same procedure for comparison purposes. These three samples do not have any preferable orientation from PEEK crystals and carbon fibers.

A.1.5 Tensile properties

The dogbone-shape samples of 65 mm long and 10 mm wide with the neck length of 20 mm and neck width of 3.15mm were stamped from the plaques. Tensile tests on these dogbone samples were performed at room temperature using an Instron Model 4204 testing machine (Instron, Grove City, PA). An extensometer was used to accurately measure Young's modulus. The load was measured with a 5 kN load cell. The crosshead speed was kept at 1.27 mm/min during all tensile tests. The average and standard deviation were calculated from measurements on at least four samples.

A.1.6 Morphological characterization

The morphology of the CNTs and the nanocomposites was analyzed by use of scanning electron microscopy (SEM). The SEM samples were prepared by breaking composite across the orientation direction in liquid nitrogen environment. SEM micrographs of the fracture surface were generated by means of a LEO 1550 SEM device with an accelerating voltage of 5 kV.

A.2 Preliminary Results and Disscussion

A.2.1 Tensile Properties

The mechanical properties, including Young's modulus, tensile strength, and elongation at break, of the PEEK and PEEK based nanocomposite are shown in Table A.1. The addition of 5 wt % CNTs does not provide any improvement on the mechanical properties, while the improvements in Young's modulus for the composites containing CFs are tremendous compared

to pure PEEK, as can be seen in Fig. A.1. PEEK used in this study has a Young's modulus of 4.749 ± 0.679 GPa, which is already very high considering it is about three times that of regular polypropylene. Compounding in 30% CF raised the composite modulus to as high as 17.548 ± 4.260 GPa, which is a 270% increase. By aligning the extrudate strands and introducing PEEK crystal and CF orientations along the flow direction, the modulus of 30 wt% CF/PEEK increased to 21.749 ± 3.327 GPa. The addition of 1 wt% CNTs provided the most improvement of the modulus for all the samples, as the modulus increased to 26.861 ± 5.163 GPa. This is a total 466% increase compared to pure PEEK matrix.

Table A.1: Mechanical properties of PEEK and PEEK based nanocomposite

Materials	Young's Modulus (GPa)	S.D.	% Increase	Yield Strength (MPa)	S.D.	% Elongation	S.D.
Pure PEEK	4.749	0.679	- -	55.77	13.28	1.51	0.66
5% CNT/PEEK	4.033	0.342	-28	52.78	15.58	1.36	0.32
30% CF/PEEK	17.548	4.260	270	204.63	40.65	1.69	0.14
30% CF/PEEK Aligned	21.749	3.327	358	206.96	17.31	1.37	0.19
1%CNT/30%CF/PEEK Aligned	26.861	5.163	466	213.21	25.76	1.55	0.08

Two preliminary conclusions could be drawn here. First, the orientation of CF is very effective in terms of improving material Young's modulus. Flowing through an extruder die can give CFs enough orientation and lead to significantly enhanced modulus. Second, the nano-scale CNT and micro-scale CF fillers may provided better reinforcement than simply addition of the two reinforcements together, because the micro-scale CFs might contribute to the CNT orientation as well. The interface interaction could be strengthened by the bridging of CNTs as well, which will be shown in the following section. The 1 wt% CNT/PEEK sample is not prepared yet at this point so no comparison can be conducted here. More comparison experiments are needed to prove this, though.

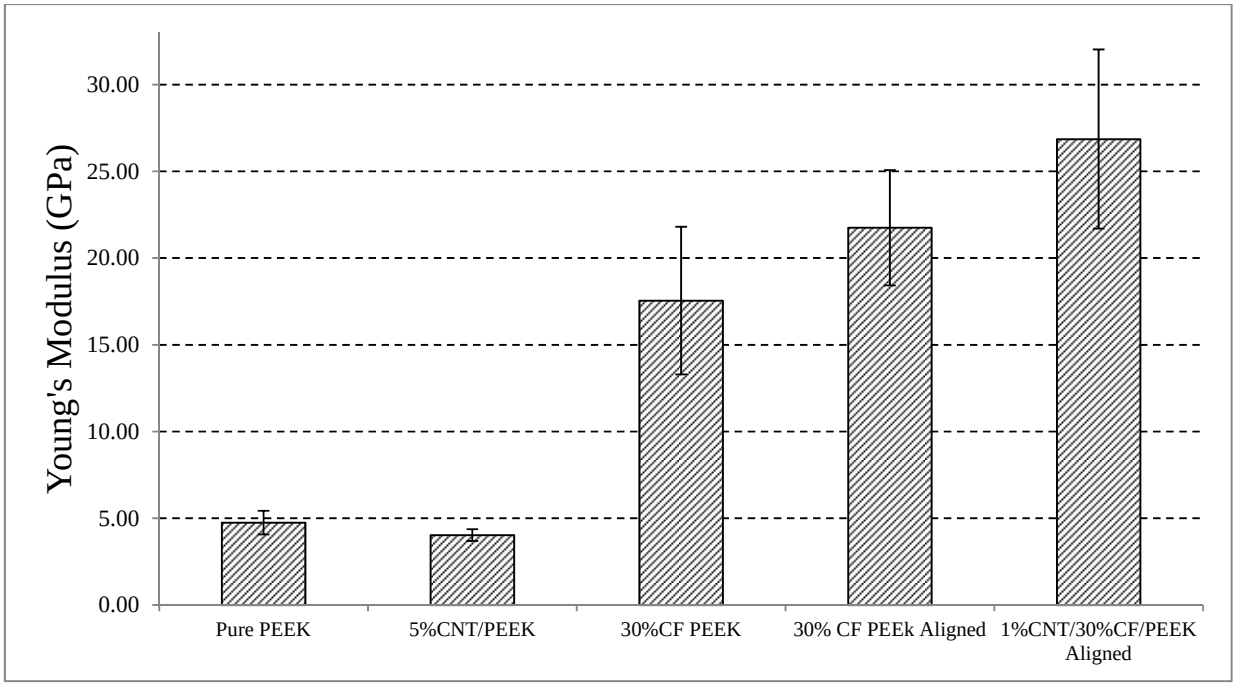

Figure A.1: Young's Molulus of PEEK and PEEK based nanocomposite

The tensile strength and elongation results of the nanocomposites are also encouraging as shown in Fig. A.2. The tensile strength of pure PEEK is 55.77 ± 13.28 MPa. Regardless of the filler type and orientating status, the tensile strengths of all composite samples are above 200 MPa. Introducing additional orientation or compounding CNTs in the composites did not affect the strength of the composites significantly. The values of elongation at break for all the samples, including the pure PEEK, are very small, ranging from 1.37% to 1.69%. It seems like the fillers did not affect the elongation at break of PEEK. This type of property will make this nanocomposite fit applications that need materials with high stiffness and low elongation at break.

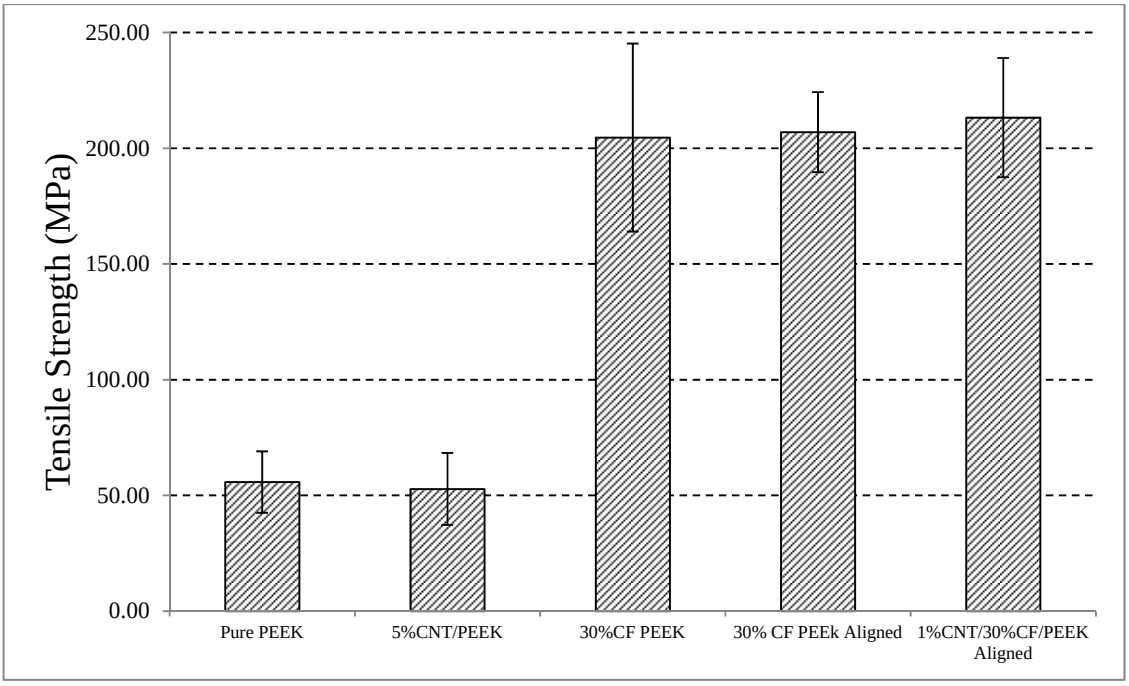

Figure A.2: Tensile strength of PEEK and PEEK based nanocomposite

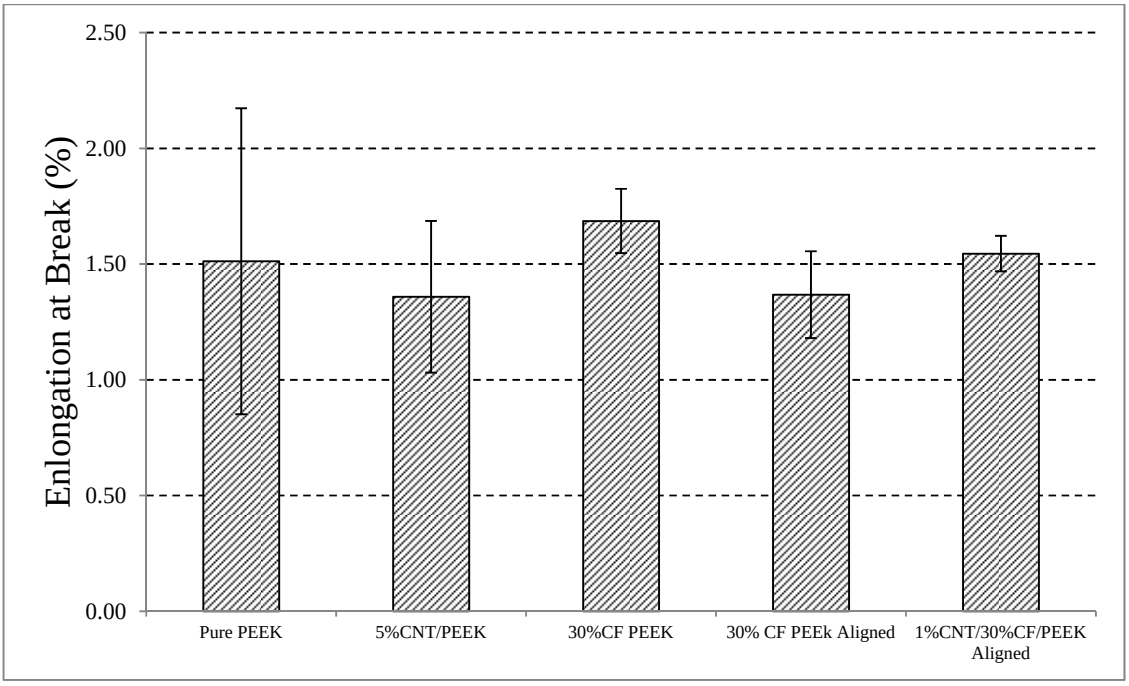

Figure A.3: Elongation at break of PEEK and PEEK based nanocomposite

A.2.2 Morphological Characterization

Scanning electron micrographs of the 1%CNT/30%CF/PEEK sample are provided here in Figures A.4 and A.5 to reveal the structure of this multi-scale reinforced composite. As can be seen in Fig. A.4, the lower magnification image, the CF orientation preference is very obvious. Most carbon fibers were aligned along the flow direction, or perpendicular to the fracture surface. This confirmed the earlier explanation for the enhanced Young's modulus from the samples with more fiber orientation. As shown in Fig. A.5 (at 20K magnification), CNTs were embedded in the polymer matrix and filled the gaps between the carbon fiber and polymer matrix. Some strings can be noticed connecting the CF and matrix which could be CNTs. The CNTs dispersed in the matrix could be reinforcing the areas that are not reinforced by the CFs, and the CNTs in the gaps could be very helpful by increasing the surface interactions between CF and PEEK matrix. These could all contribute to the tremendous modulus increase of the 1%CNT/30%CF/PEEK sample.

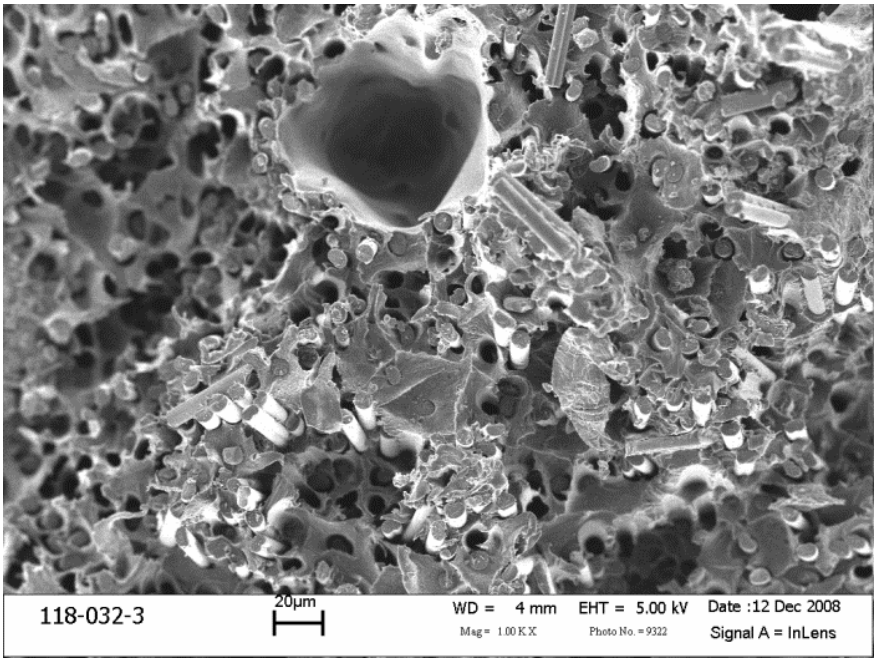

Figure A.4: Scanning electron micrograph of 1%CNT/30%CF/PEEK nanocomposite at 1k magnification

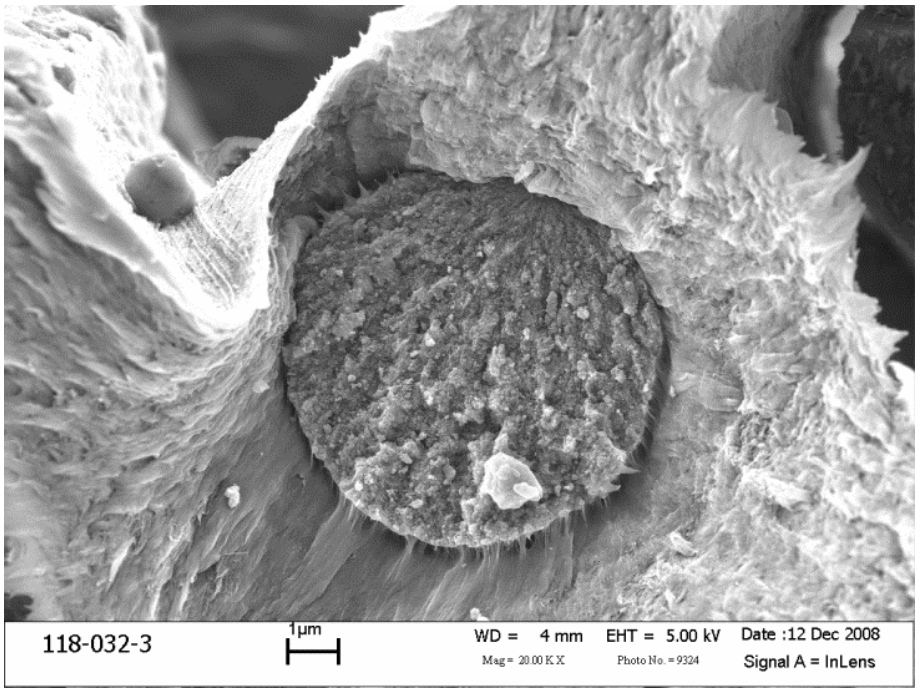

Figure A.5: Scanning electron micrograph of 1%CNT/30%CF/PEEK nanocomposite at 20k magnification

A.3 References

[1] H. Qian, E.S. Greenhalgh, M.S.P. Shaffer, A. Bismarck, J Mater Chem, 20 (2010) 4751-4762.
[2] Y. Iwahori, S. Ishiwata, T. Sumizawa, T. Ishikawa, Composites Part A: Applied Science and Manufacturing, 36 (2005) 1430-1439.
[3] T. Yokozeki, Y. Iwahori, S. Ishiwata, K. Enomoto, Composites Part A: Applied Science and Manufacturing, 38 (2007) 2121-2130.

Appendix B:

Preliminary Results on the Role of Clay Orientation on Mechanical Properties

B.0: Preliminary Results on the Role of Clay Orientation on Mechanical Properties

In addition to the degree of exfoliation of the nano-clay within the polymer matrix, the degree of orientation is another factor that affects the final mechanical properties of the nanocompoistes. The objective of this work is to determine how nanoclay orientation affects mechanical properties and whether the mechanical properties can be improved by introducing additional particle orientation.

B.1 Experimental

B.1.1 Materials and Preparation of Nanoclay/Polypropylene Composites

The polymer matrix used in this work is polypropylene (PP, Pro-Fax 6523) which was obtained from Lyondell Basell (Houston, TX) and was used as received. The melt flow index of the polymer is 4 g/10 min at 230°C and at a load of 2.16 kg. The nanoclay used was surface modified montmorillonite (MMT) (Cloisite 20A), which was obtained from Southern Clay Products, Inc. (Gonzalez, TX) and was used as-received. Cloisite 20A is a surface modified montmorillonite obtained through a cation exchange reaction, where the sodium cation is replaced by dimethyl, dihydrogenated tallow, quaternary ammonium cation. The compounding procedure in preparation of nanoclay/PP composite including clay exfoliation, extrusion and injection molding, was the same as described in Chapter 4.

B.1.2 Mechanical Stretching Procedure

The injection molded plaques were cut into strips around 6mm wide and 50 mm long. The strip was stretched using the Instron machine with a speed of 1 mm/min at a temperature of 120 °C. All the samples had a fixed elongation ratio of ~250% due to the necking behavior of the PP.

B.1.3 Small Angle X-Ray Scattering

Small angle X-ray scattering (SAXS) using a Rigaku S-Max 300 3 pinhole SAXS system was used to evaluate the orientation of nanoclay in polymer matrix. The radiation X-ray source is Cu Ka. The incident X-ray beam was attenuated to a wave length of 0.154 nm with a sample-to-detector distance of 16.0 cm.

B.1.4 Tensile Properties

The injection-molded plaques were cut into rectangular bars lengthwise along the flow direction, and were approximately 6 mm wide, 1.5 mm thick, and 80 mm long. The stretched samples are about 40 mm long, 0.6 mm thick, and 4 mm wide. Tensile tests on these samples were performed at room temperature with an Instron model 4204 testing machine (Instron, Grove City, PA). An extensometer was used to accurately measure Young's modulus. The load was measured with a 5-kN load cell, whereas the crosshead speed was kept at 1.27 mm/min during all tensile tests.

B.2 Preliminary Results and Discussion

B.2.1 Small Angel X-Ray Scattering Analysis

B.2.1.1 SAXS of 10% Clay/PP Injection molded plaques

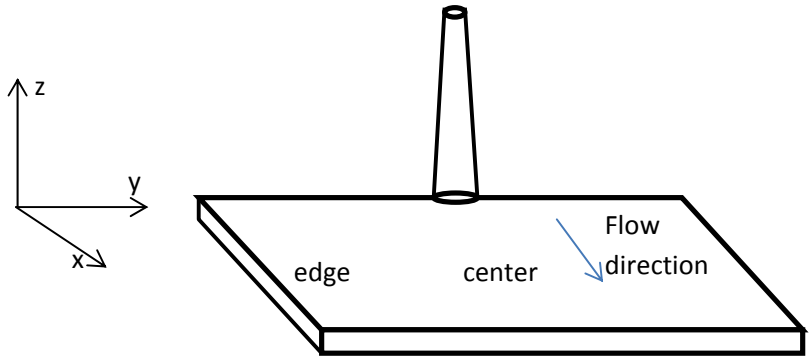

Figure B.1 Illustration of sample position and directions

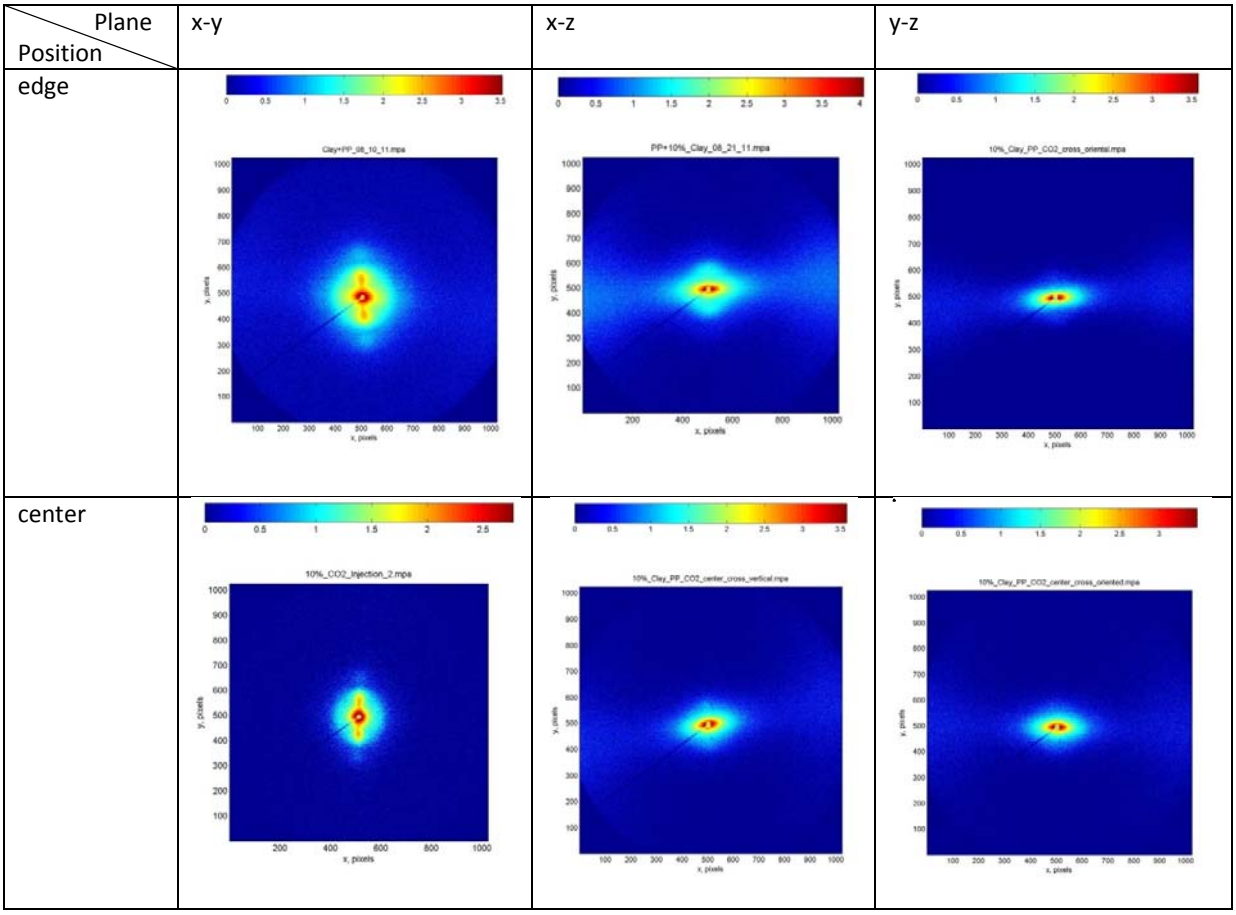

Figure B.2: SAXS patterns for 10% clay/PP composite injected plaques with different positions and directions

The terms used to describe sample directions and positions in the following are defined in Fig. B.1. As illustrated, the x axis is along the flow direction, the y axis is along the cross-flow direction, and the z axis is along the direction perpendicular to the plaque surface. The SAXS patterns for the 10% clay/PP composite injected plaques (prepared by the $scCO_2$ aided method with sequential mixing) with different positions and directions were obtained and shown in Fig. B.2. From the SAXS patterns in Fig. B.2, it can be noticed that the orientation of clay platelets depend on both sample direction and position. Regardless of the sample position (plaque edge or plaque center), strong ordered structure orientation can be observed in the x-z and y-z plane in x and y directions, respectively. This indicated that the clay platelets were orientated within the plaque plane (x-y plane). The orientations of clay platelets observed in the x-y plane varied with

different sample positions. At the edges, the amount of clay oriented in the x and y direction is about equal. While in the center, the clay platelets are mostly oriented along the y direction, which is the cross-flow direction, instead of the flow direction as we expected. This is probably because of the radial flow of the melt before it reached the mold boundary. There were only two positions of the plaques tested, and they were both sampled from same x position (about 1/3 to the plaque end). More complicated orientation of the clay platelets should be expected with more positions tested along the two directions (x and y). The flow for the composite melt within the end-gated mold is very complicated and well beyond simple flow from the gate to the mold end. Interactions between the melt and the nano-scale clay are also uncertain for now. More characterizations and analysis are needed in order to conclude the orientation behavior of clay during the injection molding process.

B.2.1.2 SAXS of Pure PP Injection Molded Plaques

PP is a semi-crystalline polymer so it has crystalline structure with orientation as well. It is important to distinguish the orientation from the nanoclays and the crystalline matrix. Therefore, the SAXS patterns for pure PP injected plaques with a few different positions and directions were obtained for comparison purposes and shown in Fig. B.3.Crytalline orientation of PP crystals is also complicated. The crystalline orientation of the PP at the edge is random in the x-y plane and is along x direction in x-z plane. The crystalline orientation in the center of the plaque is complicated. The reason for this pattern is still unclear. Although more studies will be needed for the crystalline behavior of the PP matrix, one point can be made here. The orientation of the PP crystals is reflected at larger scattering angles due to small crystal dimensions. Therefore, the introduced orientation of the nanoclay/PP samples at small scattering angles should be from the clay orientation.

Plane / Position	x-y	x-z	y-z
edge	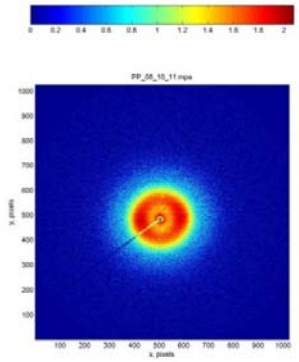	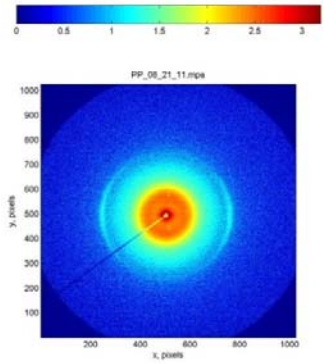	
center	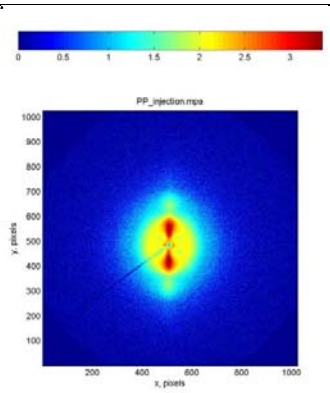		

Figure B.3: SAXS patterns for pure PP injected plaques with different positions and directions

B.2.1.3 SAXS Comparison of PP and PP Based Composites before and after Stretching

The stretching process was expected to generate orientation of both the PP crystallites and clay platelets in the stretching direction and lead to enhanced composite mechanical properties. The comparisons of the SAXS patterns between injection molded plaques before and after stretching are displayed in Fig. B.4. The differences in the SAXS patterns of the materials before and after stretching are significant. Regardless of the sample type, all samples gained more orientation along the stretching direction at a wide range of scattering angles, which suggests that both the PP crystallites and the clay platelets gained additional orientation after the stretching process.

sample	Before streching	After streching
PP (center)	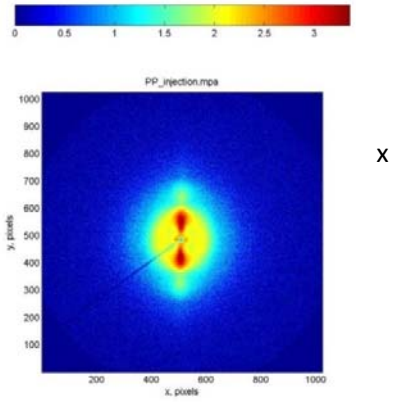 x	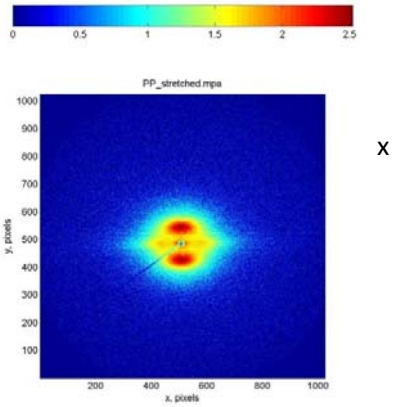 x
10% clay/PP (edge)	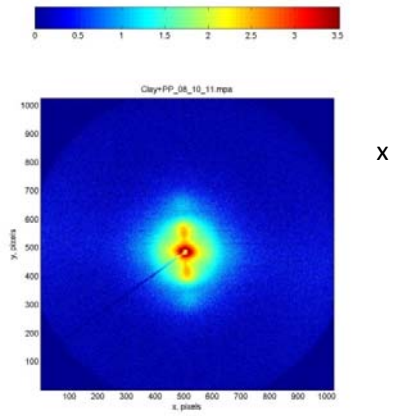 x	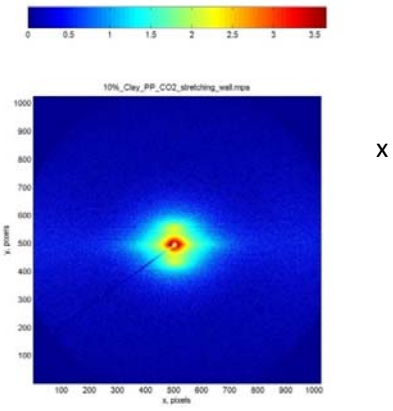 x
10% clay/PP (center)	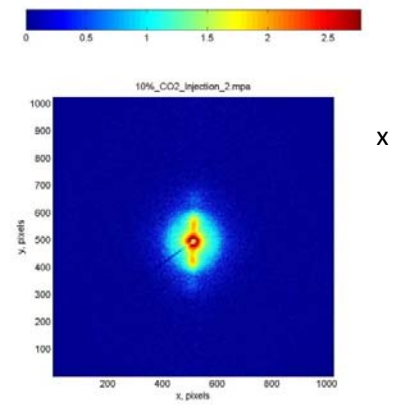 x	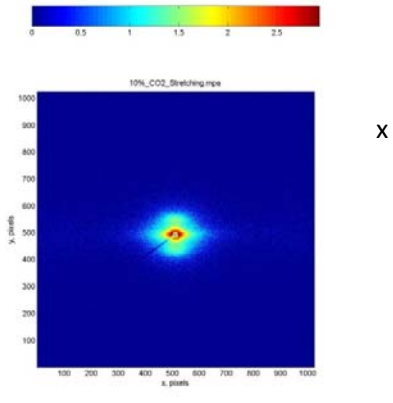 x

Figure B.4: Comparisons of SAXS patterns of injection molded plaques before and after the stretching process

B.2.2 Tensile Properties

The mechanical properties, including Young's modulus and tensile strength, of the PP, 5% clay/PP composite prepared by $scCO_2$ aided melt blending, and 10% clay/PP composite prepared by $scCO_2$ method with sequential mixing are shown in Table B.1. The Young's modulus and tensile strength results are also compared in Figs. B.5 and B.6, respectively.

Table B.1: Mechanical properties of PP and PP based nanocomposite before and after mechanical stretching process

Materials	Young's Modulus (GPa)	S.D.	% Increase	Yield Strength (MPa)	S.D.	% Increase
Pure PP (before stretching)	1.548	0.065	- -	28.80	0.69	- -
Pure PP (after stretching)	3.537	0.303	128	138.25	16.00	380
5% clay/PP CO2 (before stretching)	2.122	0.092	37	30.40	0.75	6
5% clay/PP CO2 (after stretching)	4.003	0.419	159	163.57	13.68	468
10% clay/PP CO2 sequential (before stretching)	2.484	0.050	60	30.63	0.81	6
10% clay/PP CO2 sequential (after stretching)	5.150	0.485	233	161.88	8.90	462

The mechanical properties of the PP and PP based composites exhibit a great difference before and after mechanical stretching. The modulus of the pure PP showed significant improvement as a result of the crystalline orientation gained from the stretching. The increases of Young's modulus and tensile strength for the stretched PP are 128% and 380%, respectively, compared to the injection molded PP without stretching. The modulus for the stretched 5 wt% clay/PP composite sample is higher than that of the stretched PP sample, but their difference is only around 0.5 GPa, very similar to the difference of the 5 wt% clay/PP and pure PP samples without stretching. In other words, the effect of clay orientation on Young's modulus is not obvious at 5 wt% clay loading. However, the 10 wt% nanoclay/PP sample has a larger (1.6 GPa) increase in Young's modulus compared stretched PP, which is much higher than the Young's modulus of injection molded with the same processing method and clay loading (~1 GPa). The tensile strength also increases quite a lot for the stretched nanoclay/PP samples. The tensile strength for the stretched 5% clay/PP and 10% clay/PP is about 25MPa higher than the stretched PP, while

the difference between the injection molded 5% clay/PP and PP is only 2MPa. As a preliminary conclusion, the mechanical stretching procedure is quite effective in terms of improving materials mechanical properties at relatively high clay loading (i.e. 10 wt%).

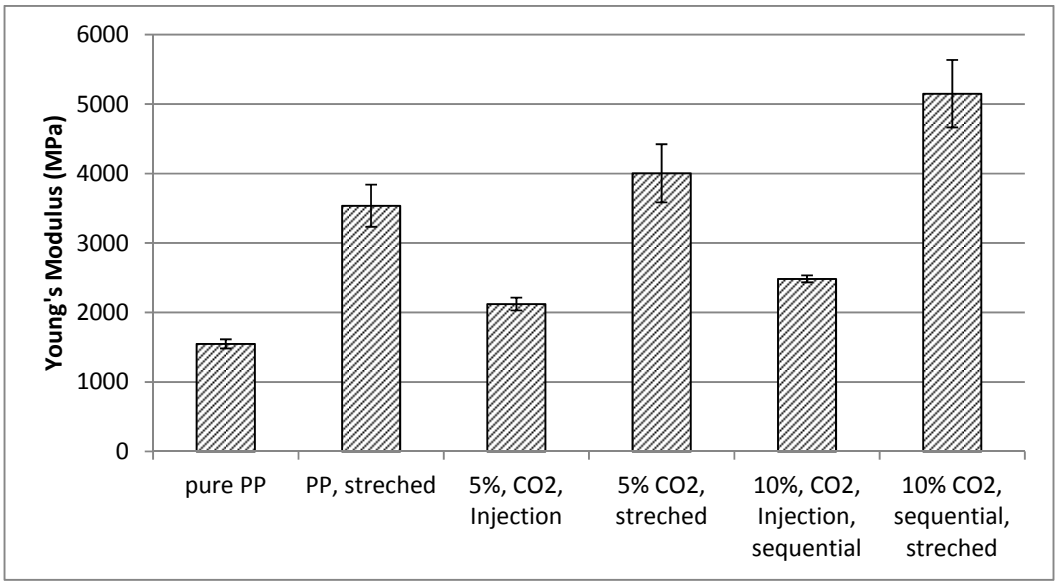

Figure B.5: Comparison of Young's moduli of PP and PP based composites before and after mechanical stretching

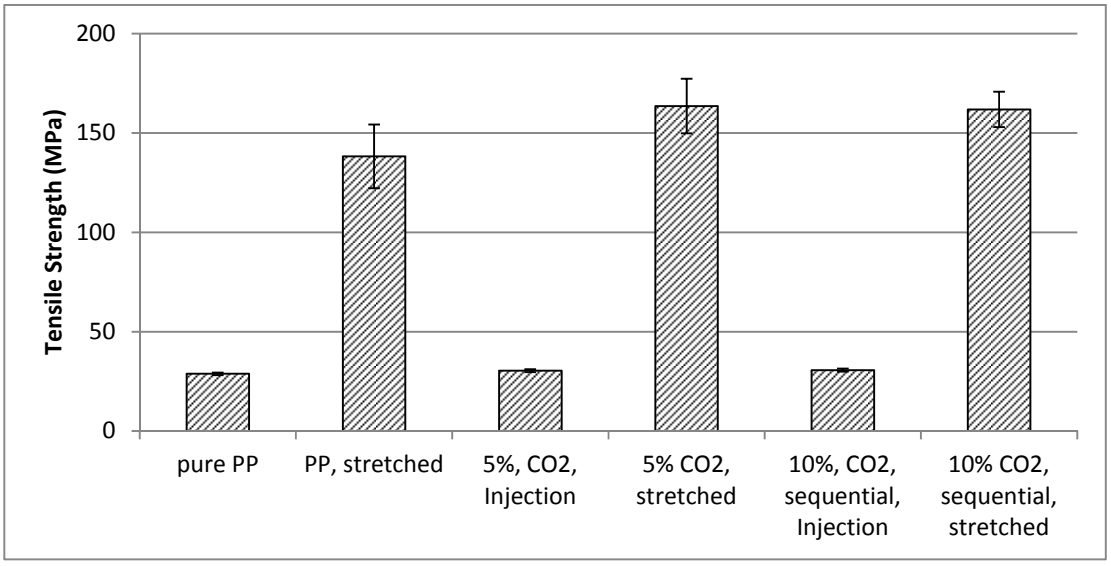

Figure B.6: Comparison of tensile strength of PP and PP based composites before and after mechanical stretching

Appendix C: Dynamic Oscillatory Rheological Data

Table C.1: Complex viscosity, $|\eta^*|$, vs. frequency, ω, for the carbon nanotubes (CNT)/poly(phenylsulfone) (PPSF) nanocomposite melts tested at a strain of 1% and at 350 °C (measured using ARES rheometer)

$\|\eta^*\|$ (Pa) / Frequency (rad/s)	PPSF	1% CNT PPSF DB	1% CNT PPSF CO2	3% CNT PPSF CO2	3% CNT PPSF DB	5% CNT PPSF DB	5% CNT PPSF CO2	7% CNT PPSF DB	7% CNT PPSF CO2
0.1	2.719E+04	4.776E+04	4.134E+04	3.408E+05	1.220E+05	2.712E+06	5.100E+06	6.029E+06	3.407E+07
0.15849	2.098E+04	3.588E+04	3.052E+04	2.561E+05	9.942E+04	1.806E+06	3.353E+06	4.013E+06	2.269E+07
0.24581	1.759E+04	2.969E+04	2.646E+04	1.963E+05	8.133E+04	1.217E+06	2.217E+06	2.668E+06	1.510E+07
0.39811	1.528E+04	2.619E+04	2.367E+04	1.531E+05	6.615E+04	8.071E+05	1.478E+06	1.773E+06	1.004E+07
0.63096	1.420E+04	2.274E+04	2.196E+04	1.224E+05	5.500E+04	5.442E+05	9.877E+05	1.186E+06	6.677E+06
1	1.301E+04	2.057E+04	2.044E+04	1.003E+05	4.677E+04	3.693E+05	6.685E+05	8.011E+05	4.444E+06
1.58489	1.229E+04	1.841E+04	1.953E+04	8.365E+04	4.042E+04	2.529E+05	4.643E+05	5.497E+05	2.965E+06
2.51189	1.165E+04	1.706E+04	1.861E+04	7.092E+04	3.523E+04	1.733E+05	3.247E+05	3.839E+05	1.985E+06
3.98107	1.119E+04	1.589E+04	1.772E+04	6.097E+04	3.099E+04	1.201E+05	2.335E+05	2.731E+05	1.334E+06
6.30957	1.091E+04	1.492E+04	1.694E+04	5.263E+04	2.735E+04	8.365E+04	1.711E+05	1.982E+05	9.005E+05
10	1.067E+04	1.420E+04	1.631E+04	4.561E+04	2.418E+04	5.878E+04	1.284E+05	1.468E+05	6.112E+05
15.84894	1.031E+04	1.370E+04	1.546E+04	3.961E+04	2.137E+04	4.165E+04	9.814E+04	1.107E+05	4.168E+05
25.11887	9.784E+03	1.300E+04	1.443E+04	3.437E+04	1.880E+04	2.969E+04	7.629E+04	8.467E+04	2.858E+05
39.81073	9.138E+03	1.207E+04	1.327E+04	2.963E+04	1.646E+04	2.136E+04	6.003E+04	6.556E+04	1.971E+05
63.09575	8.410E+03	1.103E+04	1.205E+04	2.536E+04	1.428E+04	1.544E+04	4.768E+04	5.121E+04	1.367E+05
100.00002	7.621E+03	9.870E+03	1.077E+04	2.143E+04	1.223E+04	1.120E+04	3.805E+04	4.020E+04	9.534E+04

Table C.2: Storage modulus, *G'*, vs. frequency, ω, for the carbon nanotubes (CNT) /poly(phenylsulfone) (PPSF) nanocomposite melts at a strain of 1% and at 350 °C (measured using ARES rheometer)

G'(Pa) / Frequency (rad/s)	PPSF	1% CNT PPSF DB	1% CNT PPSF CO2	3% CNT PPSF CO2	3% CNT PPSF DB	5% CNT PPSF DB	5% CNT PPSF CO2	7% CNT PPSF DB	7% CNT PPSF CO2
0.1	1.684E+03	3.477E+03	2.140E+03	2.876E+04	9.046E+03	2.672E+05	5.009E+05	5.973E+05	3.129E+06
0.15849	1.903E+03	3.496E+03	2.219E+03	3.278E+04	1.104E+04	2.826E+05	5.200E+05	6.305E+05	3.307E+06
0.25119	2.213E+03	4.281E+03	2.816E+03	3.807E+04	1.365E+04	3.010E+05	5.454E+05	6.635E+05	3.488E+06
0.39811	2.453E+03	5.187E+03	3.113E+03	4.403E+04	1.642E+04	3.162E+05	5.743E+05	6.965E+05	3.678E+06
0.63096	3.258E+03	6.192E+03	4.243E+03	5.193E+04	1.996E+04	3.359E+05	6.043E+05	7.346E+05	3.872E+06
1	3.978E+03	8.042E+03	5.808E+03	6.253E+04	2.491E+04	3.606E+05	6.416E+05	7.801E+05	4.080E+06
1.58489	5.285E+03	1.013E+04	8.358E+03	7.676E+04	3.165E+04	3.899E+05	6.936E+05	8.382E+05	4.312E+06
2.51189	7.143E+03	1.438E+04	1.254E+04	9.653E+04	4.140E+04	4.211E+05	7.567E+05	9.125E+05	4.572E+06
3.98107	1.049E+04	2.105E+04	1.948E+04	1.245E+05	5.496E+04	4.602E+05	8.395E+05	1.006E+06	4.863E+06
6.30957	1.741E+04	3.248E+04	3.138E+04	1.640E+05	7.511E+04	5.045E+05	9.465E+05	1.126E+06	5.195E+06
10	2.932E+04	5.288E+04	5.197E+04	2.212E+05	1.038E+05	5.574E+05	1.088E+06	1.284E+06	5.578E+06
15.84894	4.824E+04	8.965E+04	8.327E+04	3.044E+05	1.481E+05	6.213E+05	1.273E+06	1.486E+06	6.018E+06
25.11887	7.786E+04	1.428E+05	1.312E+05	4.246E+05	2.122E+05	6.959E+05	1.517E+06	1.749E+06	6.530E+06
39.81073	1.247E+05	2.199E+05	2.043E+05	5.981E+05	3.076E+05	7.875E+05	1.839E+06	2.092E+06	7.128E+06
63.09575	1.989E+05	3.330E+05	3.156E+05	8.452E+05	4.460E+05	8.953E+05	2.270E+06	2.540E+06	7.831E+06
100.00002	3.153E+05	4.990E+05	4.841E+05	1.192E+06	6.447E+05	1.024E+06	2.851E+06	3.136E+06	8.676E+06

Table C.3: Loss modulus, *G*", vs. frequency, ω, for the carbon nanotubes (CNT) /poly(phenylsulfone) (PPSF) nanocomposite melts at a strain of 1% and at 350 °C (measured using the ARES rheometer)

G"(Pa) / Frequency (rad/s)	PPSF	1% CNT PPSF DB	1% CNT PPSF CO2	3% CNT PPSF CO2	3% CNT PPSF DB	5% CNT PPSF DB	5% CNT PPSF CO2	7% CNT PPSF DB	7% CNT PPSF CO2
0.1	2.207E+03	4.488E+03	3.292E+03	1.240E+05	7.824E+04	1.616E+05	5.263E+05	2.207E+03	4.488E+03
0.15849	3.235E+03	6.028E+03	4.257E+03	1.318E+05	7.927E+04	1.724E+05	5.499E+05	3.235E+03	6.028E+03
0.25119	4.614E+03	8.654E+03	5.910E+03	1.432E+05	9.051E+04	1.909E+05	5.931E+05	4.614E+03	8.654E+03
0.39811	6.269E+03	1.191E+04	9.042E+03	1.608E+05	1.067E+05	2.163E+05	6.432E+05	6.269E+03	1.191E+04
0.63096	9.561E+03	1.691E+04	1.327E+04	1.858E+05	1.367E+05	2.451E+05	7.125E+05	9.561E+03	1.691E+04
1	1.407E+04	2.443E+04	2.006E+04	2.200E+05	1.711E+05	2.856E+05	7.944E+05	1.407E+04	2.443E+04
1.58489	2.125E+04	3.523E+04	3.075E+04	2.661E+05	2.268E+05	3.380E+05	8.902E+05	2.125E+04	3.523E+04
2.51189	3.194E+04	5.146E+04	4.600E+04	3.274E+05	2.942E+05	4.045E+05	9.975E+05	3.194E+04	5.146E+04
3.98107	4.844E+04	7.567E+04	6.988E+04	4.072E+05	3.868E+05	4.899E+05	1.141E+06	4.844E+04	7.567E+04
6.30957	7.413E+04	1.114E+05	1.053E+05	5.119E+05	5.112E+05	5.952E+05	1.301E+06	7.413E+04	1.114E+05
10	1.136E+05	1.635E+05	1.588E+05	6.464E+05	6.736E+05	7.276E+05	1.491E+06	1.136E+05	1.635E+05
15.84894	1.719E+05	2.363E+05	2.367E+05	7.820E+05	8.860E+05	8.912E+05	1.715E+06	1.719E+05	2.363E+05
25.11887	2.552E+05	3.381E+05	3.463E+05	9.958E+05	1.163E+06	1.091E+06	1.980E+06	2.552E+05	3.381E+05
39.81073	3.723E+05	4.782E+05	4.984E+05	1.266E+06	1.519E+06	1.334E+06	2.282E+06	3.723E+05	4.782E+05
63.09575	5.339E+05	6.665E+05	7.061E+05	1.603E+06	1.966E+06	1.625E+06	2.619E+06	5.339E+05	6.665E+05
100.00002	7.519E+05	9.154E+05	9.807E+05	2.006E+06	2.513E+06	1.965E+06	2.967E+06	7.519E+05	9.154E+05

Table C.4: Complex viscosity, $|\eta^*|$, vs. frequency, ω, for the montmorillonite (MMT) /polypropylene (PP) nanocomposite melts at a strain of 5% and at 200 °C (measured using the ARES rheometer)

$\lvert\eta^*\rvert$ (Pa) / Frequency (rad/s)	PP	5% MMT PP DB	5% MMT PP CO2	10% MMT PP DB	10% MMT PP CO2	10% MMT PP DB Sequential	10% MMT PP CO2 Sequential
0.1	3.523E+04	4.211E+04	4.452E+04	4.842E+04	5.465E+04	5.819E+04	5.028E+04
0.15849	3.216E+04	3.730E+04	4.261E+04	4.842E+04	5.390E+04	5.093E+04	4.843E+04
0.24581	3.031E+04	3.534E+04	3.776E+04	4.215E+04	4.718E+04	4.577E+04	4.223E+04
0.39811	2.857E+04	3.254E+04	3.426E+04	3.998E+04	4.305E+04	4.156E+04	3.887E+04
0.63096	2.618E+04	3.001E+04	3.176E+04	3.574E+04	3.860E+04	3.768E+04	3.539E+04
1	2.408E+04	2.707E+04	2.903E+04	3.203E+04	3.475E+04	3.366E+04	3.187E+04
1.58489	2.146E+04	2.435E+04	2.606E+04	2.852E+04	3.052E+04	2.995E+04	2.854E+04
2.51189	1.905E+04	2.146E+04	2.308E+04	2.488E+04	2.644E+04	2.758E+04	2.593E+04
3.98107	1.662E+04	1.870E+04	2.021E+04	2.157E+04	2.273E+04	2.358E+04	2.399E+04
6.30957	1.458E+04	1.608E+04	1.721E+04	1.864E+04	1.953E+04	2.044E+04	2.094E+04
10	1.261E+04	1.395E+04	1.520E+04	1.684E+04	1.733E+04	1.748E+04	1.816E+04
15.84894	1.071E+04	1.224E+04	1.371E+04	1.499E+04	1.532E+04	1.527E+04	1.615E+04
25.11887	8.972E+03	1.059E+04	1.154E+04	1.285E+04	1.306E+04	1.314E+04	1.367E+04
39.81073	7.494E+03	8.907E+03	9.947E+03	1.067E+04	1.084E+04	1.123E+04	1.145E+04
63.09575	6.160E+03	7.291E+03	8.122E+03	8.650E+03	8.745E+03	9.670E+03	9.048E+03
100.00002	4.944E+03	5.806E+03	6.391E+03	6.841E+03	6.878E+03	7.483E+03	7.001E+03

Table C.5: Storage modulus, *G'*, vs. frequency, ω, for the montmorillonite (MMT) /polypropylene (PP) nanocomposite melts at a strain of 5% and at 200 °C (measured using the ARES rheometer)

$\lvert\eta^*\rvert$ (Pa) / Frequency (rad/s)	PP	5% MMT PP DB	5% MMT PP CO2	10% MMT PP DB	10% MMT PP CO2	10% MMT PP DB Sequential	10% MMT PP CO2 Sequential
0.1	1.089E+03	9.932E+02	1.234E+03	1.392E+03	1.409E+03	1.773E+03	1.849E+03
0.15849	1.474E+03	1.619E+03	1.975E+03	2.484E+03	3.393E+03	3.241E+03	2.755E+03
0.24581	2.490E+03	2.399E+03	3.163E+03	4.156E+03	4.882E+03	4.202E+03	4.053E+03
0.39811	3.811E+03	4.232E+03	4.564E+03	5.924E+03	6.886E+03	6.362E+03	6.055E+03
0.63096	5.901E+03	6.962E+03	7.013E+03	9.096E+03	1.076E+04	9.734E+03	8.928E+03
1	9.375E+03	1.101E+04	1.186E+04	1.410E+04	1.657E+04	1.487E+04	1.397E+04
1.58489	1.475E+04	1.721E+04	1.823E+04	2.183E+04	2.482E+04	2.338E+04	2.216E+04
2.51189	2.330E+04	2.676E+04	2.844E+04	3.221E+04	3.676E+04	4.067E+04	3.740E+04
3.98107	3.589E+04	4.064E+04	4.401E+04	4.894E+04	5.486E+04	6.890E+04	6.448E+04
6.30957	5.608E+04	6.131E+04	6.955E+04	7.535E+04	8.318E+04	1.036E+05	9.740E+04
10	8.351E+04	9.463E+04	1.147E+05	1.234E+05	1.291E+05	1.566E+05	1.479E+05
15.84894	1.202E+05	1.458E+05	1.734E+05	1.856E+05	1.916E+05	2.170E+05	2.056E+05
25.11887	1.704E+05	2.121E+05	2.444E+05	2.614E+05	2.672E+05	2.922E+05	2.767E+05
39.81073	2.394E+05	2.933E+05	3.300E+05	3.529E+05	3.598E+05	3.832E+05	3.629E+05
63.09575	3.237E+05	3.897E+05	4.326E+05	4.619E+05	4.688E+05	4.914E+05	4.651E+05
100.00002	4.222E+05	5.011E+05	5.501E+05	5.885E+05	5.944E+05	6.168E+05	5.835E+05

Table C.6: Loss modulus, *G*”, vs. frequency, ω, for the montmorillonite (MMT) /polypropylene (PP) nanocomposite melts at a strain of 5% and at 200 °C (measured using the ARES rheometer)

$\lvert\eta^*\rvert$ (Pa) / Frequency (rad/s)	PP	5% MMT PP DB	5% MMT PP CO2	10% MMT PP DB	10% MMT PP CO2	10% MMT PP DB Sequential	10% MMT PP CO2 Sequential
0.1	3.278E+03	4.072E+03	4.060E+03	4.730E+03	5.344E+03	5.083E+03	4.675E+03
0.15849	4.874E+03	5.684E+03	6.055E+03	7.259E+03	8.298E+03	7.385E+03	7.163E+03
0.24581	7.188E+03	8.544E+03	8.870E+03	9.732E+03	1.119E+04	1.070E+04	9.804E+03
0.39811	1.071E+04	1.224E+04	1.285E+04	1.477E+04	1.606E+04	1.527E+04	1.424E+04
0.63096	1.542E+04	1.760E+04	1.862E+04	2.063E+04	2.232E+04	2.169E+04	2.046E+04
1	2.218E+04	2.473E+04	2.638E+04	2.876E+04	3.103E+04	3.020E+04	2.864E+04
1.58489	3.065E+04	3.455E+04	3.676E+04	3.958E+04	4.215E+04	4.130E+04	3.943E+04
2.51189	4.179E+04	4.680E+04	5.013E+04	5.354E+04	5.596E+04	5.603E+04	5.330E+04
3.98107	5.555E+04	6.236E+04	6.682E+04	7.055E+04	7.276E+04	7.857E+04	7.401E+04
6.30957	7.270E+04	8.086E+04	8.696E+04	9.028E+04	9.196E+04	1.094E+05	1.023E+05
10	9.416E+04	1.024E+05	1.111E+05	1.146E+05	1.174E+05	1.470E+05	1.369E+05
15.84894	1.195E+05	1.280E+05	1.435E+05	1.483E+05	1.516E+05	1.918E+05	1.778E+05
25.11887	1.474E+05	1.603E+05	1.815E+05	1.892E+05	1.933E+05	2.432E+05	2.241E+05
39.81073	1.780E+05	1.993E+05	2.248E+05	2.368E+05	2.412E+05	3.003E+05	2.758E+05
63.09575	2.150E+05	2.445E+05	2.732E+05	2.907E+05	2.943E+05	3.616E+05	3.311E+05
100.00002	2.569E+05	2.932E+05	3.233E+05	3.488E+05	3.498E+05	4.236E+05	3.870E+05

Table C.7: Complex viscosity, $|\eta^*|$, vs. frequency, ω, for the montmorillonite (MMT) /polypropylene (PP) nanocomposite melts at a strain of 5% and at 200 °C (measured using the RMS-800 rheometer)

$\|\eta^*\|$ (Pa) / Frequency (rad/s)	PP	5% MMT/PP DB	5% MMT/PP CO2	10% MMT/PP DB	10% MMT/PP CO2 Sequential
0.1	73894.172	86871.391	85292.609	110345.83	96136.828
0.12589	72156.219	84539.828	82159.797	105956.28	93620.859
0.15849	69894.766	81839.57	80108.344	99664.06	90874.398
0.19952	67745.852	79031.609	79049.625	98094.05	87963.313
0.25118	65359.848	76152.07	75516.43	94629.02	84414.5
0.31622	63065.758	73100.195	73100.625	90086.95	80856.859
0.39809	60409.277	70038.328	69525.195	85149.88	77166.969
0.50116	57699.398	66799.688	66754.676	80840.734	73459.391
0.63092	54996.594	63539.594	63029.699	77919.609	69728.367
0.79427	52163.438	60150.621	59158.844	72277.609	65880.727
0.99991	49303.945	56834.832	56254.582	67091.781	62030.109
1.25879	46439.512	53452.227	53317.746	64154.258	58214.203
1.58472	43597.777	50103.227	49341.211	60570.188	54375.016
1.99503	40744.543	46775.848	45409.035	55272.508	50637.848
2.51154	37899.277	43494.422	42447.801	51256.332	46900.969
3.1618	35165.539	40285.078	39566.25	47578.285	43375.668
3.98041	32477.498	37177.688	36735.98	43222.332	39911.625
5.01099	29853.588	34157.305	33010.311	39089.293	36563.789
6.30835	27337.596	31254.682	30326.693	35235.066	33363.895
7.94165	24943.461	28495.48	27767.068	31716.939	30317.807
9.9978	22624.186	25844.74	25320.281	28385.984	27431.008
12.58643	20471.844	23362.883	23018.215	25382.498	24727.479
15.84522	18427.736	21030.127	20840.863	22596.4	22188.549
19.94775	16518.885	18844.016	18513.787	20040.127	19821.098
25.1123	14765.421	16824.635	16208.063	17718.57	17650.08
31.61426	13126.667	14954.038	14157.017	15612.869	15642.224
39.7998	11624.109	13238.046	12539.253	13707.424	13812.58
50.10449	10252.302	11674.869	11065.169	12003.136	12146.449
63.07715	9002.2881	10249.85	9718.3389	10468.421	10636.904
79.4082	7871.626	8964.2461	8500.8457	9101.7598	9278.54
100	6850.1147	7800.5586	7399.8521	7873.7642	8052.3237

Table C.8: Storage modulus, *G'*, vs. frequency, ω, for the montmorillonite (MMT) /polypropylene (PP) nanocomposite melts at a strain of 5% and at 200 °C (measured the using RMS-800 rheometer)

G' (Pa) / Frequency (rad/s)	PP	5% MMT/PP DB	5% MMT/PP CO2	10% MMT/PP DB	10% MMT/PP CO2 Sequential
0.1	1378.1786	1785.3545	1373.9303	2325.0674	2234.3376
0.12589	1925.9312	2358.752	1837.731	2987.8323	2904.0745
0.15849	2520.5691	3077.0994	2477.8127	3842.2891	3731.157
0.19952	3249.5037	4021.4363	3287.9187	4865.0007	4779.5996
0.25118	4369.377	5188.1934	4287.5991	6243.5764	6158.0591
0.31622	5657.7227	6719.7383	5623.5225	7953.0754	7840.1797
0.39809	7317.7544	8623.877	7340.4761	10123.822	10058.241
0.50116	9408.9648	11061.471	9475.5654	12836.998	12707.138
0.63092	12061.646	14071.392	12157.76	16196.748	16095.771
0.79427	15325.574	17806.189	15552.162	20148.821	20148.469
0.99991	19331.953	22327.146	19756.072	25325.178	25231.109
1.25879	24278.717	27933.197	24892.756	31456.521	31362.096
1.58472	30302.664	34678.676	31162.217	38875.957	38753.664
1.99503	37520.508	42897.262	38818.574	47754.120	47635.602
2.51154	46084.457	52605.828	47867.918	58274.688	58187.266
3.1618	56513.832	64246.457	58933.258	70755.174	70644.602
3.98041	68747.797	77931.844	71863.172	85540.064	85430.898
5.01099	82879.242	93858.477	87067.727	102778.57	102657.23
6.30835	99497.328	112437.02	104707.52	122456.06	122362.57
7.94165	118708.13	133902.91	125214	145238.41	145119.09
9.9978	140447.22	158345.95	148633.11	171189.09	171074.73
12.58643	165522.84	186248.7	175409.7	200785.99	200676.53
15.84522	193502.77	217735.47	205539.23	233768.62	233676.67
19.94775	225042.16	252885.64	239696.11	270532.23	270549.09
25.1123	260357.86	292215.63	277452	311695.92	311531.25
31.61426	299184.81	335578.47	319423.81	356799.57	356697.97
39.7998	341546.94	383300.59	365079.78	406163.13	406054.34
50.10449	388091.97	435162.75	415519.94	459798.13	459697
63.07715	438231.59	491463.69	469439.84	517800.75	517688.13
79.4082	491980.25	551761.25	527749.75	579687.89	579539.75
100	549310.38	616264.75	589766.69	645441.88	645241.81

Table C.9: Loss modulus, *G*", vs. frequency, ω, for the montmorillonite (MMT) /polypropylene (PP) nanocomposite melts at a strain of 5% and at 200 °C (measured using the RMS-800 rheometer)

G" (Pa) / Frequency (rad/s)	PP	5% MMT/PP DB	5% MMT/PP CO2	10% MMT/PP DB	10% MMT/PP CO2 Sequential
0.1	7259.7886	8461.6006	7504.5571	11622.043	9350.4727
0.12589	8877.4268	10301.3	9281.8867	13078.252	11422.799
0.15849	10786.993	12545.052	11318.85	15979.797	13910.922
0.19952	13120.512	15202.503	13789.54	18815.016	16887.436
0.25118	15825.131	18335.361	16667.488	22101.258	20289.52
0.31622	19122.979	22072.051	20131.354	27522.521	24336.477
0.39809	22907.695	26427.678	24199.73	33587.695	29025.795
0.50116	27343.039	31518.75	28935.822	36344.816	34552.34
0.63092	32534.607	37429.043	34534.566	41942.082	40942.824
0.79427	38492.945	44263.801	40957.477	55391.121	48292.172
0.99991	45350.957	52077.547	48370.848	60851.352	56660.578
1.25879	53177.332	61033.727	56871.402	70339.461	66229.07
1.58472	62090.215	71177.867	66498.203	80943.242	76962.656
1.99503	72108.883	82589.883	77414.781	91734.063	89087.93
2.51154	83285.531	95366.391	89601.32	108756.59	102418.45
3.1618	95753	109583.6	103125.55	123044.14	117550.81
3.98041	109477.97	125203.35	118120.46	138742.36	133938.44
5.01099	124539.03	142370.86	134716.02	155655.97	151760.66
6.30835	140858.27	161056.59	152520.34	173855.83	171246.88
7.94165	158584.09	181217.09	171783.16	193647.28	192125.7
9.9978	177306.14	202657.7	192431.34	214300.52	214351.09
12.58643	197470.61	225688.42	214552.59	236568.84	237893.67
15.84522	218667.95	249959.86	237886.78	259733.8	262688.69
19.94775	240698.83	275308.06	262327.78	283825.09	288328.94
25.1123	264010.97	301755.69	287421.53	308819.03	315285.31
31.61426	287584.78	329053.94	313498.94	334596.31	342511.19
39.7998	312056	357002.22	340260.84	360746.88	370582.97
50.10449	336538.75	385584.72	367040.66	387634.88	398826.38
63.07715	361100.84	413727.59	394210	414239.09	426810.25
79.4082	385577.5	442464.44	420897.88	441132.59	454968.63
100	409266.22	469805.72	446937.84	466626	481728.31

Table C.10: Complex viscosity, $|\eta^*|$, vs. frequency, ω, for the montmorillonite (MMT) / high crystallinity polypropylene (HCPP) nanocomposite melts at a strain of 5% and at 200 °C (measured using the RMS-800 rheometer)

$\lvert\eta^*\rvert$ (Pa) / Frequency (rad/s)	HCPP	5% MMT/HCPP DB	5% MMT/HCPP CO2	10% MMT/HCPP DB	10% MMT/HCPP CO2 Sequential
0.1	116117.79	116657.8	109594.77	147844.36	147971.14
0.12589	112315.95	111833.41	106145.95	141786.16	141255.84
0.15849	106494.66	106822.23	102421.5	134937.14	135851.19
0.19952	101645.59	102098.02	97423.336	128345.11	128502.46
0.25118	96235.68	97005.039	92825.008	121522.78	121990.8
0.31622	91132.984	91639.336	87810.313	114262.94	115343.12
0.39809	85798.805	86332.094	82778.828	106977.45	108189.11
0.50116	80503.461	81017.094	77626.961	99963.984	101361.77
0.63092	75192.258	75758.688	72690.055	92854.805	94719.883
0.79427	70006.773	70647.969	67658.031	86116.773	88049.391
0.99991	64942.91	65540.148	62789.625	79498.414	81562.195
1.25879	60036.418	60612.348	58056.051	73157.016	75268.453
1.58472	55218.359	55794.402	53428.551	67015.336	69144.25
1.99503	50626.973	51185.723	49003.379	61178.453	63292.559
2.51154	46183.453	46754.422	44762.391	55655.754	57756.035
3.1618	42055.754	42571.898	40744.246	50462.535	52471.887
3.98041	38118.34	38598.898	36928.031	45579.438	47517.191
5.01099	34408.762	34878.797	33356.945	40995.672	42804.059
6.30835	30956.174	31400.99	30018.33	36772.777	38475.398
7.94165	27761.66	28147.557	26921.184	32883.012	34452.414
9.9978	24784.133	25131.611	24047.174	29272.104	30722.488
12.58643	22062.254	22386.986	21412.223	25994.75	27307.389
15.84522	19564.863	19856.848	18991.031	22994.619	24184.662
19.94775	17284.799	17554.018	16785.842	20273.301	21343.842
25.1123	15227.473	15466.523	14787.938	17821.299	18773.127
31.61426	13366.135	13580.476	12985.559	15614.021	16457.352
39.7998	11685.824	11885.371	11361.263	13635.425	14380.238
50.10449	10190.71	10366.89	9910.7441	11873.813	12527.301
63.07715	8851.8174	9009.1475	8615.0166	10302.554	10870.757
79.4082	7664.48	7804.1045	7461.0029	8914.0811	9406.2959
100	6608.708	6734.2827	6436.2905	7679.3179	8103.5942

Table C.11: Storage modulus, *G*', vs. frequency, ω, for the montmorillonite (MMT) / high crystallinity polypropylene (HCPP) nanocomposite melts at a strain of 5% and at 200 °C (measured using the RMS-800 rheometer)

G'(Pa) / Frequency (rad/s)	HCPP	5% MMT/HCPP DB	5% MMT/HCPP CO2	10% MMT/HCPP DB	10% MMT/HCPP CO2 Sequential
0.1	3234.9175	3216.6104	3054.5581	4731.0093	4347.6353
0.12589	4273.0688	4149.7324	4061.6479	5892.7295	5487.563
0.15849	5457.7866	5445.231	5215.9014	7538.27	7131.1709
0.19952	7002.481	6906.3052	6648.145	9558.3252	9040.3984
0.25118	8870.1768	8846.9385	8515.4189	12051.496	11428.241
0.31622	11238.113	11152.379	10780.693	15019.761	14425.255
0.39809	14080.543	13986.271	13577.601	18533.225	17862.25
0.50116	17553.439	17388.246	16872.316	22760.729	22114.064
0.63092	21751.699	21616.867	20870.984	27791.002	27368.252
0.79427	26676.486	26585.141	25668.336	33861.477	33622.867
0.99991	32610.082	32490.551	31329.805	40931.934	40915.559
1.25879	39649.387	39517.09	38055.52	49267.895	49566.113
1.58472	47769.52	47668.887	45842.539	58899.273	59596.5
1.99503	57251.328	57198.371	55037.605	70052.297	71256.367
2.51154	68198.375	68188.602	65577.094	82991.305	84792.531
3.1618	80874.969	80960.047	77653.852	97702.438	100464.83
3.98041	95315.211	95447.813	91551.391	114395.2	118076.88
5.01099	111530.59	111998.79	107237.25	133193.52	137889.22
6.30835	130075.26	130519.23	124990.49	154445.52	160526.59
7.94165	150715.02	151229.56	144948.2	178312.19	185718.02
9.9978	173686	174329.59	167071.19	204550.69	213785.75
12.58643	199234.2	200255.47	191761.06	233864.7	244870.05
15.84522	227445.27	228651.23	218971.33	265986.47	279176
19.94775	258235.92	259732.03	248780.16	301143.81	316611.91
25.1123	291956.94	293906.19	281336.91	339420.28	357304.75
31.61426	328427.75	330854.78	316727.28	381080.63	401528.69
39.7998	367546.09	370911.97	354799.63	425926.88	449192.63
50.10449	410042.25	413874.13	395886.75	474149.56	500453.38
63.07715	455048.53	459638.03	439899.72	525697.56	555084.5
79.4082	502870.28	508325.44	486343.5	580409.56	613143.88
100	553297	560050.75	535628.06	638066.38	674243.25

Table C.12: Loss modulus, *G*", vs. frequency, ω, for the montmorillonite (MMT) / high crystallinity polypropylene (HCPP) nanocomposite melts at a strain of 5% and at 200 °C (measured using the RMS-800 rheometer)

G"(Pa) / Frequency (rad/s)	HCPP	5% MMT/HCPP DB	5% MMT/HCPP CO2	10% MMT/HCPP DB	10% MMT/HCPP CO2 Sequential
0.1	11152.118	11213.603	10525.242	14007.098	14144.056
0.12589	13478.63	13453.552	12730.774	16849.104	16915.207
0.15849	15971.479	16030.604	15371.892	20013.473	20315.713
0.19952	19033.473	19164.564	18266.064	23757.188	23992.617
0.25118	22486.453	22703.135	21705.404	28044.619	28431.059
0.31622	26536.063	26745.77	25588.707	32861.945	33499.438
0.39809	31117.941	31392.982	30025.957	38342.031	39189.883
0.50116	36326.34	36690.762	35054.352	44629.031	45732.355
0.63092	42159.797	42630.168	40837.387	51572.707	53125.523
0.79427	48786.965	49415.871	47211.844	59429.844	61321.719
0.99991	56155.07	56912.996	54408.258	68142.625	70548.5
1.25879	64336.867	65267.215	62389.988	77801.695	80747.844
1.58472	73316.289	74467.969	71185.125	88370.727	91949.609
1.99503	83208.836	84594.281	80798.914	99947.531	104243.52
2.51154	93824.219	95598.313	91314.984	112477.94	117692.69
3.1618	105550.03	107534.69	102790.3	126139.93	132028.64
3.98041	118050.63	120394.22	114995.64	140814.33	147753.02
5.01099	131492.28	134176.48	128217.36	156398.41	164294.73
6.30835	145655.88	149009.23	142256.47	173087.34	182050.53
7.94165	160914.59	164617.38	157161.92	190792.23	200924.66
9.9978	176724.39	180945.38	172882.8	209301.14	220547.73
12.58643	193428.67	198225.33	189366.72	228811.5	241184.59
15.84522	210652.59	216135.2	206403.94	249009.08	262510.09
19.94775	228465.23	234847.92	224111.94	269920.88	284657.56
25.1123	246958.66	253916.8	242398.89	291685.5	307547.81
31.61426	265880.66	273614.81	261185.2	313757.72	330867.38
39.7998	284994.5	293576	280321.91	336297.13	354666.56
50.10449	304266.44	313868.44	299763.59	359340.34	378841.78
63.07715	323547.03	334163.44	319035.13	382039.94	402567.59
79.4082	342845.28	354465.28	338355.69	405188.91	426578.84
100	361403.75	373963.66	356876.59	427306.16	449531.31

Table C.13: Complex viscosity, $|\eta^*|$, vs. frequency, ω, for the montmorillonite (MMT) / maleic anhydride grafted polypropylene (PP-g-MA) nanocomposite melts at a strain of 5% and at 200 °C (measured using the RMS-800 rheometer)

$\|\eta^*\|$ (Pa) / Frequency (rad/s)	PP-g-MA	5% MMT/PP-g-MA DB	5% MMT/PP-g-MA CO2	10% MMT/PP-g-MA DB	10% MMT/PP-g-MA CO2 Sequential
0.1	10059.834	25465.131	26313.002	164178.14	39632.086
0.12589	10807.427	25220.594	25761.684	148712.98	37956.949
0.15849	10685.721	23981.979	24795.893	132533.84	36368.73
0.19952	10473.372	23144.98	23913.682	117613.04	34568.348
0.25118	9990.4678	22219.191	22734.246	104644.24	32576.539
0.31622	9801.8779	21182.293	21684.549	92568.445	30810.471
0.39809	9712.3594	20134.051	20615.502	82036.359	28987.609
0.50116	9558.3623	19117.891	19556.617	72836.875	27227.676
0.63092	9118.3926	18123.752	18428.324	64774.008	25566.357
0.79427	8809.4375	17143.674	17474.119	57732.059	23940.957
0.99991	8527.3506	16213.79	16484.613	51537.227	22432.035
1.25879	8201.5576	15284.712	15519.156	46074.293	20952.016
1.58472	7851.5864	14370.77	14554.618	41257.844	19536.377
1.99503	7512.6274	13461.429	13636.674	36989.273	18209.301
2.51154	7155.4888	12640.379	12721.622	33206.266	16895.045
3.1618	6764.3501	11774.384	11901.19	29817.018	15678.813
3.98041	6401.0571	10978.683	11075.828	26779.66	14530.153
5.01099	6013.4277	10210.499	10276.657	24054.723	13432.528
6.30835	5636.1938	9441.4854	9529.9229	21601.975	12365.76
7.94165	5265.2837	8730.9727	8804.1787	19388.154	11369.086
9.9978	4896.1421	8038.4771	8095.8887	17377.576	10412.549
12.58643	4533.9497	7393.915	7448.1274	15560.024	9523.0195
15.84522	4183.6401	6768.1055	6811.9541	13913.338	8676.9717
19.94775	3843.1946	6185.7314	6218.2949	12419.327	7884.6025
25.1123	3522.9875	5633.0664	5663.2158	11074.166	7147.9604
31.61426	3214.3967	5116.1196	5142.9741	9855.9629	6462.2764
39.7998	2924.6746	4631.6577	4650.7817	8756.6055	5823.6841
50.10449	2649.4207	4181.0376	4198.3701	7767.1919	5233.1221
63.07715	2390.8491	3760.1677	3776.1099	6874.8071	4687.0762
79.4082	2151.5469	3372.1602	3385.7363	6073.6079	4185.8945
100	1927.4131	3012.4568	3024.0708	5345.3301	3723.8994

Table C.14: Storage modulus, *G*', vs. frequency, ω, for the montmorillonite (MMT) / maleic anhydride grafted polypropylene (PP-g-MA) nanocomposite melts at a strain of 5% and at 200 °C (measured using the RMS-800 rheometer)

G' (Pa) / Frequency (rad/s)	PP-g-MA	5% MMT/PP-g-MA DB	5% MMT/PP-g-MA CO2	10% MMT/PP-g-MA DB	10% MMT/PP-g-MA CO2 Sequential
0.1	209.9529	861.40674	923.95154	13376.162	1714.3671
0.12589	200.37511	1099.8323	1156.1376	15178.93	2142.3086
0.15849	295.01169	1383.2891	1449.8755	16906.328	2555.2468
0.19952	362.82391	1704.0007	1810.5553	18694.906	3068.5237
0.25118	432.01242	2055.5764	2197.5056	20621.098	3662.7568
0.31622	568.17963	2483.0754	2707.4607	22582.412	4383.6216
0.39809	744.38672	3063.2822	3240.8403	24781.373	5195.7876
0.50116	950.2937	3693.4998	3902.9163	27235.648	6175.3242
0.63092	1336.2413	4494.1748	4695.9692	29970.027	7354.4795
0.79427	1712.0208	5434.1821	5702.9644	33080.734	8774.1553
0.99991	2261.2771	6641.1187	6874.8013	36620.82	10403.334
1.25879	2957.6489	8050.3521	8365.0352	40653.578	12431.91
1.58472	3814.9871	9807.0957	10122.251	45288.684	14817.825
1.99503	4910.5078	11845.12	12217.907	50577.137	17700.875
2.51154	6292.9873	14332.688	14884.814	56720.754	21115.863
3.1618	8014.5674	17440.174	17840.359	63822.391	25171.025
3.98041	10076.815	21058.064	21496.332	71923.289	30051.479
5.01099	12603.036	25387.457	25854.283	81243.305	35786.125
6.30835	15627.355	30341.506	30951.723	91922.414	42451.559
7.94165	19386.963	36410.41	37045.664	104095.1	50262.41
9.9978	23703.344	43397.309	44101.59	117889.02	59311.738
12.58643	28861.676	51695.199	52396.203	133618.94	70022.719
15.84522	34927.633	61148.262	61901.25	151420.64	82161.703
19.94775	41938.547	72206.023	72990.938	171491.89	96133.781
25.1123	50148.637	84871.492	85735.219	194008.92	112245.99
31.61426	59444.965	99462.57	100446.19	219397.05	130516.85
39.7998	70238.547	115973.13	116976.66	247824.78	151156.69
50.10449	82362.391	134741.75	135782.63	279543.66	174521.27
63.07715	96091.086	155858.89	157014.06	314799	200639.83
79.4082	111581.98	179538.88	180823.88	353770.81	229946.58
100	128873.43	206226.98	207469.92	396589.84	262455.34

Table C.15: Loss modulus, *G*", vs. frequency, ω, for the montmorillonite (MMT) / maleic anhydride grafted polypropylene (PP-g-MA) nanocomposite melts at a strain of 5% and at 200 °C (measured using the RMS-800 rheometer)

G" (Pa) / Frequency (rad/s)	PP-g-MA	5% MMT/PP-g-MA DB	5% MMT/PP-g-MA CO2	10% MMT/PP-g-MA DB	10% MMT/PP-g-MA CO2 Sequential
0.1	983.83435	2396.405	2463.7588	9519.7148	3573.2461
0.12589	1345.7397	2978.5142	3030.1375	10959.404	4271.3672
0.15849	1667.679	3540.2314	3652.6472	12465.71	5166.7212
0.19952	2057.9495	4292.0972	4414.4858	14183.883	6177.0308
0.25118	2471.9648	5188.7363	5270.689	16299.124	7317.1108
0.31622	3046.9836	6220.9175	6299.8394	18624.178	8700.8623
0.39809	3794.0247	7406.6216	7539.7456	21269.707	10303.671
0.50116	4695.0601	8840.5781	8990.3623	24303.938	12168.1
0.63092	5595.6445	10514.442	10636.282	27783.613	14356.162
0.79427	6784.355	12485.286	12653.278	31753.883	16870.174
0.99991	8221.2539	14789.672	14980.981	36256.242	19871.455
1.25879	9891.3057	17475.074	17653.777	41364.637	23260.359
1.58472	11843.256	20553.777	20725.15	47156.559	27183.275
1.99503	14160.635	24102.537	24307.668	53736.281	31723.873
2.51154	16833.439	28327.211	28271.832	61140.023	36805.406
3.1618	19829.121	32890.523	33131.27	69387.211	42707.555
3.98041	23401.451	38291.199	38490.395	78672.188	49415.625
5.01099	27371.035	44421.848	44535.531	89044.414	57008.938
6.30835	31936.65	51252.41	51538.09	100600.93	65444.945
7.94165	37049.203	59009.203	59299.113	113455.66	75005.664
9.9978	42828.949	67642.773	67871.281	127620.25	85553.906
12.58643	49229.641	77384.25	77735.57	143182.67	97280.141
15.84522	56342.828	88100.82	88422.875	160232.09	110238.55
19.94775	64174.676	100058.68	100292.05	178786.16	124480.24
25.1123	72884.258	113170.48	113467.95	199245.94	140077.55
31.61426	82420.125	127545.2	127853.41	221252.36	157174.64
39.7998	92821.602	143286.88	143452.25	245036.59	175710.88
50.10449	104107.8	160406.36	160664.98	270757.41	195685.22
63.07715	116230.54	178781.06	179106.88	298241.59	217142.94
79.4082	129380.63	198671.61	198961.97	327801.75	240022.03
100	143320.8	219589.14	220014.25	358388.13	264180.72

Appendix D: WAXD Data

Table D.1: WAXD data Cloisite 20A released with different storage time

Intensity (CPS) / 2 Theta	Cloisite 20A as revieved	$ScCO_2$ exfoliated Cloisite 20A tested immediately	$ScCO_2$ exfoliated Cloisite 20A tested after 1 week	$ScCO_2$ exfoliated Cloisite 20A tested after 4 weeks
1	501	129	189	239
1.02	445	145	191	213
1.04	487	124	203	179
1.06	454	129	178	208
1.08	457	117	173	208
1.1	450	103	189	207
1.12	436	114	169	186
1.14	452	133	187	215
1.16	406	127	176	196
1.18	396	116	167	231
1.2	413	115	190	218
1.22	378	99	183	205
1.24	407	90	180	180
1.26	362	110	214	207
1.28	387	108	171	185
1.3	401	75	197	200
1.32	405	104	163	202
1.34	389	120	198	219
1.36	391	101	195	187
1.38	350	114	207	186
1.4	341	84	179	201
1.42	346	101	185	183
1.44	388	107	190	188
1.46	317	128	193	191
1.48	382	101	207	183
1.5	335	100	188	204
1.52	377	117	203	210
1.54	338	94	200	204
1.56	370	94	209	209
1.58	332	109	195	224
1.6	364	105	203	235
1.62	332	96	222	224
1.64	373	114	205	241
1.66	312	108	214	245
1.68	378	118	219	231
1.7	300	98	238	221
1.72	333	112	214	205
1.74	284	111	232	242
1.76	310	112	224	218
1.78	326	113	212	230
1.8	370	109	227	223
1.82	340	106	231	235
1.84	401	127	267	240
1.86	333	150	252	282
1.88	368	129	267	252
1.9	308	134	239	259
1.92	351	114	267	258
1.94	309	141	226	261

1.96	376	133	285	261
1.98	365	120	266	270
2	406	122	276	292
2.02	334	129	275	297
2.04	396	137	288	312
2.06	368	132	281	293
2.08	369	138	301	343
2.1	359	128	311	341
2.12	332	141	285	322
2.14	337	142	307	346
2.16	400	143	283	335
2.18	362	151	319	343
2.2	378	161	331	325
2.22	374	156	345	378
2.24	368	189	324	372
2.26	394	159	316	401
2.28	359	170	337	425
2.3	394	180	347	378
2.32	395	184	346	425
2.34	416	196	364	420
2.36	460	173	350	469
2.38	456	214	367	417
2.4	410	215	348	460
2.42	456	214	390	434
2.44	526	211	404	477
2.46	437	230	387	507
2.48	474	237	412	534
2.5	490	227	375	560
2.52	478	222	442	578
2.54	493	238	451	552
2.56	508	227	445	629
2.58	502	262	409	588
2.6	548	259	456	663
2.62	514	271	463	579
2.64	523	261	528	693
2.66	520	250	501	672
2.68	565	298	512	704
2.7	559	302	473	672
2.72	586	260	525	799
2.74	601	283	530	734
2.76	572	283	518	752
2.78	662	322	520	746
2.8	644	331	569	860
2.82	645	321	602	826
2.84	597	304	525	865
2.86	656	338	568	902
2.88	652	377	593	895
2.9	680	357	615	827
2.92	663	331	599	926
2.94	687	390	558	866
2.96	661	356	602	889
2.98	709	399	620	923
3	760	329	646	928

3.02	757	436	614	848
3.04	764	403	663	958
3.06	779	478	623	862
3.08	812	434	714	939
3.1	783	482	679	863
3.12	778	422	708	929
3.14	838	483	648	854
3.16	823	446	639	864
3.18	882	484	677	854
3.2	869	481	675	881
3.22	864	504	708	813
3.24	922	510	663	780
3.26	969	496	627	761
3.28	942	494	675	788
3.3	939	522	644	748
3.32	966	520	618	757
3.34	1009	593	652	654
3.36	913	560	686	697
3.38	997	606	656	658
3.4	952	539	644	729
3.42	1050	582	614	633
3.44	932	527	621	630
3.46	1100	586	591	606
3.48	1068	560	617	570
3.5	1132	616	535	542
3.52	1069	552	625	516
3.54	1118	608	554	510
3.56	1075	523	590	498
3.58	1130	549	543	494
3.6	1088	544	564	480
3.62	1225	575	540	396
3.64	1149	526	501	452
3.66	1224	581	515	403
3.68	1095	481	485	406
3.7	1171	543	465	390
3.72	1069	529	505	369
3.74	1216	520	416	364
3.76	1061	469	469	335
3.78	1174	526	429	341
3.8	1146	466	447	351
3.82	1130	483	406	305
3.84	1122	436	428	297
3.86	1133	493	360	293
3.88	1091	425	398	251
3.9	1167	449	359	285
3.92	1010	382	343	234
3.94	1159	399	346	245
3.96	1059	380	330	249
3.98	1113	359	346	252
4	957	309	326	269
4.02	1005	344	281	211
4.04	924	339	275	242
4.06	1033	339	299	233

4.08	923	288	316	199
4.1	937	294	256	200
4.12	875	283	285	208
4.14	891	291	262	210
4.16	839	264	261	178
4.18	822	289	205	187
4.2	804	250	245	204
4.22	821	235	227	187
4.24	711	216	247	158
4.26	719	228	228	182
4.28	687	221	222	155
4.3	693	219	194	149
4.32	663	174	184	177
4.34	725	200	181	165
4.36	642	188	189	186
4.38	617	229	157	155
4.4	603	182	175	192
4.42	568	175	171	158
4.44	557	174	172	168
4.46	601	149	196	164
4.48	535	152	129	136
4.5	518	158	163	161
4.52	489	146	129	143
4.54	456	134	160	127
4.56	531	142	140	145
4.58	483	145	137	119
4.6	449	124	140	125
4.62	452	134	121	134
4.64	420	119	147	117
4.66	394	113	125	113
4.68	400	129	133	143
4.7	385	109	130	114
4.72	396	119	120	131
4.74	352	127	120	126
4.76	375	111	132	109
4.78	335	115	126	106
4.8	334	107	109	120
4.82	313	120	121	130
4.84	322	100	102	97
4.86	329	102	119	123
4.88	299	97	120	111
4.9	283	94	126	109
4.92	328	99	110	97
4.94	267	79	105	111
4.96	310	88	94	93
4.98	251	76	104	106
5	277	71	105	88
5.02	254	94	100	122
5.04	269	108	113	91
5.06	207	93	98	94
5.08	270	77	82	105
5.1	194	76	130	107
5.12	258	75	102	95

5.14	210	77	112	117
5.16	239	63	96	99
5.18	204	75	100	103
5.2	223	69	81	85
5.22	183	65	101	93
5.24	214	58	82	114
5.26	191	84	82	105
5.28	206	72	93	98
5.3	168	55	95	103
5.32	195	63	60	77
5.34	173	66	125	96
5.36	191	60	78	78
5.38	177	68	88	108
5.4	178	53	76	103
5.42	159	64	100	102
5.44	193	51	72	97
5.46	147	43	77	104
5.48	170	52	74	105
5.5	159	43	87	107
5.52	176	55	76	93
5.54	151	54	79	119
5.56	143	51	90	78
5.58	137	51	91	97
5.6	157	44	82	97
5.62	136	59	86	126
5.64	166	52	80	115
5.66	140	50	79	107
5.68	151	54	73	84
5.7	90	50	68	109
5.72	164	46	63	107
5.74	151	46	80	106
5.76	147	60	72	100
5.78	118	52	84	127
5.8	136	55	66	112
5.82	121	49	94	123
5.84	150	42	75	126
5.86	105	41	97	127
5.88	135	51	78	118
5.9	106	59	76	123
5.92	142	52	82	132
5.94	108	49	86	120
5.96	151	48	74	132
5.98	109	50	71	123
6	131	64	81	117
6.02	101	40	87	129
6.04	146	43	75	151
6.06	118	40	91	145
6.08	140	50	60	129
6.1	106	52	83	151
6.12	115	48	82	117
6.14	99	57	93	133
6.16	120	50	91	144
6.18	92	45	88	129

6.2	129	42	81	148
6.22	83	51	103	139
6.24	126	54	86	153
6.26	104	41	82	161
6.28	116	51	57	150
6.3	104	48	84	142
6.32	116	49	70	157
6.34	98	68	94	162
6.36	123	53	90	133
6.38	120	40	81	138
6.4	119	55	80	165
6.42	101	50	108	162
6.44	95	59	78	149
6.46	85	63	108	168
6.48	128	54	79	167
6.5	107	56	120	140
6.52	129	69	103	127
6.54	106	63	112	152
6.56	119	62	110	148
6.58	95	48	115	153
6.6	129	62	91	130
6.62	87	63	100	114
6.64	137	68	94	109
6.66	103	61	120	129
6.68	124	61	103	114
6.7	92	67	138	133
6.72	147	68	92	120
6.74	103	71	138	125
6.76	137	64	97	92
6.78	117	72	108	120
6.8	154	70	108	98
6.82	121	59	108	96
6.84	146	73	102	84
6.86	130	76	108	99
6.88	125	56	116	78
6.9	123	69	103	85
6.92	160	81	106	76
6.94	109	69	120	84
6.96	151	69	92	85
6.98	133	77	113	94
7	147	88	92	83
7.02	150	73	114	87
7.04	177	61	96	71
7.06	120	72	102	78
7.08	164	65	95	73
7.1	139	68	94	79
7.12	147	74	92	64
7.14	141	61	92	68
7.16	147	65	90	58
7.18	132	71	115	55
7.2	156	55	89	49
7.22	138	51	109	58
7.24	182	45	80	52

7.26	133	55	103	66
7.28	177	66	76	52
7.3	129	43	97	69
7.32	164	47	71	50
7.34	143	61	84	63
7.36	146	47	69	51
7.38	153	45	75	61
7.4	145	38	61	52
7.42	156	50	78	56
7.44	171	61	62	61
7.46	153	52	76	50
7.48	167	40	56	43
7.5	127	35	81	47
7.52	154	38	53	36
7.54	96	34	83	55
7.56	160	43	55	40
7.58	112	32	92	55
7.6	151	29	60	36
7.62	129	29	71	60
7.64	145	25	61	48
7.66	125	35	63	47
7.68	130	38	48	41
7.7	134	27	76	66
7.72	124	32	40	38
7.74	91	31	61	42
7.76	123	39	45	39
7.78	102	20	66	45
7.8	124	25	58	28
7.82	104	28	81	43
7.84	119	35	39	34
7.86	88	25	60	57
7.88	105	14	35	33
7.9	83	25	60	47
7.92	126	22	39	37
7.94	85	27	49	36
7.96	125	23	46	27
7.98	78	18	67	43
8	116	20	48	28
8.02	80	20	51	35
8.04	99	21	33	32
8.06	80	15	45	43
8.08	94	19	45	32
8.1	73	20	46	45
8.12	98	23	30	31
8.14	72	17	46	42
8.16	97	21	30	31
8.18	57	20	53	35
8.2	94	25	36	20
8.22	62	17	33	38
8.24	95	15	25	23
8.26	56	13	32	39
8.28	91	13	28	24
8.3	69	16	54	40

8.32	85	10	32	32
8.34	58	14	53	33
8.36	99	12	34	36
8.38	51	10	40	48
8.4	85	16	31	24
8.42	50	15	40	31
8.44	79	12	33	29
8.46	48	18	41	43
8.48	93	21	11	43
8.5	50	12	53	36
8.52	68	24	26	25
8.54	54	10	39	48
8.56	88	20	36	18
8.58	50	19	36	37
8.6	75	16	22	25
8.62	55	8	35	41
8.64	68	15	24	11
8.66	55	14	39	36
8.68	84	18	30	23
8.7	46	11	31	35
8.72	68	11	23	19
8.74	41	8	28	39
8.76	65	14	14	22
8.78	44	13	34	32
8.8	68	17	24	32
8.82	46	11	33	43
8.84	72	14	25	22
8.86	42	6	39	51
8.88	78	13	28	24
8.9	35	9	41	38
8.92	56	16	21	23
8.94	35	11	37	40
8.96	63	12	29	30
8.98	31	11	36	32
9	65	15	22	27
9.02	44	9	24	36
9.04	52	13	14	20
9.06	27	8	33	33
9.08	51	16	29	30
9.1	23	7	38	34
9.12	46	16	24	38
9.14	42	6	34	26
9.16	70	14	20	19
9.18	26	12	25	37
9.2	71	13	23	34
9.22	33	11	18	37
9.24	68	18	28	24
9.26	31	9	32	30
9.28	58	13	19	23
9.3	30	10	40	37
9.32	51	13	18	37
9.34	24	11	36	38
9.36	65	5	25	26

9.38	32	9	29	36
9.4	65	12	14	15
9.42	23	13	37	35
9.44	47	18	20	22
9.46	32	7	30	36
9.48	57	10	19	31
9.5	40	6	29	47
9.52	61	12		
9.54	25	9		
9.56	66	11		
9.58	34	9		
9.6	56	13		
9.62	30	9		
9.64	57	9		
9.66	30	5		
9.68	61	10		
9.7	21	9		
9.72	66	10		
9.74	44	11		
9.76	75	14		
9.78	29	15		
9.8	57	13		
9.82	24	8		
9.84	47	14		
9.86	26	18		
9.88	47	13		
9.9	26	5		
9.92	59	13		
9.94	22	8		
9.96	50	16		
9.98	27	11		
10	66	5		

Table D.2: WAXD data for pure Cloisite 20A and all nano-clay/PP composite

Intensity (CPS) / 2theta	Pure 20A	5% MMT/PP CO2 (pellet)	5% MMT/PP CO2 (plaque)	10% MMT/PP CO2 (pellet)	10% MMT/PP CO2 (plaque)	10% MMT/PP DB (plaque)	10% MMT/PP CO2 Sequential (plaque)	10% MMT/PP DB Sequential (plaque)
2.00	2662.03	470.37	509.67	442.48	503.17	590.17	800.33	503.17
2.01	2700.50	478.87	507.83	441.72	495.00	580.83	802.83	495.00
2.02	2730.80	487.30	518.17	446.72	489.33	582.33	803.33	489.33
2.03	2750.93	481.03	493.83	444.00	500.17	576.17	810.83	500.17
2.04	2770.13	479.17	499.50	434.96	516.50	587.50	794.00	516.50
2.05	2813.83	484.30	514.00	448.92	531.83	565.83	811.50	531.83
2.06	2834.33	487.97	514.67	438.16	518.67	588.83	797.33	518.67
2.07	2860.07	478.30	511.67	445.44	535.83	598.67	791.17	535.83
2.08	2872.60	484.40	517.17	433.68	524.83	599.17	802.83	524.83
2.09	2900.10	486.77	523.67	442.80	546.83	611.17	792.00	546.83
2.10	2931.27	477.63	514.67	445.92	532.00	607.33	811.83	532.00
2.11	2955.40	490.77	522.33	444.68	537.50	609.83	827.17	537.50
2.12	2982.07	491.27	516.00	449.12	542.83	603.33	814.50	542.83
2.13	2969.70	485.23	508.00	448.44	547.67	610.83	832.00	547.67
2.14	3014.77	488.97	539.00	444.76	569.33	597.17	796.17	569.33
2.15	3021.13	488.57	518.67	443.60	538.67	606.17	804.83	538.67
2.16	3038.63	487.20	522.00	455.44	580.50	588.33	825.50	580.50
2.17	3063.10	493.13	531.67	448.36	583.33	615.83	824.50	583.33
2.18	3058.93	490.43	534.50	449.84	582.00	615.33	834.50	582.00
2.19	3103.13	494.13	538.67	447.36	578.17	600.00	827.00	578.17
2.20	3110.60	491.37	537.00	447.44	575.00	629.33	833.67	575.00
2.21	3144.57	485.90	549.67	453.36	601.67	628.50	825.17	601.67
2.22	3139.23	486.53	533.17	444.16	583.17	627.17	822.50	583.17
2.23	3171.10	493.30	541.17	460.68	606.50	631.00	838.50	606.50
2.24	3185.03	493.00	549.67	459.32	609.50	638.17	856.67	609.50
2.25	3223.77	500.27	554.67	458.84	605.00	641.67	839.00	605.00
2.26	3237.83	494.50	562.33	460.44	602.17	655.67	845.67	602.17
2.27	3264.47	498.57	546.83	456.80	607.00	654.67	855.83	607.00
2.28	3260.43	499.20	561.83	458.16	619.00	649.50	857.83	619.00
2.29	3288.10	507.07	564.50	462.88	642.33	659.33	866.00	642.33
2.30	3303.37	501.77	560.67	465.12	635.67	677.33	860.17	635.67
2.31	3316.97	500.67	565.50	462.88	639.83	659.00	861.83	639.83

2.32	3342.13	509.17	555.67	464.32	637.50	678.00	873.83	637.50
2.33	3367.63	502.93	577.50	460.68	653.83	672.17	873.00	653.83
2.34	3386.50	513.10	570.50	472.76	640.50	670.50	865.83	640.50
2.35	3394.67	503.23	596.00	461.36	666.50	664.17	881.17	666.50
2.36	3422.87	506.53	564.17	470.76	654.17	689.83	876.50	654.17
2.37	3445.23	509.00	582.00	474.08	671.00	681.17	884.83	671.00
2.38	3463.07	511.00	577.50	474.96	658.00	662.83	890.00	658.00
2.39	3499.10	511.67	586.17	478.00	667.33	706.67	886.17	667.33
2.40	3505.57	510.53	609.33	474.88	671.33	696.50	891.33	671.33
2.41	3537.03	510.57	590.17	476.72	665.67	702.33	885.83	665.67
2.42	3525.40	513.17	588.67	476.60	682.83	711.50	889.50	682.83
2.43	3576.17	522.07	589.83	480.04	683.83	692.33	915.17	683.83
2.44	3599.73	524.60	605.67	488.48	670.50	705.33	899.17	670.50
2.45	3627.97	517.80	606.33	486.64	696.50	721.83	932.33	696.50
2.46	3662.93	513.87	598.17	490.48	681.83	718.50	905.50	681.83
2.47	3687.30	510.80	614.83	483.64	695.17	727.83	924.67	695.17
2.48	3699.47	520.13	614.17	487.84	711.00	743.50	917.17	711.00
2.49	3739.13	520.80	603.50	484.00	693.00	727.67	913.67	693.00
2.50	3742.13	521.17	617.83	493.88	711.33	749.33	915.17	711.33
2.51	3775.77	523.17	617.83	498.64	708.83	748.00	938.17	708.83
2.52	3834.97	520.33	612.83	497.00	703.67	790.33	917.67	703.67
2.53	3823.20	525.57	620.67	492.76	721.00	762.50	942.33	721.00
2.54	3871.77	527.00	630.50	503.36	735.33	765.33	949.33	735.33
2.55	3886.77	533.03	632.50	504.56	728.67	763.50	936.00	728.67
2.56	3927.27	537.70	636.50	507.28	740.17	787.17	962.67	740.17
2.57	3949.90	530.50	665.17	501.52	758.17	771.50	952.00	758.17
2.58	3987.03	534.60	631.33	500.52	735.33	764.83	966.33	735.33
2.59	4026.67	542.77	650.50	514.36	733.83	774.33	954.50	733.83
2.60	4037.20	539.80	623.00	512.60	736.33	790.33	960.83	736.33
2.61	4070.50	544.17	637.83	511.92	769.50	799.00	972.50	769.50
2.62	4101.57	539.40	636.67	515.12	754.33	823.00	965.83	754.33
2.63	4120.73	541.90	667.33	522.20	751.33	810.50	976.17	751.33
2.64	4164.17	560.80	652.17	517.12	757.00	822.00	973.17	757.00
2.65	4188.73	552.37	635.33	522.28	751.33	833.50	971.67	751.33
2.66	4219.33	549.63	652.17	531.72	769.17	811.17	978.67	769.17
2.67	4254.73	548.00	674.00	527.88	777.83	837.00	979.00	777.83
2.68	4276.00	548.70	686.50	538.16	775.83	830.67	984.50	775.83
2.69	4302.57	553.93	676.83	528.12	783.50	822.67	988.17	783.50

2.70	4331.77	552.37	691.00	536.52	787.00	849.33	1010.50	787.00
2.71	4364.00	552.80	668.67	543.52	802.00	865.67	1010.33	802.00
2.72	4415.43	566.07	683.50	541.64	810.17	847.17	1011.17	810.17
2.73	4434.40	564.93	693.83	545.16	780.67	864.17	1017.83	780.67
2.74	4445.83	569.43	698.83	546.88	789.83	857.67	1034.00	789.83
2.75	4507.87	564.67	690.50	554.28	815.33	858.83	997.67	815.33
2.76	4519.27	561.43	680.00	550.24	808.00	879.33	999.33	808.00
2.77	4510.27	565.97	693.83	542.08	831.17	854.17	1010.17	831.17
2.78	4566.53	571.43	707.00	547.76	830.17	892.50	1017.50	830.17
2.79	4590.93	577.13	705.00	559.80	829.00	908.17	1031.17	829.00
2.80	4612.00	576.70	702.83	563.20	817.17	915.33	1027.67	817.17
2.81	4664.40	577.20	690.83	560.12	852.00	885.17	1021.83	852.00
2.82	4676.53	575.30	711.50	564.16	833.67	917.17	1066.33	833.67
2.83	4703.57	578.37	755.50	569.00	857.50	948.67	1072.50	857.50
2.84	4742.87	582.27	706.17	574.12	833.33	932.67	1044.50	833.33
2.85	4760.80	587.33	713.17	586.64	835.33	924.00	1072.17	835.33
2.86	4791.47	596.03	747.00	585.92	858.67	958.33	1035.50	858.67
2.87	4829.60	589.73	728.33	588.64	881.33	950.17	1059.33	881.33
2.88	4829.90	595.10	744.50	580.48	849.50	943.83	1056.67	849.50
2.89	4869.77	589.43	721.83	594.24	861.00	938.17	1063.33	861.00
2.90	4903.80	593.90	754.67	604.20	887.33	956.67	1071.67	887.33
2.91	4948.50	599.03	762.50	606.16	883.17	951.00	1083.00	883.17
2.92	4945.90	599.50	754.50	595.72	880.83	972.17	1082.67	880.83
2.93	4970.13	602.47	745.00	604.92	887.33	970.83	1065.50	887.33
2.94	4988.80	599.77	739.33	605.84	887.67	970.50	1097.00	887.67
2.95	5032.20	604.33	741.33	613.96	919.17	985.67	1103.50	919.17
2.96	5043.73	613.00	762.50	622.36	872.00	996.50	1097.00	872.00
2.97	5090.70	612.23	745.17	617.44	901.83	976.50	1103.33	901.83
2.98	5121.70	609.13	766.17	619.24	882.50	987.50	1082.83	882.50
2.99	5130.53	616.40	748.67	624.08	912.83	997.17	1084.00	912.83
3.00	5135.33	609.77	788.00	620.56	926.83	1015.00	1134.00	926.83
3.01	5145.27	614.37	792.50	625.28	909.33	998.50	1102.67	909.33
3.02	5165.80	617.93	766.83	634.92	905.33	1024.33	1112.83	905.33
3.03	5224.47	626.33	761.00	638.84	931.83	1019.17	1094.17	931.83
3.04	5230.97	625.13	782.67	647.52	912.50	1037.83	1117.33	912.50
3.05	5254.70	620.50	785.83	650.04	958.50	1040.50	1106.67	958.50
3.06	5249.37	631.57	794.67	654.08	941.67	1015.50	1115.50	941.67
3.07	5242.00	630.77	793.50	654.36	939.50	1034.33	1105.83	939.50

3.08	5283.53	617.20	791.33	657.24	937.17	1055.67	1109.17	937.17
3.09	5304.83	628.00	785.50	662.56	963.50	1026.17	1132.50	963.50
3.10	5334.37	632.07	801.83	664.72	974.83	1075.50	1115.00	974.83
3.11	5341.73	639.17	779.83	673.44	971.50	1043.50	1102.50	971.50
3.12	5350.30	644.43	815.17	664.60	970.17	1074.33	1103.33	970.17
3.13	5387.73	633.50	807.00	679.76	988.17	1031.17	1110.00	988.17
3.14	5400.83	637.80	844.00	683.32	1002.67	1053.50	1144.00	1002.67
3.15	5405.43	643.27	809.83	682.48	967.00	1067.17	1127.50	967.00
3.16	5426.10	646.87	827.67	697.08	978.17	1089.17	1164.00	978.17
3.17	5442.67	643.80	797.67	699.92	984.50	1085.17	1142.50	984.50
3.18	5453.70	648.37	817.67	698.68	986.67	1099.33	1151.83	986.67
3.19	5427.43	645.47	847.83	690.08	1017.00	1109.67	1132.83	1017.00
3.20	5461.80	658.53	818.67	704.88	1009.67	1099.83	1143.00	1009.67
3.21	5487.50	654.57	823.50	704.76	1011.17	1115.83	1166.83	1011.17
3.22	5495.03	655.83	844.83	716.76	1019.67	1142.83	1163.67	1019.67
3.23	5511.30	657.23	841.83	718.24	1027.00	1126.83	1153.00	1027.00
3.24	5529.90	650.30	841.50	724.24	996.50	1116.83	1135.00	996.50
3.25	5501.50	663.57	859.83	724.32	1030.17	1117.33	1153.33	1030.17
3.26	5555.50	661.60	857.83	737.40	1025.50	1138.17	1162.00	1025.50
3.27	5520.60	669.13	845.83	731.52	1040.50	1128.33	1162.50	1040.50
3.28	5567.47	662.37	874.17	732.52	1044.17	1141.00	1140.00	1044.17
3.29	5559.20	669.70	843.50	744.84	1047.50	1128.50	1175.17	1047.50
3.30	5573.13	670.70	872.83	748.92	1045.17	1140.17	1162.00	1045.17
3.31	5600.17	665.90	865.50	746.04	1066.83	1134.33	1148.33	1066.83
3.32	5574.37	659.60	882.50	754.32	1039.33	1158.50	1142.33	1039.33
3.33	5576.53	674.63	873.00	756.92	1060.17	1168.83	1132.83	1060.17
3.34	5590.30	665.73	862.17	762.20	1082.33	1145.00	1142.83	1082.33
3.35	5587.77	671.57	885.33	769.04	1040.33	1189.50	1155.83	1040.33
3.36	5570.17	673.70	903.33	767.44	1091.67	1151.50	1166.33	1091.67
3.37	5598.60	668.10	884.83	771.36	1065.50	1163.00	1161.17	1065.50
3.38	5592.83	685.40	895.00	779.96	1078.33	1164.67	1165.50	1078.33
3.39	5604.93	669.90	900.83	789.64	1110.33	1170.83	1164.83	1110.33
3.40	5609.73	673.17	909.00	797.16	1085.67	1188.67	1140.50	1085.67
3.41	5605.00	681.67	883.50	790.32	1091.50	1184.00	1144.50	1091.50
3.42	5627.40	680.47	899.67	798.52	1109.67	1176.00	1175.83	1109.67
3.43	5607.53	682.97	932.50	795.64	1084.67	1196.17	1172.67	1084.67
3.44	5599.97	680.47	927.17	803.00	1106.50	1183.67	1158.67	1106.50
3.45	5566.27	679.57	901.17	806.68	1116.50	1194.83	1152.00	1116.50

3.46	5597.57	672.00	921.50	799.88	1129.83	1199.67	1157.67	1129.83
3.47	5593.57	685.50	914.67	821.88	1116.67	1201.17	1167.17	1116.67
3.48	5577.53	682.97	905.17	816.44	1119.83	1207.83	1177.50	1119.83
3.49	5562.47	675.50	916.67	822.56	1149.50	1218.67	1175.00	1149.50
3.50	5538.47	689.27	913.17	819.52	1131.50	1198.50	1150.00	1131.50
3.51	5543.73	686.07	929.50	823.60	1142.67	1214.83	1153.00	1142.67
3.52	5535.63	675.20	941.67	827.40	1117.83	1211.50	1145.33	1117.83
3.53	5523.97	679.23	952.17	830.28	1121.00	1209.17	1147.50	1121.00
3.54	5505.50	671.53	923.67	835.96	1136.17	1212.67	1129.83	1136.17
3.55	5502.83	672.83	951.67	831.84	1128.33	1220.83	1133.67	1128.33
3.56	5521.10	671.30	942.33	844.24	1160.50	1212.83	1142.50	1160.50
3.57	5468.80	678.13	920.00	846.44	1147.33	1209.50	1141.17	1147.33
3.58	5467.33	682.97	915.00	855.52	1138.33	1225.00	1113.00	1138.33
3.59	5448.83	678.03	920.83	846.60	1163.67	1224.17	1128.67	1163.67
3.60	5414.63	676.27	927.17	843.36	1145.00	1215.83	1113.17	1145.00
3.61	5420.93	667.30	934.83	844.04	1163.83	1271.67	1144.50	1163.83
3.62	5404.97	667.93	948.50	851.60	1169.83	1230.33	1125.83	1169.83
3.63	5346.03	668.73	933.83	847.48	1155.50	1251.83	1121.33	1155.50
3.64	5335.37	665.67	967.67	846.60	1169.00	1244.83	1073.67	1169.00
3.65	5292.10	665.03	952.00	854.08	1155.33	1249.83	1086.50	1155.33
3.66	5273.23	667.63	977.33	851.12	1178.17	1233.50	1093.83	1178.17
3.67	5263.50	665.60	968.67	860.68	1183.00	1241.83	1093.00	1183.00
3.68	5252.87	666.10	977.17	862.44	1169.67	1244.83	1111.50	1169.67
3.69	5198.97	669.40	958.17	861.84	1180.83	1275.83	1100.00	1180.83
3.70	5195.57	657.37	977.50	861.08	1176.67	1249.00	1091.33	1176.67
3.71	5143.57	660.17	989.83	865.20	1148.33	1272.17	1073.17	1148.33
3.72	5127.13	651.67	968.00	858.68	1171.83	1226.83	1080.33	1171.83
3.73	5082.33	655.30	962.67	864.00	1161.67	1238.67	1081.67	1161.67
3.74	5036.00	659.47	996.00	866.20	1186.83	1255.33	1091.17	1186.83
3.75	5001.07	648.80	983.33	859.84	1187.50	1237.50	1077.83	1187.50
3.76	4981.87	642.30	987.67	871.00	1202.83	1253.83	1069.33	1202.83
3.77	4950.67	642.93	968.67	862.40	1174.83	1239.00	1046.83	1174.83
3.78	4909.93	647.70	988.17	857.44	1182.50	1232.33	1053.83	1182.50
3.79	4845.17	638.77	956.67	859.28	1177.33	1246.17	1039.33	1177.33
3.80	4841.83	641.37	973.33	869.84	1211.00	1229.83	1018.17	1211.00
3.81	4815.77	635.03	987.50	853.96	1185.17	1233.33	1037.00	1185.17
3.82	4752.87	633.80	968.17	852.16	1208.00	1285.67	1012.67	1208.00
3.83	4711.03	628.40	997.67	850.72	1179.17	1236.17	1015.50	1179.17

3.84	4662.77	633.03	988.83	857.08	1161.67	1243.00	1006.17	1161.67
3.85	4651.00	615.77	973.17	850.32	1158.00	1253.67	1016.33	1158.00
3.86	4608.43	626.77	981.50	837.68	1189.67	1237.17	970.00	1189.67
3.87	4562.93	617.70	1000.83	845.64	1148.83	1209.17	991.00	1148.83
3.88	4522.93	619.67	971.50	833.88	1188.33	1242.17	972.50	1188.33
3.89	4472.03	602.00	986.83	840.96	1165.00	1232.83	987.83	1165.00
3.90	4426.50	601.13	981.83	828.96	1161.17	1260.00	972.17	1161.17
3.91	4386.17	606.97	982.33	838.04	1197.17	1228.67	950.00	1197.17
3.92	4345.43	602.37	979.50	825.36	1191.17	1193.33	949.67	1191.17
3.93	4290.97	598.23	975.33	819.80	1163.83	1218.67	942.00	1163.83
3.94	4223.70	598.73	984.33	827.36	1204.17	1220.00	926.50	1204.17
3.95	4191.23	591.00	958.33	824.20	1156.67	1203.83	919.00	1156.67
3.96	4157.17	580.17	966.83	826.16	1167.67	1232.50	917.00	1167.67
3.97	4119.10	572.77	987.50	821.56	1151.17	1207.67	906.00	1151.17
3.98	4083.37	578.23	990.83	810.40	1158.17	1206.17	909.67	1158.17
3.99	4013.73	567.10	973.33	797.16	1175.50	1182.00	871.83	1175.50
4.00	3993.10	571.50	986.83	801.40	1165.50	1207.33	866.00	1165.50
4.01	3926.67	567.13	955.33	800.60	1143.83	1190.17	852.67	1143.83
4.02	3882.03	563.60	957.50	787.84	1156.17	1202.50	876.50	1156.17
4.03	3828.37	560.80	964.17	787.32	1145.67	1171.83	852.67	1145.67
4.04	3786.53	550.43	970.50	781.28	1167.17	1191.33	858.00	1167.17
4.05	3727.70	555.97	956.50	782.80	1115.33	1176.00	837.00	1115.33
4.06	3685.17	549.40	943.33	766.16	1107.17	1192.00	820.83	1107.17
4.07	3664.20	542.73	941.17	774.56	1121.67	1182.17	810.67	1121.67
4.08	3616.10	538.63	932.50	766.60	1138.83	1153.67	802.33	1138.83
4.09	3540.13	531.63	949.17	767.80	1129.83	1158.33	793.50	1129.83
4.10	3509.07	531.73	928.33	754.96	1116.50	1138.17	793.33	1116.50
4.11	3465.30	523.47	962.17	751.52	1133.50	1161.17	802.67	1133.50
4.12	3422.30	520.93	952.83	726.44	1104.17	1145.00	778.50	1104.17
4.13	3382.33	518.30	909.00	742.84	1086.67	1145.50	759.33	1086.67
4.14	3311.10	516.00	920.67	731.64	1095.33	1129.00	737.17	1095.33
4.15	3284.97	508.03	920.00	723.96	1071.17	1123.17	746.33	1071.17
4.16	3231.17	502.63	910.17	720.56	1071.67	1127.83	755.17	1071.67
4.17	3200.80	509.10	899.17	711.28	1077.17	1095.17	742.17	1077.17
4.18	3161.03	497.20	920.00	705.00	1071.50	1114.17	719.50	1071.50
4.19	3125.93	486.33	921.83	701.88	1051.33	1093.33	735.33	1051.33
4.20	3071.53	484.23	908.67	701.28	1048.50	1081.50	710.83	1048.50
4.21	3025.07	484.80	902.83	683.76	1054.50	1085.33	698.33	1054.50

4.22	2989.93	476.30	884.50	676.88	1035.83	1075.17	682.33	1035.83
4.23	2960.40	470.27	893.67	680.04	1036.50	1099.83	696.83	1036.50
4.24	2894.53	468.73	884.33	664.56	1027.17	1084.00	680.50	1027.17
4.25	2863.93	464.70	887.17	670.84	1013.00	1058.83	663.83	1013.00
4.26	2833.30	459.63	882.00	656.32	1009.83	1047.17	670.17	1009.83
4.27	2783.97	456.33	870.00	643.40	1023.33	1044.17	648.33	1023.33
4.28	2740.07	451.57	867.00	638.64	996.67	1034.17	651.00	996.67
4.29	2696.00	443.87	850.33	630.28	999.00	1041.33	655.83	999.00
4.30	2663.80	445.27	842.67	639.52	988.17	1061.50	621.17	988.17
4.31	2626.63	444.47	842.17	627.36	981.83	1032.17	634.67	981.83
4.32	2582.27	430.60	818.00	624.20	973.33	994.83	612.50	973.33
4.33	2544.17	430.10	818.00	619.36	973.33	1017.83	609.67	973.33
4.34	2517.60	426.33	819.33	606.84	954.00	995.33	596.50	954.00
4.35	2453.63	429.07	822.83	613.24	956.83	988.00	581.00	956.83
4.36	2439.03	414.20	805.17	607.72	945.67	995.33	594.83	945.67
4.37	2410.63	414.30	800.50	589.20	954.17	977.17	581.67	954.17
4.38	2360.67	412.83	806.50	578.28	919.17	976.17	581.67	919.17
4.39	2345.80	409.00	788.00	580.28	910.17	958.33	569.17	910.17
4.40	2311.07	399.73	774.00	571.20	907.67	958.50	569.50	907.67
4.41	2253.63	399.67	744.17	568.04	905.33	954.00	547.50	905.33
4.42	2222.43	396.70	771.00	557.92	869.67	928.00	557.83	869.67
4.43	2183.47	391.30	750.67	563.84	868.33	922.33	538.83	868.33
4.44	2167.47	389.60	755.67	555.36	867.17	932.83	526.17	867.17
4.45	2135.40	378.60	737.83	548.68	867.50	906.83	538.50	867.50
4.46	2119.63	378.73	722.83	537.72	846.67	895.33	509.83	846.67
4.47	2076.70	376.80	725.17	522.40	854.50	881.83	518.83	854.50
4.48	2050.17	371.97	737.33	539.12	840.67	880.50	501.33	840.67
4.49	2005.57	368.43	713.17	514.80	834.00	892.00	515.00	834.00
4.50	1992.27	374.40	702.67	510.76	823.17	849.33	487.00	823.17
4.51	1953.73	358.23	701.17	506.72	802.50	845.67	498.00	802.50
4.52	1935.37	362.73	688.00	503.60	801.33	844.50	501.50	801.33
4.53	1891.47	351.97	669.33	492.72	791.83	836.83	482.33	791.83
4.54	1859.13	350.47	671.33	495.56	797.33	837.00	463.00	797.33
4.55	1853.43	351.30	663.33	490.00	780.00	844.67	473.83	780.00
4.56	1808.50	348.03	656.50	480.56	759.50	835.50	488.50	759.50
4.57	1788.70	342.30	659.17	473.80	760.17	811.50	460.17	760.17
4.58	1758.70	340.50	661.17	466.32	741.67	834.33	465.67	741.67
4.59	1736.53	328.43	649.00	472.84	745.17	798.17	444.50	745.17

4.60	1699.03	327.53	636.83	458.36	735.67	774.83	454.17	735.67
4.61	1689.13	328.97	624.00	467.00	732.00	772.83	450.83	732.00
4.62	1667.57	327.00	616.00	459.80	728.67	777.50	443.67	728.67
4.63	1641.83	318.20	618.33	446.60	710.67	774.67	426.17	710.67
4.64	1616.57	324.27	597.17	444.96	731.83	758.33	425.50	731.83
4.65	1605.53	314.53	601.83	444.84	710.83	749.67	419.67	710.83
4.66	1582.20	320.63	599.83	439.12	707.17	751.17	424.67	707.17
4.67	1561.63	309.87	584.00	426.84	693.33	750.17	416.50	693.33
4.68	1527.30	309.80	570.33	422.36	675.67	748.33	421.67	675.67
4.69	1517.00	308.13	581.00	419.56	684.33	722.83	403.33	684.33
4.70	1483.10	304.73	574.50	415.00	691.33	734.00	409.33	691.33
4.71	1463.10	302.73	562.00	415.68	680.00	724.67	412.17	680.00
4.72	1452.47	297.53	563.67	410.72	664.00	710.33	393.67	664.00
4.73	1425.93	291.97	571.50	399.92	655.33	701.83	402.50	655.33
4.74	1416.60	296.97	531.50	396.52	647.33	686.33	397.00	647.33
4.75	1393.93	288.30	542.33	399.68	642.00	681.00	386.83	642.00
4.76	1371.33	290.10	534.33	396.96	639.17	685.50	401.83	639.17
4.77	1348.13	284.37	520.83	385.20	637.00	671.17	376.67	637.00
4.78	1317.90	287.07	526.17	376.04	614.50	658.67	373.33	614.50
4.79	1320.57	281.03	518.33	371.96	603.00	666.67	374.50	603.00
4.80	1296.30	280.47	515.50	378.52	611.67	653.50	374.83	611.67
4.81	1283.80	280.87	522.83	377.12	591.50	648.17	363.67	591.50
4.82	1263.30	277.27	526.17	363.96	585.67	655.50	368.17	585.67
4.83	1252.53	274.10	502.83	366.40	578.33	632.00	345.50	578.33
4.84	1237.07	272.27	501.17	359.28	582.17	634.50	345.67	582.17
4.85	1211.03	264.97	490.83	360.36	572.33	641.67	348.50	572.33
4.86	1205.13	262.03	495.00	354.88	563.17	613.17	343.17	563.17
4.87	1192.10	265.50	478.00	356.52	553.67	626.50	351.17	553.67
4.88	1176.43	260.30	471.33	348.76	560.33	592.33	353.33	560.33
4.89	1164.47	255.63	452.17	350.44	554.83	601.00	354.83	554.83
4.90	1151.23	251.57	450.17	342.96	556.50	601.00	339.00	556.50
4.91	1132.27	257.97	456.50	338.48	544.67	592.17	332.17	544.67
4.92	1110.80	257.20	465.00	339.16	556.67	583.67	341.67	556.67
4.93	1102.73	257.83	455.17	332.72	525.67	581.67	340.50	525.67
4.94	1085.83	248.47	441.83	324.12	532.17	592.50	348.33	532.17
4.95	1069.20	247.40	436.33	322.12	515.83	560.67	322.17	515.83
4.96	1067.43	244.03	440.67	327.56	521.50	563.00	328.67	521.50
4.97	1051.27	247.17	434.67	322.52	512.17	573.00	324.50	512.17

4.98	1045.17	239.93	434.67	321.64	506.83	555.17	308.83	506.83
4.99	1027.80	239.93	430.50	317.12	502.67	555.00	317.00	502.67
5.00	1023.87	239.73	408.00	313.80	506.67	552.67	309.17	506.67
5.01	1006.77	235.43	421.17	300.68	490.67	542.67	319.33	490.67
5.02	999.37	232.30	422.50	308.20	473.33	547.33	315.00	473.33
5.03	987.63	234.33	412.17	309.68	487.67	525.33	309.50	487.67
5.04	976.47	234.67	409.50	304.64	483.50	536.83	307.83	483.50
5.05	960.10	231.03	401.17	299.00	474.50	546.83	288.83	474.50
5.06	942.30	228.13	401.67	303.44	452.17	522.50	305.33	452.17
5.07	945.23	226.13	382.83	292.44	488.33	514.83	309.67	488.33
5.08	928.10	232.40	387.17	296.48	466.67	520.83	292.00	466.67
5.09	914.73	215.73	388.17	300.20	460.00	517.17	306.00	460.00
5.10	915.87	223.20	375.17	290.64	469.67	507.33	297.67	469.67
5.11	907.97	220.27	383.33	287.80	468.17	513.17	291.83	468.17
5.12	892.00	224.27	364.00	289.40	456.33	497.67	292.50	456.33
5.13	887.23	218.00	386.17	279.20	446.17	477.67	286.83	446.17
5.14	888.90	216.90	361.00	276.12	441.50	487.17	282.33	441.50
5.15	868.50	214.57	377.00	278.96	437.67	473.50	281.00	437.67
5.16	867.60	216.77	358.83	280.92	455.50	484.33	278.67	455.50
5.17	850.63	217.80	364.83	272.48	434.67	480.67	280.67	434.67
5.18	850.83	211.23	365.67	274.12	423.33	472.50	265.33	423.33
5.19	839.37	213.03	362.17	272.32	413.17	472.67	280.17	413.17
5.20	832.93	213.53	359.33	266.20	431.00	470.67	278.00	431.00
5.21	830.63	211.33	348.83	259.96	422.00	475.00	285.33	422.00
5.22	814.47	207.83	349.83	267.56	430.67	453.00	284.00	430.67
5.23	806.27	207.70	348.33	265.04	419.83	447.00	272.00	419.83
5.24	812.67	205.97	335.83	258.32	423.50	445.00	267.67	423.50
5.25	800.43	204.40	335.17	262.68	410.67	453.33	277.67	410.67
5.26	795.63	208.13	340.67	255.68	407.67	444.17	271.67	407.67
5.27	775.40	204.23	352.83	259.92	396.50	445.83	271.33	396.50
5.28	782.43	204.83	335.67	259.24	389.50	439.50	270.50	389.50
5.29	774.00	205.53	327.67	254.80	398.67	436.33	260.00	398.67
5.30	767.97	203.50	352.50	249.68	402.33	430.67	260.00	402.33
5.31	754.10	200.73	336.17	248.76	387.50	418.67	267.83	387.50
5.32	749.27	198.23	332.50	253.96	386.00	419.83	260.33	386.00
5.33	746.73	198.10	334.67	248.52	380.83	442.00	255.83	380.83
5.34	743.27	198.30	327.67	242.36	374.50	420.17	264.50	374.50
5.35	733.03	196.13	308.33	247.32	375.00	433.83	252.50	375.00

5.36	725.07	198.97	318.50	242.04	380.50	411.50	260.00	380.50
5.37	709.33	193.37	345.67	243.84	369.00	413.67	251.50	369.00
5.38	706.40	194.27	313.17	240.48	381.17	389.00	271.00	381.17
5.39	714.33	195.87	310.83	239.08	378.83	408.33	266.50	378.83
5.40	708.07	192.33	322.83	239.80	367.67	418.50	256.50	367.67
5.41	707.60	194.97	318.67	232.88	369.00	395.17	261.83	369.00
5.42	693.10	192.60	317.50	236.20	356.83	393.50	258.83	356.83
5.43	695.53	190.57	301.00	236.16	367.33	398.33	251.33	367.33
5.44	684.63	192.37	318.83	226.72	358.00	398.33	256.33	358.00
5.45	682.20	187.80	295.83	234.84	361.83	399.50	251.50	361.83
5.46	679.33	187.13	294.33	235.00	351.00	389.50	253.50	351.00
5.47	674.77	190.30	304.17	226.32	347.67	404.50	244.17	347.67
5.48	671.53	189.47	294.00	227.52	353.33	385.00	245.67	353.33
5.49	657.33	189.57	308.33	224.80	354.50	400.33	243.83	354.50
5.50	662.17	185.83	288.67	226.48	352.00	368.17	255.83	352.00
5.51	658.80	185.07	291.67	222.08	339.33	397.33	247.17	339.33
5.52	654.87	183.30	291.17	222.76	349.17	368.50	251.00	349.17
5.53	651.27	181.03	296.50	224.48	332.83	380.83	241.83	332.83
5.54	646.33	181.43	302.17	228.28	347.67	376.17	242.83	347.67
5.55	643.37	185.43	298.67	223.60	356.50	380.83	235.83	356.50
5.56	633.33	184.33	284.33	225.68	333.00	375.00	254.50	333.00
5.57	639.80	182.53	294.33	220.48	335.17	366.83	234.67	335.17
5.58	633.20	185.43	291.17	215.56	327.17	370.17	245.67	327.17
5.59	624.83	188.30	285.67	218.68	327.50	375.00	246.67	327.50
5.60	631.53	177.40	286.67	217.72	333.67	369.33	225.67	333.67
5.61	618.10	176.87	293.50	220.08	327.17	379.50	244.17	327.17
5.62	613.87	178.60	289.83	213.80	327.67	359.83	232.50	327.67
5.63	613.50	179.77	296.50	217.64	333.50	374.17	245.17	333.50
5.64	607.63	182.83	279.33	212.28	326.50	359.83	248.67	326.50
5.65	609.57	177.30	276.50	217.04	331.33	351.50	241.83	331.33
5.66	616.00	179.53	288.00	214.60	330.00	368.33	235.33	330.00
5.67	605.70	178.33	289.00	210.56	324.67	360.67	238.83	324.67
5.68	604.63	177.60	281.17	213.28	324.00	345.00	232.50	324.00
5.69	593.50	179.20	282.67	210.28	322.33	335.17	247.00	322.33
5.70	595.57	176.53	273.17	210.56	315.67	363.00	224.50	315.67
5.71	596.13	180.03	287.17	206.92	317.17	356.00	244.50	317.17
5.72	595.93	175.63	276.33	211.84	310.67	350.67	245.33	310.67
5.73	592.60	177.23	266.17	205.40	319.00	351.00	242.17	319.00

5.74	589.90	178.10	275.67	203.44	330.83	354.50	231.33	330.83
5.75	586.13	176.23	270.33	210.96	309.33	345.67	241.33	309.33
5.76	584.83	175.37	272.50	202.92	309.17	341.33	229.50	309.17
5.77	579.67	174.87	273.33	205.84	308.00	344.83	235.83	308.00
5.78	590.07	175.40	262.50	204.24	310.67	345.33	229.17	310.67
5.79	570.10	178.97	273.00	205.56	303.00	338.50	221.83	303.00
5.80	575.67	177.13	272.83	200.96	309.33	344.00	224.83	309.33
5.81	576.13	179.63	262.33	205.80	304.50	343.67	241.50	304.50
5.82	579.00	173.57	267.33	199.68	307.67	339.33	232.83	307.67
5.83	569.53	174.37	252.00	199.40	307.33	345.00	235.83	307.33
5.84	572.47	173.80	268.83	203.52	310.33	331.50	227.67	310.33
5.85	567.67	181.13	264.33	199.92	293.33	347.00	232.50	293.33
5.86	560.03	168.77	266.00	200.52	315.33	342.50	229.17	315.33
5.87	561.97	175.03	268.83	202.52	288.17	330.17	232.83	288.17
5.88	564.80	173.97	270.67	197.32	303.00	325.50	234.17	303.00
5.89	562.73	172.97	269.50	202.84	314.17	332.67	237.83	314.17
5.90	549.20	174.80	254.17	197.36	305.17	325.33	235.83	305.17
5.91	556.87	176.00	270.33	197.56	302.50	325.83	241.17	302.50
5.92	559.47	174.93	264.50	197.60	300.67	333.00	225.00	300.67
5.93	560.33	173.93	256.83	201.68	298.33	325.50	235.83	298.33
5.94	555.93	177.03	260.67	197.24	295.50	332.00	231.00	295.50
5.95	551.47	176.53	256.83	199.28	291.00	333.00	238.67	291.00
5.96	557.37	173.97	266.17	192.52	297.50	331.67	235.00	297.50
5.97	559.90	174.27	268.17	195.60	295.83	327.17	238.50	295.83
5.98	555.77	170.87	256.83	188.48	303.83	335.50	249.50	303.83
5.99	548.40	173.90	265.33	192.64	288.50	327.00	234.50	288.50
6.00	543.00	177.07	260.50	197.32	301.83	324.17	225.17	301.83
6.01	564.83	174.97	252.33	197.40	295.67	323.17	217.50	295.67
6.02	546.20	172.43	266.00	199.04	303.00	332.50	221.50	303.00
6.03	550.83	174.67	269.33	196.76	313.83	333.50	231.67	313.83
6.04	548.57	177.67	271.50	192.56	284.33	322.83	234.33	284.33
6.05	556.27	172.53	257.83	194.56	293.33	339.83	230.67	293.33
6.06	549.57	171.60	256.67	199.52	288.00	323.50	218.83	288.00
6.07	545.50	174.93	259.00	192.28	287.83	325.83	234.50	287.83
6.08	548.77	172.53	257.50	191.84	292.17	331.00	235.17	292.17
6.09	553.40	174.23	260.17	195.12	292.33	316.83	235.83	292.33
6.10	554.27	176.90	254.50	194.24	290.67	331.83	235.17	290.67
6.11	547.53	171.70	257.17	196.20	294.67	325.33	228.33	294.67

6.12	541.90	174.63	262.33	195.12	278.67	312.17	236.00	278.67
6.13	546.60	174.70	250.33	193.24	287.67	329.67	236.67	287.67
6.14	548.77	173.97	260.17	194.48	291.17	322.33	234.00	291.17
6.15	551.87	173.17	265.17	197.36	292.67	330.17	241.50	292.67
6.16	547.30	173.77	259.50	196.24	297.83	317.17	237.67	297.83
6.17	549.80	175.60	256.17	191.20	298.50	329.00	229.50	298.50
6.18	555.20	176.20	261.17	192.32	283.00	311.67	235.67	283.00
6.19	549.37	174.30	264.50	199.24	290.33	319.00	233.50	290.33
6.20	552.50	172.37	270.67	191.56	281.17	314.33	236.50	281.17
6.21	545.73	176.10	255.17	197.72	292.67	323.33	244.67	292.67
6.22	553.77	171.50	254.17	193.60	287.33	320.83	247.17	287.33
6.23	547.13	176.87	267.17	191.88	281.50	326.67	247.33	281.50
6.24	567.47	173.77	263.17	195.12	290.17	322.00	231.83	290.17
6.25	553.30	175.20	256.00	190.36	298.00	315.00	230.67	298.00
6.26	557.37	177.17	256.17	201.36	287.50	322.00	234.33	287.50
6.27	554.73	174.33	265.17	199.84	293.33	327.00	242.17	293.33
6.28	550.37	176.50	274.33	191.00	299.67	324.33	229.33	299.67
6.29	561.60	176.20	252.83	191.68	289.50	331.67	233.00	289.50
6.30	562.77	183.47	262.67	191.24	286.33	336.00	238.17	286.33
6.31	561.17	175.60	263.33	189.48	291.83	337.67	242.67	291.83
6.32	562.60	173.80	271.83	191.56	277.00	336.33	242.67	277.00
6.33	564.40	174.60	264.33	192.64	290.00	326.83	244.50	290.00
6.34	567.40	177.57	277.00	198.72	284.50	339.17	235.50	284.50
6.35	572.37	177.03	272.33	195.92	297.33	330.33	243.00	297.33
6.36	569.87	177.87	266.17	196.40	285.17	325.17	245.00	285.17
6.37	577.87	179.80	261.83	197.32	290.17	330.83	255.67	290.17
6.38	578.20	176.20	267.50	194.04	287.83	319.00	254.83	287.83
6.39	578.97	178.83	270.50	201.88	288.67	319.83	240.67	288.67
6.40	583.37	176.17	263.67	194.04	305.67	328.83	245.17	305.67
6.41	580.60	178.17	259.67	193.16	283.33	327.17	240.00	283.33
6.42	590.30	178.47	271.83	196.44	293.83	333.83	250.67	293.83
6.43	592.47	180.67	258.50	198.60	297.00	326.67	246.50	297.00
6.44	593.43	177.23	269.50	200.16	288.83	327.50	238.50	288.83
6.45	593.27	181.63	254.83	202.08	287.33	338.50	246.67	287.33
6.46	599.70	182.13	270.83	198.40	281.83	335.83	240.17	281.83
6.47	595.00	181.83	267.33	196.44	293.83	342.00	252.67	293.83
6.48	594.17	180.70	266.33	202.16	293.83	332.17	240.67	293.83
6.49	603.17	180.83	269.83	203.16	293.17	338.33	253.50	293.17

6.50	603.57	181.20	269.67	200.96	294.67	328.33	244.67	294.67
6.51	609.43	185.27	274.17	200.20	287.17	317.00	247.83	287.17
6.52	609.00	181.83	275.00	199.36	293.33	339.83	252.83	293.33
6.53	617.10	180.67	270.83	200.68	295.50	337.33	249.50	295.50
6.54	618.97	180.13	268.83	197.60	301.67	344.33	246.67	301.67
6.55	631.30	180.77	257.83	203.40	305.50	342.83	258.33	305.50
6.56	627.13	183.43	274.50	208.32	300.50	338.17	250.33	300.50
6.57	627.00	184.27	266.83	201.28	306.83	336.67	263.33	306.83
6.58	625.73	183.33	269.50	204.24	297.83	346.67	252.17	297.83
6.59	638.57	184.80	270.50	197.24	305.17	339.67	245.00	305.17
6.60	638.23	183.57	256.17	205.16	299.33	339.17	246.67	299.33
6.61	640.33	179.20	261.67	205.92	304.83	351.00	254.17	304.83
6.62	646.70	183.83	279.33	205.80	307.67	357.50	247.00	307.67
6.63	642.70	184.27	270.50	207.56	295.67	355.33	252.17	295.67
6.64	652.40	185.63	279.50	208.36	295.00	353.83	262.67	295.00
6.65	659.67	188.53	273.17	213.32	307.00	356.83	252.17	307.00
6.66	660.37	186.17	275.00	204.76	307.83	366.67	256.67	307.83
6.67	664.00	189.10	274.67	208.40	306.00	360.00	261.67	306.00
6.68	667.30	185.03	276.33	208.68	309.00	363.50	271.33	309.00
6.69	677.13	183.13	285.50	203.60	314.67	371.33	257.17	314.67
6.70	675.63	184.97	276.67	206.12	304.00	346.50	258.67	304.00
6.71	676.60	191.67	277.00	212.00	325.17	369.33	266.33	325.17
6.72	692.23	189.87	278.33	209.96	321.50	352.67	252.00	321.50
6.73	690.50	187.43	286.33	208.24	316.50	365.67	272.67	316.50
6.74	686.00	187.50	289.33	205.08	296.33	365.83	272.33	296.33
6.75	693.23	191.50	286.83	210.88	321.67	373.33	261.67	321.67
6.76	696.03	185.53	278.67	209.84	321.00	370.33	273.50	321.00
6.77	708.83	189.70	284.33	216.16	315.17	367.50	265.83	315.17
6.78	709.57	191.63	280.83	216.48	309.33	379.50	279.83	309.33
6.79	714.83	191.27	277.67	218.04	319.00	382.17	251.83	319.00
6.80	721.30	189.63	272.17	209.60	309.17	367.50	253.50	309.17
6.81	728.47	189.07	276.17	213.76	310.00	377.17	275.67	310.00
6.82	728.47	189.97	277.67	216.52	311.17	366.33	269.00	311.17
6.83	734.20	194.53	286.83	215.00	325.50	378.17	259.83	325.50
6.84	732.70	188.97	280.83	213.28	317.33	384.17	276.00	317.33
6.85	740.27	192.87	293.83	221.96	329.50	383.83	271.00	329.50
6.86	740.53	189.33	280.00	221.48	334.67	383.00	272.33	334.67
6.87	744.07	189.47	281.50	218.64	325.83	379.00	272.83	325.83

6.88	762.47	193.83	297.17	221.04	330.00	374.50	275.00	330.00
6.89	755.87	194.33	287.50	219.20	325.00	384.33	277.67	325.00
6.90	760.87	191.80	303.17	223.16	324.83	399.67	270.67	324.83
6.91	760.60	193.77	291.17	222.04	321.67	394.17	258.67	321.67
6.92	773.17	195.60	285.83	216.80	340.00	385.00	278.83	340.00
6.93	770.80	186.67	280.83	225.84	315.00	393.50	266.00	315.00
6.94	776.20	194.40	302.17	219.64	326.17	387.67	272.83	326.17
6.95	776.83	194.63	292.83	222.84	328.83	395.50	269.50	328.83
6.96	784.43	193.43	303.33	229.96	323.50	401.67	262.67	323.50
6.97	780.47	194.57	295.00	221.68	323.50	398.17	266.67	323.50
6.98	787.43	191.13	300.33	223.96	335.33	383.00	269.50	335.33
6.99	784.10	194.40	294.67	223.56	320.33	388.83	268.00	320.33
7.00	794.70	196.93	302.00	221.32	339.33	396.67	260.67	339.33
7.01	793.57	193.53	289.67	229.60	327.50	402.83	253.17	327.50
7.02	796.30	198.43	302.67	226.56	338.83	401.17	275.17	338.83
7.03	802.97	191.57	280.83	226.96	346.50	401.17	255.33	346.50
7.04	798.13	192.47	295.83	221.88	333.33	406.17	266.83	333.33
7.05	800.93	197.53	290.83	228.56	327.50	406.67	282.67	327.50
7.06	800.40	191.77	296.17	224.40	341.33	401.83	271.33	341.33
7.07	799.73	193.10	318.33	232.68	336.50	395.83	274.50	336.50
7.08	797.63	194.27	295.83	228.28	347.83	409.17	269.50	347.83
7.09	796.63	194.40	299.17	231.72	334.00	398.50	271.33	334.00
7.10	804.70	195.87	298.67	234.68	337.67	411.67	263.17	337.67
7.11	802.50	196.80	283.33	228.28	346.67	401.17	274.17	346.67
7.12	798.30	196.37	287.00	230.88	337.33	403.50	256.17	337.33
7.13	800.37	199.87	307.67	227.60	346.33	419.17	269.83	346.33
7.14	806.93	201.63	306.67	230.64	340.67	409.17	280.67	340.67
7.15	798.47	197.43	294.00	227.48	346.33	408.33	250.17	346.33
7.16	801.00	198.30	304.00	236.68	345.83	413.83	261.33	345.83
7.17	790.30	193.97	307.17	236.60	347.33	411.00	266.33	347.33
7.18	795.47	195.60	317.17	234.96	367.50	406.00	266.17	367.50
7.19	794.93	195.57	301.50	231.32	348.17	410.17	252.00	348.17
7.20	800.00	197.33	308.33	235.00	341.33	396.83	260.00	341.33
7.21	795.20	198.13	307.00	238.00	342.17	415.67	257.50	342.17
7.22	801.83	196.20	290.67	238.28	343.17	424.00	270.00	343.17
7.23	799.83	197.50	314.00	238.56	356.50	412.83	264.00	356.50
7.24	784.70	193.33	318.00	238.68	340.17	409.33	256.67	340.17
7.25	772.30	195.33	309.67	239.76	341.50	408.17	261.33	341.50

7.26	764.90	198.47	305.33	238.48	341.17	414.00	249.17	341.17
7.27	768.97	200.37	317.00	237.44	346.17	405.00	262.50	346.17
7.28	772.87	196.60	312.00	242.84	349.67	414.83	257.00	349.67
7.29	768.07	195.60	329.17	235.84	346.83	406.00	251.17	346.83
7.30	752.97	194.63	314.00	236.32	326.50	400.17	256.33	326.50
7.31	747.20	195.20	309.67	241.76	343.67	409.83	256.17	343.67
7.32	746.77	194.93	304.00	242.24	344.17	413.00	264.00	344.17
7.33	743.30	192.33	311.67	241.16	341.67	402.17	240.33	341.67
7.34	737.73	196.80	311.00	241.80	355.50	416.17	252.00	355.50
7.35	731.33	192.43	302.33	235.64	350.00	414.33	258.67	350.00
7.36	729.00	196.97	317.00	241.08	340.00	409.33	247.33	340.00
7.37	724.47	197.63	310.83	244.24	340.00	412.67	260.33	340.00
7.38	712.77	189.03	303.83	243.12	350.50	415.33	249.17	350.50
7.39	716.27	194.00	293.50	240.56	348.00	406.17	253.50	348.00
7.40	699.67	191.60	313.17	243.28	338.17	386.17	247.33	338.17
7.41	701.47	195.07	312.83	242.48	346.00	418.17	252.50	346.00
7.42	690.57	193.17	320.50	237.60	339.67	413.67	252.33	339.67
7.43	689.90	195.60	300.83	239.52	352.17	419.83	240.83	352.17
7.44	679.87	197.07	299.00	244.28	337.17	414.67	246.00	337.17
7.45	669.03	191.40	315.83	236.00	331.83	397.17	241.33	331.83
7.46	667.70	193.60	306.83	241.48	336.00	413.67	246.83	336.00
7.47	650.43	194.80	320.50	240.40	346.17	389.00	249.00	346.17
7.48	657.23	194.83	299.33	242.08	342.50	413.50	245.67	342.50
7.49	647.97	194.67	307.67	247.28	322.67	404.17	235.67	322.67
7.50	643.13	193.57	319.00	243.88	341.67	402.67	231.33	341.67
7.51	642.20	192.80	323.83	243.88	332.67	400.00	235.33	332.67
7.52	622.27	194.60	304.50	239.20	329.83	407.00	237.33	329.83
7.53	625.20	190.87	312.50	243.68	331.00	390.17	226.33	331.00
7.54	617.07	188.47	314.83	239.76	345.67	395.83	244.33	345.67
7.55	601.57	187.47	306.17	248.76	335.33	382.17	231.50	335.33
7.56	601.70	197.57	309.33	242.20	330.33	390.67	224.83	330.33
7.57	589.43	189.70	316.33	242.24	326.00	399.50	247.83	326.00
7.58	595.40	189.20	299.00	240.80	331.83	394.33	224.83	331.83
7.59	577.80	190.57	311.17	243.12	329.17	388.00	236.67	329.17
7.60	566.30	195.13	308.17	240.52	317.67	374.83	234.17	317.67
7.61	568.83	189.90	306.00	239.24	328.33	370.67	217.00	328.33
7.62	551.57	188.90	310.00	245.60	333.33	386.67	230.50	333.33
7.63	555.20	191.40	325.17	239.64	314.17	379.33	225.17	314.17

7.64	544.30	185.80	313.17	236.28	308.33	388.17	229.33	308.33
7.65	544.90	190.00	313.00	239.92	320.67	382.50	226.67	320.67
7.66	531.43	185.07	292.67	241.36	315.50	373.83	238.17	315.50
7.67	532.97	191.37	306.83	243.56	317.33	374.83	239.33	317.33
7.68	519.90	190.83	309.50	240.20	316.17	366.33	225.50	316.17
7.69	514.17	189.63	291.17	238.48	316.83	374.17	231.17	316.83
7.70	507.30	191.67	295.83	241.36	313.00	366.83	220.00	313.00
7.71	497.53	192.40	312.33	230.68	311.33	369.00	236.17	311.33
7.72	490.30	187.30	287.17	238.76	306.83	368.50	228.17	306.83
7.73	488.00	189.43	290.33	234.00	298.83	364.50	225.00	298.83
7.74	485.90	187.77	299.33	239.80	312.17	362.83	222.00	312.17
7.75	477.50	186.40	294.50	238.88	307.00	359.17	216.33	307.00
7.76	463.70	185.60	292.17	238.00	308.33	361.83	230.17	308.33
7.77	459.97	187.20	303.83	234.20	305.33	342.33	226.33	305.33
7.78	458.47	187.63	298.00	237.56	307.67	360.83	218.17	307.67
7.79	451.50	192.40	301.67	229.92	303.83	342.50	208.17	303.83
7.80	446.80	189.53	300.67	234.52	301.17	336.17	213.83	301.17
7.81	439.07	185.77	295.67	234.44	296.83	334.67	209.83	296.83
7.82	435.23	185.70	282.67	237.16	304.17	345.50	215.67	304.17
7.83	428.37	183.57	294.83	234.92	302.17	338.67	222.50	302.17
7.84	419.50	187.00	287.50	234.96	304.00	336.33	214.00	304.00
7.85	415.87	187.20	296.00	227.16	289.83	326.67	216.17	289.83
7.86	406.70	180.93	294.00	230.56	287.17	345.50	205.00	287.17
7.87	401.40	181.63	289.83	226.56	295.33	330.33	209.00	295.33
7.88	400.67	186.00	299.67	230.44	284.50	321.67	207.50	284.50
7.89	390.33	190.03	288.00	229.72	299.50	318.67	220.17	299.50
7.90	384.90	184.73	301.67	227.96	288.17	318.00	211.67	288.17
7.91	381.37	183.80	299.50	232.08	292.33	315.83	211.33	292.33
7.92	377.30	181.80	283.67	227.80	298.17	320.00	216.17	298.17
7.93	371.47	183.23	287.83	227.64	277.83	317.67	202.83	277.83
7.94	363.60	184.47	306.00	225.48	288.67	319.50	213.83	288.67
7.95	361.07	183.60	292.33	225.68	283.00	319.50	212.50	283.00
7.96	352.37	184.80	294.50	222.84	293.50	322.17	204.17	293.50
7.97	352.93	184.23	292.83	222.28	279.00	318.50	210.17	279.00
7.98	347.17	179.87	280.83	222.80	289.00	319.00	209.67	289.00
7.99	344.50	178.47	281.33	220.52	287.50	314.17	218.33	287.50
8.00	335.10	179.77	295.50	220.64	292.00	305.67	197.00	292.00
8.01	337.63	186.57	292.50	219.12	285.83	295.33	197.33	285.83

8.02	321.70	183.07	280.83	222.96	281.17	305.33	200.83	281.17
8.03	319.17	183.30	278.67	217.44	256.83	303.67	208.17	256.83
8.04	315.17	185.43	295.83	215.60	267.67	294.83	191.33	267.67
8.05	314.83	179.97	282.17	217.68	294.67	298.83	201.00	294.67
8.06	311.53	182.03	283.00	220.24	266.17	295.83	207.67	266.17
8.07	308.80	181.50	276.00	220.00	271.00	292.83	209.17	271.00
8.08	301.43	182.97	291.50	217.48	257.17	288.50	203.67	257.17
8.09	295.53	178.50	278.33	212.48	266.00	289.67	207.67	266.00
8.10	293.33	181.97	287.00	217.72	275.67	294.83	202.17	275.67
8.11	288.27	177.17	294.50	205.16	262.17	297.33	211.33	262.17
8.12	284.97	179.13	274.50	208.72	259.50	282.83	198.00	259.50
8.13	283.90	178.93	295.17	210.48	260.00	281.00	201.17	260.00
8.14	275.83	179.03	274.33	212.48	262.67	288.33	201.50	262.67
8.15	270.63	177.87	288.33	210.52	252.17	287.50	206.00	252.17
8.16	273.37	175.63	281.17	212.16	263.00	283.67	194.00	263.00
8.17	269.70	184.47	286.67	205.04	257.83	276.83	188.50	257.83
8.18	265.57	183.53	278.50	210.08	259.00	274.33	200.33	259.00
8.19	258.57	176.10	273.00	205.04	272.67	264.17	199.50	272.67
8.20	256.20	180.40	273.33	208.00	256.17	273.33	182.67	256.17
8.21	253.37	181.33	281.83	208.56	267.00	277.83	195.33	267.00
8.22	252.43	179.17	275.67	202.88	249.83	275.00	201.33	249.83
8.23	244.43	175.33	274.17	203.48	264.67	267.33	191.83	264.67
8.24	246.83	181.87	262.83	203.64	258.67	272.17	200.33	258.67
8.25	245.50	177.37	288.00	201.68	250.67	262.67	200.33	250.67
8.26	239.03	176.27	280.00	200.52	246.67	270.50	199.33	246.67
8.27	234.87	178.47	282.83	200.80	247.50	279.00	197.83	247.50
8.28	232.63	180.37	270.00	200.40	247.33	264.33	192.00	247.33
8.29	230.27	180.30	271.00	200.32	254.50	269.17	201.33	254.50
8.30	228.70	179.57	281.83	197.56	244.50	262.83	203.00	244.50
8.31	225.63	182.50	262.33	202.00	260.17	279.50	198.33	260.17
8.32	221.90	180.10	262.50	202.80	242.50	265.67	196.00	242.50
8.33	224.77	180.13	265.17	202.24	241.83	251.67	197.50	241.83
8.34	216.67	176.83	270.33	195.00	245.00	267.50	202.67	245.00
8.35	217.67	175.10	268.50	196.56	242.83	249.17	190.33	242.83
8.36	209.93	179.77	279.00	192.48	244.50	249.67	200.83	244.50
8.37	207.67	176.97	289.50	190.84	237.33	272.33	192.33	237.33
8.38	207.87	177.10	279.50	189.68	251.83	250.83	184.00	251.83
8.39	202.67	181.03	277.33	195.00	250.67	253.50	206.67	250.67

8.40	204.73	179.50	273.83	194.96	243.83	250.17	201.50	243.83
8.41	198.43	179.87	285.83	191.92	244.67	261.00	198.83	244.67
8.42	196.40	176.03	273.00	192.92	239.50	250.50	195.50	239.50
8.43	194.17	175.17	271.33	190.52	242.33	251.17	185.67	242.33
8.44	202.07	182.93	268.17	195.88	235.67	247.00	208.67	235.67
8.45	195.10	179.23	275.83	195.88	231.83	251.17	194.33	231.83
8.46	190.03	177.00	273.17	191.72	246.17	248.17	210.33	246.17
8.47	188.30	180.30	277.83	190.68	245.00	249.83	199.00	245.00
8.48	189.17	180.83	274.00	187.44	233.83	253.67	208.00	233.83
8.49	184.37	178.97	265.00	190.76	240.50	236.50	197.00	240.50
8.50	187.23	178.07	271.17	190.04	240.83	248.83	208.17	240.83
8.51	184.53	179.43	270.00	189.60	247.67	247.50	197.33	247.67
8.52	181.30	175.87	259.00	188.32	240.67	245.67	208.67	240.67
8.53	180.37	178.37	261.17	185.24	236.00	251.17	198.50	236.00
8.54	183.00	178.73	269.00	188.20	232.00	237.83	194.83	232.00
8.55	180.03	181.87	278.00	189.04	242.50	246.17	202.67	242.50
8.56	174.40	181.37	279.67	189.68	247.00	225.00	198.50	247.00
8.57	176.77	179.30	268.50	190.36	242.00	237.50	191.00	242.00
8.58	169.43	176.10	276.50	183.16	232.00	239.33	193.00	232.00
8.59	174.27	184.63	267.67	188.96	233.17	240.50	188.67	233.17
8.60	171.00	178.90	261.67	180.68	222.83	236.50	196.50	222.83
8.61	172.30	182.70	264.00	185.48	233.50	249.00	197.67	233.50
8.62	166.70	181.83	269.67	182.72	229.17	232.83	186.33	229.17
8.63	166.07	177.07	271.83	187.04	236.33	253.00	202.50	236.33
8.64	166.20	182.83	268.50	182.80	234.50	226.17	199.67	234.50
8.65	161.13	184.17	274.33	183.80	246.17	233.67	193.83	246.17
8.66	163.10	182.70	275.50	183.08	235.50	245.50	208.17	235.50
8.67	160.50	180.87	275.50	183.16	229.33	225.67	194.33	229.33
8.68	163.13	180.73	270.33	179.92	223.83	230.17	204.83	223.83
8.69	159.93	184.03	282.50	181.80	231.17	234.00	192.50	231.17
8.70	156.53	180.97	284.00	181.88	236.17	234.83	192.67	236.17
8.71	158.33	183.40	277.67	179.12	224.17	237.33	197.83	224.17
8.72	156.23	179.40	280.00	181.80	232.17	233.50	195.67	232.17
8.73	154.47	184.07	271.83	184.64	230.67	232.50	205.00	230.67
8.74	155.80	181.73	267.83	181.60	232.33	221.33	194.00	232.33
8.75	153.33	182.93	271.50	181.24	231.50	240.67	195.33	231.50
8.76	150.00	179.87	278.17	175.00	216.50	224.00	192.33	216.50
8.77	150.00	183.03	258.17	181.88	229.67	230.17	207.17	229.67

8.78	149.97	183.60	262.17	179.52	229.00	234.67	202.83	229.00
8.79	147.50	185.03	276.50	179.76	224.50	235.33	203.83	224.50
8.80	147.83	181.07	280.17	177.52	218.33	235.33	210.50	218.33
8.81	145.20	189.47	289.83	181.44	226.33	233.33	196.83	226.33
8.82	146.90	180.53	268.83	177.56	236.50	227.67	205.17	236.50
8.83	140.57	183.67	269.00	178.40	226.83	233.17	215.00	226.83
8.84	142.53	186.83	282.17	178.40	238.00	222.67	186.50	238.00
8.85	142.60	186.77	279.50	175.84	229.67	228.50	204.83	229.67
8.86	141.60	183.93	286.67	174.00	234.67	229.00	195.33	234.67
8.87	142.43	183.43	275.67	178.60	237.00	225.33	201.83	237.00
8.88	141.67	185.23	279.17	179.00	220.67	226.50	200.67	220.67
8.89	138.57	185.90	266.17	181.76	229.17	221.83	208.67	229.17
8.90	140.23	189.40	278.33	180.48	229.50	232.17	214.83	229.50
8.91	136.33	186.97	266.50	178.44	227.00	242.00	210.67	227.00
8.92	135.57	186.50	285.17	178.20	242.50	218.83	203.33	242.50
8.93	137.93	186.40	283.17	179.24	231.33	228.00	208.00	231.33
8.94	135.33	182.53	272.83	177.52	225.67	216.83	196.17	225.67
8.95	136.67	192.30	279.33	183.52	235.67	223.83	199.33	235.67
8.96	132.53	188.03	283.50	179.20	239.67	230.00	211.17	239.67
8.97	131.37	187.13	287.33	182.32	238.33	231.17	203.17	238.33
8.98	132.53	189.83	269.83	177.28	233.67	228.00	203.50	233.67
8.99	133.13	191.40	280.50	175.64	229.00	216.67	203.67	229.00
9.00	128.63	188.50	275.50	177.96	239.67	233.17	210.67	239.67
9.01	133.47	189.60	282.50	179.20	231.83	231.33	210.17	231.83
9.02	132.23	189.07	283.17	175.80	233.50	230.50	207.67	233.50
9.03	127.77	188.73	289.67	180.44	237.50	230.50	203.50	237.50
9.04	131.60	190.47	273.67	174.08	221.17	242.00	212.17	221.17
9.05	127.90	190.10	276.17	175.24	226.33	231.00	211.83	226.33
9.06	125.40	195.47	293.83	176.88	224.83	224.50	208.17	224.83
9.07	128.03	188.97	281.50	182.04	235.67	219.17	209.50	235.67
9.08	125.70	191.77	287.17	174.24	218.17	219.17	202.83	218.17
9.09	125.53	192.50	286.83	175.96	234.83	217.83	201.17	234.83
9.10	128.40	190.07	291.67	179.20	231.33	219.83	211.83	231.33
9.11	125.10	192.50	293.17	180.68	233.33	233.17	220.33	233.33
9.12	123.43	195.53	287.83	183.88	230.50	227.17	211.67	230.50
9.13	125.20	193.67	278.50	180.60	230.33	220.33	218.50	230.33
9.14	124.00	194.77	282.50	179.72	227.33	229.50	209.17	227.33
9.15	120.67	193.20	280.83	180.72	228.83	232.00	220.17	228.83

9.16	120.67	192.97	297.00	178.24	233.50	227.67	221.17	233.50
9.17	125.53	198.23	294.83	180.56	234.33	227.17	219.00	234.33
9.18	120.00	196.97	295.00	180.04	225.83	220.83	215.00	225.83
9.19	117.33	188.83	285.67	182.80	239.17	228.50	210.00	239.17
9.20	119.80	194.30	280.83	180.28	239.83	228.17	225.67	239.83
9.21	121.43	192.63	282.83	184.04	231.17	229.50	216.50	231.17
9.22	116.73	189.73	290.33	182.44	233.17	229.67	212.83	233.17
9.23	122.93	196.37	295.00	178.32	232.83	235.33	221.00	232.83
9.24	116.33	203.87	285.17	178.76	232.33	225.00	224.33	232.33
9.25	119.07	197.30	301.33	184.32	244.67	229.67	217.67	244.67
9.26	117.90	196.27	300.50	183.76	232.33	223.00	221.33	232.33
9.27	120.13	196.90	300.83	183.48	248.00	223.17	224.33	248.00
9.28	121.77	194.47	285.33	180.00	245.17	233.17	222.67	245.17
9.29	115.43	196.70	311.17	179.68	235.83	241.67	229.67	235.83
9.30	114.17	201.43	290.83	185.76	243.17	234.33	213.00	243.17
9.31	118.43	201.90	300.17	182.24	220.33	221.17	218.50	220.33
9.32	118.87	206.00	291.67	181.52	224.50	236.83	226.17	224.50
9.33	113.97	198.23	283.67	182.76	240.00	237.50	232.50	240.00
9.34	116.23	201.57	309.83	181.96	243.00	236.00	223.67	243.00
9.35	115.40	200.33	290.00	182.68	238.17	231.83	228.50	238.17
9.36	116.03	202.30	301.33	186.32	240.83	238.67	224.17	240.83
9.37	113.30	198.37	305.00	183.08	254.83	242.67	229.33	254.83
9.38	115.17	201.27	308.67	185.08	254.50	227.33	223.17	254.50
9.39	114.70	202.23	309.67	184.64	248.33	232.50	227.67	248.33
9.40	110.10	206.50	319.17	183.64	238.33	229.17	228.67	238.33
9.41	112.33	206.50	309.17	189.48	234.33	236.00	233.33	234.33
9.42	107.83	202.50	304.00	185.44	249.83	230.50	227.50	249.83
9.43	115.57	207.93	299.67	189.20	242.67	230.83	226.00	242.67
9.44	110.43	205.67	321.50	188.36	241.17	223.50	247.50	241.17
9.45	112.40	211.27	315.50	184.04	245.83	240.67	229.17	245.83
9.46	110.93	205.43	321.33	189.24	229.17	232.17	233.00	229.17
9.47	112.63	207.33	298.17	187.24	245.50	239.67	238.83	245.50
9.48	112.60	205.03	310.17	190.76	235.17	235.83	224.50	235.17
9.49	112.20	208.17	314.00	185.08	245.67	236.33	243.83	245.67
9.50	111.73	207.20	326.17	191.32	240.50	222.50	224.17	240.50
9.51	110.47	209.47	308.67	188.72	247.00	243.67	233.50	247.00
9.52	113.23	210.93	305.50	181.96	249.67	227.50	240.00	249.67
9.53	112.17	213.57	306.83	193.36	247.17	229.50	232.17	247.17

9.54	109.67	207.10	314.33	186.84	253.00	238.67	240.83	253.00
9.55	114.33	210.17	313.67	189.40	245.00	230.83	234.83	245.00
9.56	110.60	208.47	312.17	190.68	248.00	239.17	234.00	248.00
9.57	108.33	213.30	341.00	190.60	255.17	237.50	232.67	255.17
9.58	111.70	209.03	312.67	195.40	252.50	232.00	227.33	252.50
9.59	109.57	212.60	334.50	194.44	256.00	245.50	228.17	256.00
9.60	111.83	215.87	327.50	196.52	251.00	239.50	234.50	251.00
9.61	106.90	219.63	316.17	190.40	239.00	242.17	236.50	239.00
9.62	111.60	212.70	307.67	188.48	256.17	236.67	236.83	256.17
9.63	107.70	217.33	322.50	197.40	247.33	241.50	238.33	247.33
9.64	108.17	210.07	312.50	193.80	241.17	237.50	244.17	241.17
9.65	108.47	218.63	332.00	193.56	246.00	230.50	243.83	246.00
9.66	104.97	215.07	312.50	197.68	250.17	258.50	241.67	250.17
9.67	108.07	217.20	319.33	188.68	259.67	236.67	236.17	259.67
9.68	109.63	216.97	333.00	195.32	256.17	248.00	248.00	256.17
9.69	109.10	216.07	312.50	192.72	246.83	250.67	249.50	246.83
9.70	111.23	219.17	324.17	191.68	252.83	242.50	246.83	252.83
9.71	109.30	218.37	330.67	194.56	253.83	242.50	246.67	253.83
9.72	110.13	218.93	335.17	203.88	264.50	244.33	246.17	264.50
9.73	107.50	221.03	316.50	196.56	260.83	253.17	251.00	260.83
9.74	105.13	212.30	332.83	197.80	274.17	239.00	246.83	274.17
9.75	110.47	220.97	322.83	197.00	263.50	250.50	243.17	263.50
9.76	110.70	219.10	339.50	196.68	261.50	245.17	247.50	261.50
9.77	110.27	224.40	326.67	205.04	257.83	250.17	253.17	257.83
9.78	112.00	221.10	326.17	204.16	249.17	250.50	251.00	249.17
9.79	106.77	224.20	325.67	206.48	266.67	240.67	253.17	266.67
9.80	109.83	223.33	345.67	202.40	262.83	256.67	256.00	262.83
9.81	109.80	224.13	336.00	203.68	261.83	259.50	260.00	261.83
9.82	111.07	229.17	337.67	197.56	268.17	270.00	261.17	268.17
9.83	106.57	224.60	339.50	200.84	268.67	248.17	262.67	268.67
9.84	108.77	225.07	330.50	199.92	255.83	257.00	249.67	255.83
9.85	108.27	224.57	343.83	206.08	266.33	243.50	254.00	266.33
9.86	108.43	227.27	346.67	201.12	268.17	255.00	244.50	268.17
9.87	107.60	228.80	345.00	207.24	260.83	263.33	263.17	260.83
9.88	106.57	229.37	336.83	206.88	256.00	243.50	252.83	256.00
9.89	109.57	229.83	347.17	203.36	279.33	240.00	260.50	279.33
9.90	108.37	230.27	332.83	202.12	271.50	256.00	255.33	271.50
9.91	106.80	228.90	336.33	206.68	265.00	248.33	257.67	265.00

9.92	107.27	230.70	338.17	204.48	254.17	268.17	276.00	254.17
9.93	105.80	227.87	357.17	205.16	266.33	266.50	268.50	266.33
9.94	105.07	234.47	354.00	210.44	272.50	252.50	262.17	272.50
9.95	108.03	234.03	339.00	209.36	263.83	265.67	263.50	263.83
9.96	105.33	234.73	358.67	211.88	264.00	258.83	263.17	264.00
9.97	106.33	238.57	352.33	205.28	278.17	266.33	271.50	278.17
9.98	105.43	231.90	341.83	210.12	274.33	270.50	260.83	274.33
9.99	103.67	234.07	347.33	204.28	268.83	263.50	251.83	268.83
10.00	107.73	236.23	359.83	212.36	288.00	264.33	266.67	288.00